Carbohydrate-based detection as the basis of new diagnostics for infectious diseases

Pedro J. Hernando Callejo

(student number 100302124)

This thesis is submitted in fulfilment of the requirements of the degree of Doctor of Philosophy at the University of East Anglia

Department of Gut Microbes and Health

Quadram Institute Bioscience

November 2022

Declaration

I declare that the work contained in this thesis submitted by myself for the Degree of Doctor of Philosophy is my work, except where due reference is made to other authors, and has not previously been submitted by me for a degree at this or any other university.

Pedro J. Hernando Callejo

ABSTRACT

Carbohydrates cover the surface of mammalian and bacterial cells, playing crucial roles in biological processes including pathogen-host recognition. The intrinsically weak carbohydrate-mediated interactions are compensated in Nature by a multivalent exhibition of the sugar ligands generating a “velcro” type of interaction known as glycocluster effect.

There is an unmet need for simple, reliable, and portable devices for the early detection of pathogens. In this research work, we explored the development of a rapid carbohydrate-based assay for the detection of glycan-binding proteins, lectins, in relation to the detection of bacteria. To allow a visual read-out of the test, gold nanoparticles have been applied on a paper-based diagnostic assay.

A set of carbohydrates was chemically and/or enzymatically modified with an azidopropyl tether, allowing the functionalisation of alkyne-modified bovine serum albumin through Cu(I)-catalysed alkyne-azide cycloaddition. The multivalent neo-glycoproteins were immobilised on the surface of *ca.* 40 nm gold nanoparticles following passive adsorption methodology. The synthesised glyconanoparticles were employed as detection agents in a dipstick assay for the detection of a selection of lectins. To further understand the impact of the nanoparticle size and the presentation of glycans on the assay performance, *ca.* 150 nm gold nanoshells and *ca.* 40 nm gold nanoparticles covalently functionalised with glycans were investigated.

A lectin relevant to the early detection of the opportunistic pathogen *Pseudomonas aeruginosa* was targeted. A carbohydrate-based ligand was tailored for the detection of the *P. aeruginosa* surface lectin LecA. The detection of LecA in bacterial samples employing antibodies was investigated through Western Blot. Preliminary results against *P. aeruginosa* strain are presented using flow cytometry to evaluate the potential detection of the target bacteria exploiting its interaction with glyconanoparticles.

The results presented in this thesis show the potential of glyconanoparticles for the cost-effective detection of lectins, paving the way for the rapid detection of pathogens.

CONTENTS

LIST OF FIGURES

LIST OF SCHEMES

LIST OF TABLES

ABBREVIATIONS

δ	Chemical shift
λ_{max}	Maximum of absorbance
Å	Armstrong
Ab	Antibody
Ac	Acetyl
ACN	Acetonitrile
AcO	Acetate
Ac_2O	Acetic anhydride
A. oryzae	*Aspergillus oryzae*
AP	Alkaline phosphatase
Aq.	Aqueous
Asc	Ascorbate
Asp	Aspartic acid
ATR	Attenuated total reflection
AuNP	Gold nanoparticles
AuNS	Gold nanoshells
BCIP	5-Bromo-4-chloro-3'-indolyphosphate
BLI	Biolayer interferometry
Bn	Benzyl
Boc	*Tert*-butyloxycarbonyl
Boc_2O	Di-*tert*-butyl carbonate
BSA	Bovine serum albumin

Bz	Benzoyl
c	concentration (g/100 mL)
ca.	*circa*
calcd	calculated
Cat.	catalytic
CC-BY	Creative Commons Attribution License
Cit.	Citrate
C. jejuni	*Campylobacter jejuni*
ConA	Concanavalin A
COSY	Correlated spectroscopy
CRD	Carbohydrate recognition domain
CT	Cholera toxin
CTB	Cholera toxin B subunit
CuAAC	Copper(I)-catalysed azide-alkyne cycloaddition
d	doublet
dd	doublet of doublets
ddd	doublet of doublets of doublets
dt	doublet of triplets
DTT	Di-thiothreitol
DCM	Dichloromethane
DLS	Dynamic light scattering
DMAP	4-Dimethylaminopyridine
DNA	Deoxyribonucleic acid
E. coli	*Escherichia coli*
EDC	1-(3-Dimethylaminopropyl)-3-ethylcarbodiimide
ELLA	Enzyme-linked lectin assay
Eq	Equivalents
ESI-MS	Electrospray ionisation mass spectrometry
EtOH	Ethanol
FCM	Flow cytometry
FITC	Fluorescein isothiocyanate
2'FL	2'-Fucosyllactose

FRET	Förster resonance energy transfer
FSC	Forward light scattering
FT-IR	Fourier transform infrared spectroscopy
Gal	Galactose
GalNAc	*N*-acetylgalactosamine
gAuNP	Gold glyconanoparticle
gAuNS	Gold glyconanoshell
Glc	Glucose
GlcNAc	*N*-acetylglucosamine
Gly	Glycine
GM1	Ganglioside mono-sialic acid 1
GPC	Gel permeation chromatography
gQD	Glyco-quantum dot
HBOt	*N*-Hydroxybenzotriazole
HEPES	4-(2-Hydroxyethyl)-1-piperazineethanesulfonic acid
Hex	Hexane
HILIC	Hydrophobic interaction liquid chromatography
His	Histidine
HMO	Human milk oligosaccharide
HPLC	High-performance liquid chromatography
HR-MS	High-resolution mass spectroscopy
HRP	Horseradish peroxidase
HSQC	Heteronuclear single quantum coherence
IC_{50}	Half maximal inhibitory concentration
IPA	Isopropanol
IPTG	β-D-1-thiogalactopyranoside
ITC	Isothermal titration calorimetry
$J_{a,b}$	Coupling constant between a and b
K_D	Dissociation constant
Lac	Lactose
LB	Lysogeny broth
LDS	Lithium dodecyl sulfate

Lit.	Literature
LOD	Limit of detection
LTBh	Heat-labile enterotoxin
Lys	Lysine
M	multiplet
MALDI-TOF	Matrix-assisted laser desorption/ionisation time of flight
Man	Mannose
α3α6-Man	α3,α6-mannotriose
MBL	Mannose-binding lectin
MeOH	Methanol
MES	2-(N-Morpholino)ethanesulfonic acid hydrate
MS	Mass spectrometry
NBT	nitro-blue tetrazolium
NHS	N-Hydroxysuccinimide
NMR	Nuclear magnetic spectroscopy
NOESY	Nuclear overhauser enhancement spectroscopy
NP	Nanoparticle
NTP	Nucleotide triphosphate
OD	Optical density
o.n.	Over night
OTf	Trifluoromethanesulfonate, triflate
PAA	polyacrylamide
P. aeruginosa	*Pseudomonas aeruginosa*
PAGE	Polyacrylamide gel electrophoresis
PB	Phosphate buffer
PBS	Phosphate buffer saline
PCR	Polymerase chain reaction
PDB	Protein database
PEG	Poly(ethylene glycol)
Phe	Phenylalanine
PHEA	Poly(*N*-hydroxyethyl acrylamide)
ppm	Parts per million

PVP	Poly(vinylpyrrolidone)
QD	Quantum dot
RAFT	Reversible addition-fragmentation chain transfer
RBP	Relative binding potency
RCA_{120}	*Ricinus communis* agglutinin 120
R_f	Retention factor
RT	Retention time
rtPCR	Real time polymerase chain reaction
r.t.	Room temperature
s	singlet
SDS	Sodium dodecyl sulfate
3'SL	3'-Sialyllactose
SLT-1	Shiga-like toxin 1
SLT-2	Shiga like toxin 2
SNFG	Symbol nomenclature for glycans
SPR	Surface plasmon resonance
SSC	Sidelight scattering
S. suis	*Streptococcus suis*
Stx1	Shiga toxin 1
Stx2	Shiga toxin 2
t	triplet
T. cruzi	*Trypanosoma cruzi*
TcTs	*Trypanosoma cruzi* trans-sialidase
TEA	Triethylamine
TEM	Transmission electron microscopy
TFA	Trifluoroacetic acid
THF	Tetrahydrofurane
THPTA	Tris(3-hydroxypropyltriazolylmethyl)amine
Thr	Threonine
TLC	Thin layer chromatography
T_m	Protein melting point
Tol	Toluene

Tris	Tris(hydroxymethyl)aminomethane
TSA	Thermal shift assay
UEA I	*Ulex europaeus* agglutinin I
UV-Vis	Ultraviolet-visible
WGA	Wheat germ agglutinin

ACKNOWLEDGEMENTS

I would like to start with a big thank you to Rob, for giving me the experience of a PhD and for guiding me throughout the last three years. Thank you for your patience and understanding, and for hammering when I needed it. Thank you, Simone, for being there, always ready for a call, always there to calm me down and to bring some positivity to the conversation. María, thank you very much for always welcoming me into your office with a smile. Thank you for teaching me the value of looking at the details and for helping me communicate better my research. Nathalie, thank you so much for your kindness, and for your warm welcome to your group. Thank you, Paz, for opening the doors of your lab and hosting me these last months. Thank you to all the people that have supported me at QIB and JIC: Dimitris, Andy, Ryan, Manu, Sergey, Martin, Carlo and Gerhard, for your help and advice when I have needed it.

Thank you to all the Iceni family, for being there, for being fun and for your willingness to help. Thank you, Simona, Giulia, Trudy, Mike, Lloyd, Chris and Tanya; I am going to miss you all. A special thank you to Irina, my *hooligan* mate. Thank you for coaching me in the lab, for checking on me every day, and for being a friend whenever I needed it. Iako, I wish you the best to finish your PhD, I know you will overcome any difficulty that comes your way. Be as you are: you will reach far. Gaiomix, I think we have kept our promise: "we are all in this together", until the very day of our vivas. I thank you so much for listening to my problems, and for letting me be part of your life. Cheers mate.

Thank you, Ana, for being there from the very beginning. I wish you the best in your next adventure… I hope Bilbao is ready for you. Wouter, Victor, Anne, Helene and María G., I am going to miss the time with all of you, and I wish you the best in finishing your studies. Mar and Markus, thank you for being such lovely friends and housemates, for welcoming me to Mardle St and for letting me put a 55" TV in the living room. A special thank you, Carla, for being so thoughtful, for sharing so much with me, and for letting me share with you. I hope you have the best experience in the US.

No podría haber llegado hasta aquí sin mi familia. Papá, mamá, siempre os estaré agradecido por enseñarme a valorar mi educación, por apoyarme en cada paso que he dado, y mantenerme a flote durante esta aventura. A mi brother, muchas gracias por estar ahí, por preocuparte por mí y por cuidarme cuando vuelvo a casa. Y por todos los juegos de la Switch que te he robado. Anita, muchas gracias por ser tan alegre y por tener siempre una sonrisa. Jiminou, muchas gracias por sumarte a esta aventura. Has sido mi zona segura cada vez que lo he necesitado. Gracias por cuidar de mí, por enseñarme tu pasión por los juegos de mesa, y por compartir tanto conmigo.

Muchas gracias a todos.

Esta tesis está especialmente dedicada a mi abuela.

Esté donde esté, seguirá preguntando qué tal me va en Medicina. Ya casi soy doctor, yaya.

CHAPTER 1

INTRODUCTION

The following chapter introduces the state of the art of the research work discussed in this thesis. It is divided into three main sections: chemical biology, microbiology and nanotechnology. General aspects of carbohydrates and their role in biological systems are discussed, together with the instrumental techniques developed to assess the interactions of carbohydrates with glycan receptors. The biological importance of carbohydrates is exemplified with the specific case of *Pseudomonas aeruginosa* and one of its glycan receptors, the lectin LecA. Finally, the general properties of gold nanoparticles (AuNPs) and other examples of nanometric structures employed in assays in solution for the detection of lectins are discussed.

This project has been financed by the Marie Skłodowska-Curie Actions (MSCA) within the European Framework Horizon 2020 (grant agreement 814102). It is part of the Sweet Crosstalk Innovative Training Network (SCT-ITN), which aim is to gain insights and develop a deeper knowledge of the relationship between health, glycans and microbiota.[1] Six different pillars hold the approach of the consortium, comprising tools and techniques from different fields of Chemistry and Biology (**Figure 1.1**).

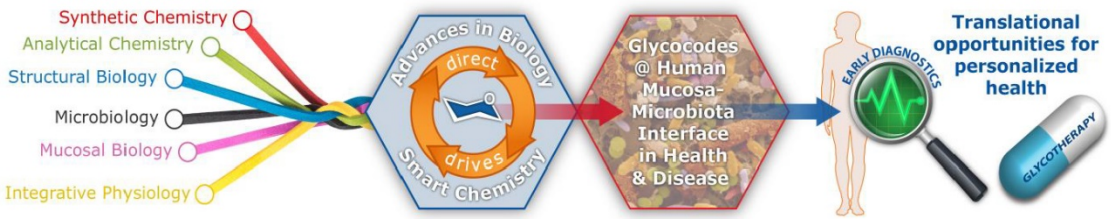

Figure 1.1. Flow chart of the approach adopted in the SCT-ITN to investigate the relationship between human health, glycans and microbiota.[1]

1.1. Chemical Biology of glycans

Carbohydrates are ubiquitous in the cell surface, in the so-called glycocalyx (**Figure 1.2**) of both mammalian and bacterial cells. The carbohydrate structures forming the glycocalyx play different biological roles including recognition, targeting and regulation of cell-cell and cell-environment interactions.[2] The variety of processes that glycans are involved in is achieved by the diversity of stereochemistry, configurations, linkages, chemical variations, and branched structures that carbohydrates present in Nature.[3] However, the knowledge about glycans is still limited by the complexity of these molecules. Due to the unbalance between abundance and specific knowledge, carbohydrates have received the name of the dark matter of Biology.[4]

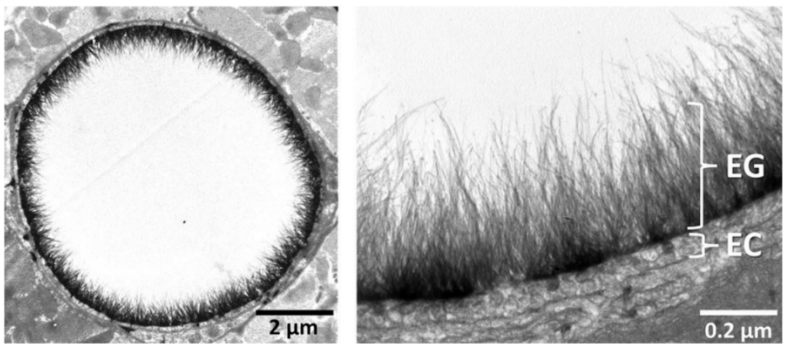

Figure 1.2. Transmission electron microscopy (TEM) image of a goat coronary capillary, zoomed in to emphasise the size of the endothelial glycocalyx (EG) which is several fold thicker than an endothelial cell (EC). Reproduced from Gaudette *et al.*[5] with permission from John Wiley and Sons.

1.1.1. The role of glycans in the recognition and infection process

Despite the key role of carbohydrates in many biological processes, their interaction with proteins is weak, with dissociation constants (K_Ds) in the µM to mM range.[6] To increase the strength of the interaction, carbohydrates are often exhibited on cell surfaces in a multivalent manner, facilitating a cluster glycoside effect.[7] The clustering effect is a phenomenon based on the cooperation between neighbouring glycan units from a same ligand leading to an enhancement of interaction. An example of the clustering effect is the glycosylation on the surface of mammalian cells or viruses, which is well known to play a key role in the recognition process either to trigger the host invasion (**Figure 1.3A**) or to alert the immune system for the presence of a pathogen in their environment (**Figure 1.3B**).[8] In the process of biological recognition, not only the presence of the specific carbohydrates is needed for the interactions

to take place, but also the right receptors on the surface of the counterpart. Glycan receptors on biological membranes are often proteins known as lectins, which present a high specificity towards precise glycans and conformations, being able to distinguish between linkages and stereochemistry.[9] The difference between a lectin and other kinds of glycan-binding proteins such as enzymes, is that the role of lectins is limited to the interaction with the glycans counterpart for adhesion or recognition processes, without modifying them.

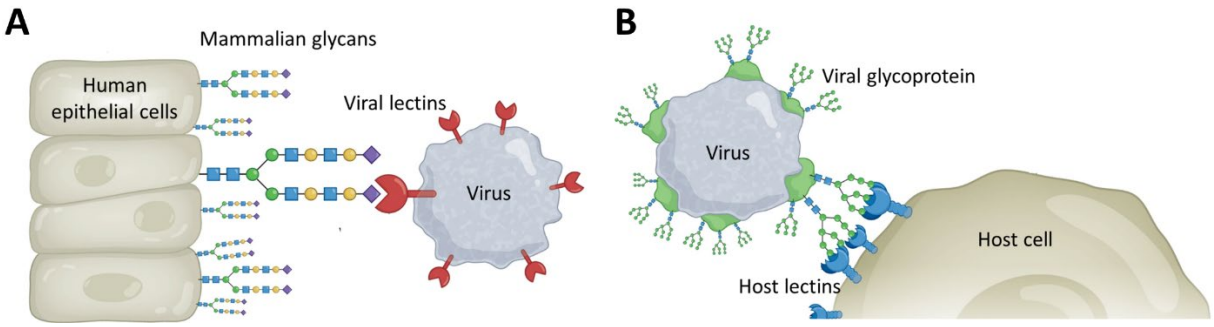

Figure 1.3. The multivalent presentation of glycans is key in biological processes such as recognition between virus and mammalian cells during either (**A**) host invasion or (**B**) pathogen detection showing lectin clustering effect. Reproduced from Dugan *et al.*[8] with permission from Springer Nature.

Host cell-bacteria interaction is a crucial step for the infection process, and it is usually mediated by cell-surface carbohydrate recognition.[10,11] It has also been proved that bacteria can vary their preference in surface glycan recognition depending on the stage of infection of the host cell.[12] After identifying and characterising six lectins on the surface of *Helicobacter pylori*, it was found that four of them were involved in the adherence process, showing a preference for lactoceramides and fucosylated glycans. The other two lectins were involved in the colonisation stage, showing preference for with sialylated glycans.

1.1.2. Lectins: mode of binding

Lectins possess a binding pocket called the carbohydrate recognition domain (CRD).[13] In fact, lectins are often multivalent, comprising several CRDs to tighten the interaction with carbohydrates, exploiting the glycoside clustering effect.

The mechanism of binding between glycans and lectins is controlled mainly by hydrogen bonds and aromatic interactions, followed by metal ion coordination and the formation of salt bridges.[14] Hydrogen bonds occur between the hydroxyl groups on the glycan and polar side chain groups of the amino acids in the binding pocket, such as serine or glutamine (**Figure**

1.4A).[15] The hydroxyl groups act cooperatively, being both acceptor and donor of interactions. Not only the hydroxyl groups but also amines present in some glycans can participate in the interaction. Hydrophobic fragments, such as alkyl groups, can also participate in hydrophobic interactions with hydrophobic regions of the binding pocket such as aromatic amino acids phenylalanine, tryptophan or serine (**Figure 1.4B**).[16] The stabilising coordination of hydroxyl groups to a metal ion, often Ca(II), is a common feature, although not exclusive, in C-type lectins (**Figure 1.4C**) such as the DC-SIGN receptors or the mannose-binding lectin (MBL) in humans.[17] Less commonly, electrostatic interactions can be found between charged glycans such as sialic acid, and amino acids like serine, forming a salt bridge (**Figure 1.4D**).[18]

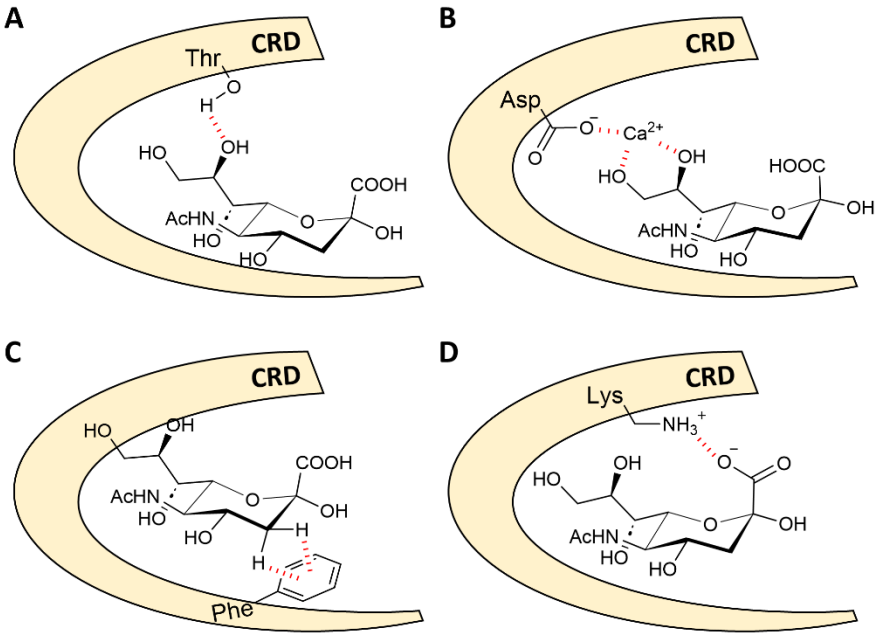

Figure 1.4. Schematic representation of the CRD of a general sialic acid-binding lectin showing (**A**) hydrogen bonds through a threonine (Thr), (**B**) calcium coordination through an aspartic acid (Asp), (**C**) hydrophobic interactions with phenylalanine (Phe) or (**D**) salt bridges formed with a lysine (Lys) residue.

1.2. Quantification of lectin-carbohydrate interactions

1.2.1. Isothermal titration calorimetry

To allow the quantification of the binding intensity of biomolecules in solution, isothermal titration calorimetry (ITC) is often the technique of choice. ITC is versatile as it can be used for both small and macromolecules, measuring the heat exchanged upon association and

dissociation of the ligand and analyte (**Figure 1.5**).[19] The system includes two cells, one for the sample and one for the reference, whose temperatures are constantly monitored. During the assay, a solution of the ligand is titrated with a solution of the analyte, measuring the difference in temperature between the sample and reference cells to evaluate the heat exchanged in the binding event. One of the shortcomings of this technique is the compatibility of buffers, as both ligand and analyte need to be used in the same one to avoid heat exchange by the combination of different buffers.

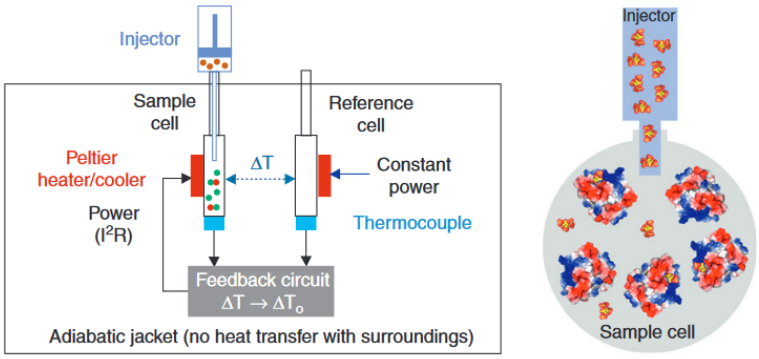

Figure 1.5. Scheme of a typical ITC experiment to investigate the interaction between a ligand and an analyte in solution. The heat exchanged between both is measured in a sample cell in comparison with a constant reference cell. Reproduced from Lambright[19] with permission from Elsevier.

ITC has been widely used to measure different types of interactions such as protein-small molecule,[20] protein-DNA[21] or protein-protein interactions.[22] An example of the application of this technique in Glycoscience is a study on the mannose-binding lectin concanavalin A (ConA, described in *Section 1.3.2.*).[23] The authors designed and synthesised a series of di-, tetra-, hexa- and octavalent mannose ligands to investigate their different avidity for ConA (**Figure 1.6**). The data obtained from the ITC experiments showed a K_D of 15 µM for the divalent mannose derivative, which was six times lower than the one obtained using the methyl α-mannoside monosaccharide. However, the decrease of K_D was found to be not proportional to the increase in multivalency, with a value of 0.4 µM found for the tetravalent ligand, and 0.2 µM for the hexavalent one. The octavalent ligand exhibited the lowest K_D of this series, 74 nM. The authors commented on the enthalpy contribution to the energy of binding being proportional to the multivalency of the ligand, whereas the entropy contribution was higher. That observation suggested that the increase in binding reported is linked to the presentation

of glycans matching the requirements of the CRD, and not only to the multivalency of the ligands.

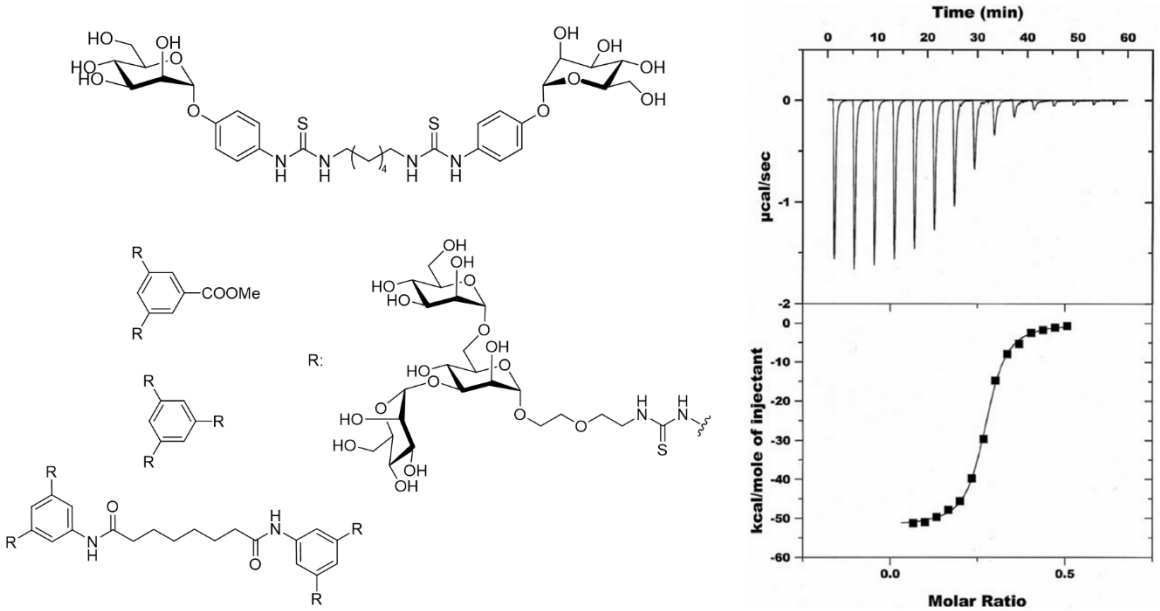

Figure 1.6. Mannosylated structures assayed *via* ITC. A solution of ConA is titrated with the ligand, with additions every five minutes. The heat exchanged upon interaction is plotted (top graph) and integrated (bottom graph) to calculate the thermodynamic parameters of the association equilibrium. Adapted from Dan *et al.*[23] (CC-BY)

ITC analysis has often been employed to evaluate glycan-lectin interactions, and several examples are reported in *Chapter 4* to evaluate *P. aeruginosa* LecA inhibitors. However, this technique requires quantities of both protein and ligands, typically in the sub-milligrams for carbohydrate systems, which might not be ideal in case of valuable or not easy to access materials. ITC informs a good candidate for the thermodynamic study of known inhibitors rather than the initial screening of libraries of ligands, not only because of the amounts needed but also because of the assay time required, often of 1-2 h per ligand. An ideal experiment, performed in triplicate and including the necessary controls, could take as long as 10 hours, which makes it unviable for large libraries of compounds. However, ITC presents the highest sensitivity in comparison to the other techniques described in this thesis, reaching K_Ds in the nanomolar and even picomolar range.

1.2.2. Glycan microarrays

To allow a high throughput screening of numerous glycans (or other biologically active molecules), glycan microarrays have been developed. In this section, the main techniques

employed to evaluate the binding between glycans and lectins are presented, with special attention to surface plasmon resonance (SPR) given its relationship to AuNPs. It must be noted that these techniques are often very dependent on assay conditions, leading to a lack of reproducibility between different reports. It is also important to complement data from different assays, as the format (*i.e.* in-solution as opposed to surface-bound assays) plays a key role in the presentation of glycans and can sometimes lead to different recognition by lectins. As a complementary technique, lectin microarrays have also been developed to screen a range of lectins against glycoproteins, tissues and pathogens to investigate their carbohydrate profile.[24] Those applications have been of special importance in the study and image of the over-glycosylated surface of cancer cells.

1.2.3. Enzyme-linked lectin assay

Based on the covalent functionalisation of glass slides often pre-activated with NHS esters, enzyme-linked lectin assays (ELLAs) allow an easy functionalisation with a series of amine-ending ligands to be tested in an organised fashion (**Figure 1.7**).[25] The slides are stained with the lectin of interest, often conjugated with alkaline phosphatase (AP) or horseradish peroxidase (HRP) to develop the assay.[26] Otherwise, the lectin can be used unconjugated, followed by a labelled antibody which recognises the lectin in a sandwich manner. After washing to remove the unbound ligands, the slide is then read, often in a confocal scanner to allow quantification of the fluorescence.

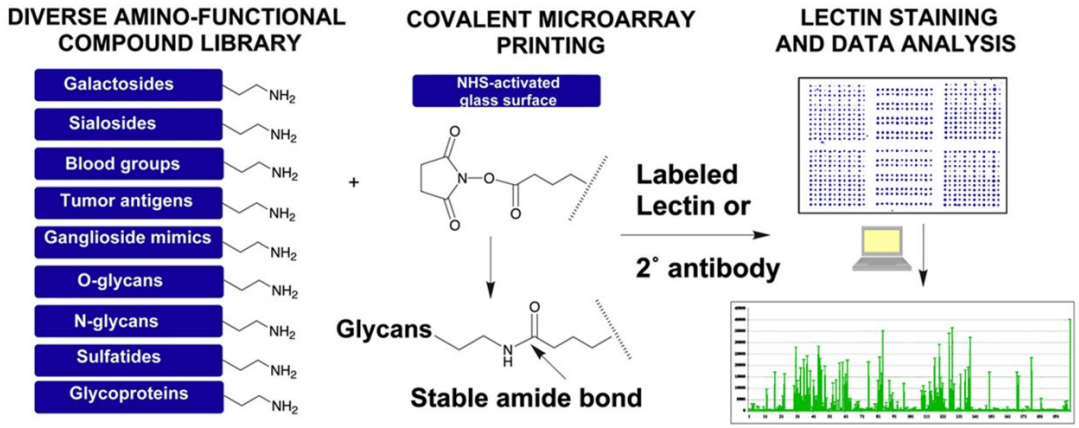

Figure 1.7. Flow chart of an ELLA to test the interaction between a range of carbohydrates and a lectin. Aminoalkyl-functionalised probes are bound to an NHS ester-activated glass slide, which is then stained with either a fluorescently labelled lectin, or a lectin and a fluorescently labelled antibody. The fluorescence is quantified to compare the interactions. Adapted from Blixt *et al.*[25] with permission from the National Academy of Sciences.

Historically, ELLA is the technique of choice when aiming at screening a high number of ligands to investigate the binding preferences of lectins, given the ease to perform the assay (several examples are reported in *Section 1.3*). This assay does not provide binding information from a thermodynamic or kinetic point of view, and it is often used to collect preliminary data before employing a more sophisticated technique such as ITC. However, the binding can be quantified as a half maximal inhibitory concentration (IC_{50}), which is the concentration of ligand in solution at which only half of the lectin binds to the surface of the microtiter well. An ELLA assay was developed to investigate the binding of four glucose-centred mannose clusters to ConA (**Figure 1.8**).[27] The wells of a microtiter plate were coated with mannan (polymeric α-mannose) and the binding of HRP-labelled ConA was studied upon incubation of the lectin in the presence of the different ligands in solution. The ligands successfully inhibited the binding of the lectin, followed by peroxidase reactions to observe fluorescence. The anomeric configuration of the glucose core did not seem to influence the results of the assay, with IC_{50} values found of 27 and 31 μM respectively for the α and β anomers. The exchange of the aglycone sulphur atom for a thiourea moiety in the terminal mannose residues led to a dramatic change in affinity, with an IC_{50} value of 640 μM, possibly due to the rigidity of the system. A pentadecavalent ligand was synthesised, and even though there was an improvement in affinity, it was not proportional to the increase in multivalency, with an IC_{50} value of 18.5 μM.

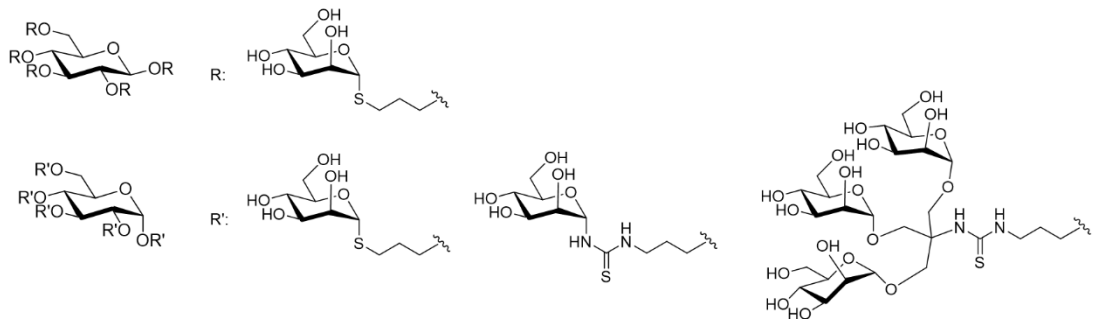

Figure 1.8. Mannosylated structures assayed *via* ELLA by Kohn *et al*.[27] to assess their inhibitory power against the binding of ConA to a mannan-coated surface.

1.2.4. Surface plasmon resonance

The phenomenon of SPR appears upon the interaction between light and metal surfaces. It has been widely used to quantify the binding of biomolecules and analytes (**Figure 1.9**),[28] with several arrays discussed throughout this thesis. Glycoarrays often use gold chips pre-

functionalised with streptavidin, avidin or neutravidin to investigate the interaction of lectins with biotinylated glycans.[29] Incident light applied to the metal surface is reflected through a prism, to measure the change in reflected angle (SPR angle) upon attachment of the analyte to the ligand-bound surface. As molecules bind to the surface, the intensity of a chosen SPR angle decreases proportionally to the mass of the analyte attached, allowing to follow the binding events in real-time. SPR is possibly a better-balanced option for thermodynamic studies over ITC, however, the information obtained through both techniques is complimentary, as SPR provides information on the surface-bound interactions, while ITC evaluates the interactions in solution.

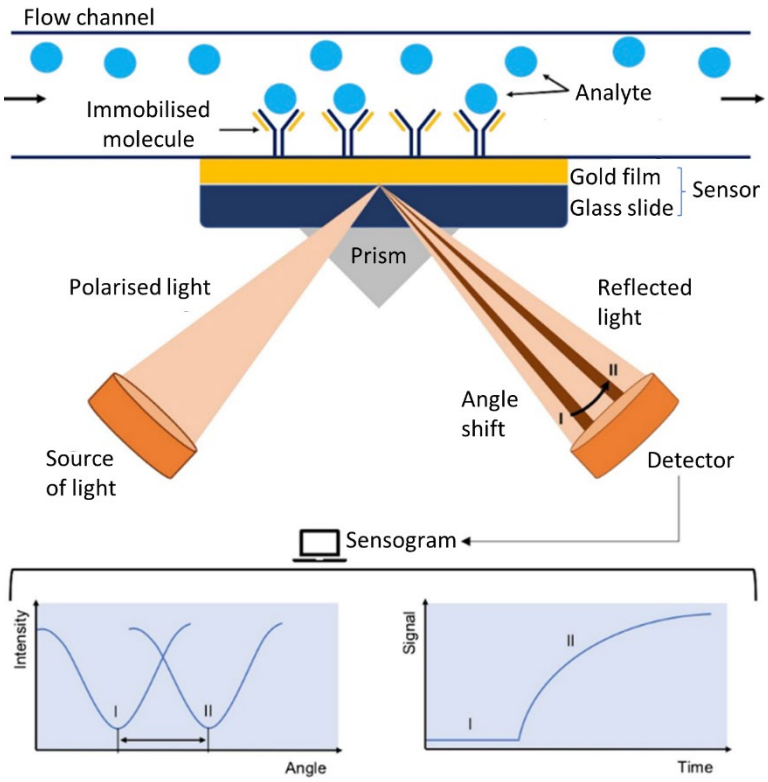

Figure 1.9. Scheme of a typical SPR experiment to investigate the interaction between an analyte in solution and a biomolecule immobilised on a gold chip. Monochromatic light is applied to the sensor to measure the change of light intensity reflected from the angle I to angle II, following the binding event. Adapted from Boguszewska *et al*.[28] (CC-BY).

SPR microarrays can be used to test libraries of compounds as well as to investigate the effect of the surface density of carbohydrates on the binding properties of a lectin. The binding of a linear mannotrioside with ConA was investigated in a SPR microarray to study the influence of glycan density (**Figure 1.10**).[30] Gold sensors were coated with different ratios of polyethylene glycol (PEG) and the mannotrioside functionalised with a PEG chain of similar

length, both with a terminal thiol to allow immobilisation on the gold surface. A systematic "dilution" of the ligand density on the surface was obtained ranging the proportion of the two molecules from 0 to 100%. RNase A and B were used as negative and positive controls, respectively, given the known presence of a high mannose moiety on RNAse B and the absence of it in the A isomer.[31] The results clearly showed an increasing interaction of ConA at the mannosylated surface with increasing densities of the glycan.

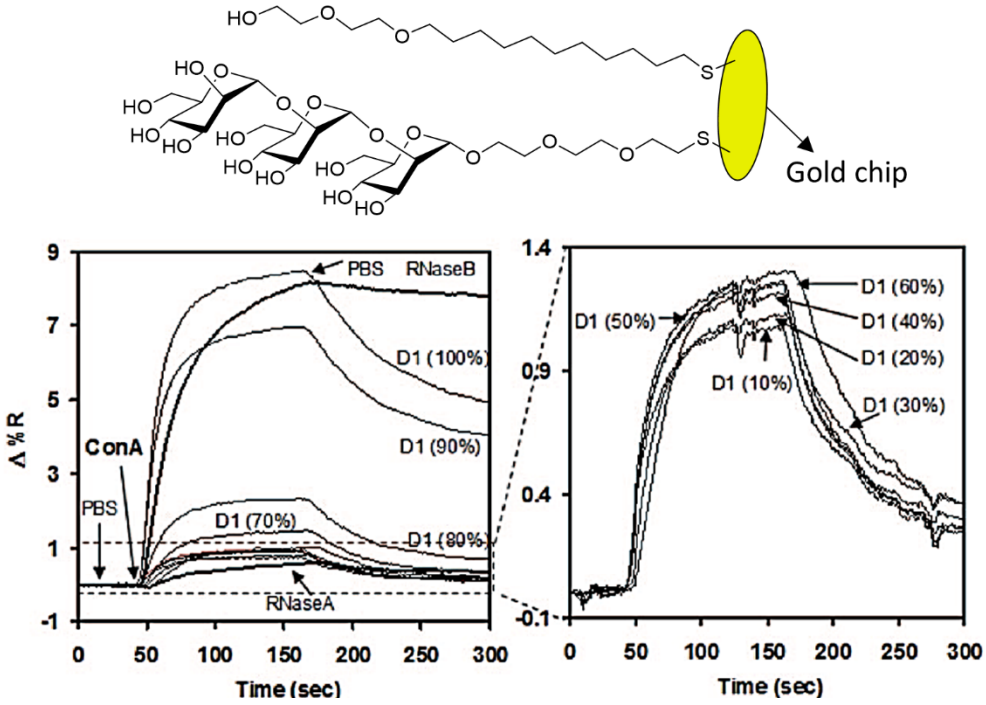

Figure 1.10. SPR array to investigate the influence of carbohydrate density on the interaction between ConA and a linear mannotrioside. The glycan was bound to a gold sensor in different ratios with a PEGylated linker. The sensograms from the experiments clearly show an increasing interaction between the lectin and the surface with increasing sugar densities. Adapted from Dhayal *et al.*[30] with permission from the American Chemical Society.

1.2.5. Gold nanoparticles: surface plasmon resonance and more

With the emergence of disciplines such as nanoengineering or nanobioelectronics, colloidal nano-sized particles have kept attracting the attention of researchers for many years.[32,33] Nanoparticles (NPs) are nanostructures with a size comprised between 1 and 100 nm whose preparation started to be studied about thirty years ago.[34] The importance of AuNPs lies in the unique features that their structures have. On the nanometre scale, the conduction electrons oscillate in resonance with incident electromagnetic radiation, resulting in the previously mentioned phenomenon named SPR (**Figure 1.11**).[35,36] As a consequence, optical

properties are governed by size, particle distance, shape and the nature of the metal core. In the case of noble metals such as gold or silver, the surface plasmon absorption band appears in the visible region of the electromagnetic spectra. Therefore, a wide range of intense colours can be observed by combining different metal atoms and particle sizes.[37]

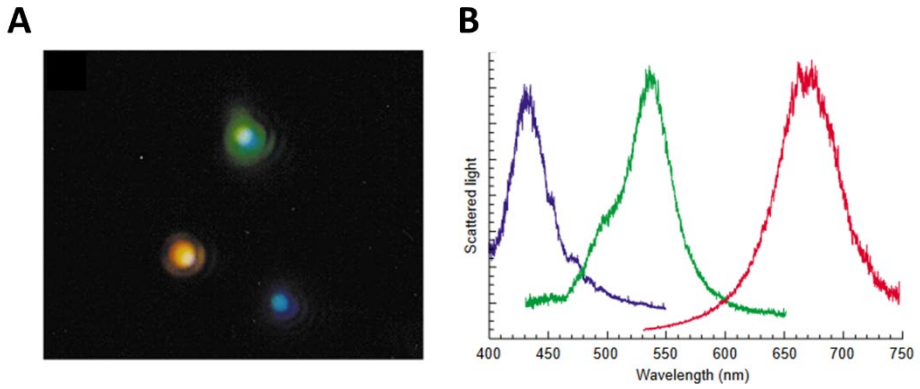

Figure 1.11. Surface plasmon resonance of silver and gold nanoparticles (type not specified). (**A**) Photograph of NPs suspension illuminated with white light. (**B**) Overlayed normalised UV-Vis spectrum of the three NPs, showing the maximum of surface plasmon absorbance. Adapted from Schultz[35] with permission from Elsevier.

Given the spheric shape of AuNPs, these exhibit a high surface area to volume ratio, allowing the installation of numerous ligands on their surface. This is a highly beneficial feature for their application in the study of carbohydrate interactions, as the multivalency of glycans is very important to overcome their weak binding (discussed in *Section 1.1* and will be discussed throughout this thesis). The field of the glyconanoparticles (gAuNPs) is based on the seminal work of Penadés and collaborators who employed thiolated lactose and Le^x trisaccharide to functionalise 2 nm AuNPs for the study of Ca(II)-mediated cell adhesion processes.[38] A follow-up publication explored in depth the methodology for the preparation, functionalisation and characterisation of gAuNPs,[39] including thiolated carbohydrates and also a fluorescent ligand for the labelling of 2-6 nm gAuNPs. In their pioneering work, Penadés *et al*. presented gAuNPs as mimics of the glycocalyx layer in biological surfaces, with potential to control the particle size and the density of sugars on their surface. Since then, the interest in gAuNPs rose considerably in just a few years.[40] The influence of the nanoparticle size on the target binding has been studied, concluding that nanoparticles with larger sizes favour carbohydrate-target interactions due to their flatter surfaces.[41]

Colour-change based assays

The multivalent functionalisation of AuNPs with a suitable ligand, such as carbohydrates, allows its binding to multivalent targets like lectins. This process decreases the interparticle distance, leading to the clustering of AuNPs, especially in the presence of a multivalent target (**Figure 1.12A**). As previously mentioned, the SPR is a distance-dependant phenomenon, therefore the aggregation of AuNPs can cause a shift in the maximum of absorbance, typically towards the blue spectrum (purple colours), which can be followed either visually (**Figure 1.12B**)[42] or through the measurement of the UV-Vis spectra (**Figure 1.12C**).[43] The aggregation of particles can be also followed through TEM (**Figure 1.12D**).[44]

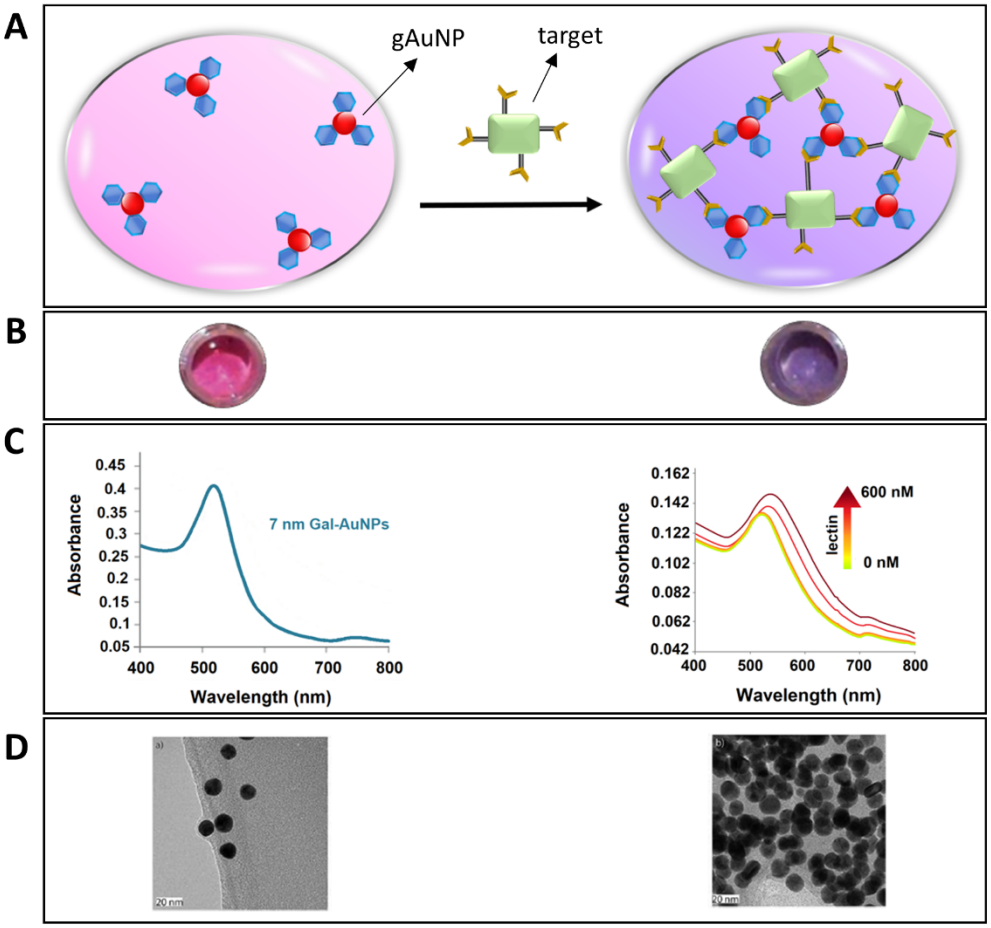

Figure 1.12. (**A**) Schematic representation of a gAuNPs aggregation-based assay for the detection of lectins or pathogens. This type of assay can be evaluated through (**B**) the colorimetric detection due to the plasmon shift,[42] (**C**) a shift of the plasmon resonance absorption band in the UV-vis spectra,[43] or (**D**) visualisation of nanoparticle aggregation *via* TEM.[44] Figure adapted from Hernando *et al*.[45] (CC-BY).

A wide range of bioassays has been developed taking advantage of the colour, UV-Vis and TEM changes upon clustering of AuNPs in the presence of a target.[46] The discussion below covers detection assays in solution based on gAuNPs, whereas those in lateral flow or dipstick formats are presented in *Chapter 3*.

Although the aggregation-induced colour change above mentioned was due to a shift in the UV-Vis absorption, it is also possible that the aggregates formed are not stable in the suspension, precipitating and leading to a loss in colour intensity. Previous work in our group showed that gAuNPs-based assays enable discrimination between pathogens taking advantage of their interactions with specific carbohydrates.[47] The assay developed benefited from different binding preferences between human and avian influenza viruses. These haemagglutinin-mediated interactions allowed the development of a bioassay to discriminate the two viruses. Whereas the avian influenza virus binds to Neu5Ac-α(2,3)-Gal, the human influenza virus prefers the α(2,6) analogue. The disaccharide was coupled to a thiolated trimeric tether for the subsequent functionalisation of *ca*. 16 nm AuNPs. The density of the glycosides on the surface of the particles was adjusted by combining the trimeric glycoside with a PEG ligand, finding an optimal glycoside-PEG ratio of 25:75. The system exhibited a decrease in UV-vis absorption that could also be observed visually upon addition of influenza H3N2 virus (human strain) to a solution of the gAuNPs. The addition of the avian strain H5N1 did not cause any appreciable aggregation (**Figure 1.13**). Other studies have also exploited the specific binding of influenza virus strains to distinguish between them. Copper(I)-catalysed azide-alkyne cycloaddition (CuAAC) has been used to install a di-thiolated linker on the sugars, to subsequently functionalise 13 nm AuNPs *via* thiol interactions.[48] In another work, a sialoglycopeptide extracted from egg yolk was used to functionalise 12 nm AuNPs for the colorimetric detection of the human influenza virus.[44] In brief, a multistep methodology was developed to extract the N-glycan-containing glycoprotein from lyophilised egg yolk. The isolated glycoprotein was finally purified through solid-phase extraction in a carbon/celite column. The protein part of the glycoprotein was cleaved with a protease and purified through gel permeation chromatography (GPC), and finally derivatised to form a sialyl oligosaccharide disulfide ligand. Under reductive conditions, the disulfide function was converted to a thiol for the installation on the surface of *ca.* 20 nm AuNPs. Experiments were initially performed with haemagglutinin and then with two H1N1 strains, A/PuertoRico/8/34 and A/New

Caledonia/29/1999, respectively binding to α2,3-linked and α2,6-linked sialic acid. The system showed selectivity towards A/New Caledonia/29/1999, in the presence of which the nanoparticles aggregated and a colour change could be observed. The study achieved the selective detection of the human influenza virus (over the avian one) with a LOD of 141 nM.

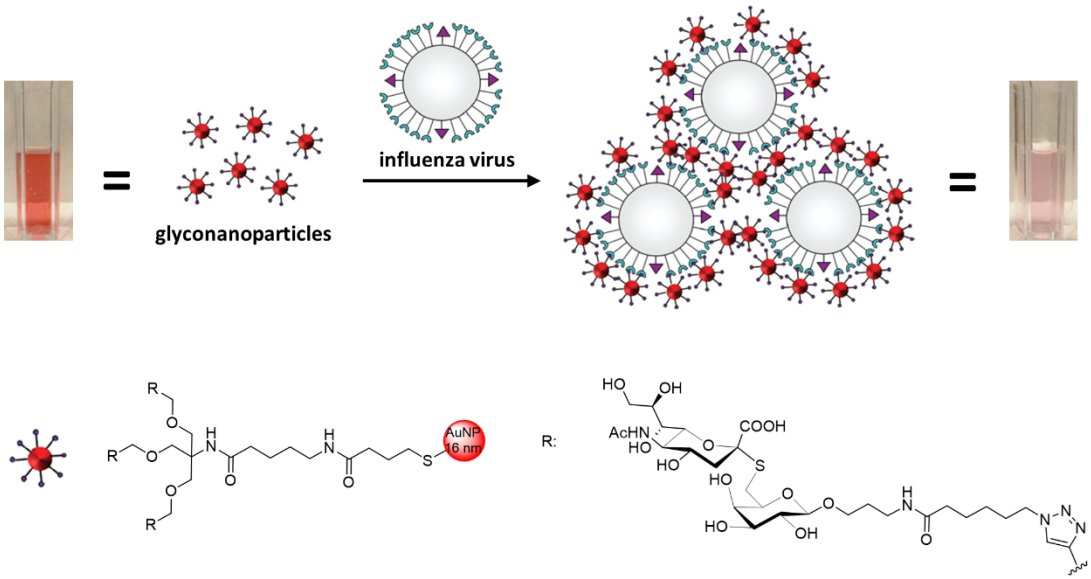

Figure 1.13. Schematic representation of aggregation of trivalent sialic acid-functionalised gAuNPs for the detection of influenza virus. Adapted from Marín *et al.*[47] with permission from the Royal Society of Chemistry.

Authors have designed gAuNPs in different ways and with different sorts of tethers, for the detection of biologically relevant targets. The use of thiolated ligands is a pivotal methodology for the functionalisation of AuNPs. In many works, thiolated glycosides are directly used for the functionalisation of the gold surface, although thiolated alkynes or activated esters have also been used to synthesise pre-activated AuNPs that would be subsequently coupled to the glycoside decorated with a suitable reactive counterpart.

To mimic the presentation of sugars on the cell surface, a sphingolipid ceramide has been functionalised with galactose or lactose and derivatised with a disulfide group for their installation on the surface of 20 nm AuNPs (**Figure 1.14**).[49] The aggregation assay was applied for the detection of the phytotoxin ricin from *Ricinus communis* and its less toxic variant, *R. communis* agglutinin 120 (RCA_{120}, described in *Section 1.3.1.*). The addition of the agglutinin to a solution of either galactose- or lactose-functionalised AuNPs induced a rapid blue-shift of the colour of the nanoparticle suspension, which was reverted upon the addition of an excess of free lactose. The assay worked in a range of 28-55 nM of RCA_{120}, although, interestingly,

ricin only interacted with the lactose-ceramide-functionalised AuNPs, and not with the galactose-ceramide ones.

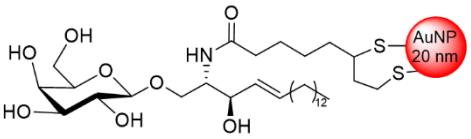

Figure 1.14. Representation of 20 nm gAuNPs functionalised with a thiolated galactosyl ceramide by Uzawa *et al.*[49] for the detection of the phytotoxin ricin.

With the aim of developing a system to detect ricin, thiolated galactosides have been synthesised and installed on the surface of *ca.* 16 nm AuNPs (**Figure 1.15**).[50] The authors performed a systematic study to evaluate the effect of the density of the glycans on the surface of the particles. It was found that a galactoside ligand-PEG ratio of 70:30 was optimal for the detection assay. The developed system reached a LOD of 7 nM, with a linear range between 0-100 nM.

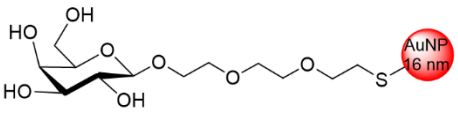

Figure 1.15. Representation of 16 nm gAuNPs functionalised with a thiol-ending PEGylated galactoside by Schofield *et al.*[50] for the detection of the phytotoxin ricin.

Another toxin that has attracted considerable attention in the field of diagnostics is cholera toxin (CT) from *Vibrio cholerae*. Once inside the intestine, the B subunit of the toxin (CTB) binds to the GM1 ganglioside containing a pentasaccharide containing terminal sialyl-galactose units. It was found that galactose alone could mimic this receptor,[51] thus lactose-derivatised AuNPs were synthesised, allowing to detect the presence of this toxin through the aggregation of the nanoparticles, causing a redshift of the plasmon resonance absorption band (**Figure 1.16**).[52]

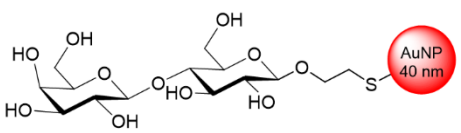

Figure 1.16. Representation of 40 nm gAuNPs functionalised with a thiolated lactoside by Schofield *et al.*[52] mimicking the Galβ(1-3)GalNAcβ(1-4)[Neu5Acα(2-3)]Galβ(1-4)Glc-lipid receptor at the GM1 ganglioside.

A later work reported the synthesis of *ca.* 16 nm AuNPs bearing sialic acids for the detection of SIGLECs (sialic acid-binding lectins which are overexpressed in cancer cells).[53] To validate the interaction between monovalent siglecs, these were crosslinked using antibodies to allow the formation of divalent targets that caused aggregation of the sialic acid-functionalised AuNPs. Aiming at proving the potential to investigate the cellular distribution and biological roles of SIGLECs, these lectins were overexpressed in Chinese hamster ovary cells and the binding of the gAuNPs was observed through TEM. Also in the field of cancer research, a 2-3 nm gAuNPs system dually functionalised with lactose as a targeting agent and phthalocyanine as a photosensitiser was developed (**Figure 1.17**).[54] The gAuNPs successfully interacted with the galactoside-binding galectin, whose over-expression is typically related to cancer.[55] The system was applied to breast cancer cells, showing that the presence of lactose favoured the accumulation of gAuNPs on the surface of the cells, and also that a shorter linker (C3 as opposed to C11) between the photosensitiser and the gAuNPs was also preferred in this system.

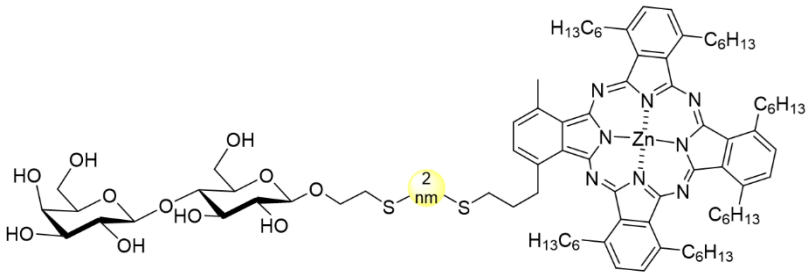

Figure 1.17. Representation of 2 nm gAuNPs dually functionalised with a thiolated lactoside and the photosensitiser phthalocyanine by Garcia-Calavia *et al.*[54] for the treatment of breast cancer cells.

The impact of the length of thiolated glycosides for the detection of fimbriae adhesins such as the mannose-binding FimH from *E. coli* has been studied (**Figure 1.18**).[42] Particles functionalised with thioglucose were able to detect ConA through SPR shift and a visual colour change induced by aggregation of the particles, however they presented low saline stability, resulting in false positives due to aggregation (NaCl concentrations tested 0 – 1 M, although it was not specified at which point the nanoparticles aggregated). To overcome this problem, a thiolated PEG-3k was clicked to the glycosides, further stabilising the particles to prevent them from aggregating at higher NaCl concentrations. The assay successfully allowed to distinguish between two standard strains of *E. coli*: the FimH+ K-12, and the FimH- TOP10.

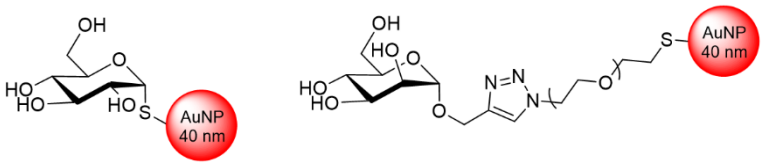

Figure 1.18. Representation of 40 nm gAuNPs functionalised with either thioglycosides or a thiol-ending PEGylated glycoside by Richards *et al.*[42] for the detection of ConA and two strains of *E. coli.*

A more elaborated thiol-ending glycopolymer has also been synthesised through reversible addition-fragmentation chain transfer (RAFT) polymerisation and subsequent reductive amination to install sialic acids targeting influenza virus (**Figure 1.19**).[56] The 100:25 copolymer of HPMA (*N*-2-hydroxypropyl methacrylamide) and APMA (*N*-3-aminopropyl methacrylamide) allowed the installation of nearly 25 units of sialic acid per polymer. The polymer was linked to the surface of *ca*. 20 nm AuNPs through the thiol, and the interaction with influenza virus was monitored *via* TEM and dynamic light scattering (DLS). A control was performed with the lactose-functionalised AuNPs, which did not show interaction with the virus, verifying that the interaction observed with the sialylated AuNPs was specific.

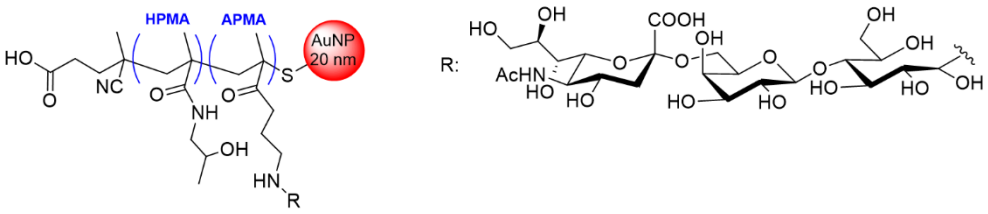

Figure 1.19. Representation of 20 nm gAuNPs functionalised with a sialylated polymer synthesised through RAFT polymerisation by Zhang *et al.*[56] for the detection of influenza virus.

A key feature of the reports discussed above is the cluster glycoside effect described in *Section 1.1.1*, highly related to the multivalency of the particles. Imberty and collaborators have contributed substantially to better understand the importance of multivalency in glycan-mediated interactions. A collection of galactosylated 1-2 nm AuNPs was synthesised with galactose loadings ranging from 17-90% using a thiolated glucoside to dilute the galactoside on the particle surface (**Figure 1.20A**).[57] The sugar density was estimated by ^{1}H-NMR and confirmed by elemental analysis, correlating the loading with the sugar valency of the gAuNPs, which ranged from 12 to 67 glycans per particle. The avidity of these gAuNPs for the galactose-binding LecA (for the binding specificities of the lectin, refer to *Section 1.3.3.*) was studied by

SPR and ITC, with the expected discrepancies depending on the type of assay used (*i.e.*, surface-bound as opposed to in solution). However, both techniques converged to similar K_D values in the nanomolar range. More examples of multivalent inhibitors of LecA, specifically galactose dimers, are discussed in *Chapter 4.* In a follow-up work, the group employed analogous gAuNPs functionalised with mannose targeting the lectin BC2L-A from another opportunistic pathogen, *Burkholderia cenocepacia*.[58] The gAuNPs were evaluated similarly through SPR and ITC, with similar results and K_Ds again in the nanomolar range.

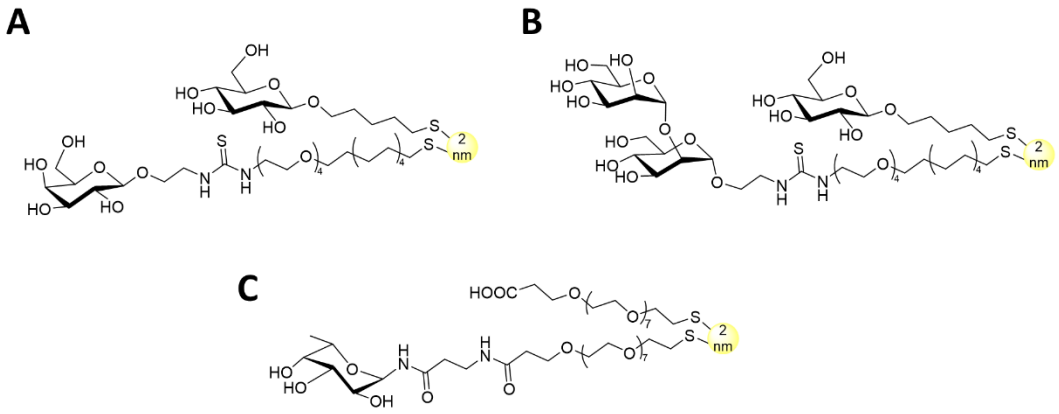

Figure 1.20. Representation of 2 nm gAuNPs functionalised with thiolated glycosides in different ratios to modulate the carbohydrate density by (**A**) Reynolds *et al*.,[57] (**B**) Chiodo *et al.*[59] and (**C**) Arosio *et al*.[60]

A later publication of the group developed an ELISA assay based on mannosylated and galactosylated gAuNPs (**Figure 1.20B**).[59] The assay was established with the detection of anti-HIV antibodies, which are reported to bind to high mannose clusters on the surface of the virus.[61] The protocol followed was analogous to other ELLAs discussed before, and consisted in the coating of a 96-well plates with functionalised gAuNPs followed by incubation with the protein of interest. The proteins were detected with HRP-functionalised antibodies, and the assay reported a 3000-fold higher sensitivity than the one found in other antibody-based assays. With the system in place, the method was preliminarily applied to the detection of the HIV receptor DC-SIGN with successful results. In a follow-up work, the detection of that lectin was achieved with fucosylated gAuNPs following a similar strategy (**Figure 1.20C**).[60] The system was taken further, attempting to block viral infection using fluorescently labelled beads functionalised with the HIV protein gp120 as a mimic of the virus, and DC-SIGN-expressing mice cells as a host. The gAuNPs successfully blocked the interaction of the HIV

mimic with the host, and they were found to trigger a fucose loading-dependent gAuNPs internalisation.

Another type of mannose-functionalised 5 nm AuNPs have been developed more recently to block the HIV infection-related DC-SIGN/R lectins.[62] In the reported assay, four different ligands were prepared: a single mannoside, a single Man-α(1,2)-Man, a trimeric mannoside, and a trimeric Man-α(1,2)-Man (**Figure 1.21**). The four gAuNPs successfully interacted with fluorescently labelled DC-SIGN/R, leading to nanosurface energy transfer (NSET) and quenching the fluorescence of the lectin at higher rates and from longer distances than the more widely used Förster resonance energy transfer (FRET). A mathematical analysis of the quenching efficiency led to the calculation of the apparent binding constant, showing how the trimeric ligands exhibited K_Ds up to 4 times lower than the ones of monovalent ligands.

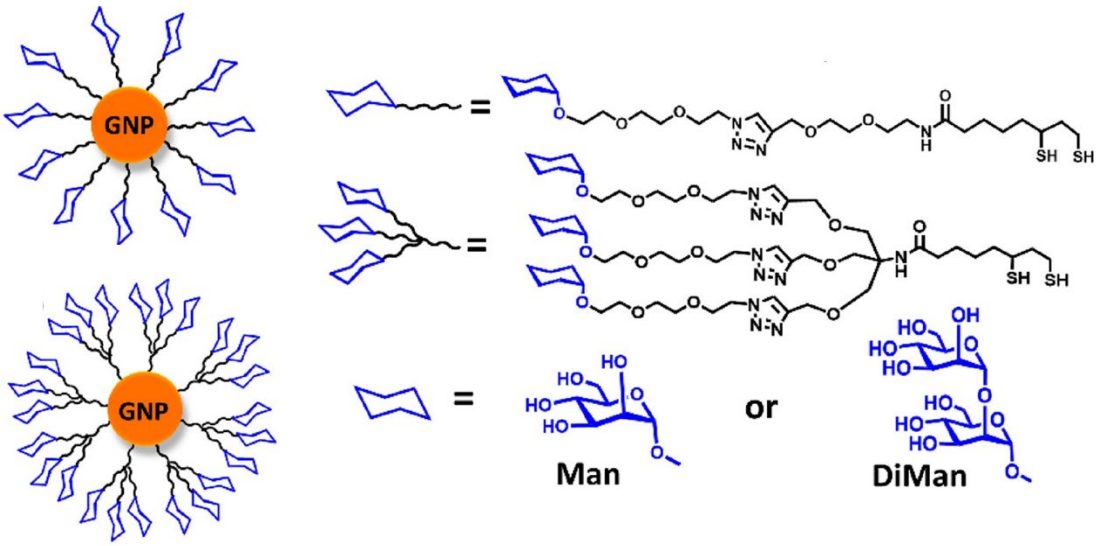

Figure 1.21. Representation of 5 nm gAuNPs functionalised with thiolated mannosides and di-mannosides, in monomeric and trimeric fashions for the interaction with DC-SIGN/R lectins. Reproduced from Scanian *et al.*[62] (CC-BY).

Even though the thiol-gold interaction is a widely used methodology for the functionalisation of gAuNPs, it is not the only one. Similarly to the formation process of the fucoidan-based gAuNPs described above, the fluorescent self-assembled polymer glyco(bis) acrylamide can act as a reducing agent to form *ca.* 10 nm gAuNPs (**Figure 1.22A**) which quench the fluorescence.[63] The developed assay informed a ConA detection system based on restoring the quenched fluorescence of glyco(bis) acrylamide upon the subtraction of glycan moieties by the lectin. This system allowed a LOD of 1.6 nM, with a 0 – 600 nM linear range. Another

common AuNP functionalisation methodology is the passive adsorption of proteins onto the gold surface due to electrostatic interactions arising between the negatively-charged metal surface, and the positively-charged protein.[64] However, this methodology has been mostly reported for the installation of antibodies on the surface of AuNPs (**Figure 1.22B**).[65] Up to date, only a few reports about the passive adsorption of neoglycoproteins on the surface of AuNPs are available. A methodology was developed to evaluate the glycosylation pattern of proteins through their passive adsorption on AuNPs (**Figure 1.22C**) and subsequent assessment of lectin-binding proteins.[66] That constituted a proof-of-concept work in which the presence of Man and GlcNAc was confirmed in RNase B and rituximab, respectively, through DLS.

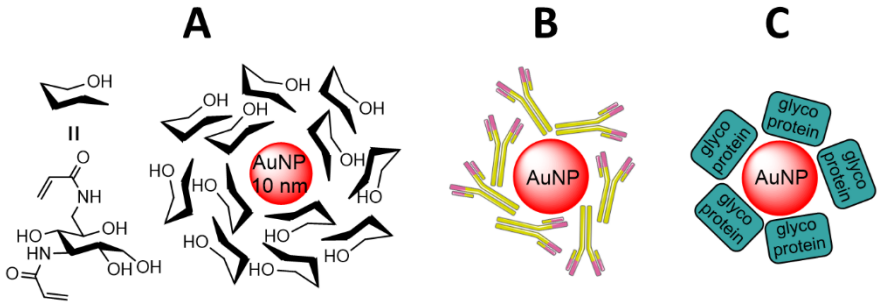

Figure 1.22. Alternative methodologies to the use of thiolated ligands for the synthesis of functionalised AuNPs, including (**A**) one-pot synthesis with an electron-donating fluorescent Glc(bis)polyacrylamide,[63] (**B**) classical passive adsorption of antibodies[65] or (**C**) less explored passive adsorption of neoglycoproteins.[66]

Recently, a more elaborated methodology was published for the development of a glycoprotein-based gAuNP system for the detection of Shiga toxins from *Shigella dysenteriae*.[67] A novel *N*-glycosyltransferase discovered in the cell cytoplasm was employed for the installation of globotriose on up to 15 asparagine sites of its substrate protein DANYTK. The glycoprotein was passively adsorbed on the surface of *ca.* 25 nm shell@core Au@FePor-TFPA-COP (iron porphyrin tris(4-formylphenyl)amine covalent organic polymer). These gAuNPs were successfully implemented in an ELISA where the toxin was firstly bound to the wells of a 96-well plate. After appropriate washings and the addition of the globotriose-functionalise gAuNPs, the addition of tetramethylbenzidine (TMB) and hydrogen peroxide triggered a peroxidase reaction catalysed by the iron porphyrin from the AuNP core. After 30 minutes of incubation, a blue colouration and measurement of the absorbance at 652 nm allowed the detection of the toxin, with a LOD of 7 ng/mL (0.1 nM) and a linear range of 0.1 ng/mL – 100 µg/mL (1 pM to 1.5 µM).

As it will be described in *Chapter 2*, bovine serum albumin (BSA) exhibits advantages as a carrier protein and has been widely used to prepare different glycoconjugates, most of them towards the development of vaccines. Even though the methodology for simple conjugation of proteins on the surface of AuNPs has already been published, gAuNPs bearing BSA glycoconjugates have not been reported up to date. The results reported in *Chapter 2* explore the easy and reproducible bioconjugation of BSA neoglycoconjugates on the surface of *ca.* 40 nm AuNPs.

Fluorescent glyconanoparticles in detection systems

Very small semiconductor nanoparticles, known as quantum dots (QDs) have been used for imaging purposes due to their exceptional fluorescent properties. CdS QDs were functionalised with a thiol-ending PEGylated mannoside targeting the FimH on the surface of the *E. coli*.[68] The incubation of different concentrations of the pathogen with the glyco-QDs (gQDs) led to bacterial aggregation that was observed through fluorescence confocal microscopy (**Figure 1.23**)

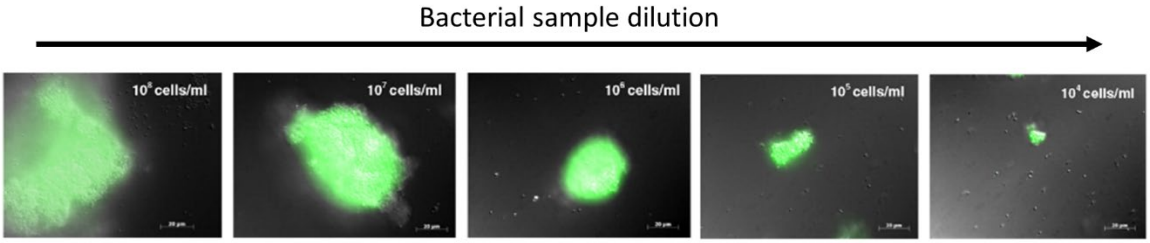

Figure 1.23. Confocal microscopy images of *E. coli* samples aggregated upon incubation with mannosylated QDs. (**A-E**): serial dilutions of the cellular samples. Adapted from Mukhopadhyay *et al*.[68] with permission from Elsevier.

Many assays in the field of detection and diagnostics take advantage of the phenomenon of fluorescence. Even though AuNPs are not inherently fluorescent, some gAuNP-based studies have included fluorophores or QDs to benefit from their properties. The combination of AuNPs with certain fluorescence-emitting species leads to quenching processes known as FRET. This effect has been exploited in switch-on (**Figure 1.24A**) or switch-off (**Figure 1.24B**) assays for the detection of proteins and pathogens.

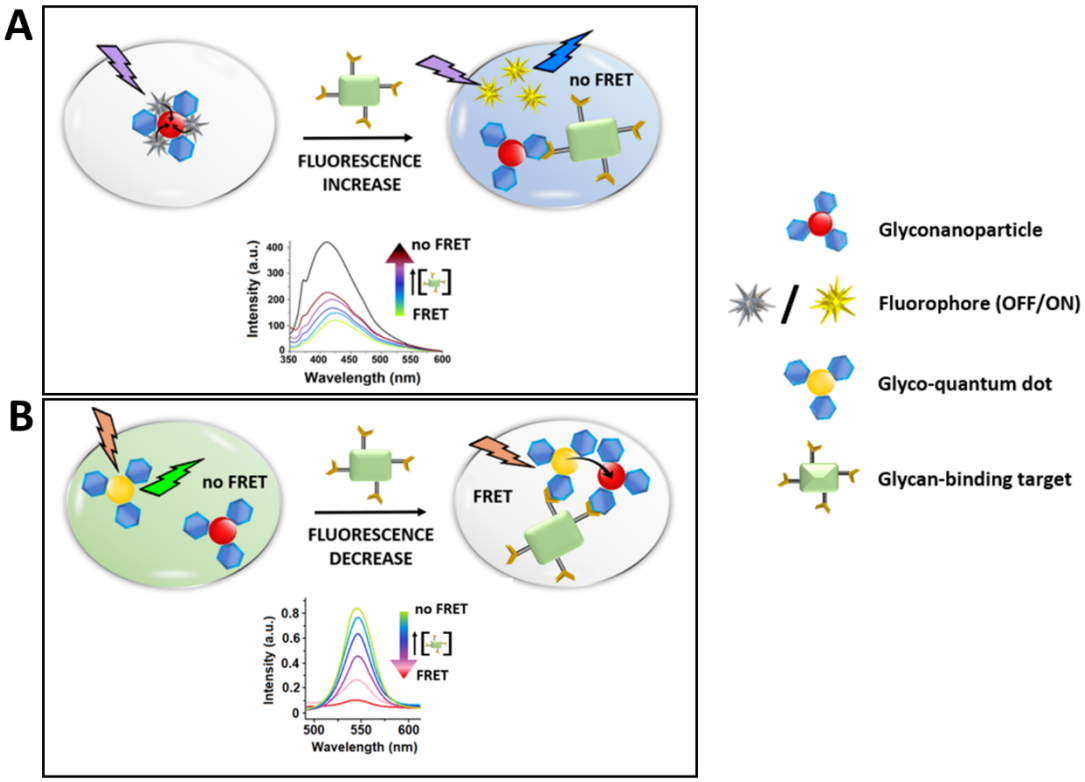

Figure 1.24. (**A**) The FRET effect causes fluorescence quenching upon attachment of a fluorophore to a gAuNPs. The fluorescence is activated due to the displacement of the fluorophore in the presence of the glycan-binding target. (**B**) gQDs can be used as fluorophores together with gAuNPs. In the presence of the glycan-binding target, the crosslinking of gQDs and gAuNPs leads to fluorescence quenching. Adapted from Hernando *et al*.[45] (CC-BY).

An example of a fluorescence switch-on bioassay for the detection of CTB was designed using galactose-functionalised AuNPs and amine-functionalised QDs.[69] The formation of hydrogen bonds between the amines on the QDs and the hydroxyl groups of galactose-AuNPs allowed proximity between donor and acceptor, leading to fluorescence quenching of the QDs. However, in the presence of CTB, hydrogen bonds were disrupted and the amine-QDs were released, activating their fluorescence. Glycoacrylamides have been reported as fluorescent polymers due to the π interactions upon aggregation.[70] Poly(Glc-bis(acrylamide))-functionalised 10 nm AuNPs were synthesised *in situ* by polymerising the fluorescent sugar in presence of $HAuCl_4$ at basic pH. The glycoacrylamides-AuNPs aggregate did not exhibit fluorescence, but in the presence of a glucose-binding target the Glc-bis-AuNP aggregate is disrupted, and the fluorescence is reactivated (**Figure 1.25**).

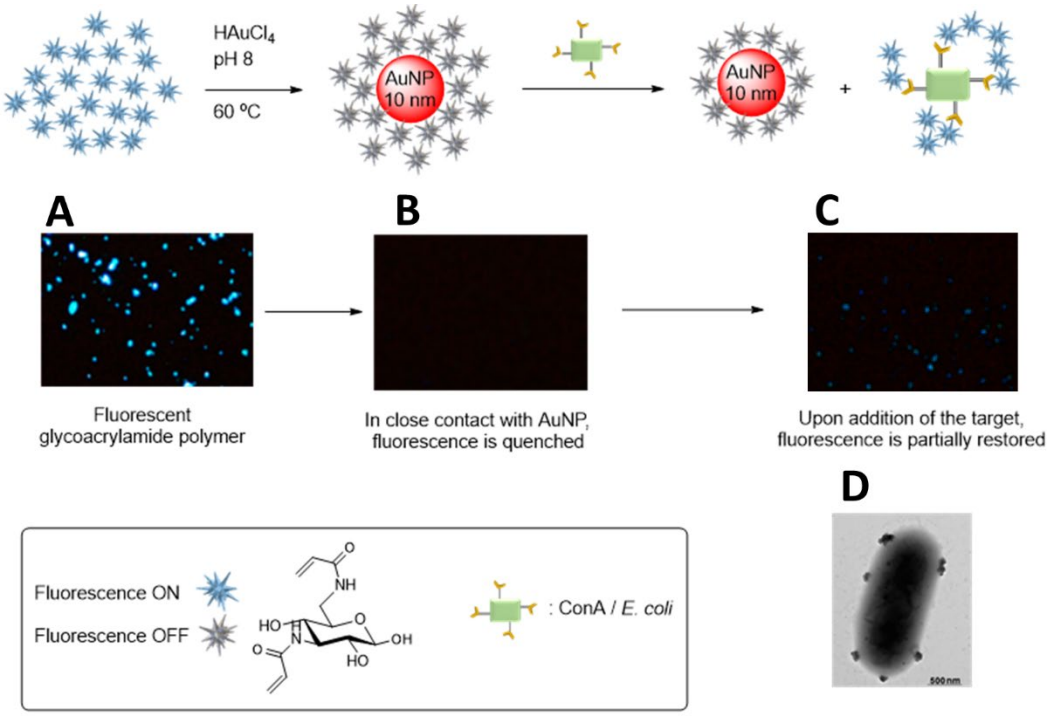

Figure 1.25. (**A**) Poly(Glc-bis(acrylamide)) presents fluorescence but (**B**) upon functionalisation of 10 nm AuNPs, the emission is quenched. (**C**) In the presence of either ConA or *E. coli*, the polymer is partially displaced from the surface of the AuNP and the fluorescence is partially restored. (**D**) TEM image showing aggregation of the glycoacrylamide polymer on the surface of *E. coli.* Figure adapted from Hernando *et al*.[45] (CC-BY).

The lectins LecA and LecB from *P. aeruginosa* have also been targeted with gAuNPs. An approach based on click chemistry between azide-functionalised glycosides and alkyne-activated *ca*. 40 nm AuNPs has been developed to treat *P. aeruginosa* biofilms.[71] The particles were firstly activated with a thiolated cyclooctyne moiety, that was subsequently coupled with an azide-ending PEGylated galactoside or fucoside, targeting the pathogen's lectins LecA and LecB, respectively. Not only the particles successfully interacted with the pathogen, but they could also encapsulate the photosensitiser ceftazidime to evaluate the eradication properties of the system against biofilm through photodynamic therapy upon irradiation at 600 nm. With a strategy similar to the work of Scanian *et al.*[62] discussed above (see **Figure 1.21**), a FRET approach was reported in an assay combining mannose-functionalised ZnS/CdSe 5 nm QDs and 13 nm AuNPs.[72] Both kinds of particles were functionalised with a PEGylated mannoside to develop a fluorescence switch-off bioassay designed for the detection of the plant lectin ConA. In the absence of the targeted lectin, a suspension containing Man-AuNPs and Man-QDs exhibited fluorescence. However, in the presence of ConA, the fluorescence of the QDs

was quenched upon clustering between the AuNPs due to their binding with the lectin. Very recently, a mannosylated gQDs system targeting the DC-SIGN/R lectins has been published (**Figure 1.26**).[73] The di-Man-functionalised QDs successfully interacted with the protein and, upon the association, the QDs would suffer the FRET effect, observing a drop in fluorescence intensity. However, the energy was not lost but transferred to a dye previously conjugated to the lectin (Atto-594), becoming fluorescent emitting at a non-overlapping wavelength with the fluorescence of the QDs. Upon dissociation, the dye would become non-fluorescent, whereas the QDs would recover the lost fluorescence. The reported system allowed to study the kinetics of the gQDs-lectin interaction.

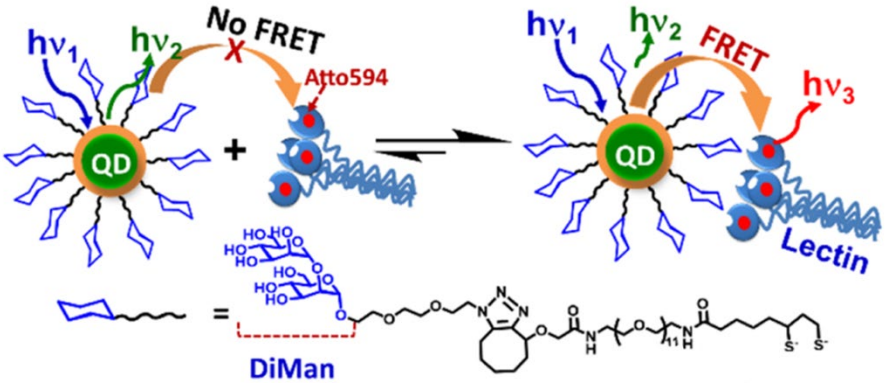

Figure 1.26. Representation of the dually fluorescent system based on diMan-QDs developed to target DC-SIGN/R lectins. Adapted from Hooper *et al*.[73] (CC-BY).

1.2.6. Biolayer interferometry

Following on surface-bound biomolecules to quantify their interactions with analytes, biolayer interferometry (BLI) is among the most sensitive techniques, allowing the use of very small amounts of material.[74] BLI measures the interference pattern of reflected white light incident on a fibre optic biosensor tip (**Figure 1.27**). The surface of the biosensors is pre-activated (often with streptavidin or with NHS esters) and coated with the ligand of interest (loading). This allows to measure the baseline before dipping the tip in a solution of the analyte, which binds to the ligand-coated biosensor. The changes in thickness on the biosensors cause a shift in the interference pattern, allowing to study the association process. This is followed by a washing step to allow the dissociation of the ligand-analyte conjugate. BLI is, like ELLA, a high-throughput technique, typically allowing the measurement of 8 samples in parallel, and the automatization of 96-well plates (similarly to SPR). This technique provides a thermodynamic

study of protein-ligand interactions with quantity requirements up to ten times smaller than ITC, although with a lower sensitivity (K_Ds in the millimolar to the nanomolar range). Given that the readout of BLI is dependent on the actual size of the ligands and analytes, it is often used to quantify the binding of proteins to macromolecules such as glycoproteins and lectins, rather than single (poly)saccharide molecules.

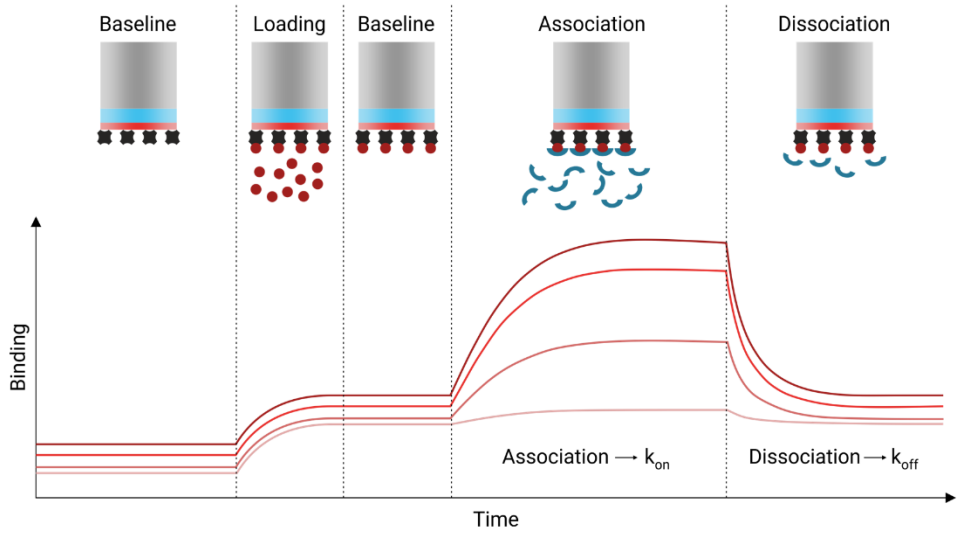

Figure 1.27. Scheme of a typical BLI experiment to investigate the interaction between an analyte in solution and a biomolecule immobilised on a fibre optic biosensor. The increased thickness of the sensor translates into a shift of wavelengths of incident white lite, leading to a different interference pattern. Adapted from 2Bind Molecular Interactions®.

BLI is a relatively newer technique, since the release of the Octet by ForteBio (USA) in 2005. As opposed to other techniques such as ELLA or SPR, fewer BLI glycoarrays have been published up to date, with no one covering ConA. However, a report was published to evaluate galactosylation levels on samples of antitumor necrosis factor immunoglobulins produced on large scales, as quality control during the production of antibodies (**Figure 1.28**).[75] To investigate the presence of the galactose residues, biotinylated RCA_{120} was bound to a streptavidin-coated sensor and dipped in a solution of the antibodies. A first attempt to study the antibodies in their native form failed to show any interaction with the BLI sensor. To ensure that the oligosaccharides were accessible by the sensor, the antibodies were treated with mercaptoethanol and iodoacetamide to reduce the disulfide bonds, causing the unfolding of the proteins. The experiment successfully detected the presence of galactose moieties in the antibodies, with a linear dose response.

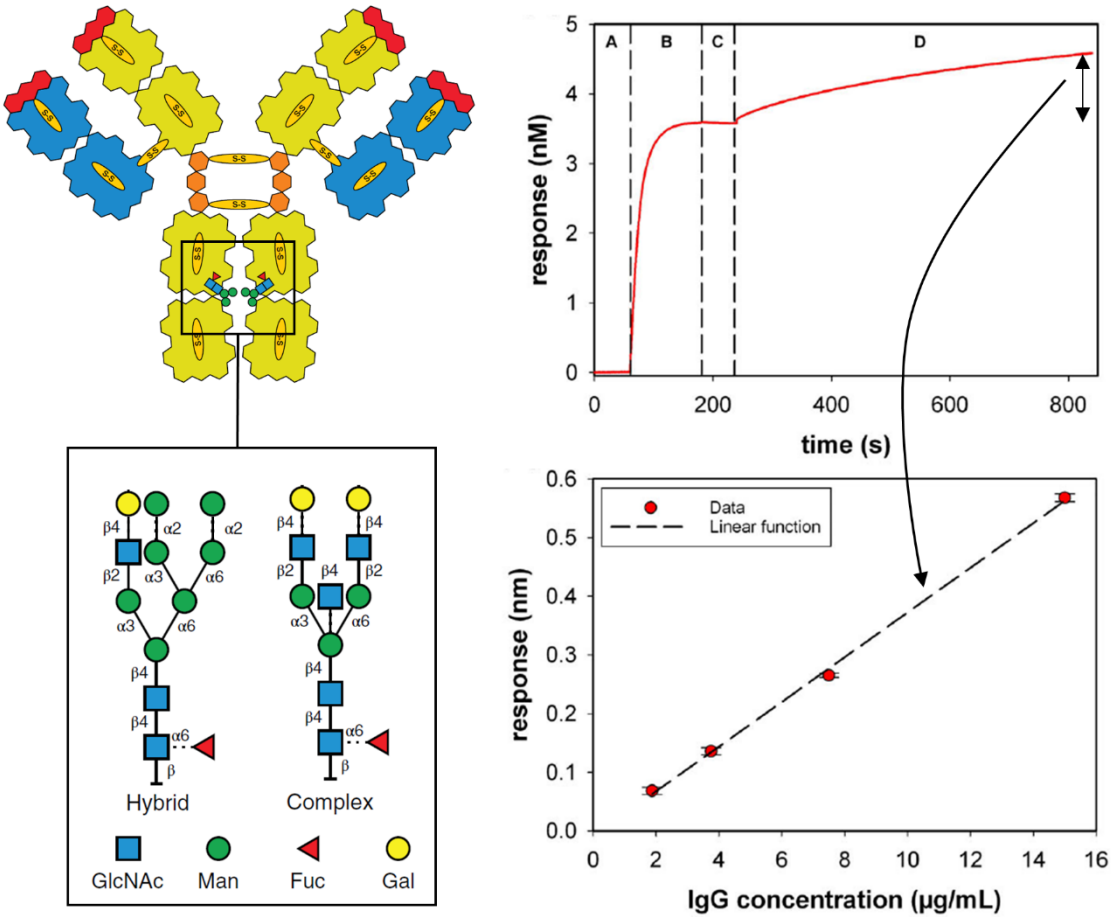

Figure 1.28. Investigation of the glycosylation pattern of antitumor antibodies through BLI. To detect the presence of terminal galactose residues, biotinylated RCA_{120} was bound to a streptavidin-coated sensor. Recombinant antibodies were assayed at different concentrations, showing a linear dose-response. Adapted from Wallner *et al.*[75] (CC-BY-NC).

1.2.7. Thermal shift assay

An alternative approach to measure the interaction between a protein ligand and an analyte is to quantify the stabilisation effect of such interaction on the protein through a thermal shift assay (TSA) (**Figure 1.29**).[76] Although dedicated instruments are available, this technique can be performed in most real-time polymerase chain reaction (rtPCR) thermocyclers that allow to progressively increase the temperature until the proteins in the sample are denatured and therefore unfolded. This technique typically involves the addition of an environment-sensitive dye such as Spyro orange, which presents an enhancement of fluorescence upon attachment to the hydrophobic pockets of the unfolded protein. The maximum of fluorescence intensity over the temperature gradient marks the melting point of the protein (T_m), which is often increased due to the intramolecular forces occurring in the presence of an analyte interacting

with the binding site. In contrast with ITC, TSA requires smaller amounts, potentially micrograms or sub-micrograms. This technique is somehow comparable to ELLA as quantities of reagents and assay time required are similar, although ELLA requires the fluorescent labelling of the ligands added to the coated well, which is not needed in TSA. More importantly, this is a high-throughput technique, as it is often performed in 96-well plates and large libraries of compounds can be measured in roughly the same amount of time required to assay one sample through ITC. However, this technique will not provide a full thermodynamic study as ITC does, although quantitation of the binding intensity has been proved possible through a titration experiment, studying the variation in T_m at different concentrations of the analyte.[77] This technique is a very good candidate for the preliminary screening of large libraries, before in-depth study with other techniques such as ITC. The combination of both would allow the study of protein-ligand interactions in solution.

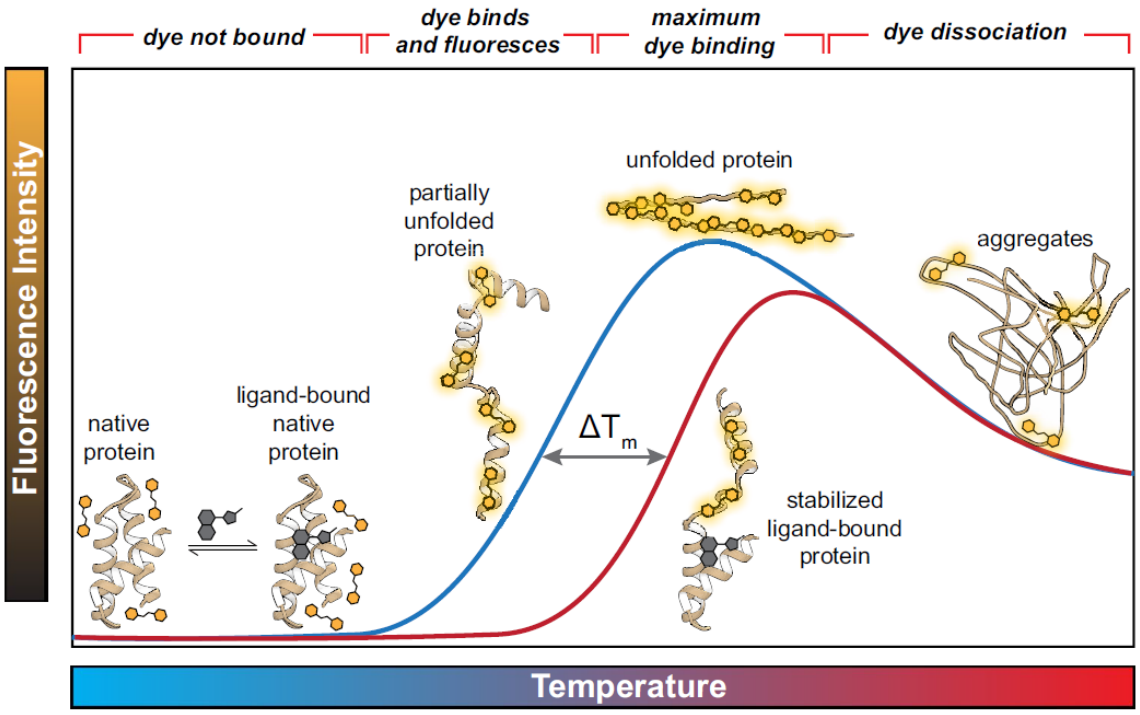

Figure 1.29. Schematic representation of a typical TSA experiment to investigate the interaction between a protein and an analyte in solution. The progressive increase in temperature causes protein denaturation, which unfolds to exhibit hydrophobic pockets that interact with an environment-sensitive fluorescent dye (**blue**). The presence of a protein binder causes stabilisation of the structure, leading to denaturation at higher temperatures (**red**). Reproduced from Samuel *et al.*[76] (CC-BY).

TSA is perhaps the least explored technique in the field of Glycoscience, given that its main use is to investigate protein stabilisation instead of quantification of binding as such. However,

a proof-of-concept work was published very recently on the use of this technique to quantify the binding of maltose and maltotriose to the *Escherichia coli* maltose-binding protein (**Figure 1.30**).[78] Spyro dye was used during the assay to observe fluorescence upon unfolding of the protein. The unfolding temperature T_m of the native protein was 43 °C which increased to 45 °C in presence of 1 µM of maltose and progressively to 53 °C with 1 mM. Interestingly, the experiment could distinguish two sets of T_m values with their respective shifts, one starting at 43 °C and the other at 54 °C. This is potentially due to the partial and total unfolding of the protein, although this was not discussed in the publication.

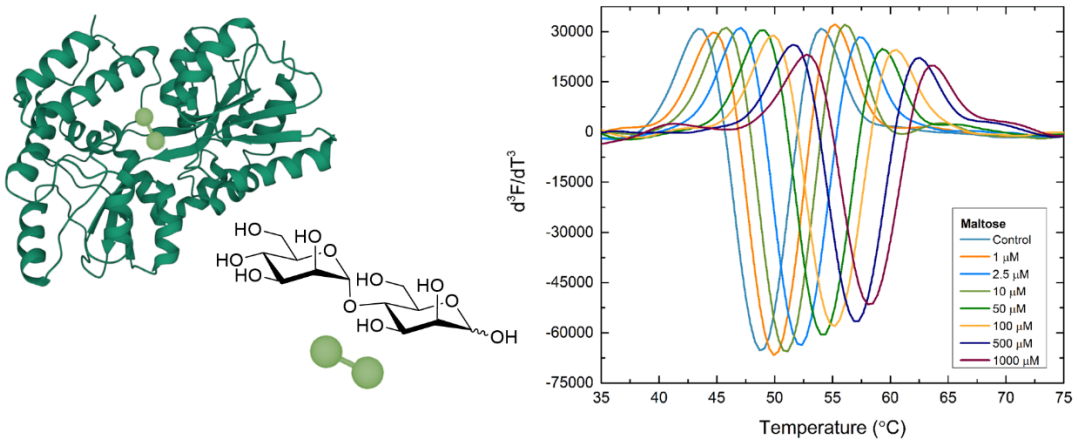

Figure 1.30. Investigation of the stabilisation of the *E. coli* maltose-binding protein through TSA. Two sets of melting temperatures were observed for the maltose binding protein (PDB 1MPD), with their related shifts upon interaction with increasing concentrations of maltose. Adapted from Bhayani *et al.*[78] (CC-BY).

1.3. Lectins of study

1.3.1. Targeted lectin: *Ricinus communis* agglutinin 120 (RCA_{120})

A major focus of this research work is the development of a sensitive and selective detection assay for RCA_{120}. Not only as a proof-of-concept work, but the development of a detection system for RCA_{120} is also of biological relevance given its relationship with the lethal ricin toxin form *R. communis*, which has been reported to have a lethal dose of 20 mg/kg in humans.[79] Ricin is a ribosome-inactivating 60 kDa protein composed of two subunits, RTA and RTB, both linked through a disulphide bond (**Figure 1.31**).[80] This toxin has attracted interest in the field of diagnostics due to its potential as a warfare agent.[81] The mechanism of action of ricin has

been widely studied and it starts with the binding of RTB to terminal galactoside residues on cell membranes.[82] Upon endocytosis, the RTA-RTB dimer is degraded by a protein disulphide isomerase which allows RTA to reach and attach to 28S ribosomal RNA, hindering protein elongation.[83]

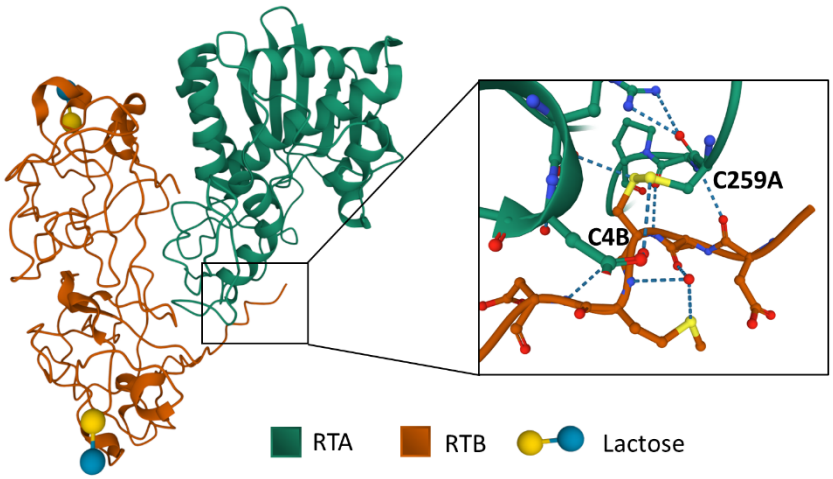

Figure 1.31. Structure of ricin co-crystallised with lactose (PDB 2AAI), expanding on the disulphide bond linking RTA and RTB chains between the cysteine-259 (chain A) and cysteine-4 (chain B) residues.[80]

Given its lower toxicity, RCA_{120} has been extensively employed instead of ricin for research purposes. RCA_{120} is a dimer of ricin-like units (RCA_{60}) with divalent galactose-binding activity, as a result of a tyrosine-to-histidine-248 mutation in the binding pocket of ricin.[84,85] With homology rates ranging from 80-90% between both proteins, it has been found that ricin-binding ligands tend to interact with RCA_{120} too and vice-versa.[86]

Different arrays have proven the binding specificity of this lectin over the last 40 years. A set of branched glycopeptides exhibiting terminal Gal, GalNAc and Neu5Ac moieties was assayed against both RCA_{60} and RCA_{120}, probing the binding to Galβ-(1,3)-GlcNAc and the decrease of interaction upon the addition of terminal Neu5Ac residues.[87] The assay used consisted in the precipitation of iodinated glycopeptides bound to the lectins of interest to then measure the radioactivity of ^{125}I in a gamma counter. Soon after that, a lectin high-performance liquid chromatography (HPLC) was developed using RCA_{120}-bound silica columns in the so-called frontal affinity chromatography.[88] A set of di-branched Gal, Man and Neu5Ac-ending oligosaccharides were passed through the column to assess the retention time (RT), that can be correlated to the intensity to lectin binding. This type of assay was revised years later to

compare the specificity of RCA_{120} and *Erythrina* lectins towards 96 linear and branched oligosaccharides (**Figure 1.32A**).[89] The developed assay confirmed the results obtained before applying different fractions collected from the RCA_{120}-bound chromatography columns in an ELLA. The microarray allowed to investigate the range of lectins that would interact with each fraction of oligosaccharides (**Figure 1.32B**).

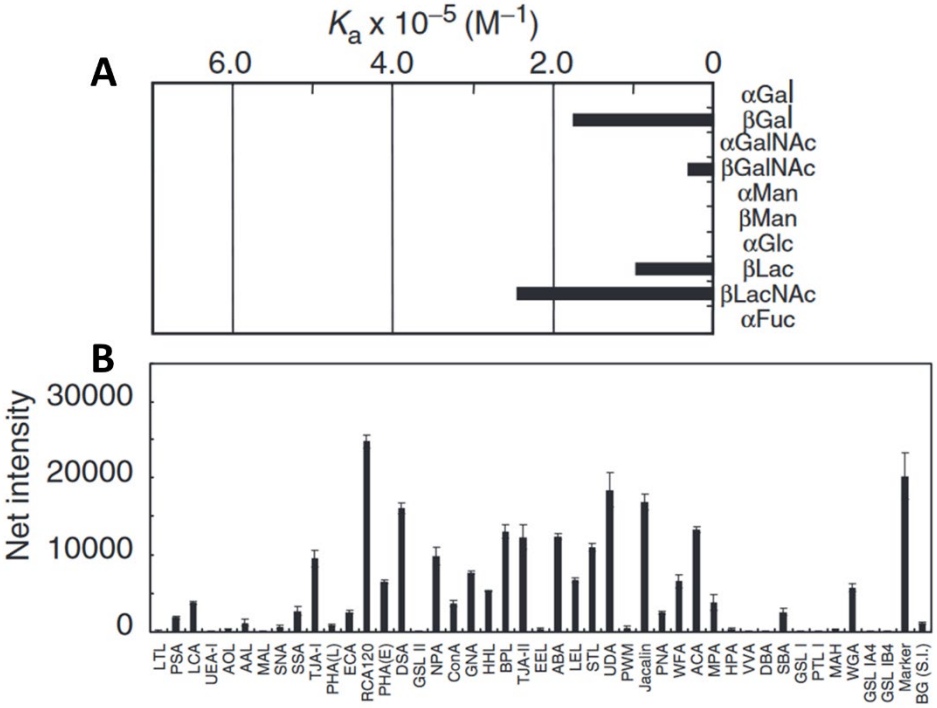

Figure 1.32. (**A**) Summary of the binding specificity of RCA_{120} investigated by HPLC using an RCA_{120}-agarose column. (**B**) Lectin microarray of one of the HPLC fractions to investigate the interaction with a range of lectins, including RCA_{120}. Adapted from Itakura *et al*.[89] with permission from Oxford University Press.

A library of 87 glycans containing Gal, GalNAc, Glc, GlcNAc, Man, Fuc and Neu5Ac moieties was screened in the form of BSA or polyacrylamide (PAA) glycoconjugates in an ELLA (**Figure 1.33**).[90] This assay helped profiling the specificity of RCA_{120} among other lectins, showing interaction with β-galactose residues but not with α-galactose, and with specificity for Galβ-(1,4) linkages over Galβ-(1,3). Modifications of LacNAc (Galβ-(1,4)-GlcNAc) in positions 2 or 3 with fucose or sialic acid hampered the binding.

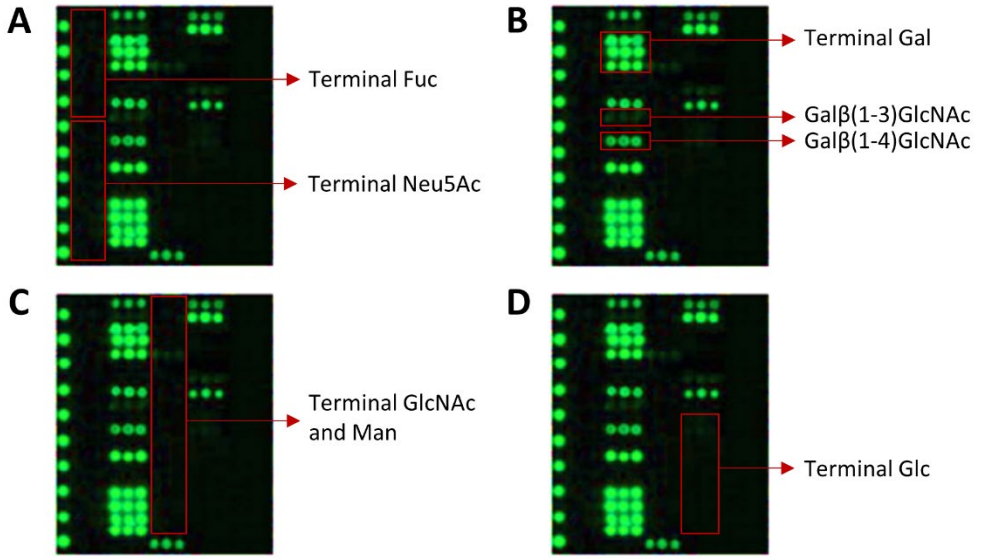

Figure 1.33. ELLA assay to investigate the specificity of RCA_{120} in terms of glycans and linkages. (**A**) Terminal fucose and sialic acid moieties inhibited the binding, whereas (**B**) terminal galactose would interact strongly with the lectin. However, the Gal-β(1,4)-GlcNAc linkage was preferred over β(1,3). (**C**) Terminal GlcNAc, and in many cases, the previous β(1,3) linkage would exhibit no interaction. Reproduced from Tateno *et al.*[90] with permission from Oxford University Press.

Those findings were confirmed soon after in different publication by Field and Russell, which assayed a collection of 40 biotinylated oligosaccharides containing similar moieties as before in an SPR glycoarray.[29] Having established the specificity of RCA_{120}, other variations in the structure of terminal galactose-exhibiting oligosaccharides have been attempted to study the effect of the interaction. A series of modified sulphated galactan (galactose oligomers) were assayed in an ELLA format.[91] The results obtained showed that sulphate substitution in the 4 position abolished the binding, although an enhancement was observed if the substitution was in the 2 or 6 positions. A later report attempted to find RCA_{120} binders among human milk oligosaccharides (HMOs).[92] BSA or glycine glycoconjugates were bound to gold chips to be assessed *via* SPR. This assay confirmed that only the core structure Galβ-(1,3)-GlcNAcβ-(1,3)-Galβ-(1,4)Glc would interact with the lectin, while fucosylation in many different positions would prevent the binding.

1.3.2. Control lectins

In this thesis, three lectins have been used as negative controls: *Ulex europaeus* agglutinin I (UEA I), wheat germ agglutinin (WGA) and ConA.

UEA I is a lectin isolated from gorse seeds which appears as a 110 KDa dimer of protomers consisting of two different subunits each.[93] This lectin has a reported affinity for L-fucose,[94] and more specifically for L-Fuc-α(1,2)-Gal terminus in oligosaccharides (**Table 1.1**).[95,96] UEA I has been employed in lectin microarrays, for example, the one showed in **Figure 1.32B** above.[89] However, to explore the affinity of UEA I for a wider variety of glycans, our group performed an ELLA assay whose results matched published data obtained with different techniques and complemented on the affinity for more sialylated and mannosylated oligosaccharides (data discussed in *Chapter 3*).

Table 1.1. Binding specificity of UEA I for different carbohydrates. Adapted from Allen *et al*.[96]

Carbohydrate	IC_{50} (mM)
p-Nitrophenyl β-D-fucopyranoside	>10
β-D-fucopyranosyl azide	>10
Methyl α-D-mannopyranoside	>10
D-Galactose	>10
Methyl 2-*O*-α-L-fucopyranosyl-β-D-galactospranoside	5
p-Nitrophenyl 3-*O*-β-L-fucopyranosyl-β-D-galactopyranoside	3
6-*N*-Trifluoroacetylaminohexyl-β-L-fucopyranoside	2.5
Benzyl 2-*O*-β-L-fucopyranosyl-β-D-galactopyranoside	2.5
β-L-Fucopyranosyl amine	2.5
L-Fucose	2.5
2-*O*-β-L-Fucopyranosyl-D-galactoside	1.25
p-nitrophenyl 3-*O*-α-L-fucopyranosyl-β-D-galactospyranoside	1

UEA I has been reported to allow discrimination of the fucose-ending Lewis a and the sialyl-ending Lewis x (**Figure 1.34**),[97] the latter being a tumour marker. The affinity of UEA I for fucosylated structures has proved useful for the imaging of carcinoma cells[98] and ovarian cancer cells.[99]

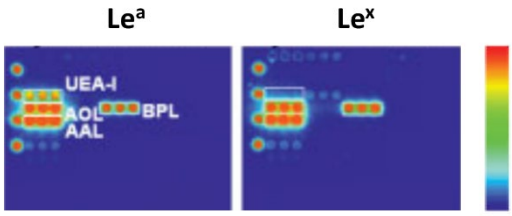

Figure 1.34. ELLA assay to discriminate between the fluorescently labelled Lewis antigens Le^a and Le^x, exhibiting terminal fucose and sialic acid, respectively. Adapted from Uchiyama *et al.*[97] with permission from John Wiley and Sons.

WGA is found in the seeds of *Triticum vulgaris*, appearing as a 36 KDa dimer with a reported affinity for Neu5Ac and GlcNAc (**Table 1.2**),[100] although the latter has been more widely explored in literature.[101,102] However, a later publication investigating the binding requirements of blood groups present on the surface of erythrocytes in an SPR lectin microarray found that WGA would only bind to linear oligosaccharides.[103] They observed that branched structures containing GlcNAc and Neu5Ac moieties would exhibit no interaction with the lectin. Given the biological importance of sialic acids in host-pathogen interactions,[104,105] this research will exploit the affinity of WGA for Neu5Ac.[106] As mentioned for UEA I, the specificity of WGA has not been widely explored in literature, the reason why the ELLA results obtained by Iceni Glycoscience will be commented on in *Chapter 3*.

Table 1.2. Binding specificity of WGA for different carbohydrates. Adapted from Mukhopadhyay *et al*. [100]

Carbohydrate	IC_{50} (nmol)
N-acetyl-D-galactosamine	810
N-acetylneuraminic acid methyl ester	600
N-acetylneuraminic acid	540
N-acetylneuraminyl methyl α-ketoside	540
N-acetylneuraminyl methyl β-ketoside	470
Sialyllactose (α2,3 and α2,6)	370
N-acetyl-D-glucosamine	160

A more commonly studied lectin is ConA, due to its readily availability in jack beans.[107] It is a tetramer of 26 KDa subunits,[108] although at neutral pHs the structure is organised in a dimer-tetramer equilibrium.[109] The affinity of ConA for high mannose structures was reported more

than thirty years ago through frontal affinity chromatography.[110] Soon after that, the groups of Oscarson and Toone reported the avidity of ConA for α-mannose terminal residues and to a lesser extent to α-glucose residues, with their hydroxyl groups in positions 3, 4 and 6 playing key roles in the interaction (**Figure 1.35**).[111,112] Those studies observed an enhancement of the interaction when increasing the valency of the mannoside using α3,6-mannotriose. The available literature reporting the effects of multivalency on the avidity of ligands for ConA is discussed in *Chapter 2*.

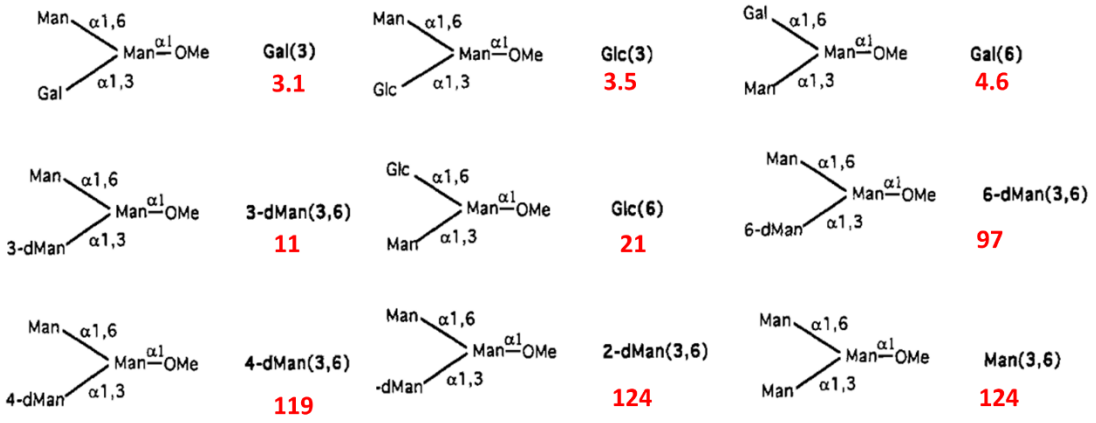

Figure 1.35. Structures tested by Mandal *et al.*[111] to assess the linkage specificity of ConA. In **red**, the relative binding potency compared with methyl α-mannoside measuring the IC_{50} value.

1.3.3. Case of study: Pseudomonas aeruginosa LecA

The growth of antimicrobial resistance species, combined with the profiles that different strains are developing, depict the biggest enemy to be defeated in the battle against infections.[113,114] The World Health Organisation identifies a particular interest in the research and development of new antibiotics for specific bacteria species, among which *Pseudomonas* is identified as a critical priority.[115] *P. aeruginosa* is a flagellate rod-shaped Gram-negative bacteria, which has the distinguished ability among Pseudomonas of growing at temperatures as high as 42 °C.[116] It is a major source of hospital-acquired infections, mainly affecting immunosuppressed patients and causing respiratory pathologies[117] and urinary tract infections,[118] being strongly related to cystic fibrosis and pneumonia.[119,120]

The agglutination of erythrocytes by proteins from the surface of *P. aeruginosa* has been studied for the past 50 years, probing the inhibition of such process in the presence of D-galactose.[121] Two lectins, LecA (PA-I) and LecB (PA-II), have been isolated from *P.*

aeruginosa,[122] and their involvement during the adhesion to respiratory epithelial human cells has been proven.[123] It has been reported that the interaction of the pathogen with the host occurs through glycosphingolipids,[124] where LecA binds preferentially to D-galactose residues, and LecB to L-fucose.[125,126] LecA has been specifically assayed against various glycosphingolipids of various polysaccharide lengths using iodinated lectin as staining agent on TLC plates.[127] Interestingly, although many of those glycosphingolipids included terminal β-galactose residues, only the ones containing polysaccharides with at least four glycan units exhibited binding (**Table 1.3**). Screening the free carbohydrates without the ceramide side showed that monosaccharides would bind to the lectin, probing that not only the glycan has to be present, but it also needs to be available, as the lipidic part of the macromolecules possibly hindered the interaction.

Table 1.3. Binding specificity of LecA for different glycosphingolipids. Reproduced from Lanne *et al*.[127] (++): tight binding, (+): normal binding, (–): no binding.

Carbohydrate	Binding
Gal-β-Cer	–
SO_3-3-Gal-β-Cer	–
Gal-β(1,4)-Glc-β-Cer	–
Neu5Ac-α(2,3)-Gal-β(1,4)-Glc-β-Cer	–
Gal-α(1,3)-Gal-β(1,4)-Glc-β-Cer	+
Gal-α(1,4)-Gal-β(1,4)-Glc-β-Cer	++
GalNAc-β(1,4)-Gal-β(1,4)-Glc-β-Cer	–
Gal-β(1,3)-GalNAc-β(1,4)-Neu5Ac-α(2,3)Gal-β(1,4)-Glc-β-Cer	–
Gal-β(1,3)-GalNAc-β(1,4)-Gal-β(1,4)-Glc-β-Cer	–
GalNAc-β(1,3)-Gal-α(1,4)-Gal-β(1,4)-Glc-β-Cer	–
Gal-β(1,4)-GalNAc-β(1,3)-Gal-β(1,4)-Glc-β-Cer	–
GalNAc-α(1,3)-GalNAc-β(1,3)-Gal-α(1,4)-Gal-β(1,4)-Glc-β-Cer	–
Gal-α(1,3)-Gal-β(1,4)-GlcNAc-β(1,3)-Gal-β(1,4)-Glc-β-Cer	++
Gal-α(1,4)-Gal-β(1,4)-GlcNAc-β(1,3)-Gal-β(1,4)-Glc-β-Cer	++
GalNAc-α(1,3)-[Fuc-α(1,2)]-Gal-β(1,4)-Gal-β(1,4)-Glc-β-Cer	–
Gal-α(1,3)-[Fuc-α(1,2)]-Gal-β(1,4)-Gal-β(1,4)-Glc-β-Cer	–

LecA will be studied in this research as a potential target for the detection of pathogens *via* carbohydrate interactions. Current diagnosis methodologies are based on bacteria culture or genetic studies via PCR.[128] Isolation of bacteria and subsequent cultivation is, although not expensive, time-consuming. The PCR method is not only faster, taking about one hour instead of up to three days, but it also provides a sensitivity three times higher than a traditional bacteria culture diagnosis.[129]

1.3.4. Summary of lectins specificities

Table 1.4 below summarises the glycan specificity of the lectins outlined in this section.

Table 1.4. Specificity of lectins used in this thesis

Lectin	RCA_{120}	UEA I	WGA	ConA	LecA	LecB
Specificity	β-D-Gal	α-L-Fuc	Neu5Ac	α-D-Man	β-D-Gal	α-L-Fuc

1.4. Aims

The main objective of the present research work is the development of a carbohydrate-based assay for the rapid detection of lectins as a model of binding for more complex targets such as the pathogen *P. aeruginosa*. The colorimetric properties of AuNPs ensure a visual result for the assay, preventing the need for sophisticated equipment that requires high investment and technical skills to be used. Previous work in our research group has shown that the gAuNPs system was able to bind to *P. aeruginosa* strain PA01. This will allow the establishment of the appropriate methodology to assess the binding between the carbohydrate-based probe developed and bacteria.

The synthetic strategy and optimization of the target carbohydrate probes will be discussed. Characterisation techniques such as ^{1}H- and ^{13}C-NMR, ESI-MS, optical rotation and infrared spectroscopy will be used to confirm the synthetic products. The initial planning includes the chemical derivatisation of a series of carbohydrates to install an azidopropyl tether. Alkyne functionality will be introduced on BSA following an epoxide-opening based methodology previously developed in the group. CuAAC chemistry will be employed to couple the alkyne functionalised protein to azidopropyl glycosides. The neoglycoprotein adducts will be

analysed through MALDI-TOF, comparing the molecular weight of the initial alkyne-BSA and the final glycoprotein to estimate the number of glycans immobilised. The synthetic BSA glycoconjugates will be installed on the surface of 40 nm AuNPs following passive adsorption methodology. The synthesised gAuNPs will be characterised by UV-Vis, DLS and TEM. Successful functionalisation of the nanoparticles will be tested in the format of a dipstick assay for the detection of a selection of lectins including RCA_{120}, UEA I, WGA and ConA.

With a functional detection system for carbohydrate-binding proteins, a ligand will be designed for the targeted detection of the *P. aeruginosa* lectin LecA. The synthesis of the designed ligand will be attempted and the binding will be quantified employing ITC and/or BLI. Flow cytometry experiments are envisioned to allow the evaluation of gAuNPs-bacteria interactions.

CHAPTER 2

SYNTHESIS OF BOVINE SERUM ALBUMIN GLYCOCONJUGATES TO ENABLE GLYCAN MULTIVALENCY

2.1. Introduction

The following chapter illustrates the synthesis and characterisation of a library of azidopropyl glycosides designed to build a collection of BSA glycoconjugates. The retrosynthetic pathways, synthetic strategies followed and issues encountered during the synthesis are discussed. Most of the glycosides were synthesised chemically, and one was synthesised enzymatically. BSA was functionalised with propargyl moieties to allow coupling *via* CuAAC between the glycosides and the protein, yielding the final glycoconjugates.

2.1.1. Carbohydrate chemistry: selection of glycans

To establish a carbohydrate-based assay for the detection of pathogen-related proteins, four plant lectins were selected as a model of binding to glycans. This included RCA_{120}, UEA I, WGA and ConA, which are galactose-, fucose-, sialic acid- and mannose-binding lectins, respectively. Glycan microarrays to understand the specific interactions between the model lectins and carbohydrates has been discussed in detail in *Chapter 1*. Therefore, the selection of glycans employed in this research work (**Figure 2.1**) included galactose (Gal), lactose (Lac), 2'-fucosyllactose (2'FL), glucose (Glc), mannose (Man), α3,α6-mannotriose (α3α6-Man) and 3'-siallylactose (3'SL).

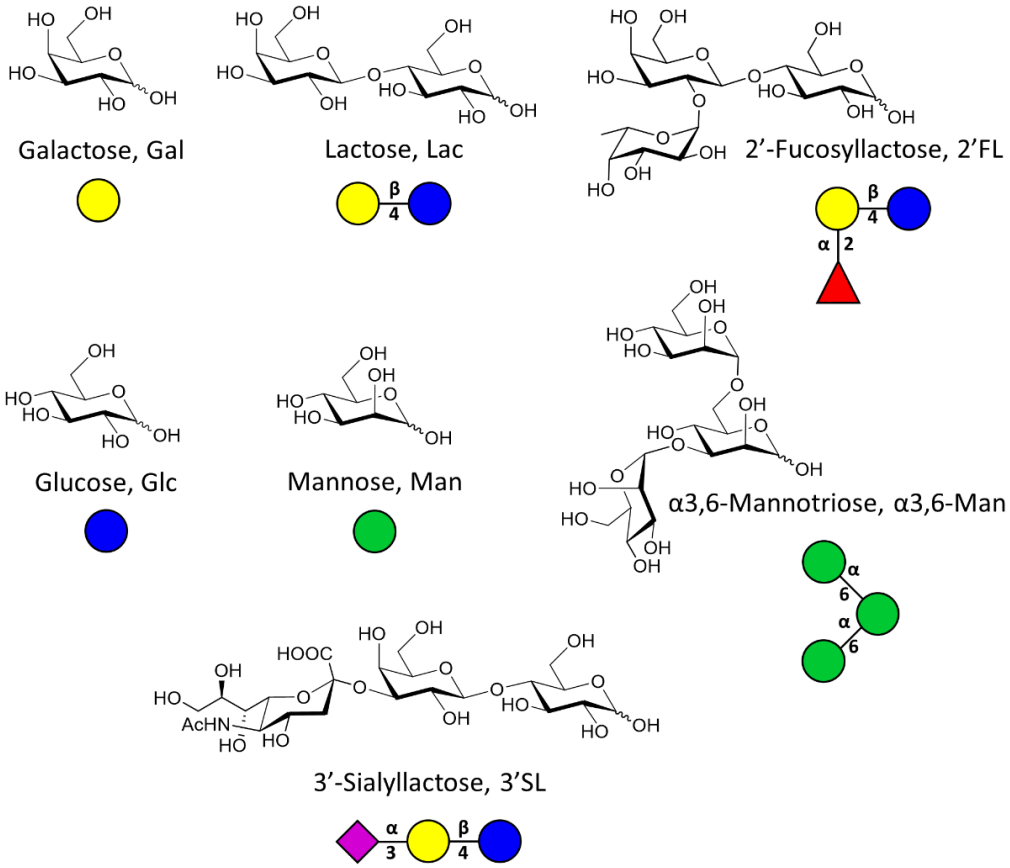

Figure 2.1. Chemical structures of the glycans used in this thesis. Below each chemical structure, the name, the abbreviation used throughout this work, and the corresponding symbol nomenclature for glycans (SNFG)[130] are reported.

2.1.2. The importance of multivalency in the development of carbohydrate-based ligands

Glycoarrays to understand multivalency

Given the weak nature of carbohydrate interactions (K_D values in the mM – µM range), the multivalent presentation of glycans on biological surfaces is required to enhance the affinity for glycan receptors.[7] This phenomenon – the cluster glycoside effect – has been discussed in *Chapter 1*, together with the use of glycan microarrays to understand the effect of glycan multivalency in their interactions with lectins.[131–133]

The well-known Man-ConA interaction has been extensively employed as a binding model to study carbohydrate-lectin interactions. Toone *et al.* synthesised a series of di, tetra and hexavalent mannose ligands based on a benzene 1,3,5-tricarboxylic acid scaffold.[134] The affinity of the set of ligands for ConA was evaluated through ITC, observing a binding potency of the tetravalent ligand up to 31 times higher than that of methyl α-mannoside. The

hexavalent ligand showed a 13-fold improvement of the binding with respect to the methyl α-mannoside, proving that a higher multivalency does not necessarily correlate with a more efficient binding of the ligand to the target lectin. The authors further investigated the origin of the binding enhancement by analysing the X-ray structure of the glycan-lectin conjugates formed. A detailed analysis of the data suggested that the binding enhancement could be attributed to a crosslinking process leading to the formation of soluble glycan-lectin aggregates. Using a similar scaffold, mannose dendrimers from mono- to octa-valent (**Figure 2.2**) were printed on maleimide-functionalised aluminium oxide chips to compare their avidity for FITC-labelled ConA.[135] The assay showed preferential binding to the octamer, although the progression in binding strength (measured as K_D) was not proportional to the valency of the ligand. The K_D value obtained for the monomer (960 nM) decreased almost by a factor of two for the dimer (540 nM), however, the value for the tetramer did not decrease as much (510 nM). A similar decrease was observed for the octamer, with a K_D of 440 nM.

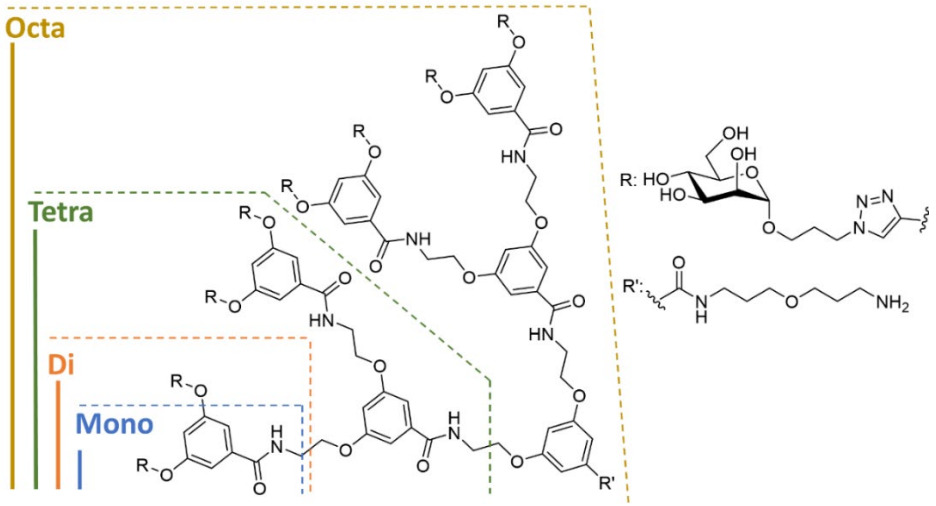

Figure 2.2. Structure of the mannose monomer, dimer, tetramer and octamer employed by Branderhorst *et al.*[135] to study the effect of multivalency on the Man-ConA binding.

A recent report found similar results when functionalising NHS ester-activated glass slides with analogous mannose monomers, dimers and tetramers at various concentrations.[136] Upon incubation with fluorescently labelled ConA, it was confirmed that higher glycan densities (as a result of the higher concentrations used for the functionalisation) and a higher multivalency (mannose dendrons over mannose monomers) granted a higher avidity for the lectin. It was also observed that saturation of the fluorescent signal was reached faster for the glycodendrons due to the saturation of the binding sites of the lectin (**Figure 2.3**).

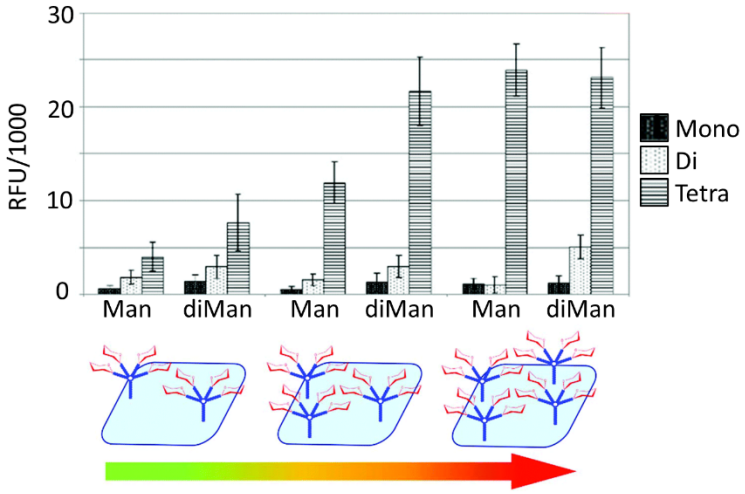

Figure 2.3. Fluorescence quantification of ConA in a glycoarray with mannose and α1,2-di-mannose at increasing concentrations and with increasing degrees of multivalency in the form of dendrons. Adapted from Maio *et al.*[136] (CC-BY-NC 3.0).

The multivalency in microarrays has also been achieved by pre-organising the binding sites of a scaffold bound to glass slides to couple monovalent ligands. Tetrapeptides formed by glycine and propargylglycine were prepared with a combinatorial approach to access sixteen isomers, followed by a CuAAC to couple monovalent ligands (**Figure 2.4**).[137] The panel was decorated with six different ConA-binding ligands, including derivatives of α-mannose, α/β-glucose, α1,6-di-mannose and α1,2-di-mannose. The K_D values were reported for the sixteen compounds, finding values ranging from 4 to 1 μM. This approach provided a systematic methodology to vary glycan density on surfaces in a controlled manner, and reducing the complexity involved in multivalent carbohydrate-based ligand synthesis.

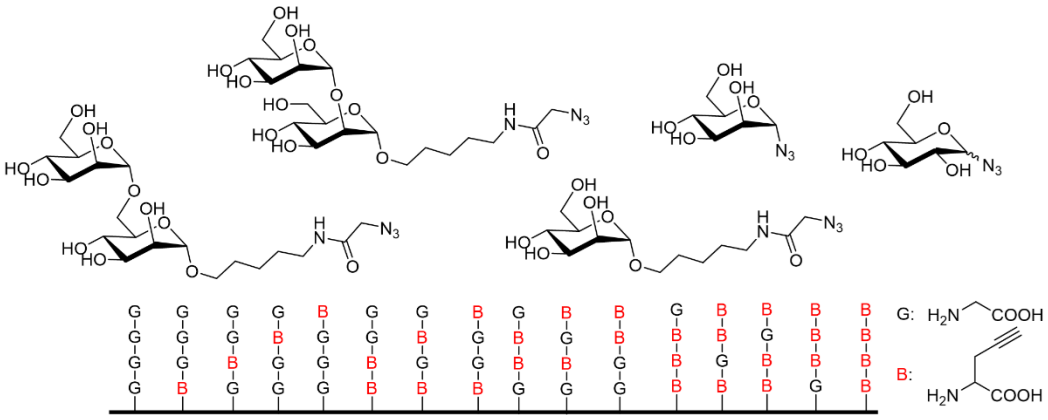

Figure 2.4. The strategy developed by Mende *et al.*[137] for the CuAAC coupling of different ConA ligands on a surface functionalised with propargylglycine-containing tetrapeptides.

Thiolated silane chips decorated with glycan ligands have been used to study the ConA-mannose system combining a microfluidics printer for the manufacturing and fluorescence microscopy for the analysis.[138] The chips were functionalised following a thiol-ene addition with a mixture of alkenyl mannoside and allyl alcohol in a gradient of molar fractions to achieve different glycan densities (**Figure 2.5**). The increasing gradient of glycan density immobilised on the chip led to a gradual decrease of the K_D value. The change was also studied at different concentrations of ConA, observing tighter interactions at lower concentrations of the lectin.

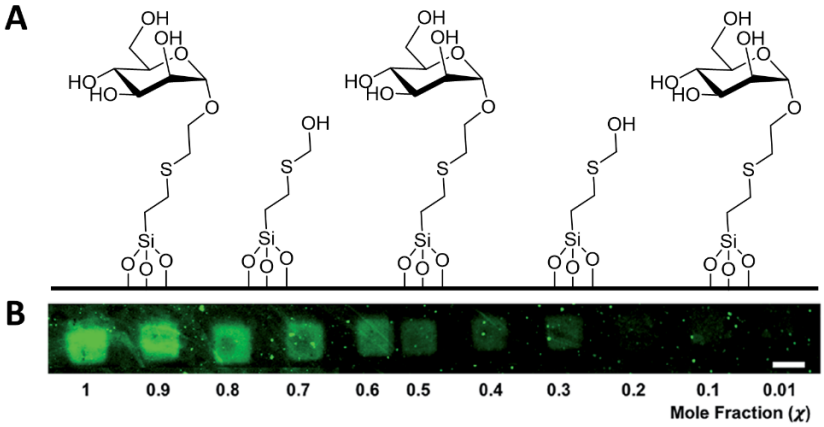

Figure 2.5. The strategy developed by Valles *et al.*[138] for the functionalisation of a thiolated silane surface to study the influence of glycan density on the binding between mannose and ConA. (**A**) Example of a chip functionalised with mannose at a molar ratio of 0.6 with allyl alcohol. (**B**) Fluorescence observed in the test due to the binding of FITC-labelled ConA. Reproduced from Valles *et al.*[138] with permission from the Royal Society of Chemistry.

The same thiol-ene approach was employed two years later by the same group to functionalise a copolymer of ethylene glycol dimethacrylate and pentaerythritol tetrakis(mercaptopropionate) photo-polymerised *in situ* on thiolated glass slides.[139] The degree of polymerisation was correlated with the capacity of the polymer to allocate glycan residues, hence reporting a precise estimate of the density of glycans on the surface.

Cyclopeptides have been employed to create glyco-clusters to study the interactions of carbohydrates with pathogens and to develop carbohydrate-based vaccines.[140] Aiming at targeting WGA, GlcNAc-based ligands with an unprecedented increase of binding potency were developed.[141] The developed method compared two tetramers of GlcNAc differing in the linkage and tether employed to link the glycoside to a cyclic nonapeptide core (**Figure 2.6A**). Both glycopeptides showed a different relative binding potency (RBP) in comparison to

GlcNAc, measured as IC_{50}, achieving up to a 25500-fold increase when the shorter tether was employed.

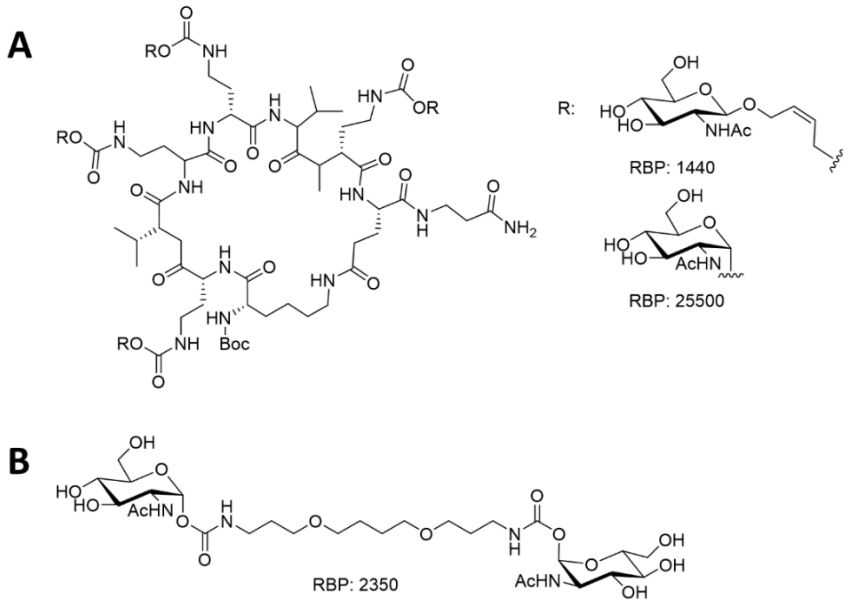

Figure 2.6. GlcNAc-based multivalent ligands reported by Schwefel *et al*.[141] for enhanced binding to WGA. (**A**) Two cyclic nonapeptide-supported GlcNAc tetramer differing in the tether length connecting the glycosides to the backbone. The one with a shorter tether exhibited a higher RBP. (**B**) Example of GlcNAc dimer synthesised in the same work to investigate the contribution of the GlcNAc-GlcNAc bridge to the increased binding.

The binding enhancement observed in the above-described glycopeptide was further studied to understand the contribution of the different pieces of the synthesised ligand to the binding. A set of fragments from the glycopeptide with different glycoside conformations and distance between glycans was evaluated. The use of an α- or β-GlcNAc glycoside did not show a significant difference in binding potency. Three GlcNAc dimers differing in bridge length (the medium one shown in **Figure 2.6B**) were assayed. The medium-sized dimer seemed to have the most significant contribution to the binding, with a noticeable drop in ligand affinity if the tether was shorter or longer. A series of crystal structures and NMR experiments showed the mode of binding and conformation adopted by three isomers of WGA and either the glycopeptide or the GlcNAc dimer. That work represents how a systematic approach can achieve high affinity between carbohydrate-based ligands and lectins by carefully tuning the structural features of a synthetic probe.

In the latest follow-up work by the same group, a similar approach was adopted for the synthesis of linear tetravalent GlcNAc ligands (**Figure 2.7A**).[142] The authors successfully

targeted simultaneously four binding sites of WGA by including a PEGylated bridge to link two GlcNAc dimers, achieving RBP values over 2,000,000 with respect to GlcNAc when using PEG_{10}, PEG_{11} and PEG_{12}. A combination of ITC, DLS and electron paramagnetic resonance permitted to report a detailed mode of binding between the ligand and the lectin (**Figure 2.7B**). The reported K_D values were in the nanomolar range as observed in the case of carbohydrate-lectin high-affinity interactions.

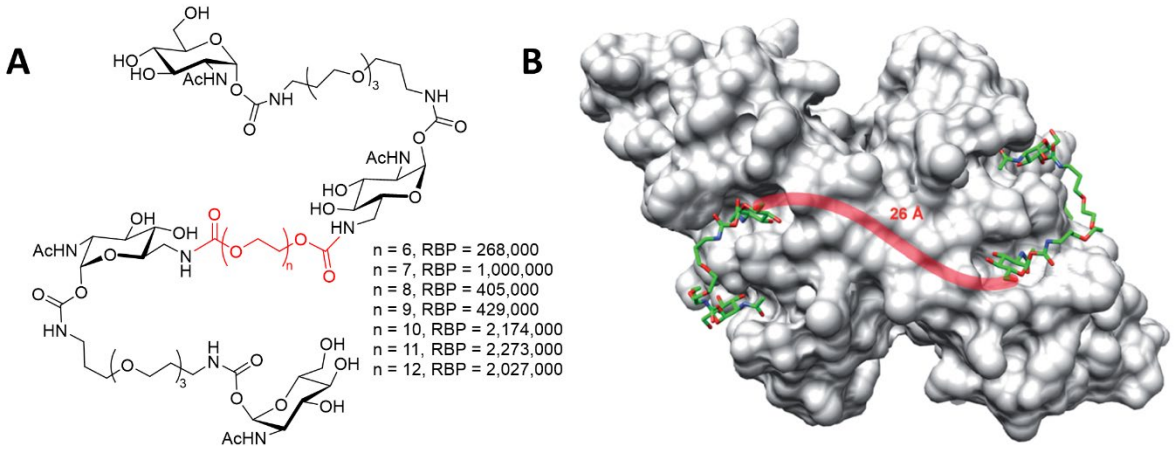

Figure 2.7. (**A**) Structure and (**B**) representation of the mode of action of the tetravalent GlcNAc linear ligands targeting four binding sites of WGA (adapted from Rohse *et al.*[142], CC-BY-NC). RBP values were measured as IC_{50} compared to GlcNAc.

Many lectins have been targeted to develop tools for the detection of pathogens or treatments of the generated infections. The DC-SIGN receptor of dendritic cells, also used by viruses like HIV, Ebola or Dengue as an entry gate into the host cells, has been targeted for antiviral therapies. The DC-SIGN receptor binds to the trimeric residues of mannose contained in the lipopolysaccharide ManLAM on the pathogens surface,[143] therefore trimeric mimics have been developed to block the receptor and prevent binding, hence infection, of the pathogens. For example, phenylene-ethynylene was used by Ordanini *et al.* as a rigid rod scaffold to build mannose dendrimers to target DC-SIGN (**Figure 2.8**).[144] The reported work compared eight hexavalent and eight divalent rods with different bridging lengths and glycan substituents. The carbohydrate ligands synthesised were proven to bind to the targeted lectins with an average RBP of 10 (IC_{50}, compared to mannose). The highest value was achieved by the hexavalent ligand including a three-member rod in the linker, which had an RBP value of 17. Furthermore, they also showed the ability to block HIV infections. Detection

of the HIV antigen p24 in lymphocyte cultures after 3 days in presence of the hexavalent compounds showed successful blocking of viral infection.

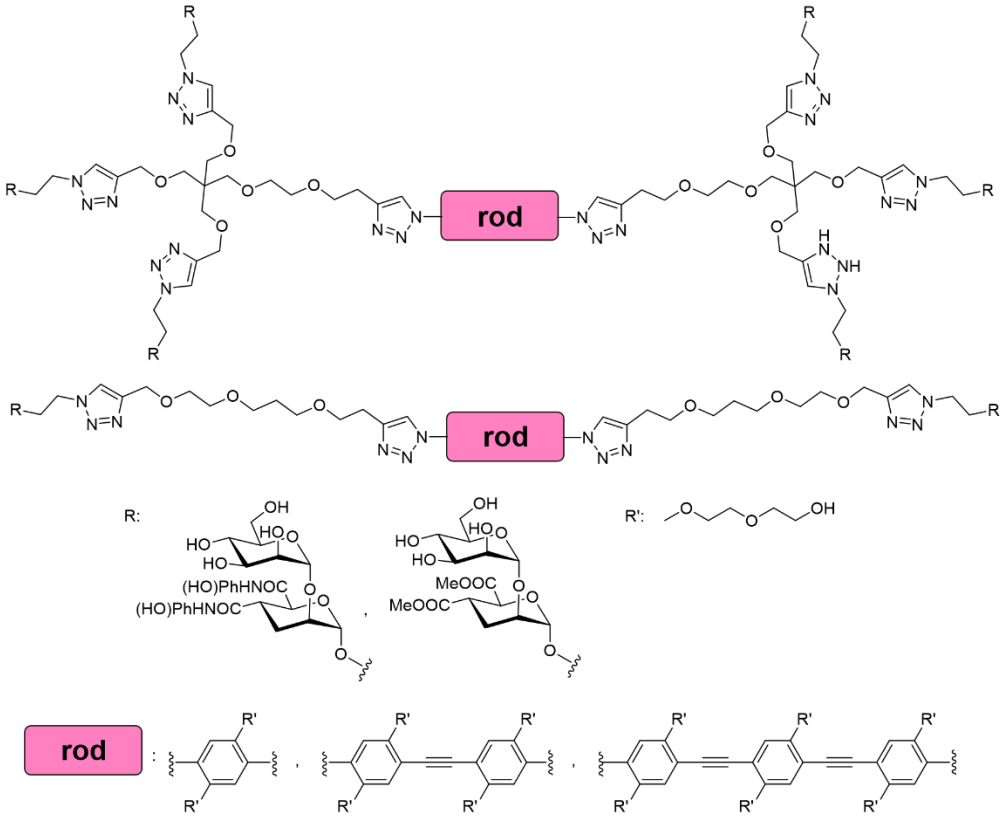

Figure 2.8. Hexavalent and divalent mannose-ending rods synthesised by Ordanini *et al.*[144] targeting DC-SIGN lectins.

Tuning the density of glycan probes

Most of the examples presented so far have achieved multivalency by installing glycans directly on glass slides and measuring their performance using fluorescently labelled lectins. Fewer examples tuned the density of glycans *via* the installation of the carbohydrates on peptides or polymer backbones. The density of glycan probes can also be tuned by incorporation of the carbohydrates into proteins forming glycoconjugates. This strategy and the examples reported in the literature using this approach will be reviewed in *Section 2.1.*3. High glycan density, and optimisation of this parameter, can also be achieved with gAuNPs.[41,145] The development of gAuNPs-based assays and the approaches to tune their glycan density are discussed in *Chapter 1* (bioassays in solution) and *Chapter 3* (flow assays).

2.1.3. Glycoconjugates of bovine serum albumin. Various approaches including amide formation, epoxide-opening and click chemistry

Glycosylation is a very common post-translational modification in Nature where glycans are installed on the surface of proteins.[146] The glycosylation pattern is heavily linked to many biological functions of proteins and the development of diseases such as cancer or inflammatory bowel disease. The functionalisation of proteins with specific glycans has a high relevance in order to understand biological processes involving glycoproteins and in particular their glycans. The process to obtain glycoproteins has been the subject of numerous studies to develop methodologies targeting specific functional groups in the side chains of amino acids such as lysine, to attach carbohydrates in different ways.[147] BSA has been widely used as a carrier protein due to its biocompatibility, stability, high water solubility, low cost and the number of lysine residues available. In this research work, BSA will be employed for the multivalent presentation of carbohydrates targeting lectins. Glycoconjugates have often been modified employing carbonyl-related functional groups such as oximes, thioureas, hydrazides, squaramides and amides. Different tethers have been used to bridge the glycan units to the proteins, allowing flexibility for the glycan moiety to be accessible for the target.

Oximes have been used as a linkage between rhamnose and BSA as a potential methodology for the development of glycoconjugate-based vaccines (**Figure 2.9**).[148] The authors developed an efficient method based on aminooxy-activated BSA synthesised through an NHS coupling of the functional tether to be further reacted with an aldehyde-terminal carbohydrate unit. The construct allowed the installation of up to 22 glycans per protein unit, which was determined by MALDI-TOF.

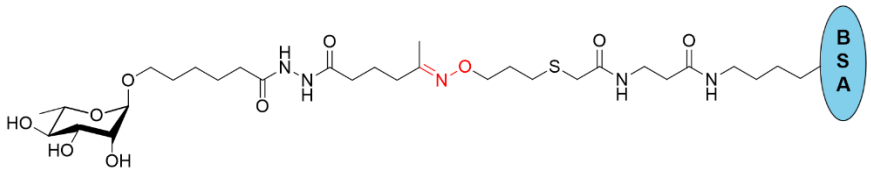

Figure 2.9. Oxime-linked BSA glycoconjugate synthesised by Kubler-Kielb *et al.*[148] using aminooxy-activated BSA and an aldehyde-ending rhamnoside.

Thioureas have been synthesised employing thiophosgene to obtain a mannose-6-phosphate-BSA (M6P-BSA) glycoconjugate to target insulin-like growth factor in hepatic cells (**Figure 2.10A**).[149] The BSA-glycoside ratio was optimised to allow the installation of up to 10

mannoside residues per BSA unit, as determined by the well-known phenol-sulphuric acid assay.[150] The glycoconjugate was successively precipitated in ethanol to form nanoparticles encapsulating sodium ferulate and employed as a drug delivery system for the treatment of hepatic fibrosis. The M6P-BSA binding to hepatic cells was efficient in delivering the drug that accumulated in the liver of mice showing potential to be further developed as a therapeutic methodology. A similar approach but using more complex glycoside derivatives was used to develop a vaccine candidate against *Neisseria meningitidis*.[151] With a remarkable synthetic effort it was possible to access the bacterial LPS core carbohydrate, Hep_2Kdo_2, starting from a mannose building block. BSA was decorated with 4 units of the tetrasaccharide (**Figure 2.10B**) and successfully applied as a glycoconjugate-based vaccine for the immunisation of rabbits.

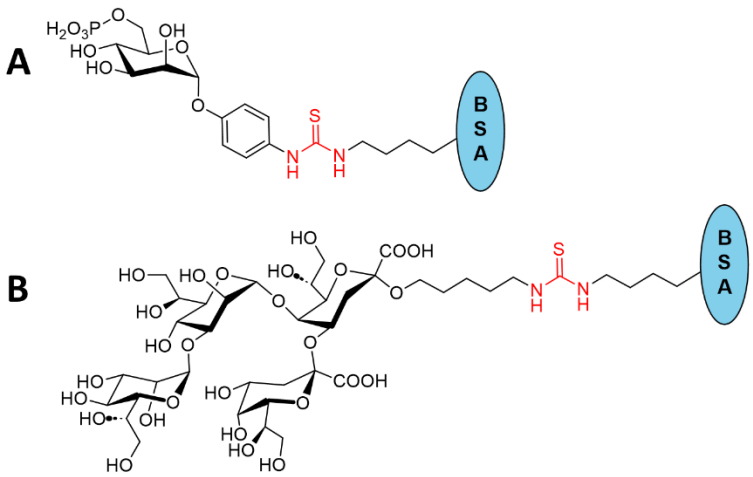

Figure 2.10. Thiourea-linked BSA glycoconjugates synthesised by (**A**) Li *et al.*[149] and (**B**) Kong *et al.*[151] using thiophosgene.

Bis-acyl hydrazides have been employed as crosslinking agents to bridge glycans and proteins (**Figure 2.11**).[152] Targeting lysine residues on BSA, EDC-activation allowed the coupling of a bis-hydrazide-functionalised pulmonary trisaccharide β-D-GalNAc(1-4)-β-D-Gal(1-4)-β-D-Glc. The glycoconjugates were employed to develop a biosensor for the detection of *P. aeruginosa* infection.

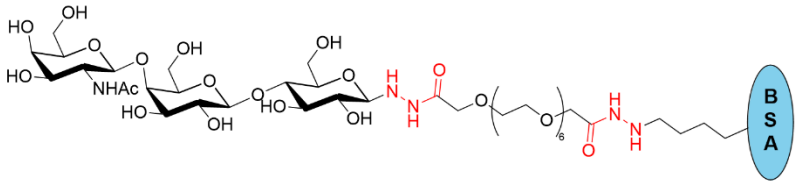

Figure 2.11. Hydrazine-linked BSA glycoconjugate synthesised by Adak *et al.*[152] using a PEGylated bis-acyl hydrazide spacer.

The application of squaramides to functionalise BSA with glycans has allowed access to novel glycoconjugates. A mannose-BSA-FITC glycoconjugate was prepared and employed for the bioimaging of MCF-7 cancerous cells to develop targeted therapies against cancer (**Figure 2.12A**).[153] The bi-functional conjugate was prepared *via* an aminohexyl α-D-mannoside derivative coupled to methyl squarate and successively installed on terminal amines of a BSA-FITC conjugate. The final glycoconjugate contained 10 copies of the glycoside per BSA unit, as determined by MALDI-TOF. The authors confirmed the binding of the construct to ConA and *E. coli* strain K12, and finally targeted epithelial MCF-7 cancer cells, observing the binding through fluorescence imaging. A similar strategy was employed for the attachment of carbohydrates to BSA, using squaramide-linked 3-(2-aminoethylthio)propyl Le^x (β-D-Gal(1-4)-β-(α-L-Fuc(1-3)-D-GlcNAc) glycoconjugates with 35 copies of the tetrasaccharide per BSA (**Figure 2.12B**), as determined by the phenol-sulphuric acid assay.[154] The Le^x glycoconjugate was recognised by anti-Le^x antibodies paving the way for the development of a Le^x-based anti-cancer vaccines.

Targeting the development of glycoconjugate-based vaccines against the *Brucella* species, mannosylated BSA neoglycoconjugates have been reported.[155] The vaccine candidate was prepared using BSA as a carrier decorated with an average of 14 copies (determined by MALDI-TOF) of a 4,6-dideoxy-4-formamido-α-D-mannopyranose-based mimic of the *O*-polysaccharide antigen present on surface of the pathogen.

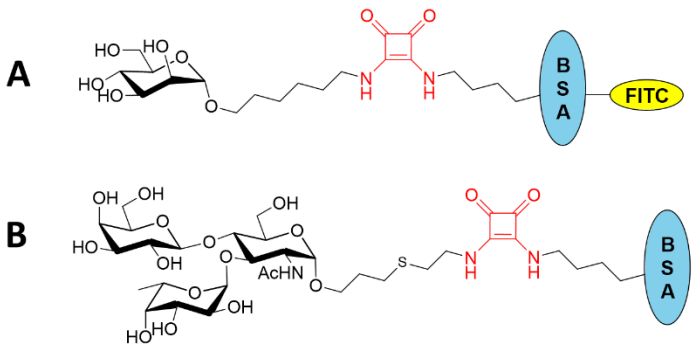

Figure 2.12. Squaramide-linked BSA glycoconjugates synthesised by (**A**) Marradi *et al.*[153] and (**B**) Wang *et al.*[154] designed for the imaging and prevention of cancer, respectively.

The most common methodology to decorate BSA relies on the formation of amide bonds. The Lewis A trisaccharide has been functionalised with a 1-octanecarboxylic acid tether to form an amide bond with terminal side chain amines of BSA residues (**Figure 2.13A**).[156] The methodology involved the installation of a hydrazide tether on the trisaccharide and the subsequent formation of the reactive acyl azide intermediates *in situ* to finally achieve a novel glycoconjugate containing 30 glycans per BSA, determined by the phenol-sulphuric acid method. The glycoconjugate was used for the immunisation of goats to study the production of anti-Le^a antibodies. Besides the application for vaccine development, sialylated glycoconjugates have also been used as prophylactic agents to prevent infection by influenza virus.[157] For this purpose, sialic acid was functionalised with an azide at the anomeric position and successively reduced to an amine to allow coupling to one end of a bis-NHS ester tether. The other end was subsequently used for the coupling with BSA (**Figure 2.13B**), yielding a glycoconjugate with 13 carbohydrate units per BSA (determined by MALDI-TOF) that successfully inhibited the binding of influenza virus to chicken erythrocytes in a haemagglutination inhibition assay. With a similar strategy, a GlcNAc-BSA glycoconjugate (**Figure 2.13C**) containing an average of 10 carbohydrate units per BSA (determined by MALDI-TOF) was prepared in a synthetic report.[158] PEGylated glycosides have also been employed to form glycoconjugates *via* amide formation (**Figure 2.13D**).[159] A thiodigalactoside was firstly "clicked" to an NHS ester-ending PEG-5 chain, which was used for the coupling to BSA. The methodology yielded neoglycoconjugate with 7 and 19 glycans, whose glycan loading was assessed through an indirect methodology, the trinitrobenzene-sulfonic acid assay, which determines the unfunctionalised lysine residues of the protein.[160] The performance of the glycoconjugates for the inhibition of galectin-3 was investigated, leading to IC_{50} values of 2 nM

for the more glycosylated conjugate and 19 nM for the less glycosylated one. By comparing with a monovalent ligand, whose IC_{50} value was of 9030 nM, the importance of the multivalent presentation of glycans for lectin-binding processes was proven.

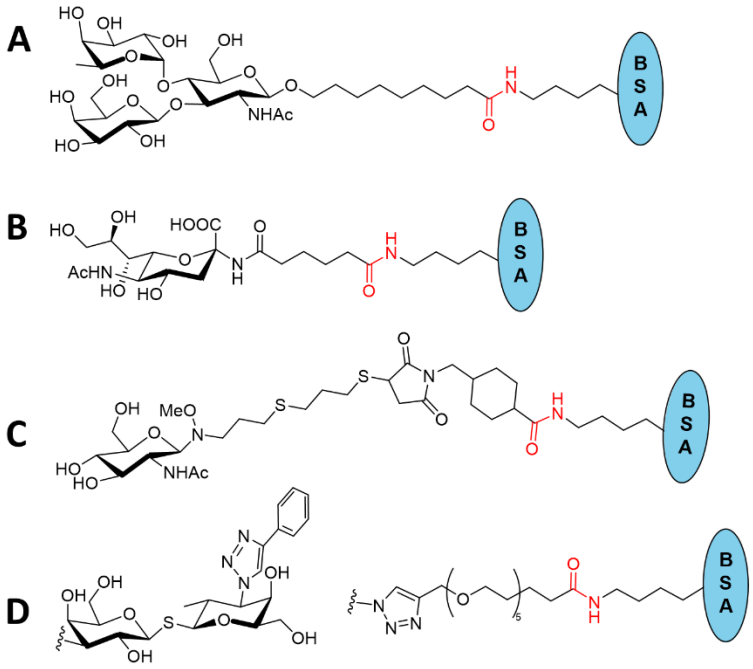

Figure 2.13. Amide-linked BSA glycoconjugates synthesised by (**A**) Lemieux *et al.,*[156] (**B**) Zhong *et al.,*[157] (**C**) Munneke *et al.*,[158] and (**C**) Zhang *et al.*[159] for the development of novel vaccines and anti-virals.

BSA contains 60 lysine residues of which 39 are accessible for conjugation,[161] which have been targeted for glycosylation by the methodologies described above. However, the higher number of acidic residues in BSA, approximately 100,[162] might present an opportunity for functionalisation of the protein. A potential approach consists in the activation of the available terminal carboxylic acids present in glutamic acid or aspartic acid residues with 1-(3-dimethylaminopropyl)-3-ethylcarbodiimide (EDC) to successively react with aminoalkyl glycosides. However, this approach must be considered carefully as the activated carboxylic acids can lead to intermolecular BSA coupling generating crosslinked BSA units. A representative crosslinking polymerisation of BSA units *via* lysine-glutamic acid coupling is reported in **Scheme 2.1**. The polymerisation of BSA upon EDC-activation has been employed for the synthesis of self-assembled BSA-Au nanoclusters.[163] The conjugation described reported a straightforward synthetic methodology and characterisation of the nanoclusters, studying the shape and surface granularity with varying concentrations of EDC for the BSA polymerisation.

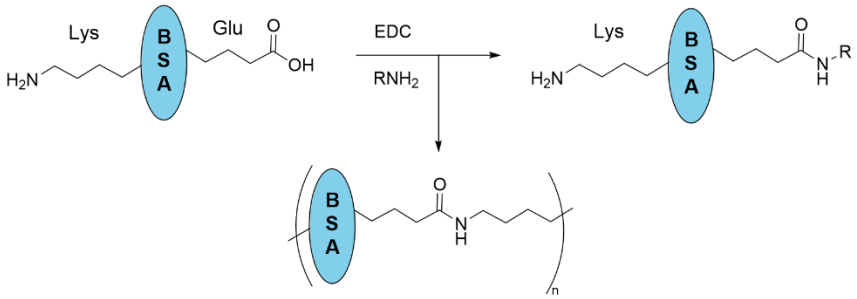

Scheme 2.1. Representation of polymerisation of BSA *vs.* coupling with a primary amine upon activation with EDC.

The modification of BSA often exploits the amine terminal group of lysine side chains, which might affect the ability of the protein to create hydrogen bonds, with an impact in the protein conformation, solubility and therefore its stability. In an attempt to functionalise BSA while preserving the hydrogen bond capability of the protein a click chemistry-based approach is reported in this thesis. Click chemistry has emerged with opportunities to create large combinatorial libraries of chemical compounds due to its efficiency and ease to perform.[164] The concept of click chemistry was firstly introduced by the twice-Nobel prize winner Prof Sharpless and collaborators as a "modular, wide in scope and high yields, stereospecific, with simple reaction conditions (ideally non-sensitive to oxygen and water) and without the need of purification through chromatographic methods". Click reactions include cycloadditions (such as CuAAC),[165,166] nucleophilic ring openings (especially strained rings such as epoxides), carbonyl chemistry not based in aldols (such as the formation of ureas) and additions to carbon-carbon multiple bonds (such as epoxidations).

CuAAC is a 1,3 dipolar cycloaddition between azides and terminal alkynes that results in 1,4-triazole derivatives, with applications found in many fields, although this discussion will focus on Glycoscience. It is a versatile reaction widely used for the creation of libraries of compounds, for example, the conjugation of carbohydrates to PEG,[159,167,168] naphthalimide fluorescent probes[167] or the surface of alkyne-functionalised gold nanoparticles.[168] CuAAC chemistry has already been explored for the synthesis of BSA glycoconjugates as described above; however, this has often implied the functionalisation of BSA with alkyne moieties through an amide bond. For example, heparinoids, polysaccharides derived from heparin with repeating units consisting of glucosamine and uronic acid, have been functionalised with a terminal azide to allow copper-free click chemistry with BSA (**Figure 2.14**).[169] In the

methodology described, BSA was modified with a cyclooctyne moiety attached through an amide bond to the surface of the protein. Although only 6 cyclooctyne moieties were installed per BSA, all of them reacted with the azide-functionalised heparin, as determined by MALDI-TOF. The neoglycoconjugate was implemented in an assay to evaluate its ability to control cell proliferation through its interaction to the fibroblast growth factor 2, leading to inhibition of cell growth.

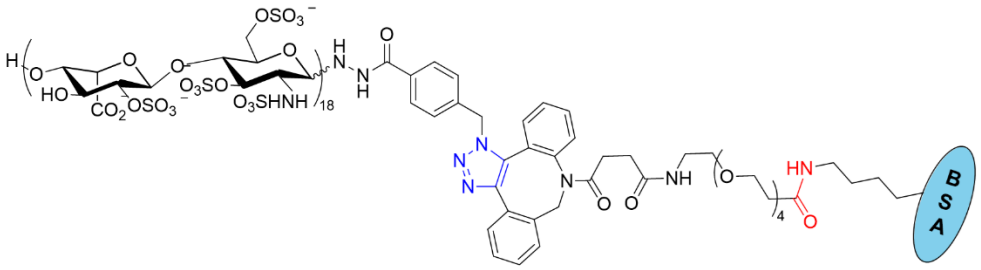

Figure 2.14. Glycoconjugate synthesised through copper-free click chemistry by Lemieux *et al.*,[169] highlighting the amide bond created to install the cyclooctyne moiety, and the triazole ring formed upon the coupling with the heparin derivative.

Epoxides are three-membered cyclic ethers very reactive due to their ring strain.[170] The reactivity of glutamic or aspartic acid residues towards epoxide moieties was assessed more than 50 years ago in a study to identify amino acids in the binding pocket of lysozyme (**Figure 2.15**).[171]

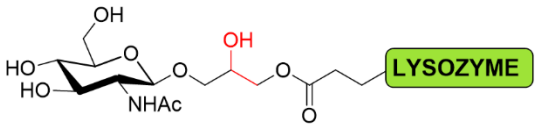

Figure 2.15. Glycoconjugate synthesised through epoxide-opening chemistry by Thomas *et al.*[171] targeting glutamic and aspartic acid residues of lysozyme.

However, epoxides are better known for their reactivity in the presence of primary amines for the synthesis of β-aminoalcohols.[172] The reactivity between lysine residues and epoxide derivatives in neutral pH conditions has been known for more than 25 years. Using *N'*-acetyl-lysine-4-methylcoumarin-7-yl-amide as a model of protein-bound lysine, the reaction with different γ-hydroxy-α,β-unsaturated epoxides was successfully tested for the first time.[173] Several years later, a library of different reagents including diazo compounds, enamides, halides and glycidol reactive cores were screened to fluorescently label a range of proteins.[174] The panel of proteins included human carbonic anhydrase II (HCA II), ConA, BSA, kinase A and

glyceraldehyde-3-phosphate. Among twelve probes, the glycidol compound (**Figure 2.16A**) was the only one specifically targeting HCA II, which was due to the presence of the reactive epoxide facilitating the coupling with the surface of the protein. Those results served as the basis for a later report where several epoxide-ending fluorophores were used to label the same protein (**Figure 2.16B**).[175] Not only that one-pot methodology allowed to label the site pocket of the enzyme, but also the fluorophore could be cleaved to restore the enzymatic activity of HCA II.

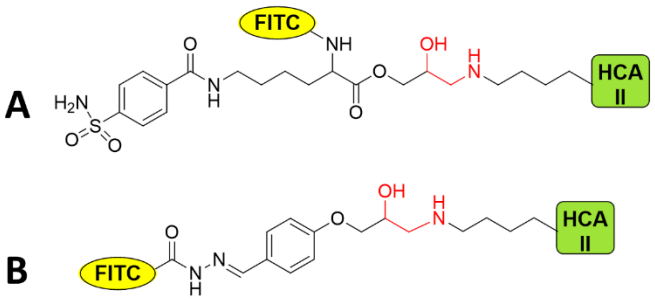

Figure 2.16. Two examples of the fluorescent β-aminoalcohol-linked HCA II conjugates synthesised by (**A**) Chen *et al.*[174] and (**B**) Takaoka *et al.*[175] to study the active site of the enzyme.

Other enzymes have been targeted with multivalent glycoconjugates. The enzymatic degradation of collagen type I has been studied with collagen conjugates synthesised through epoxide opening chemistry (**Figure 2.17**).[176] Two different epoxides were used, glycidol and butyl glycidyl ether, to study the different effects of the side chain on the affinity for the degrading enzymes collagenase, trypsin, acetylated trypsin, and cathepsin B. They concluded that a longer, hydrophobic chain was more beneficial than a shorter, hydrophilic one.

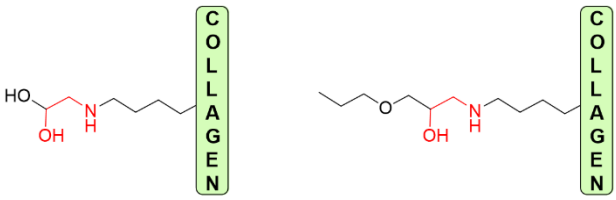

Figure 2.17. β-aminoalcohol-linked collagen conjugates synthesised by Gratzer *et al.*[176] to study the affinity for collagen degrading enzymes.

The examples above discussed illustrate the versatile applications of epoxides for the functionalisation of protein units. Bi-functionalised reagents bearing terminal epoxides such as ethylene glycol bis glycidyl ether (EGDE) have been used to crosslink proteins while granting

better water solubility properties, creating new biomaterials.[177] Fibrous proteins such as keratin are biocompatible candidates to be used as scaffolds for cell cultures. EGDE has been used to crosslink keratin fibres (**Figure 2.18A**) targeting not only lysine residues but also histidine, tyrosine, proline, glutamic acid and aspartic acid, creating 3D cell cultures with good potential for tissue engineering.[178] A similar approach has been taken using the corn protein zein and a triglycidyl ether crosslinking reagent to develop a bone tissue regeneration system (**Figure 2.18B**).[179] The developed system showed a good cell viability; however, issues of cytotoxicity have been recently encountered when using modified zein as a result of unreacted epoxide moieties pending from the fibre structure.[180] To overcome the issue, the authors added a second step following the crosslinking reaction, using a lysine buffer to quench the unreacted epoxide moieties. Other biomaterials have been synthesised following the same methodology, including a tubular prosthesis for blood vessel regeneration made from crosslinked silk fibroin,[181] or a gelatine filamented yarn which was used to knit gloves.[182]

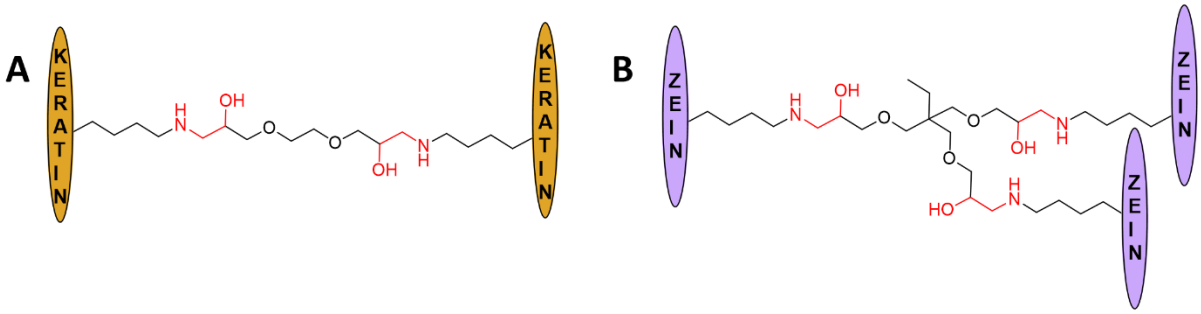

Figure 2.18. Examples of β-aminoalcohol-crosslinked (**A**) keratin fibres and (**B**) zein fibres synthesised by Fan *et al.*[178] and Cardenas-Turner *et al.*[179] (respectively) for the development of tissue regeneration technologies.

Besides proteins, other biomolecules have been used for the development of materials through epoxide-opening chemistry. The epoxide-ending reagent γ-glycidoxypropyltrimethoxysilan (GPTMS) has been used on many occasions over the past years to functionalise chitosan, which can undergo a crosslinking process *via* trimethoxysilane condensation upon heating (**Figure 2.19**).[183] Due to the high hydrophilic nature of chitosan, this application resulted to be useful for the development of separation membranes,[184–186] allowing to separate azeotropic mixtures.[187] The crosslinked polysaccharide has also been implemented in biomedical applications; for example, in the formation of hydrogels as carriers of bone-bonding biomaterials in bone surgery.[188]

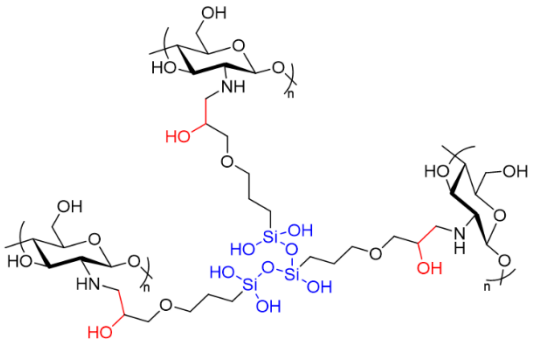

Figure 2.19. Structure of GPTMS-crosslinked chitosan through epoxide-opening chemistry and silane condensation.

2.2. Aims

The present chapter describes the development of a synthetic methodology to prepare BSA glycoconjugates through click chemistry (**Scheme 2.2**). The synthesised glycoproteins will serve in *Chapter 3* as lectin-binding ligands to be installed on the surface of AuNPs to develop a dipstick assay for the detection of carbohydrate-binding proteins.

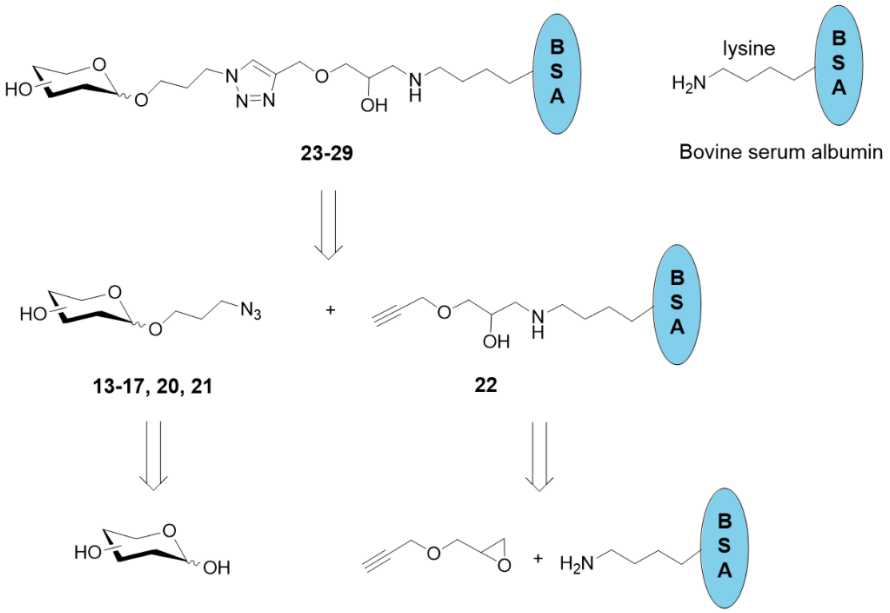

Scheme 2.2. The scientific aim described in *Chapter 2*. Retrosynthetic pathway of a set of BSA glycoconjugates.

2.3. Results and discussion

2.3.1. Synthesis of azidopropyl glycosides

A library of 3-azidopropyl derivatives of galactose (Gal), lactose (Lac), 2'-fucosyllactose (2'FL), glucose (Glc), mannose (Man), α3,6-mannotriose (α3α6-Man) and 3'-sialyllactose (3'SL) was synthesised following or adapting published methods.

Galactose, lactose, 2'-fucosyllactose, glucose and mannose

Due to the similarities in chemical structure and reactivity of the carbohydrates employed in this work, a similar synthetic route was employed for the synthesis of their 3-azidopropyl derivatives, which is summarised in **Scheme 2.3**.

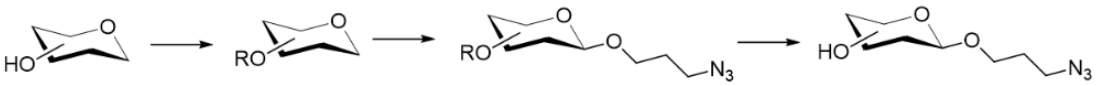

Galactose	a1.	(**1**, 98%)	b.	(**7**, 42%)	c.	(**13**, 63%)
Lactose	a1.a2.	(**2**, 85%)	b.	(**8**, 34%)	c.	(**14**, 95%)
2'-Fucosyllactose	a1.	(**3**, 85%)	b.	(**9**, 25%)	c.	(**15**, 93%)
Glucose	a1.	(**4**, 99%)	b.	(**10**, 27%)	c.	(**16**, 38%)
Mannose	d.	(**5**, 92%)	e. / f.	(**12**, 62%)	g.	(**17**, 95%)

Scheme 2.3. Synthesis of 3-azidopropyl glycosides of galactose, lactose, 2'-fucosyllactose, glucose and mannose. Reagents and conditions: **a1.** NaOAc, Ac_2O, DMAP (cat.), 120 °C, 1 h; **a1.** Pyridine, Ac_2O, DMAP (cat.), r.t., o.n.; **b.** 3-azidopropan-1-ol (**6**), $BF_3{\cdot}OEt_2$, DCM, N_2, 0 °C to r.t., o.n.; **c.** MeONa, MeOH, r.t., 1 h; **d.** Pyridine, BzOCl, DMAP (cat.), r.t., o.n., N_2; **e.** HBr, DCM, 0 °C, 1.5 h; **f.** 3-azidopropan-1-ol (**5**), AgOTf, toluene, -20 °C to r.t., o.n., N_2. The yields shown here are unoptimized.

Peracetylated galactose (**1**), lactose (**2**), 2'-fucosyllactose (**3**) and glucose (**4**) were obtained under thermodynamic control conditions to obtain a higher ratio of β-acetate in the anomeric mixture.[189] The ratio of α- and β- peracetates correlates with the equilibrium between the two anomers, which is temperature-dependent. Kinetic conditions (low temperatures) allow a higher amount of α-anomer as the reaction conditions do not provide enough energy to cross the enthalpic energy barrier to equilibrate from the α to the β-anomer. Employing thermodynamic conditions (higher temperatures) provides the sufficient energy to allow the conversion from α- to β-anomer, shifting the equilibrium to obtain a higher amount of the β-peracetate. Most of the desired anomer could be isolated by recrystallisation from hot

ethanol. However, because of the higher stability of α-anomer (hence lower reactivity) in the following glycosylation conditions, it was possible to proceed to the next step using the α/β mixture of peracetates, where an easy separation of the two anomers was not feasible. In the specific case of lactose, the NaOAc-Ac_2O acetylation conditions did not reach a full conversion to the peracetylated disaccharide, as evidenced from the up-fielded doublets in the ^{1}H-NMR spectrum (**Figure 2.20**), which are diagnostics of a partially acetylated intermediate. Analysis performed by ESI-MS confirmed the presence of both the octa-*O*-acetate (found m/z 701.3 $[M+Na]^+$, calcd for $C_{26}H_{36}O_{19}Na$ 701.2) and the hepta-*O*-acetate (found m/z 659.4 $[M+Na]^+$, calcd for $C_{28}H_{38}O_{19}Na$ 659.2). This result has been reported before[190] and it is associated with the lower reactivity of the hydroxyl group in position 3.[191] The partially acetylated mixture was resubmitted to acetylation, using pyridine in the presence of a catalytic amount of 4-(dimethylamino)pyridine (DMAP). The mixture was converted to the fully acetylated product.[192]

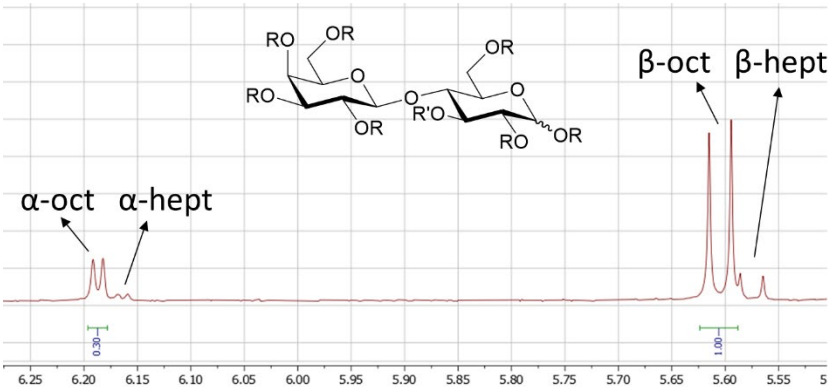

Figure 2.20. Characterisation of the mixture of octa- (α-oct and β-oct; R = R' = Ac) and hepta-*O*-acetate (α-hept and β-hept; R = Ac, R' = H) derivatives of lactose. A down-fielded pair of doublets was found through ^{1}H-NMR corresponding to the α- and β- anomers.

The first attempt for the preparation of peracetylated mannose (**5b**) was performed under thermodynamic conditions as described above. This methodology led to a mixture of products containing the expected α- and β-mannose pentaacetates, and a secondary pair of carbohydrates whose anomeric protons appeared slightly down-fielded in the ^{1}H-NMR of the crude (**Figure 2.21**). The same result has been previously reported and attributed to the presence of a small percentage of the per-*O*-acetyl-α- and β-D-mannofuranosides.[193] Detailed studies on the pyranose-furanose equilibrium at high temperatures are still missing for several carbohydrates. However, a recent study reported the increase of the molar ratio of furanose

species for ribose, reporting the inversion of the pyranose-furanose ratio at 134-156 °C from predominantly pyranose, to predominantly furanose.[194]

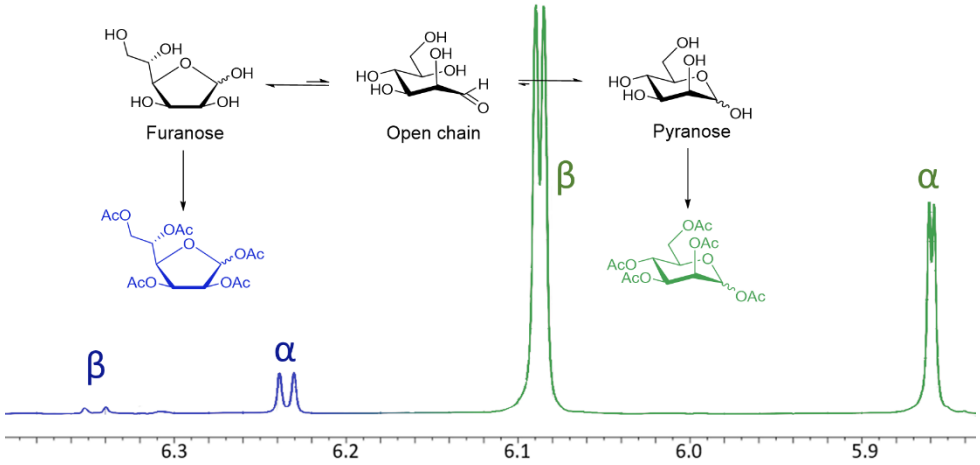

		α-Pyranose		β-Pyranose		α-Furanose		β-Furanose	
		δ_{H-1}	$J_{1,2}$	δ_{H-1}	$J_{1,2}$	δ_{H-1}	$J_{1,2}$	δ_{H-1}	$J_{1,2}$
Man	lit.	Percec *et al.*[195]		Percec *et al.*[195]		Stevens[196]		Stevens[196]	
		5.85	1.2	6.07	2.0	6.24	3.4	6.35	4.8
	this work	5.86	1.2	6.09	1.8	6.23	3.3	6.34	4.9

Figure 2.21. The ^{1}H-NMR spectrum of the crude mixture of pyranosides and furanosides found after acetylation of mannose using NaOAc and Ac_2O at 120 °C for 45 minutes. Most of the material was successfully acetylated into mannose pentaacetate. NMR shifts of the anomeric protons (δ_{H-1}, ppm) and H1-H2 coupling constants ($J_{1,2}$, Hz) are described and compared with the literature.

The synthetic pathway followed for the peracetylation of mannose was reconsidered. Due to the C-2 axial configuration of mannose, the α-anomer is the thermodynamically favourite species found in Nature.[197] To direct the synthesis towards the α-anomer, benzoyl was chosen as a protective group. Perbenzoylated mannose (**5**) was obtained following standard published methods using benzoyl chloride in pyridine under kinetic control conditions.[198]

The protected glycans **1-4** were subsequently coupled to 3-azidopropan-1-ol (**6**) *via* $BF_3{\cdot}OEt_2$-promoted glycosylation[199] to afford acetylated azidopropyl galactoside (**7**), lactoside (**8**), 2'-fucosyllactoside (**9**) and glucoside (**10**). Acetate groups are often the choice of leaving groups in glycosylations promoted by BF_3, since they participate in the mechanism, stabilising the

oxacarbenium ion formed upon S_N1 cleavage of the acetate group in the anomeric position (**Scheme 2.4**).[200] After the attack of the anomeric acetate to the promoter, a positive charge is generated, which is stabilised by the carbonyl group of a neighbouring acetate through its coordination to the anomeric carbon. That leads to a second nucleophilic attack from a hydroxyl-containing acceptor. This reaction step is moisture-sensitive, as the presence of water will lead to the hemiacetal by-product.

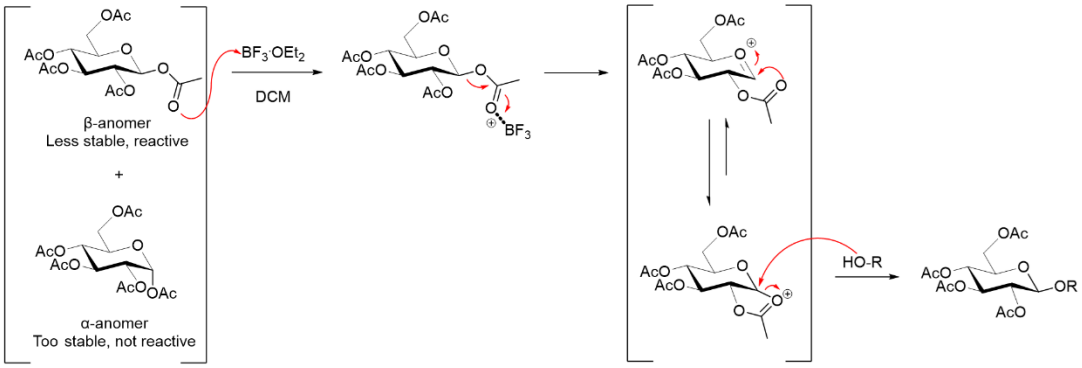

Scheme 2.4. Mechanism of the $BF_3{\cdot}OEt_2$-promoted glycosylation with the participation of an acetate protecting group. For R = H (moisture), the mechanism leads to a hemiacetal by-product.

In the case of mannose, the classical Koenigs–Knorr glycosylation with a silver salt promoter such as silver trifluoromethanesulfonate (AgOTf) was chosen as strategy to obtain the α-anomer.[201] AgOTf-promoted glycosylation requires a glycosyl halide as a donor, hence a benzoylated mannosyl bromide (**11**) was chosen, which is more stable than the acetylated analogue. The perbenzoylated mannoside **5** was subsequently brominated in the anomeric position to obtain the corresponding benzoylated mannosyl bromide.[202] This reaction is α-stereospecific due to the loss of chirality upon formation of the oxacarbenium ion and the subsequent addition of the bromide. The reaction was followed by TLC and once the starting material was completely converted to another compound with higher R_f the reaction was stopped. Due to instability of glycosyl bromides, product **11** was not characterised and it was directly used in the following AgOTf-promoted glycosylation[203] with **6** to yield benzoylated azidopropyl mannoside (**12**). The reaction follows a very similar mechanism to the one promoted by $BF_3{\cdot}OEt_2$, with a rapid subtraction of the bromide by the silver salt, forming insoluble silver bromide that leaves an oxacarbenium cation that is stabilised by the participation of a benzoyl group, directing the reaction towards the α-anomer (**Scheme 2.5**).[201]

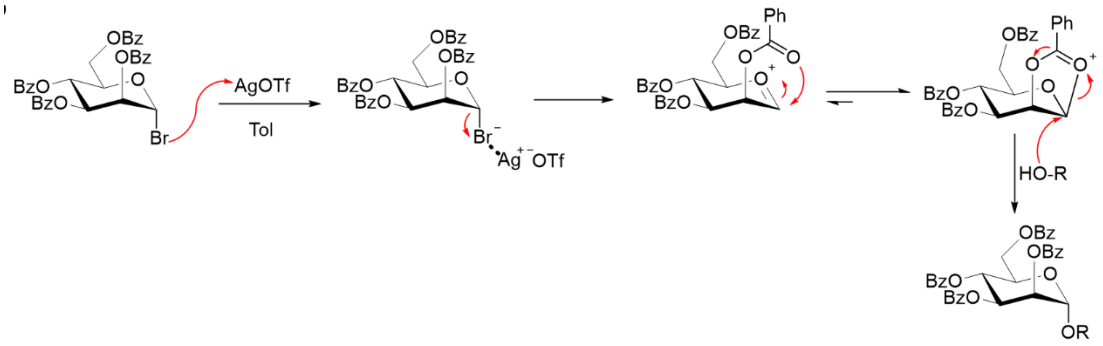

Scheme 2.5. Mechanism of the AgOTf-promoted glycosylation with the participation of one benzoyl group. For R = H (moisture), the mechanism leads to a hemiacetal by-product.

For all the products **7**, **8**, **9**, **10** and **12**, the glycosylation was confirmed by ^{1}H- and ^{13}C-NMR assignment of the respective anomeric peaks, the $J_{1,2}$ coupling constants values, and by comparison with the available literature data (**Table 2.1**). The chemical shift of the glycosylated carbohydrate was *ca.* 1.2 ppm upfield for the β-anomeric proton and *ca.* 9 ppm downfield for the β-anomeric carbon if compared to the corresponding anomeric acetate starting material.[204–215] Due to the little difference in R_f between the glycosides **7, 8, 9, 10** and **12** and their respective unreacted starting materials, the purification of this reaction is not efficient by either silica gel chromatography or by recrystallisation. The purification resulted more efficient through silica gel (for monosaccharides) or gel permeation chromatography (for disaccharides) after deacetylation. The protective groups were removed *via* standard Zemplen deacetylation with sodium methoxide in methanol,[209] affording azidopropyl galactoside (**13**, overall yield 26%), lactoside (**14**, overall yield 27%), 2'-fucosyllactoside (**15**, overall yield 20%), glucoside (**16**, overall yield 10%) and mannoside (**17**, overall yield 54%). Complete removal of protective groups was confirmed through the disappearance of their respective peaks in ^{1}H- and ^{13}C-NMR.

Table 2.1. NMR shifts of the anomeric proton ($\delta_{H\text{-}1}$, ppm) and carbon ($\delta_{C\text{-}1}$, ppm), and H1-H2 coupling constants ($J_{1,2}$, Hz) for the respective fully protected glycans (benzoylated for mannose, acetylated for the rest), protected glycosides, and deprotected glycosides of the monosaccharides synthesised in this thesis. (*) The discrepancy was found with the reported data. Not only these peaks, but the whole spectrum was shifted in comparison. (**) As no literature is available for the azidopropyl glycoside, we compared it with the corresponding methyl glycoside. (***) No available literature with assigned NMR data. (****) As no literature is available on the azidopropyl glycoside, we compared it with the butyl one.

		Protected glycan			**Protected glycoside**			**Unprotected glycoside**		
		$\delta_{H\text{-}1}$	$J_{1,2}$	$\delta_{C\text{-}1}$	$\delta_{H\text{-}1}$	$J_{1,2}$	$\delta_{C\text{-}1}$	$\delta_{H\text{-}1}$	$J_{1,2}$	$\delta_{C\text{-}1}$
Gal	lit.	Lebedel *et al.*[204]			Fekete *et al.*[205]			Lu *et al.*[206]		
		5.69	8.2	92.3	4.48	8.0	101.3	4.40	7.8	102.9
	this work	5.70	8.2	92.3	4.47	8.0	101.5	4.41	8.0	102.9
Lac	lit.	Šardzí *et al.*[207]			Demchenko *et al.*[208]			Yu *et al.*[209] (*)		
		5.64	8.3	91.6	4.46	8.0	100.8	4.36	7.7	103.4
	this work	5.67	8.2	91.7	4.46	7.9	101.2	4.46	7.8	102.9
2'FL	lit.	Wang *et al.*[210]			Scheppokat *et al.*[211] (**)			(***)		
		5.69	8.2	91.5	4.39	7.9	101.7	-	-	-
	this work	5.67	8.0	91.9	4.47	8.0	101.0	4.45	7.7	102.3
Glc	lit.	Michihata *et al.*[212]			Huang *et al.*[213]			Lu *et al.*[206]		
		5.71	8.2	91.8	4.51	8.0	101.0	4.43	8.1	102.3
	this work	5.71	8.1	91.8	4.47	7.8	100.9	4.47	7.8	102.9
Man	lit.	Sail *et al.*[214]			Meldal *et al.*[215] (****)			Meldal *et al.*[215] (****)		
		6.61	2.0	91.4	5.13	1.8	97.7	4.85	1.5	100.0
	this work	6.63	1.9	91.5	5.11	1.8	97.9	4.88	1.6	99.8

α3,6-Mannotriose

For the synthesis of an α3,α6-mannotrioside (**Scheme 2.6**), a mannoside acceptor with positions 2 and 4 selectively protected is required. The preparation of a similar mannotrioside has been reported before *via* orthoester chemistry.[203]

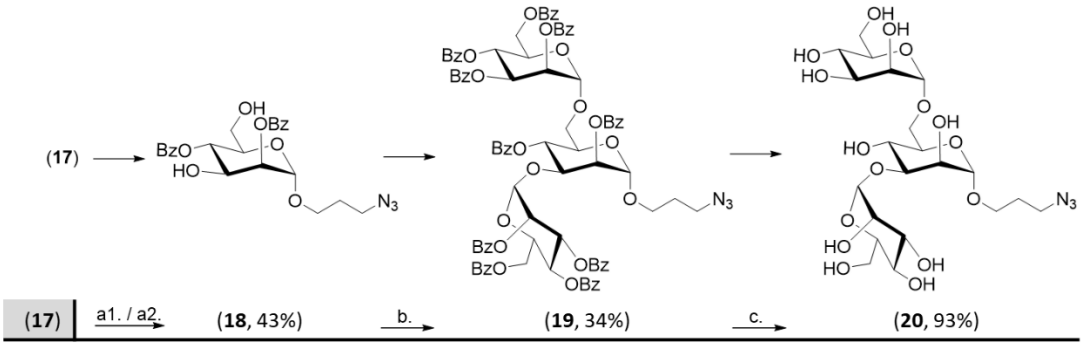

Scheme 2.6. Synthesis of 3-azidopropyl mannotrioside Reagents and conditions: **a1.** $BzOEt_3$, p-tol sulfonic acid (cat.), TFA, acetonitrile, r.t., 25 min; **a2.** TFA (aq.), acetonitrile, r.t., 15 min; **b.** (**11**), AgOTf, toluene, -20 °C to r.t., o.n., N_2; **c.** MeONa, MeOH, r.t., 1 h. The yields shown here are unoptimized.

The deprotected mannoside **17** was selectively benzoylated to afford azidopropyl 2,4-di-*O*-benzoyl mannoside (**18**). The mechanism of this reaction is reported in **Scheme 2.7** where the first step consists in the elimination of a methoxy group from the trimethyl orthobenzoate to give methanol (step **A**). The newly formed carbocation is rapidly stabilised by the primary hydroxyl group of the glycan moiety (step **B**). Due to the catalytic acidic conditions, the elimination of a second methoxy group is promoted by the neighbouring hydroxyl group at C-4 of mannose forming a cis-methoxybenzylidene derivative of the glycoside (step **A'**). The repetition of these steps (**A**, **B**, **A'**, and **B'**) between the positions 2 and 3 leads to the formation of a complex mixture of (2,3):(4,6)-di-*O*-methoxybenzylidene derivatives, given that two new stereogenic centres have been created in the process (*i.e.* four isomers). TLC-ESI-MS confirmed the presence of such intermediates (ESI-MS: found m/z 522.2 $[M+Na]^+$, calcd for $C_{25}H_{25}N_3O_8Na$ 522.2). The resulting complex mixture was directly used for the following step without need of isolating the single species.

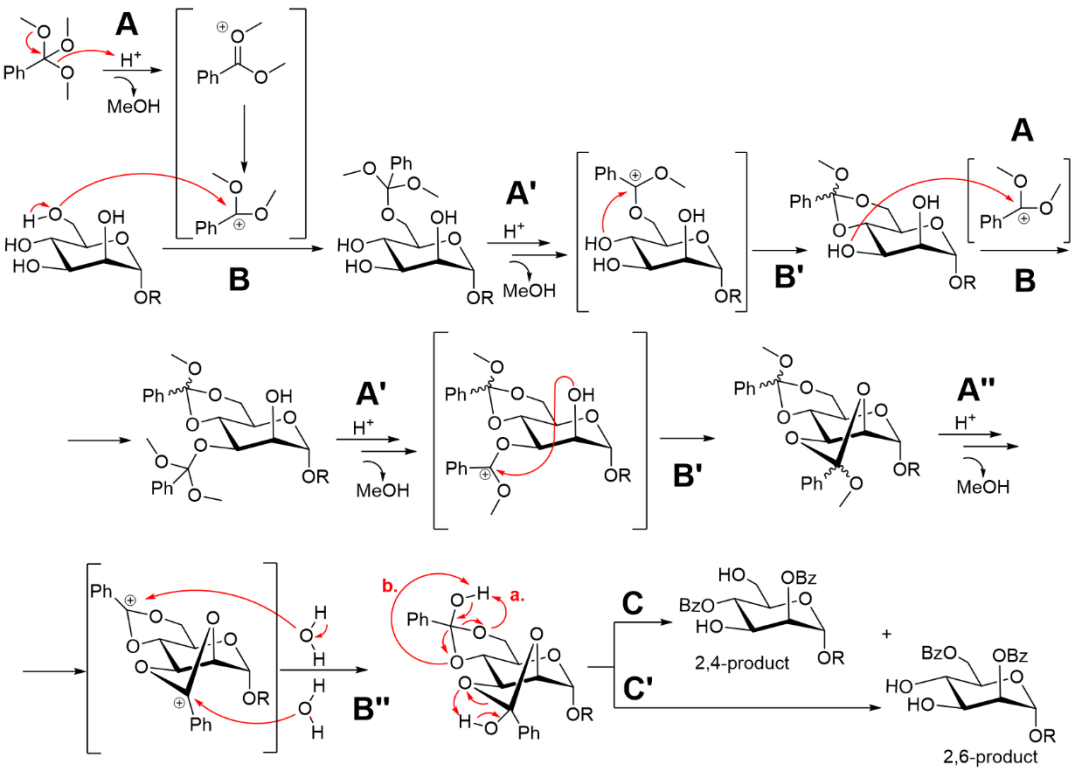

Scheme 2.7. Proposed mechanism for the synthesis of a 2,4-di-*O*-benzoyl mannoside *via* orthoester formation and opening with trimethyl orthobenzoate in acidic conditions. The mechanism is a repetition of (step **A**) acidic elimination of a methoxide group from the orthobenzoate, (step **B**) stabilisation of the positive charge by a hydroxyl group from the glycan and (step **A'**) acidic elimination of another methoxide group from the orthobenzoate and (step **B'**) stabilisation of the positive charge by a neighbouring hydroxyl group. (Step **A'')** A last catalytic elimination of a methoxide group generates a positive charge which (step **B''**) is stabilised by water molecules, leading to (steps **C/C'**) a final rearrangement to give a 2,4- or 2,6-di-*O*-benzoyl mannoside.

Upon addition of a stoichiometric amount of aqueous trifluoroacetic acid (step **A''**, **B''**), the 2,3-linked orthoester opens selectively in position 3, leaving position 2 benzoylated. This is due to the steric hindrance at position 2, which prevents the cleavage of the ester leading to more than 95% of the axial ester-equatorial alcohol derivative.[216] However, the opening of the 4,6 linked orthoester occurs in a 1:1 ratio since both positions are relatively accessible, leading to the mixture of 2,4- and 2,6-di-*O*-benzoyl mannosides.[217]

The structural differences between 2,4- and 3,6-di-*O*-benzoyl mannosides allowed the isolation of the desired azidopropyl 2,4-di-*O*-benzoyl mannoside **18** through silica gel chromatography. ^{1}H-NMR allowed the unambiguous identification of the desired product, based on the diagnostic chemical shift of the protected 4-position (**Figure 2.22**).

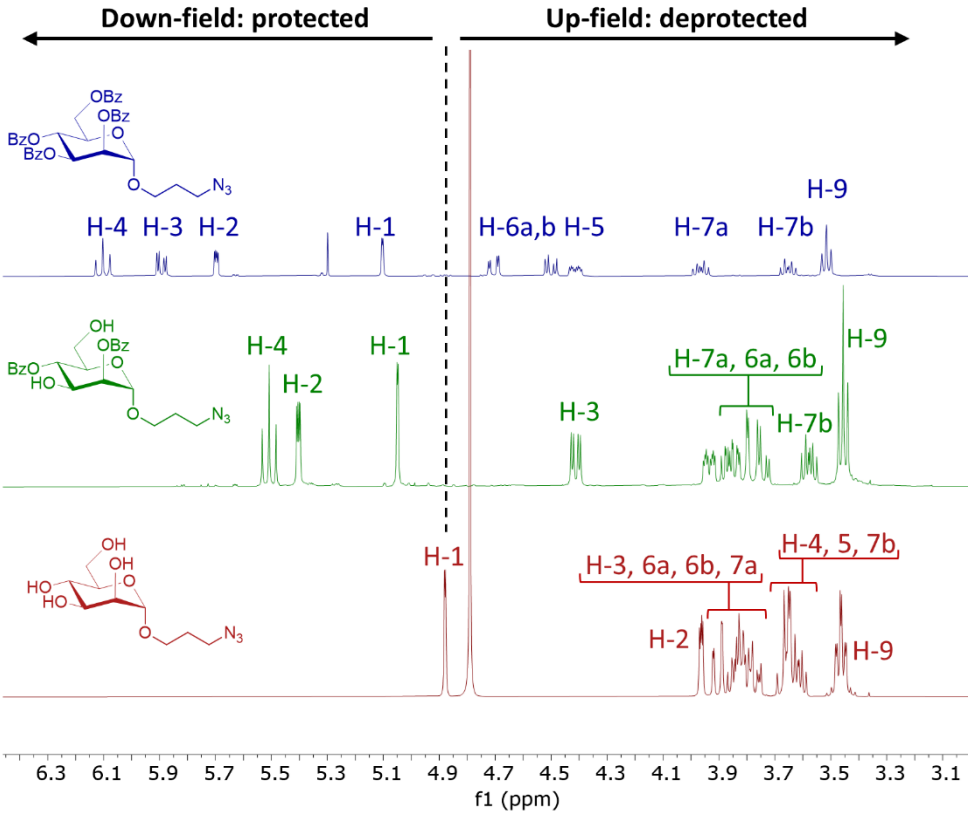

		2,4-di-*O*-benzoyl			2,6-di-*O*-benzoyl		
		δ_{H-1}	δ_{H-4}	δ_{H-6}	δ_{H-1}	δ_{H-4}	δ_{H-6}
Man	lit.	Oscarson *et al.*[203]			Oscarson *et al.*[203]		
		5.00	5.8	3.72	4.92	3.92	4.55 + 4.76
	this work	5.05	5.51	3.74 + 3.81	Not isolated		

Figure 2.22. Stacked ^{1}H-NMR spectra for benzoylated azidopropyl mannoside (**12**, **blue**), azidopropyl 2,4-di-*O*-benzoyl mannoside (**18**, **green**) and azidopropyl mannoside (**17**, **red**). The comparison between them helps to conclude that positions 3 and 4 have remained benzoylated upon hydrolysis of the orthoester precursor. ^{1}H-NMR shifts ($\delta_{H-x,}$ ppm) are described and compared with those reported in the literature for a similar octyl 2,4-di-*O*-benzoyl mannoside.[203]

Glycoside **18** was successfully reacted as acceptor with benzoylated mannosyl bromide as a donor following AgOTf-promoted glycosylation conditions. The reaction yielded a benzoylated azidopropyl α3,α6-mannotrioside (α3α6-Man, **19**), which was deprotected to afford the azidopropyl α3,α6-mannotrioside (**20**, overall yield 7%). In this case, the complexity of the NMR spectrum for both **19** and **20** prevented a full report of coupling constants and specific shifts for ^{1}H, which is not unprecedented.[203] However, the anomeric protons could be assigned

via comparison with an aminoethyl α3,α6-mannotrioside reported in the literature (**Table 2.2**).[218]

Table 2.2. NMR shifts of the anomeric proton ($\delta_{H\text{-}1}$, ppm) and H1-H2 coupling constants ($J_{1,2}$, Hz) for the anomeric peaks of the azidopropyl α3,6-mannotrioside, in comparison with published literature. (*) Not measured, the peak was an apparent singlet.

		$\delta_{H\text{-}1}$	$J_{1\text{-}2}$	$\delta_{H\text{-}1}$	$J_{1\text{-}2}$	$\delta_{H\text{-}1}$	$J_{1\text{-}2}$
20	Lindhorst *et al.*[218]	5.05	1.6	4.84	1.6	4.79	(*)
	This work	5.03	1.5	4.83	1.4	4.76	1.4

3'-Sialyllactose

Given the biological importance of sialic acid in the pathogen-host interactions,[219–221] an azidopropyl 3'-siallylactoside was designed and synthesised. To afford the compound more efficiently, enzymatic installation of sialic acid on the previously synthesised azidopropyl lactoside **14** was performed using *Trypanosoma cruzi* trans-sialidase, which is known to have the desired specificity (**Scheme 2.8**).[222] The expression and purification of this enzyme are described in *Appendix 1*. Briefly, an ampicillin-resistant plasmid encoding for the enzyme was induced in *E. coli* and the bacteria were cultured in the presence of ampicillin to discard non-competent cells. The gene expression was induced by the addition of isopropyl β-D-1-thiogalactopyranoside (IPTG).[223] The cells were lysed and the expressed enzyme was purified *via* metal ion affinity chromatography.

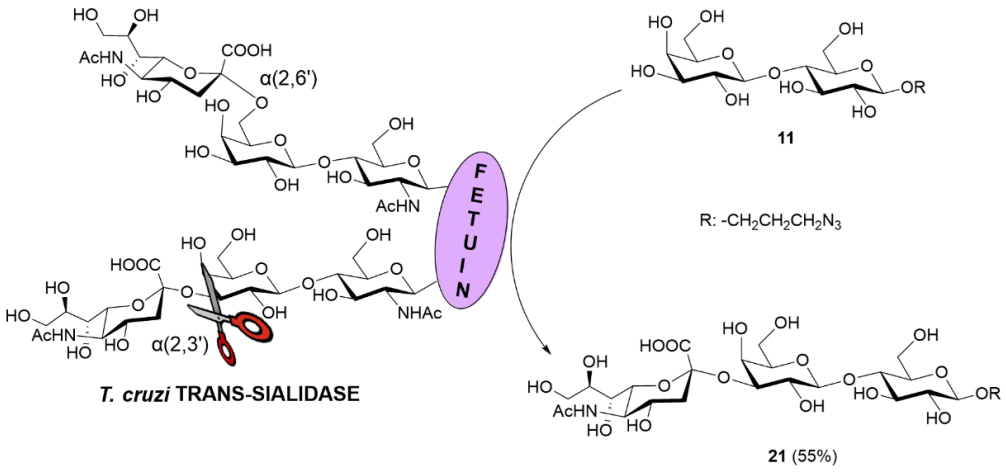

Scheme 2.8. Enzymatic installation of sialic acid on the 3'-position of azidopropyl lactoside (**14**) using *T. cruzi* trans-sialidase and fetuin as a source of sialic acid. Reagents and conditions: Tris-HCl buffer 50 mM pH 8.39, 37 °C, o.n. The yield shown here is unoptimized.

Bovine fetuin was employed as a source of sialic acid, as it has been reported to contain 8.7% of sialic acid (w/w, leading to 13 units per protein) in the form of bi- and tri-antennary sialic-acid terminal *N*-glycans.[224] However, only 38% of the sialic acid content is α(2,3')-linked and therefore suitable substrate for the trans-sialidase,[225] which accounts for a 3.3% (w/w, leading to 5 units per protein) content of "useful" sialic acid. For the reaction, *ca.* 60 mg of fetuin (2 mg of "useful" sialic acid) were employed per mg of azidopropyl lactoside, which translates into a molar ratio of sialic acid-lactose of 2.5. The reaction mixture was easily purified through anion exchange chromatography, taking advantage of the negatively charged carboxylic group from the sialic acid moiety *vs.* the uncharged starting material that is not retained in the cartridge. The enzymatic reaction worked with a yield of 54%, affording the desired azidopropyl 3'-sialyllactoside (3'SL, **21**, overall yield of 15% from lactose). The NMR spectra (^{1}H and ^{13}C) were in agreement with data reported in literature,[226] as detailed in **Table 2.3**.

Table 2.3. NMR shifts of the anomeric proton ($\delta_{H\text{-}1}$, ppm) and carbon ($\delta_{C\text{-}1}$, ppm), and H1-H2 coupling constants ($J_{1,2}$, Hz) for the azidopropyl sialyllactoside **21**. (*) Not assigned in the publication.

		$\delta_{H\text{-}1}$	$J_{1\text{-}2}$	$\delta_{C\text{-}1}$	$\delta_{H\text{-}1'}$	$J_{1'\text{-}2'}$	$\delta_{C\text{-}2''}$	$\delta_{H\text{-}NAc}$
21	Wu *et al.* [226]	4.49	8.0	(*) 102.2	4.53	7.9	(*) 99.9	2.03
	This work	4.50	7.9	102.1	4.54	7.7	99.8	2.04

Glycoside synthesis: summary

A collection of azidopropyl glycosides including Gal, Lac, 2'FL, Glc, Man, α3α6-Man and 3'SL has been synthesised. The glycosides have been fully characterised with all data in agreement with published literature, when available. In the following step, this collection served to develop a CuAAC set of BSA neoglycoconjugates, which will be used in *Chapter 3* for the synthesis of gAuNPs to target lectins in a dipstick assay.

2.3.2. BSA functionalisation

To study the multivalent presentation of carbohydrates on the surface of AuNPs (*Chapter 3*), BSA-based glycoconjugates have been designed employing click chemistry. Using the 3-azidopropyl glycosides **13**, **14**, **15**, **16**, **17**, **19** and **21** described in *Section 2.3.1*, a set including Gal-, Lac-, 2'FL-, Glc,- Man-, α3,6-Man- and 3'SL-bearing BSA glycoconjugates was synthesised.

Functionalisation of BSA with a propargyl moiety

BSA was first functionalised with a propargyl moiety (**22**) to allow CuAAC chemistry with azidopropyl glycosides (**Scheme 2.9**). This was achieved through epoxide ring-opening methodology using glycidyl propargyl ether to allow the nucleophilic attack of terminal amines in lysine residues from BSA to the epoxide. It is worth mentioning that the glycidyl propargyl ether is acutely toxic by inhalation and adequate health and safety measures must be kept during any work with this reagent.

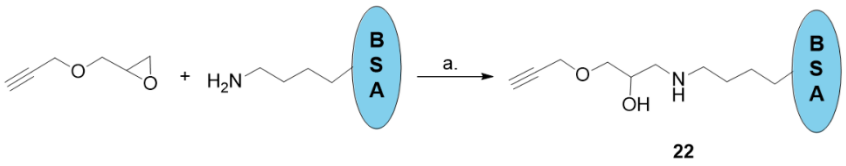

22

Scheme 2.9. Epoxide-opening reaction between glycidyl propargyl ether and BSA, targeting its available lysine residues to yield a propargylated BSA adduct (**22**). Reagents and conditions: (**a**) $NaHCO_3$ (aq., 10 mM), darkness, 37 °C, o.n.

The reaction is promoted under basic conditions obtained with $NaHCO_3$ (10 mM, pH 8.2) that shift the acid-base equilibrium of the lysine residues towards the neutral state. Given the high pKa of the side chain of this amino acid (10.4),[227] at pH 8.2 most of the amines are present as protonated species. However, a further increase of the pH in the reaction mixture would result in the opening of the epoxide by the excess of hydroxyl groups in the solution. For this reason,

the reaction is left overnight to allow a nearly full conversion of the available lysine residues to propargyl moieties. The reaction vials were covered with aluminium foil during the functionalisation due to the photosensitivity of the epoxide reagent. The excess of epoxide was removed from the mixture *via* dialysis against Mili-Q water over 48 hours, with a change of the water after the first 24 hours. The propargylated BSA **22** was characterised by MALDI-TOF analysis, evaluating the increase in average molecular weight after functionalisation of the protein. The outcome of the reaction was variable between experiments, with an average increase in molecular weight of 2900 Da (different experiments afforded values between 2500 and 3300 Da). **Equation 2.1** shows the simple mathematical approach to calculate the average number of propargyl units installed on BSA. The stacked spectra in **Figure 2.23** illustrate the difference observed, in this case of 2899 Da, resulting in 26 propargyl units per BSA.

$$\mathrm{M_{BSA}} = 66569\ \mathrm{Da}, \mathrm{M_{alk}} = 112\ \mathrm{Da},$$

$$\mathrm{M_{alk-BSA}} = 69468\ \mathrm{Da} \rightarrow\ \Delta\mathrm{M} = 2899\ \mathrm{Da}$$

$$2899\ \mathrm{Da} \cdot \frac{1\ \text{propargyl unit}}{112\ \mathrm{Da}} \approx 26\ \text{propargyl units per BSA}$$

Equation 2.1. Calculation of the average number of propargyl units installed on BSA.

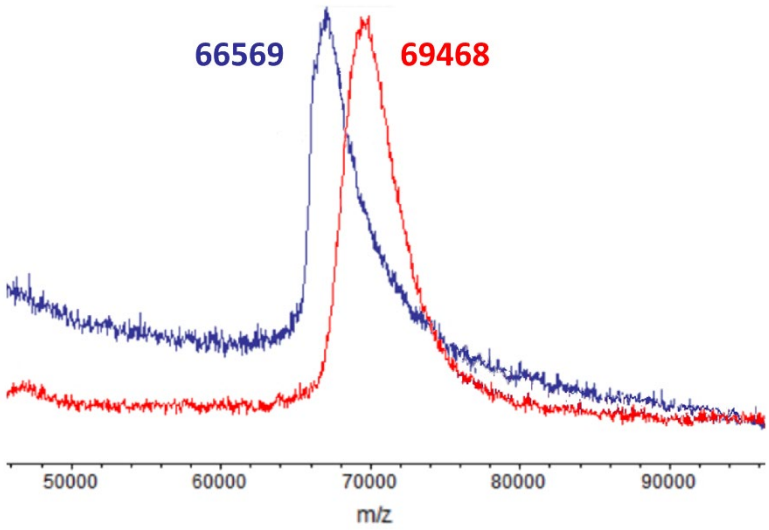

Figure 2.23. Overlapped MALDI-TOF spectra of **BSA** and **propargylated BSA (22)**. The difference in mass between the two species allows to calculate the degree of functionalisation of the BSA adducts.

Functionalisation of BSA with azidopropyl glycosides

The propargylated BSA was glycosylated *via* CuAAC chemistry with the collection of 3-azidopropyl glycosides **13-17**, **20** and **21** (**Scheme 2.10**).

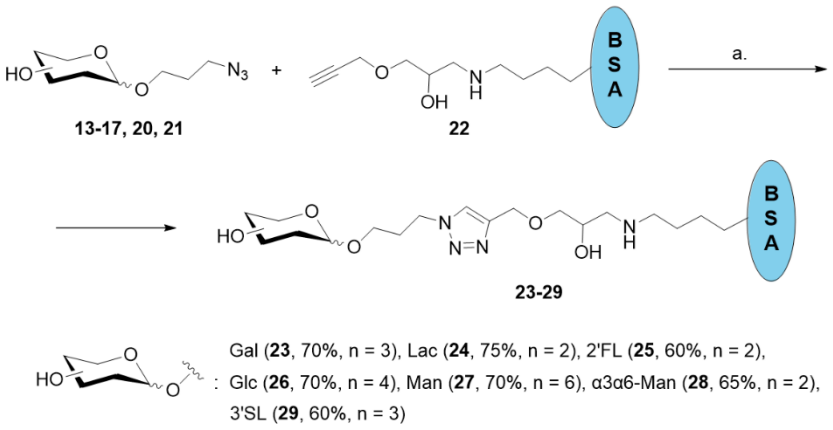

Scheme 2.10. CuAAC reaction between the collection of 3-azidopropyl glycosides **13-17, 20** and **21**, and BSA. Reagents and conditions: (**a**) $CuSO_4$ (aq., 4.5 mM), THPTA (aq. 11 mM), NaAsc (aq., 1.1 mM), 37 °C, o.n. **n**: number of glycan units installed on the glycoprotein.

In this reaction, catalytic Cu(II) ions from the sulphate salt are reduced *in situ* by sodium ascorbate (NaAsc) to their Cu(I) active, yet unstable, form. The oxidation of NaAsc produces different species, such as hydrogen peroxide or dehydroascorbate, that can react with the protein oxidising residues such as cysteine or methionine, leading to cross-linking and precipitation of the protein in the reaction vial.[228,229] To avoid this, tris(3-hydroxypropyltriazolylmethyl)amine (THPTA) is used to intercept the reactive oxygen species and act as a sacrificial reductant. THPTA is usually mixed beforehand with copper sulphate and then added to the reaction vial. Only after THPTA is present in the reaction mixture, sodium ascorbate can be safely introduced into the system. The optimal THPTA-Cu ratio reported in the literature to guarantee an optimal turnover in the catalytic cycles was found to be to be 5:1.[230] However, in previous work at Iceni Glycoscience different concentrations were tested and no improvement was found beyond a 2:1 ratio. Similarly, the recommended concentration of NaAsc was 2.5 mM, which had been optimised at Iceni Glycoscience to 1.1 mM.

Small molecular weight reagents (catalyst, salts and unreacted glycosides) were removed through dialysis against Mili-Q water and the remaining solution was freeze-dried to isolate the target glycoprotein. The characterisation of the BSA glycoconjugates **23-29** was performed

through MALDI-TOF, similarly to the propargylated BSA **22**, evaluating the difference in average molecular weight before and after the coupling reaction. A representative example of the spectrum corresponding to glycoconjugate **23** is shown in **Figure 2.24**.

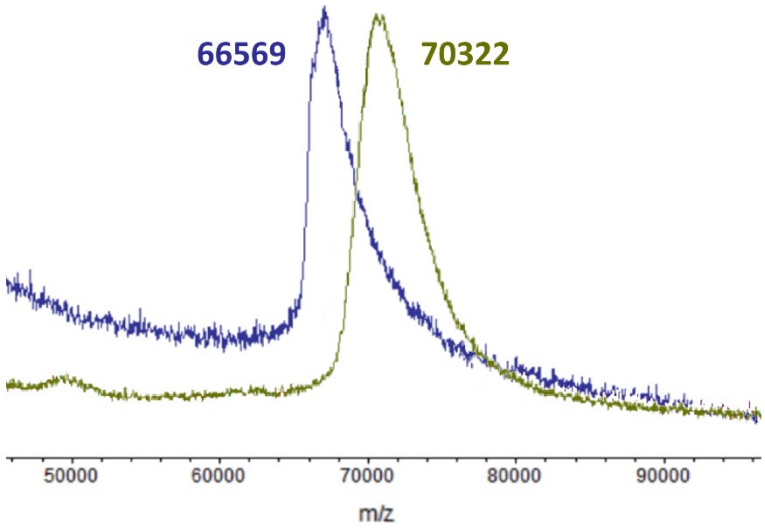

Figure 2.24. Overlapped MALDI-TOF spectra of **BSA** and **Gal-BSA (23)**. The difference in mass between the two species allows to calculate the degree of functionalisation of the BSA adducts.

A representative example of how the degree of functionalisation is calculated for the Gal-BSA glycoconjugate is shown in **Equation 2.2**.

$$\mathrm{M_{alk-BSA}} = 69468\ \mathrm{Da}, \mathrm{M_{gal}} = 263\ \mathrm{Da},$$

$$\mathrm{M_{alk-BSA}} = 70322\ \mathrm{Da} \rightarrow\ \Delta\mathrm{M} = 854\ \mathrm{Da}$$

$$854\ \mathrm{Da} \cdot \frac{1\ \mathrm{galactoside\ unit}}{263\ \mathrm{Da}} \approx 3\ \mathrm{galactoside\ units\ per\ BSA}$$

Equation 2.2. Calculation of the average number of galactoside units installed on BSA.

The number of glycans installed on the surface of BSA varied for the different glycoconjugates (data shown in **Table 2.4**). Furthermore, trials for the synthesis of Gal-BSA provided some variability in the degree of functionalisation of the protein, with different batches showing between 3 and 11 galactose units per BSA. However, for similarity with the rest of glycoconjugates **24**-**29**, the Gal-BSA glycoconjugate **23** used throughout this thesis refers to the glycoconjugate functionalised with 3 galactose units per BSA.

Table 2.4. Mass spectrometry data for the glycoconjugates **23-29** synthesised in this thesis. M_{found}: m/z average for the product of the bioconjugation. $M_{glycoside}$: molecular weight of the glycoside used for the bioconjugation. n: number of glycans installed BSA, resulting from the difference of mass observed between the glycosylated (M_{found}) and propargylated BSA ($M_{alk\text{-}BSA}$ = 69468), divided by $M_{glycoside}$.

Glycoconjugate	M_{found}	ΔM	$M_{glycoside}$	n
23	70322	854	263	3
24	70138	670	425	2
25	70596	1128	571	2
26	70539	1071	263	4
27	71094	1626	263	6
28	70539	1071	587	2
29	71267	1799	716	3

An additional experiment was performed to try to favour the CuAAC reaction by reducing the amount of oxygen present in the reaction media. The coupling reaction between 3-azidopropyl galactoside (**13**) and propargylated BSA (**22**) was performed using degassed water as solvent for both the reaction and the preparation of stock solutions of the reagents. For this purpose, nitrogen was bubbled through a sealed flask containing Mili-Q water under sonication for 2 hours before the reaction. This reaction led to the installation of 14 galactose units on the surface of BSA (Gal_{14}BSA, **23b**), which was the highest rate achieved in this research. This glycoconjugate will be compared with glycoconjugate **23** for the detection of lectins in *Chapter 3*, to evaluate the impact of the amount of glycans exhibited on the BSA in binding events.

2.4. Conclusions

Representative examples of glycoarrays developed to dissect the role of glycan density and multivalency in lectin interactions have been discussed. A thorough literature analysis has been reported in this chapter to discuss the most relevant examples of BSA glycoconjugates, the chemical approaches for their synthesis and the type of application of the neoglycoproteins. Special attention has been drawn to the state of art for reports on glycoconjugates synthesised *via* epoxide-opening chemistry, as directly relevant to the

approach adopted in this research. Surprisingly, to the best of our knowledge no BSA glycoconjugate has been reported to date using an epoxide-opening chemistry approach as the one suggested in this research work. Although many different synthetic approaches have been developed to install glycans on the surface of proteins (oximes, thioureas, amide bonds, squaramides, click chemistry, etc.), it is difficult to draw a general trend in terms of rates of functionalisation. However, most of the reports yielded glycoconjugates bearing around 10 glycan units per BSA.

A library of 3-azidopropyl glycosides has been chemically synthesised including derivatives of galactose (**13**, 26%), lactose (**14**, 27%), 2'-fucosyllactose (**15**, 20%), glucose (**16**, 10%), mannose (**17**, 54%), α3,6-mannotriose (**20**, 7%), and also enzymatically in the case of 3'-sialyllactose (**21**, 15%). For known compounds, the anomeric peaks from ^{1}H- and ^{13}C-NMR have been compared with available literature. For novel compounds only varying in aglycon with respect to literature, a similar reported compound has been used for comparison.

A novel, click methodology has been explored to functionalise BSA with propargyl moieties following epoxide-opening chemistry targeting the available lysine residues. The terminal propargyl moiety has been employed to functionalise BSA with the 3-azidopropyl glycosides through CuAAC. These glycoconjugates benefit from BSA, which is commonly used as a carrier protein. The library has been characterised through MALDI-TOF to establish the number of glycan units installed on the surface of the protein, which has ranged between 2 and 6. Only one glycoconjugate had a higher rate of functionalisation, namely Gal_{14}BSA (**23b**). This glycoconjugate will be used to investigate the impact of glycan density on lectin detection in *Chapter 3.*

The collection of BSA glycoconjugates will be used in *Chapter 3* for the synthesis of a library of gAuNPs for the detection of plant lectins in a dipstick assay format. The distribution of glycans and their spacing on the surface of the protein might provide benefits in the detection assay in comparison with the direct attachment of glycosides into the surface of the AuNPs.

2.5. Future work

The developed methodology has yielded neoglycoconjugates with a relatively uniform loading of glycans. However, it would be interesting to perform an optimisation of the BSA functionalisation conditions, allowing to control both the installation of propargyl moieties and glycans (**Figure 2.25**). In the present work, two variants of the Gal-BSA neoglycoconjugate were synthesised, with loadings of 3 and 14 galactose units of per protein (namely Gal-BSA and Gal_{14}-BSA). A collection of Gal_n-BSA neoglycoconjugates in hand bearing a range of glycan density would allow a better understanding of the role of multivalency in the gAuNP-based dipstick assay developed in the following chapter for the detection of lectins.

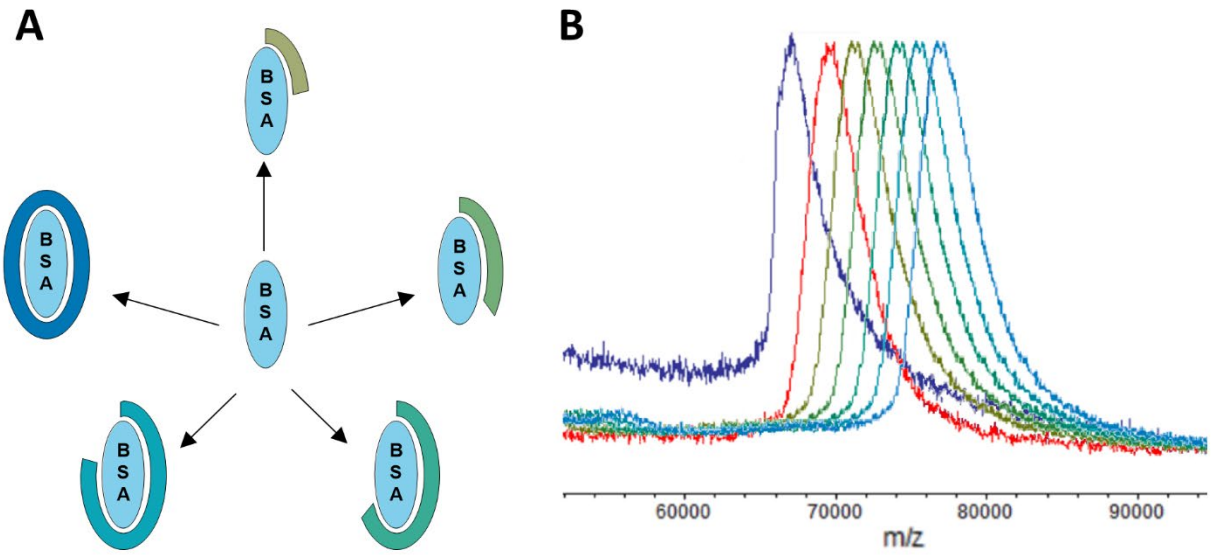

Figure 2.25. Potential future work following the results obtained in *Chapter 2*. (**A**) Schematic representation of the synthesis of a set of BSA glycoconjugates covering different degrees of glycosylation, represented as an outer ring around the BSA. (**B**) Expected overlapped MALDI-TOF spectra of **BSA**, **propargylated BSA**, and the different glycoconjugates ( ).

CHAPTER 3

A GLYCONANOPARTICLE-BASED DIPSTICK ASSAY FOR THE DETECTION OF LECTINS

3.1. Introduction

The following chapter illustrates the synthesis and characterisation of a set of gAuNPs, including *ca.* 40 nm AuNPs and *ca.* 150 nm gold nanoshells (AuNSs), and their application for the detection of lectins. The synthetic strategies and the issues encountered during their functionalisation are discussed. Different arrangements of carbohydrates on the surface of the particles, *i.e.* through a BSA glycoconjugate or covalently attached to the surface through an amide bond, were evaluated and compared for the detection of lectins in a dipstick assay. The dipstick assay has been optimised with three kinds of glyconanomaterials: 40 nm AuNPs functionalised with BSA glycoconjugates, and either 40 nm AuNPs or 150 nm AuNSs functionalised with glycan derivatives through an amide bond. The three of them will be investigated to find the best system for the detection of plant lectins in terms of sensitivity of cross-reactivity with other lectins. In this chapter, lectins are used as binding-models for the detection of bacterial proteins and adhesins.

An introduction to the general properties of AuNPs and to “in solution” bioassays, based on colour changes induced by the aggregation of a suspension of gAuNPs, is given in *Chapter 1*. The introduction in this chapter covers a literature review on the application of gAuNPs in lateral flow and dipstick assays.

3.1.1. Flow assays: lateral flow *vs.* dipstick assay

The lateral flow assay

LFAs are paper-based diagnostic tools frequently used for the detection of a wide range of pathogens and biomarkers.[231] LFAs consist of different nitrocellulose strips assembled to allow the flow of a sample across the strip. The strips used to build the LFA differ in thickness, porosity and loading of reagents such as detergents. A schematic representation of a typical Ab-based non-competitive LFA is shown in **Figure 3.1** where Abs are used as biorecognition units, although carbohydrates and aptamers have also been exploited for the development of this rapid tests. First, a specific amount of liquid sample is deposited on the sample pad (**Figure 3.1A**) and the solution flows towards a conjugation pad due to capillarity. In the conjugation pad, the sample interacts with the detection agent pre-deposited in the strip. The detection agents used in LFA are often a combination of targeting ligands such as antibodies, linked to a colorimetric label such as AuNPs (*i.e.* Ab-AuNPs), and are designed to capture the analyte of interest in the sample, (**Figure 3.1B**). The analyte-Ab-AuNPs conjugates, the sample matrix and other reagents (buffer components, detergents..) continue to flow until the test line, where a secondary Ab against the analyte of interest has been printed to capture the analyte-Ab-AuNP conjugate, often in a sandwich manner (**Figure 3.1C**). When the analyte of interest is present in the sample, this sandwich-like interaction will lead to the development of a coloured line that will indicate a positive sample. The remaining unconjugated Ab-AuNPs, the matrix and reagents continue to flow until a control line, where a secondary Ab against the primary Ab has been printed to capture the unconjugated Ab-AuNPs, developing a line that allows verification of correct flow and manufacturing of the test (**Figure 3.1D**). The rest of the matrix, reagents and unbound Ab-AuNPs continue flowing until the end of the strip, from where a cotton wick is causing the pulling force driving the assay (**Figure 3.1E**).

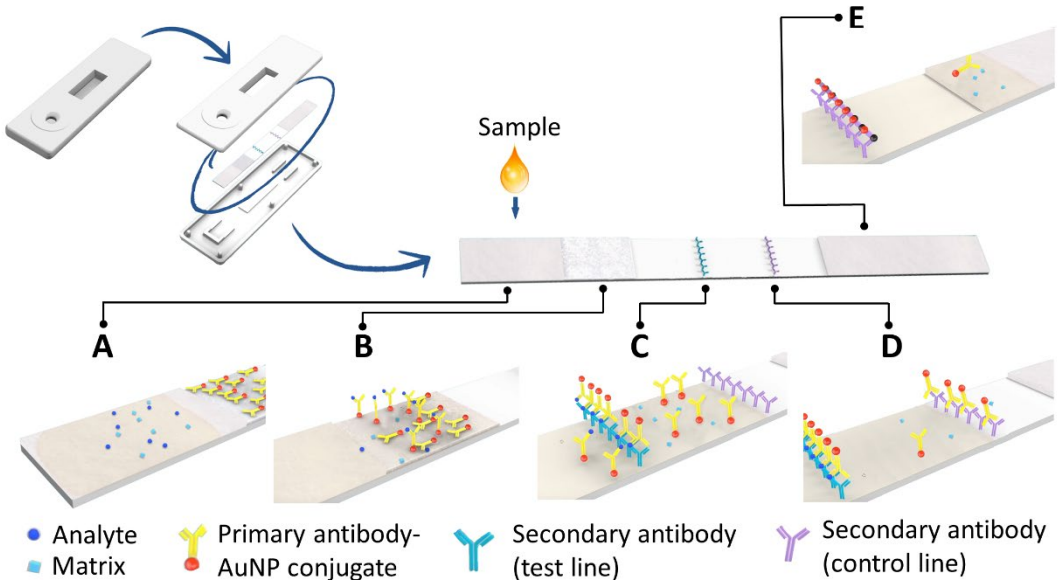

Figure 3.1. Representation of a typical Ab-based LFA. (**A**) A liquid sample is deposited on the sample pad, and it starts flowing towards (**B**) a conjugation pad where typically Ab-AuNPs have been deposited to capture the analyte present in the sample. (**C**) The captured analyte-AuNPs conjugate, sample matrix and remaining reagents continue to flow until the test line, where typically an Ab line has been printed to capture the analyte-AuNP adduct, often in a sandwich manner. (**D**) The remaining components continue to flow until the control line, where typically a secondary Ab line has been printed to capture the Abs from the AuNPs. (**E**) The remaining matrix and unbound reagents finally flow towards the end of the strip. Image adapted from Abingdon Health®.

LFAs are available for the detection of a very wide range of biomarkers, metabolites and drugs. A few representative examples of non-carbohydrate-based LFAs are discussed below, although more comprehensive reviews are recommended for a wider discussion.[232,233]

Detection assays for FDA-approved biomarkers have been developed in the last two decades. Many other LFAs have been developed over the last 25 years similarly for the diagnosis of many diseases, for example, leprosy,[234] leishmania,[235] AIDS,[236] dengue,[237] malaria,[238] or SARS-CoV-2.[239] These are often satisfactorily compared with ELISA-based detection protocols, which probes the potential of LFA as diagnostic tools. An example of this is the detection of the kidney injury molecule (KIM-1 in humans) in urine samples for the early diagnosis of acute kidney injury.[240] The detection agents in the developed assay were *ca*. 40 nm AuNPs functionalised with a polyclonal anti-KIM-1 Ab that would act in a sandwich manner with a test line composed of an epitopically distinct anti-KIM-1 Ab (**Figure 3.2**). The control line was made of an anti-rabbit Ab for the capture of the functionalised AuNPs. The assay was employed using three different nephrotoxicity models: cadmium-, gentamicin- and ischemia-

induced damage. The test reached a LOD of 0.8 ng/mL of KIM-1, in parallel to results previously obtained with ELISA-based testing. The developed assay was applied on two real post-surgery patients that had received cisplatin chemotherapy, to monitor their potential kidney damage.

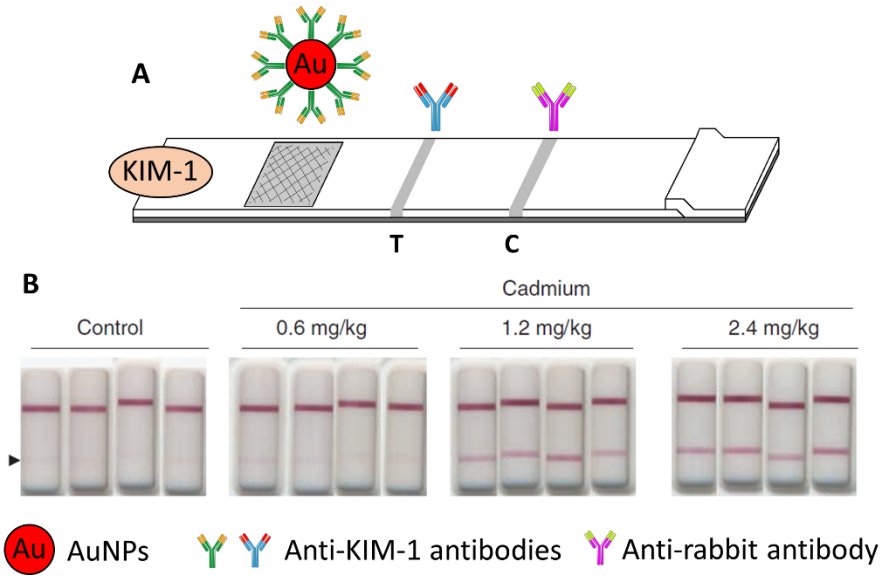

Figure 3.2. (**A**) Schematic representation of the sandwich assay developed for the detection of the KIM-I biomarker. The assay employed 40 nm AuNPs functionalised with an anti-KIM-1 Ab, a test line with an epitopically different Ab, and an anti-rabbit Ab in the control line. (**B**) Representative results of one of the three different nephrotoxicity models studied in that work, where doses of cadmium were administrated to rats. Figure reproduced from Vaidya *et al.*[240] with permission from Elsevier.

Ab-based LFAs have also been reported for the detection of pharmacologically active compounds and drugs. For example, a competitive LFA was developed for the detection of indomethacin, an anti-inflammatory drug whose stability in water represents a risk of intoxicating aquatic systems,[241] in water samples from Chengdu (China).[242] Competitive LFAs are slightly different to the one described in **Figure 3.2**, also known as sandwich assays. In the competitive format, the test line contains the analyte rather than the anti-analyte Ab. Therefore, the presence of the analyte in the sample leads to blocking the Ab-AuNPs before they reach the test line, which prevents their interaction with the analytes deposited in the test line. When no analyte is present in the sample, the Ab-AuNPs are captured by the test line. The assay for the detection of indomethacin included *ca.* 20 nm AuNPs functionalised with anti-indomethacin Ab, a test line consisting of an indomethacin-ovalbumin conjugate, and a control line made of anti-rabbit Abs (**Figure 3.3A**). The developed assay detected

indomethacin in water in a rapid and efficient manner. The results obtained showed a visual LOD of 0.1 ng/mL (**Figure 3.3B**), which is comparable with the testing through ELISA.

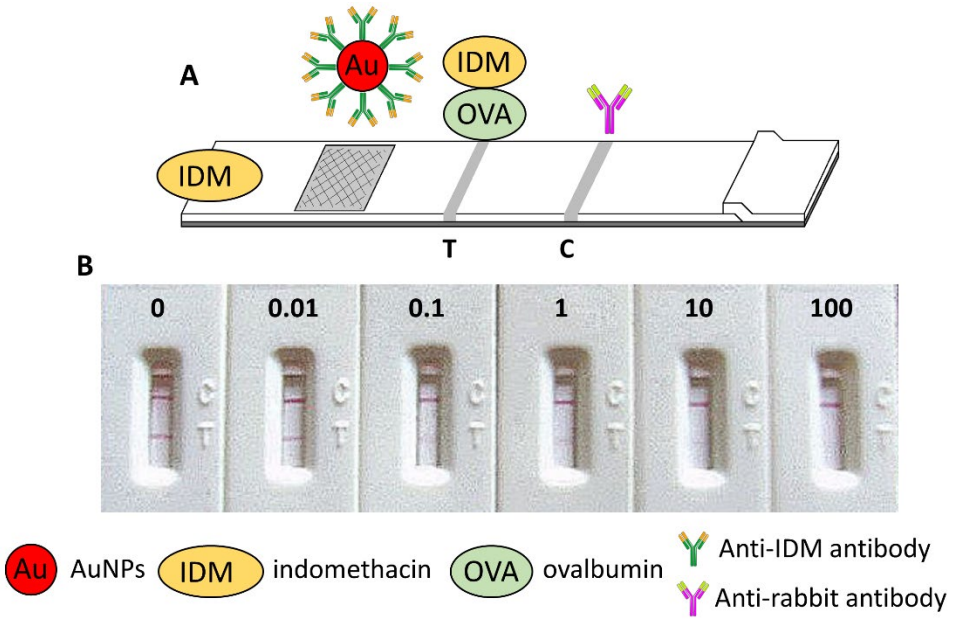

Figure 3.3. (**A**) Schematic representation of the competitive assay developed for the detection of indomethacin. The assay employed *ca*. 20 nm AuNPs functionalised with an anti-indomethacin Ab, a test line with indomethacin-conjugated ovalbumin and a control line with an anti-rabbit Ab. (**B**) Assessment of the sensitivity of the assay for the detection of indomethacin in the 0 – 100 ng/mL range. Figure reproduced from Li *et al.*[242] with permission from Elsevier.

Similar technologies have been developed over the years for the detection of other drugs in water, such as ibuprofen,[243] diclofenac,[244] morphine,[245] fentanyl[246] or cocaine,[247] among many.

The dipstick assay

In a dipstick assay, the analyte is bound to the surface of a nitrocellulose strip overlapped with a cotton wick to generate a pulling force in the assay (**Figure 3.4A**). The dipstick assay starts with the deposition of a specific analyte on the nitrocellulose strip (**Figure 3.4B**), which is then conditioned with a buffer to block the rest of the strip (**Figure 3.4C**). In the next step, a solution containing the detection agent is allowed to flow along the strip (**Figure 3.4D**) to develop a signal due to the interaction with the target (**Figure 3.4E**). The dipstick format is ideal to test interactions between AuNPs functionalised with biorecognition molecules and an analyte under controlled conditions as a preliminary step before developing a LFA.

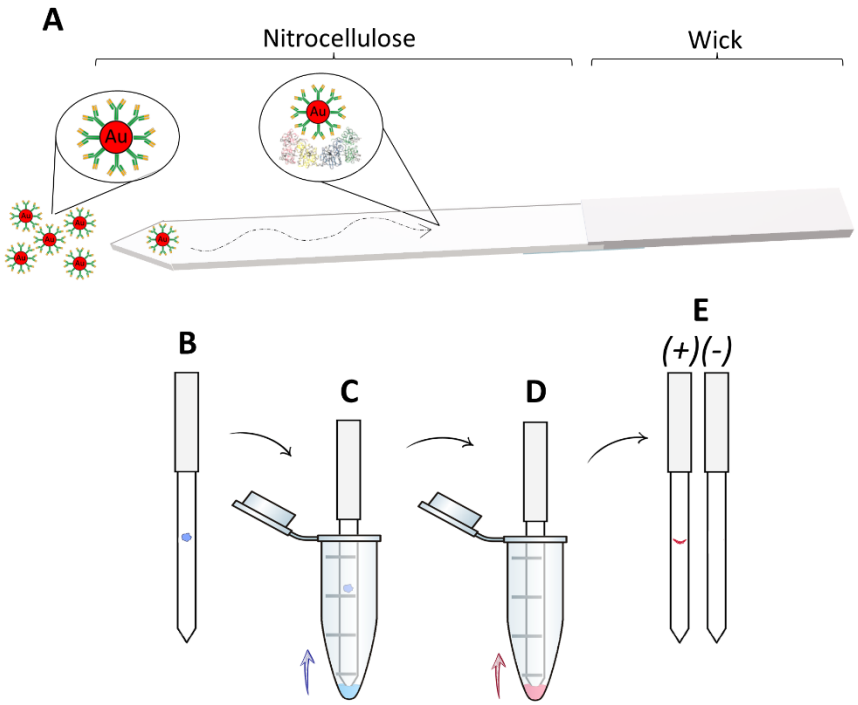

Figure 3.4. Schematic representation of the workflow of a typical dipstick assay. (**A**) Magnified dipstick showing the interaction of a functionalised AuNP with a pre-deposited analyte. The dipstick assay starts with (**B**) the deposition of an analyte that will bind to the nitrocellulose strip and (**C**) blocking the strip allowing a buffer to run along. (**D**) The nitrocellulose strip is dipped in a solution of the functionalised AuNPs of interest, which flows until they reach (**E**) the deposited target to develop a colorimetric signal.

The dipstick format explained in **Figure 3.4** is the one adopted in this thesis; however, there is no specific definition for what constitutes a dipstick assay, other than the need to dip a nitrocellulose strip on a solution of the detection agent. In many cases, the assay format also includes a conjugation pad with functionalised AuNPs, so the only difference with a LFA is the application of the sample, which is absorbed in the nitrocellulose strip directly from a vial instead of deposited into the sample pad. The dipstick technology has been adopted for the detection of many analytes including toxins and drugs, very often incorporating Ab-AuNPs in the assay as detection agents. Examples of targeted analytes include, for example, the detection of salmonella Abs,[248] aflatoxin,[249,250] the meningitis-related cryptococcal polysaccharide capsule,[251] or heroin.[252]

3.1.2. Carbohydrates as an alternative to antibodies for detection assays

Traditionally, AuNP-based assays have benefitted from the high selectivity and sensitivity that Abs feature for detection purposes. However, Abs are subjected to availability, storage limitations, restrictive assay conditions and the high economic investment to produce them.[253]

Carbohydrates are potentially suitable biomolecules as alternatives to Abs in detection assays.[45] Not many head-to-head comparisons of the performance of Abs and carbohydrates are available in the literature, however, a report was published comparing both for the detection of ricin in a quartz crystal microbalance experiment.[254] That technique involved the exposure of a layer of either the ganglioside mono-sialic acid 1 (GM1) or anti-RTB Ab to ricin to measure in an extremely sensitive way mass changes upon loading of the analyte. The results showed a LOD of 0.1 µM when using Abs, which was improved by the application with GM1 to 0.04 µM. The linear range of the assay was also improved when carbohydrates were used as biorecognition molecules, from 25 – 50 µg/mL of RTB for the Ab-based assay to 5 – 100 µg/mL of RTB when GM1 was used. However, even though there is potential to improve sensing properties, the use of glycans for detection applications inherently brings a decrease in specificity. Abs, especially monoclonal ones, are designed to target only one antigen, while a glycan such as galactose will bind to a range of different structures (*i.e.* RCA_{120}, ricin, LecA…).

A series of LFAs have been developed and compared for the detection of *V. cholerae* CT.[255] To compare the performance of GM1, aptamers and Abs as ligands in either the capturing agent (AuNPs/liposomes) or the test line, four different assays were developed. The first one (**Figure 3.5A**) included GM1-functionalised liposomes, a test line with CT-binding aptamer CT916 and a control line with CT to capture the liposomes. The second one (**Figure 3.5B**) was a competitive assay where the test line contained CT to trap CT916-functionalised AuNPs in case of a negative test, with a control line containing a complementary aptamer for CT916. The third assay (**Figure 3.5C**) was a sandwich one using CT916-AuNPs as detecting agents, with an anti-CT Ab in the test line to capture a CT-CT916-AuNPs conjugate in a positive sample, and a CT916 complimentary aptamer-based control line. The fourth assay (**Figure 3.5D**) was a variation of the third one, adding a pre-incubation step to mix the sample with a solution of a primary anti-CT Ab to capture the CT from a positive sample. Once the pre-incubated sample is applied to the test, an Ab-CT-CT916-AuNP conjugate is formed. The test line included secondary anti-rabbit Abs to capture the Ab-CT-CT916-AuNP conjugate. The assays were

tested for concentrations of toxin ranging from 0 – 10,000 µg/mL, with visual limits of detection of 10, 100, 10 and 1 ng/mL, respectively, for the respective approaches. This work represented a good comparison of the different approaches that can be taken for the development of LFAs. Even though the GM1-based assay did not provide the best performance in this comparison, it was probed to be a good candidate with results comparable to the ones coming from Abs.

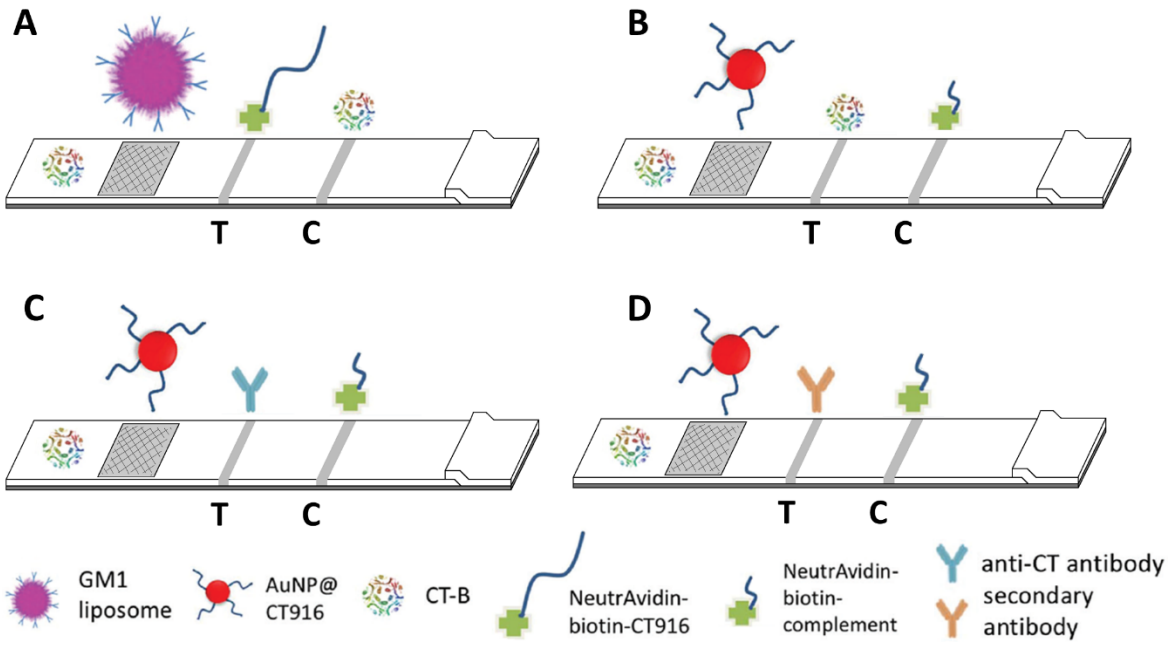

Figure 3.5. Schematic representation and comparison of four different LFAs for the detection of cholera toxin. (**A**) GM1-functionalised liposomes with a test line composed of CT-binding aptamer CT916 and a control line composed of CT. (**B**) CT916-AuNPs with a test line composed of CT and a control line composed of a complementary aptamer for CT916. (**C**) CT916-AuNPs with a test line composed of anti-CT Ab and a control line composed of a complementary aptamer for CT916. (**D**) The sample is pre-mixed with a solution of a primary anti-CT antibody to capture CT. The pre-mixed sample is applied to the test, where Ab-CT-CT916-AuNP are formed. The test line was composed of a secondary Ab for the anti-CT Ab, and a control line composed of a complementary aptamer for CT916. Reproduced from Frohnmeyer *et al.*[255] with permission from the Royal Society of Chemistry.

3.1.3. Glyconanoparticle-based flow assays

Despite the promising results of gAuNPs in detection assays and the broad range of "in solution" aggregation-based bioassays that have been developed to date (as discussed in *Chapter 1*), their potential has not been widely explored in flow assays yet. This point was

made in a recent review by Baker *et al.*[256] The available literature regarding carbohydrate-based lateral flow and dipstick assays is discussed below.

The first example of gAuNP-based dipstick assay reported in the literature employed reversible addition-fragment chain transfer (RAFT) polymerisation for the synthesis of thiol-ending p-(*N*-acrylamidophenyl)-α-galactoside for the detection of the galactose-binding Shiga toxin Stx1.[257] Upon attachment of the glycopolymer to a gold surface, the interaction with Stx1 was proven *via* SPR (**Figure 3.6A**). The glycopolymers were also attached to *ca*. 40 nm AuNPs (**Figure 3.6B**) and an aggregation assay probed the interaction with peanut agglutinin (PNA) as a model lectin of binding to galactose. The work attempted for the first time a gAuNPs-based paper-based assay. The authors reported the detection of 1 µg of Stx1 (**Figure 3.6C**); however, the intensity of the spot was too poor to verify an actual interaction.

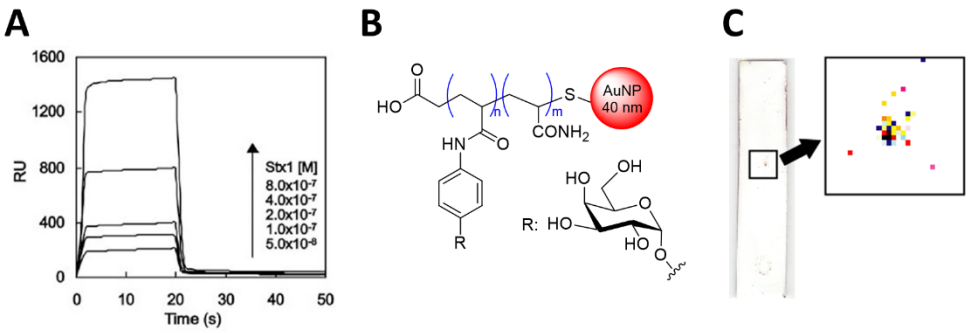

Figure 3.6. First example of a gAuNP-dipstick. (**A**) SPR results confirming the interaction between the poly-[p-(*N*-acrylamidophenyl)-α-galactoside] and Stx1. (**B**) Synthesised glycopolymer-functionalised 40 nm AuNPs applied to (**C**) a dipstick assay for the detection of 1 µg of Stx1. Reproduced from Toyoshima *et al.*[257] with permission from Springer Nature.

In a follow-up work, the authors investigated the development of a LFA implementing the synthesised glycopolymer, with a special interest in the optimisation of the glycan density on the surface of the AuNPs.[258] In that work, RAFT polymerisation afforded thiol-ending co-polymers of p-(*N*-acrylamidophenyl)-α-mannoside and acrylamide in different ratios (0%, 6%, 12% and 50% of sugar loading was tested) that were installed on the surface of *ca.* 40 nm AuNPs for the detection of ConA in a LFA (**Figure 3.7A**). A first screening of the four gAuNPs showed that, whereas the ones containing 6 and 12% of glycan loading in the polymer would successfully detect ConA, the ones with a higher ratio (50%) aggregated at the bottom of the dipstick. The evaluation of the assay showed a 10-fold sensitivity improvement when using the particles containing 6%, in comparison with the ones containing 12% (**Figure 3.7B**). The

importance of tuning the density of glycans on the surface of AuNPs for detection bioassays has been discussed in *Chapter 1*. Importantly, that work showed for the first time the potential use of carbohydrate ligands for the rapid and visual detection of glycan-binding analytes in a lateral flow format.

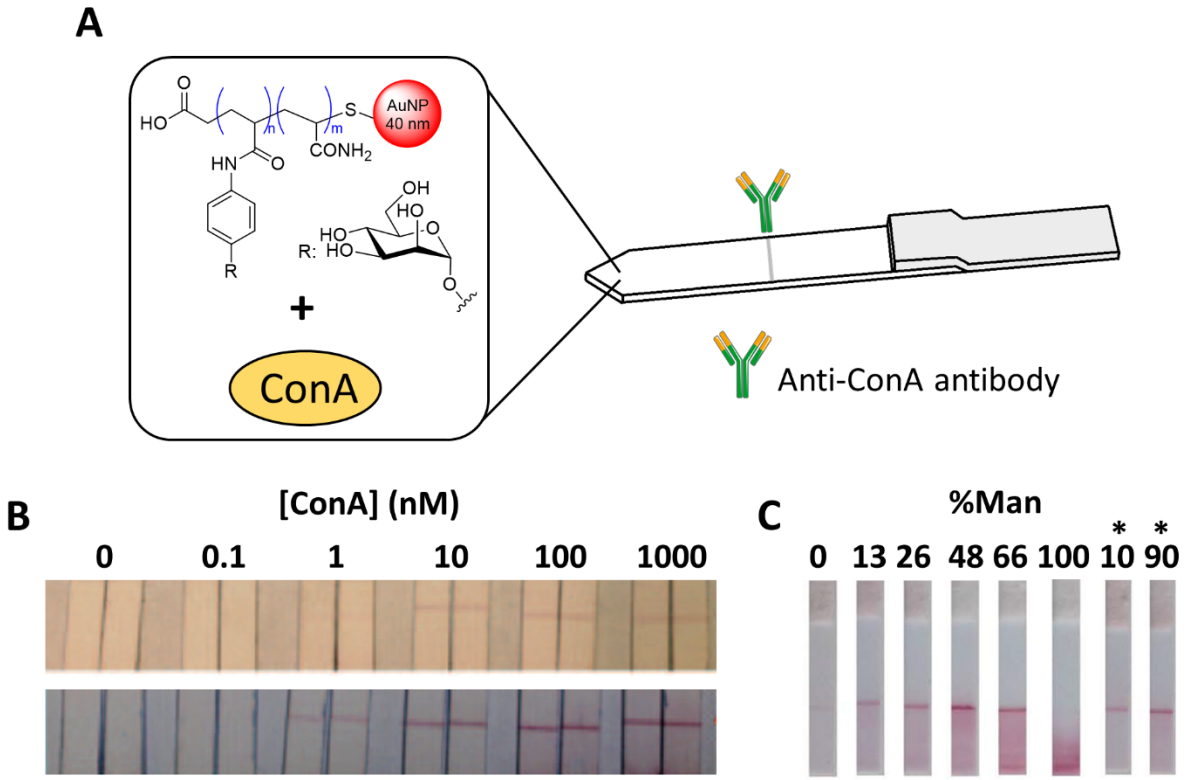

Figure 3.7. (**A**) Schematic representation of a dipstick assay for the detection of ConA employing 40 nm AuNPs functionalised with a co-polymer of p-(*N*-acrylamidophenyl)-α-mannoside and acrylamide. (**B**) Sensitivity studies for the detection of ConA at different concentrations. The top and bottom employed, respectively, gAuNPs containing glycopolymers with 6 and 12% of glycan loading (adapted from Ishii *et al.*[258] with permission from CSJ Journals). (**C**) Extension of the study, assessing the performance of gAuNPs functionalised with the glycopolymer containing different loadings (%) of mannose for the detection of ConA (240 nM). (*) Instead of varying the glycan loading in the glycopolymer, those gAuNPs were synthesised with a mixture of glycopolymer containing 100% Man and acrylamide (the percentage given represents the glycopolymer). Adapted from Takara *et al.*[259] with permission from the Royal Society of Chemistry.

The same authors published an extension of that work a few years later, with a more detailed study of the glycan loading in the glycopolymer.[259] Employing the same assay and type of thiolated acrylamide glycopolymer, gAuNPs were synthesised with different loadings of mannose. Glycan loadings were measured as the ratio of monomers used for the synthesis of the glycopolymer. The performance of these gAuNPs in the dipstick assay (**Figure 3.7C**)

showed the difference between using only glyco-polyacrylamide (100% mannose) or diluting the surface of the AuNPs (10%, 90%) with polyacrylamide. The latter option was probed to help the gAuNPs to flow better along the nitrocellulose strip, preventing the smearing and yielding a more efficient detection assay.

More recently, and with the need for rapid and cost-efficient assays for the detection of SARS-CoV-2 due to the covid-19 pandemic, other examples implementing gAuNPs in flow assays have been reported. The first report of this series employed RAFT polymerisation to synthesise a sialic acid-ending poly(*N*-hydroxyethyl acrylamide) (PHEA) (**Figure 3.8A**).[260] In that work, the length of the polymer ($PHEA_{40}$, $PHEA_{50}$, $PHEA_{58}$) and the size of the AuNPs (16 nm, 35 nm) were evaluated to find the optimal presentation of glycans on the particle aiming at the detection of the spike protein of the virus (**Figure 3.8B**). The dipstick assays showed the superior performance of 35 nm AuNP functionalised with either the $PHEA_{40}$ or $PHEA_{50}$ glycopolymers, with a visual LOD of the spike protein of 0.008 mg/mL.

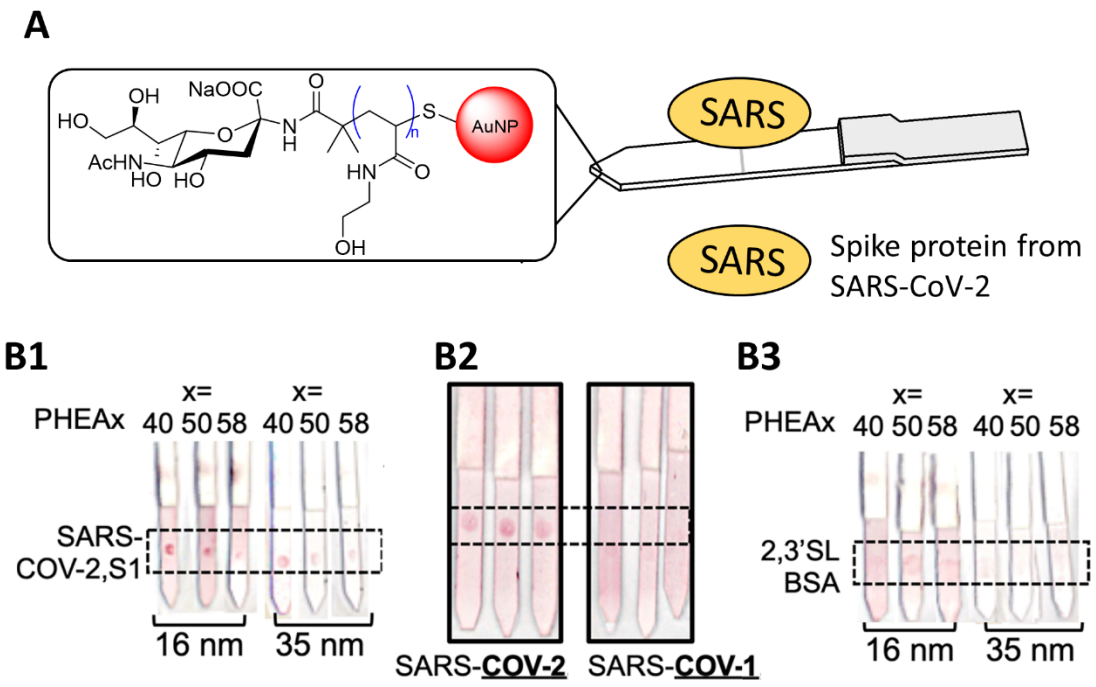

Figure 3.8. (**A**) Schematic representation of the dipstick assay for the detection of the SARS-CoV-2 spike protein (SARS-COV-2,S1) with sialic acid-functionalised AuNPs. (**B1**) Detection of the spike protein with all the gAuNPs synthesised, comparing the length of the glycopolymer ($PHEA_{40}$, $PHEA_{50}$, $PHEA_{58}$) and the size of the AuNPs (16 nm, 35 nm). (**B2**) Detection of SARS-CoV-2 with $PHEA_{50}$-functionalised 35 nm AuNPs, and SARS-CoV-1 as control. (**B3**) Controls performed with sialyllactose-functionalised BSA (2,3'SL-BSA) for all the gAuNPs synthesised. Adapted from Baker *et al.*[260] (CC-BY).

The authors published a follow-up work soon after for the development of a lateral flow device.[261] That report explored the concept of "flow-through" assay, as the samples from patients were not applied in a sample pad but deposited in the nitrocellulose strip to form a test line instead. The system was tested for the detection of SARS-CoV-2 in PCR-validated patient samples, achieving sensitivity rates of 85%. To improve the sensitivity of the assay, the authors indicated the need to optimise the assay buffer to minimise non-specific interactions, and also the possibility of false negatives due to the gAuNPs not interacting with heat-inactivated viruses (which may present damaged spike proteins). Importantly, the specificity of the assay was tested, showing no cross-reactivity with other respiratory pathogens such as the human and avian influenza virus.

The same authors progressed in the development of their gAuNPs-based flow assays, with a special interest in optimising the particle size, length of the glycopolymer and density of glycans on the surface of the gAuNPs (**Figure 3.9A**).[262] For this, a galactose-ending thiolated PHEA was synthesised using the previously developed RAFT polymerisation, yielding four different glycopolymers ($PHEA_{26}$, $PHEA_{40}$, $PHEA_{72}$, $PHEA_{110}$). Those polymers were used to functionalise AuNPs of either 16 or 40 nm, combined with non-glycosylated PHEA in different percentages (0, 33, 66, 100%) to allow the dilution of glycan density on the surface of the AuNPs. The assessment of the 32 types of gAuNPs consisted of the detection of the galactose binding soyben agglutinin (SBA) at 0.05 mg/mL in a dipstick assay. The authors observed that more intense signals were obtained with longer glycopolymers, although non-specific binding also increased. A higher glycan density on the surface of the AuNPs, and 40 nm gAuNPs, produced a higher signal-to-noise ratio. Taking those observations into account, the choice of optimal gAuNPs was Gal-$PHEA_{72}$-functionalised 40 nm AuNPs. The optimised gAuNPs were implemented in a sandwich LFA for the detection of SBA, where the test line was a Galα1-3-Galβ-1-4-GlcNAc-BSA glycoconjugate, reaching a visual LOD of 0.05 mg/mL (**Figure 3.9B**).

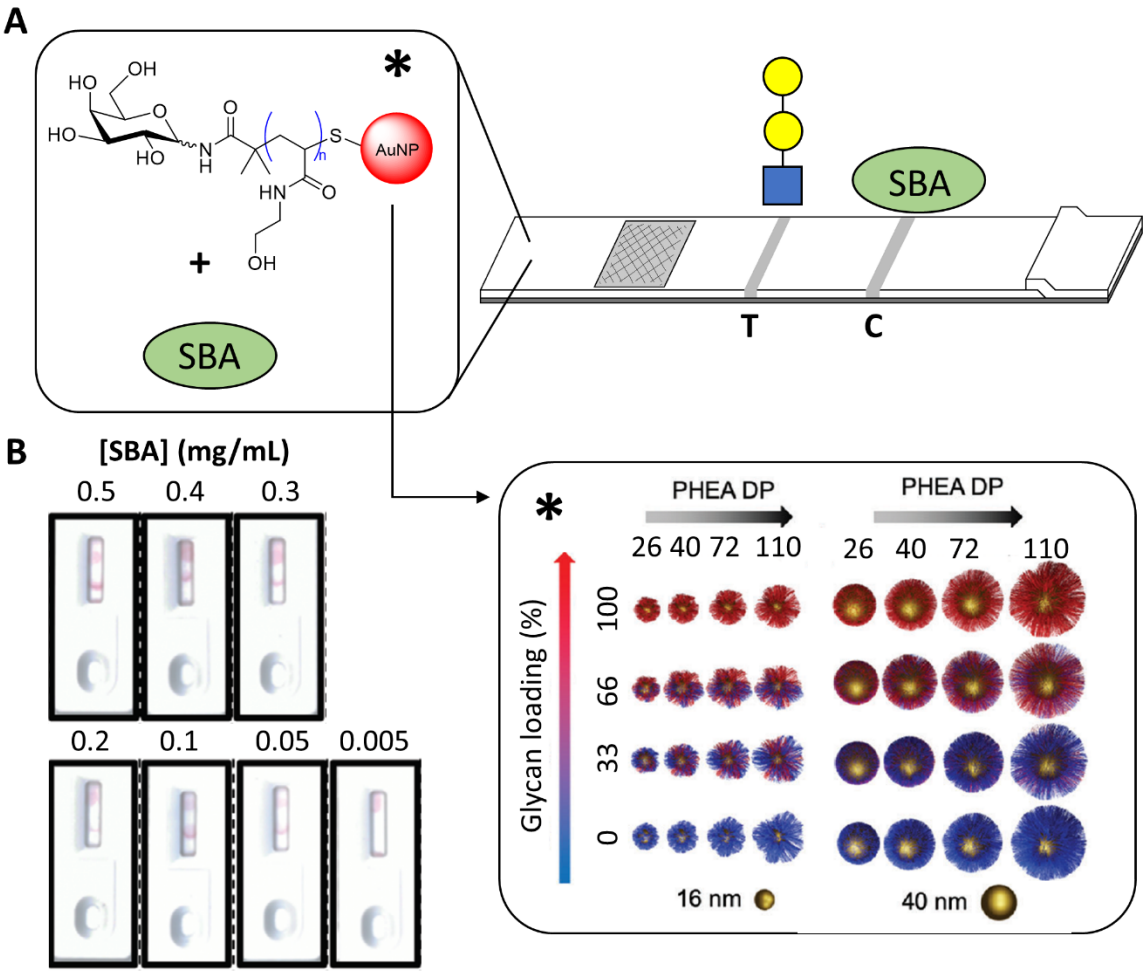

Figure 3.9 (**A**) Schematic representation of the developed lateral flow device for the detection of SBA. 24 different gAuNPs were synthesised in a preliminary study to optimise the length of the glycopolymer (degrees of polymerisation 26, 40, 72 or 110), the diameter of the AuNPs (16 or 40 nm) and the loading of glycans on the surface (0, 33, 66. 100%). (**B**) Lateral flow devices show a dynamic range of 0.5 – 0.005 mg/mL of SBA, with a visual LOD of 0.05 mg/mL. Adapted from Baker *et al.*[262] (CC-BY).

Efforts have been made to further improve glycan-based flow assays, tuning not only the detection agents but also the test lines. Very recently, poly(vinylpyrrolidone) (PVP) was proposed as an alternative to the traditional Ab-based test lines.[263] The availability of NHS-ester-activated PVP opens a door to the design of polymeric test lines functionalised on demand for the detection test, for example, GalNAc-PVP to develop interactions with SBA, or biotinylated PVP to interact with streptavidin-AuNPs. This work probed that the molecular weight of the polymer, as well as the concentration applied to the test line, had a direct impact on the performance of the assay, but the trends were not clear, *i.e.*, it has to be evaluated on a case-by-case basis. Another example of protein-free test lines in glycan-based LFAs, took advantage of the cell glycocalyx to develop a LFA for SARS-CoV-2.[264] The namely GlycoGrip

technology exploited glycosaminoglycans from the cellular glycocalyx as a multivalent means to capture the virus due to their binding affinity for the spike protein. Anti-spike Ab-labelled 40 nm AuNPs allowed the labelling of the virus, being able to detect the different variants of the virus, both in buffer and in human saliva.

3.1.4. Gold nanoshells in flow assays

As discussed in the previous section, the impact of the size of the AuNPs in the design of LFAs has been investigated. Traditionally, *ca*. 30 – 40 nm AuNPs were used for LFAs due to their bright colour and contrast, while being reasonably stable.[265] Assays employing AuNPs in the 16 – 100 nm range have reported that bigger sizes can improve the sensitivity of the colorimetric assays.[262,266] However, the increase in AuNP size also brings technical challenges related to the stability of the particles and their diffusion through the nitrocellulose strip. Another option to allow better stability due to a lighter core while still exhibiting a large gold surface are shell@core Au@Si nanoshells (gold nanoshells, AuNSs, **Figure 3.10**), which are under-represented in current LFA literature. Up to date, reports involving AuNSs are less advanced and mostly proof-of-concept works, as the optimal methodologies for their implementation in bioassays and advantages against AuNPs have not been fully understood. To the best of our knowledge, no examples of gold glyconanoshells (gAuNSs) have been reported in the literature up to date.

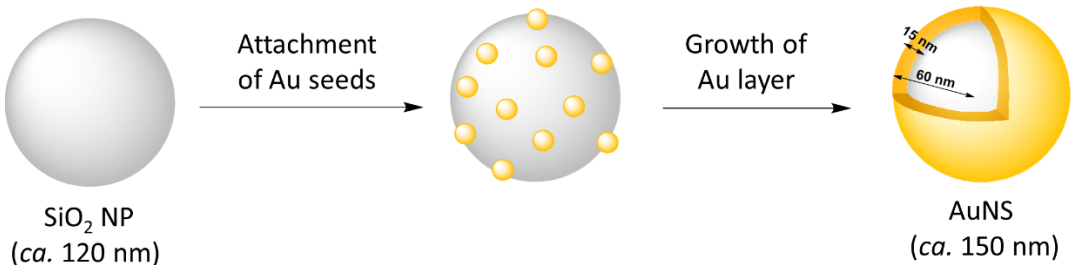

Figure 3.10. Representation of the seeding and growth of a layer of gold around a pre-synthesised silica NP to form a AuNS.

Following the same trend of traditional AuNPs, functionalised AuNSs can also undergo aggregation in the presence of a multivalent target, which can be followed visually and through UV-Vis. As a proof-of-concept, an aggregation-based assay in solution was reported with Ab-functionalised shell@core 118 (22@96) nm AuNSs for the detection of rabbit immunoglobulin in human whole blood samples.[267]

A rapid diagnostic tool was developed with *ca.* 150 (20@110) nm AuNSs for the detection of three immunogenic peptides from *Onchocerca volvulus* (onchocerciasis).[268] In that work, commercially available AuNSs were functionalised with Abs following an NHS-ester activation and subsequent protein bioconjugation. The assay allowed the detection of the targeted biomarkers with a sensitivity comparable to the one obtained through ELISA, although some cross-reactivity with viral, malaria and other parasite-related peptides was observed. This was a proof-of-concept work, helping to establish new methodologies for less explored colorimetric labels such as AuNSs. A comparison between *ca*. 15 nm AuNPs and a series of AuNSs ranging 130 – 210 (15@100-150-180) nm was performed in a dot immunoassay.[269] As a preliminary work, all the particles were functionalised with an anti-rabbit Ab to detect normal rabbit serum. These results indicated that the biggest nanoshells tested could improve the detection limit of the assay from 16 ng to 0.2 ng, with a working range of 0.1 to 1,000 ng (**Figure 3.11**).

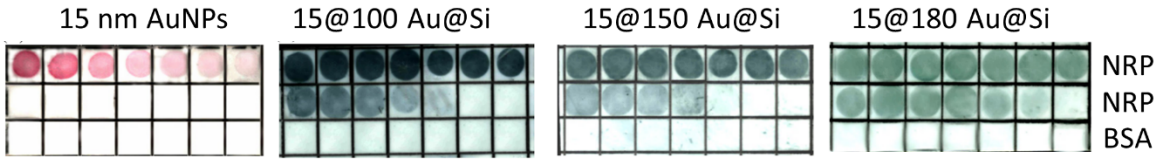

Concentration guide (µg)

1000	500	250	125	62	31	16
8	4	2	1	0.5	0.2	0.1
10	10	10	10	10	10	10

Figure 3.11. Dot immunochromatographic assay for the detection of normal rabbit serum (NRP) in serial dilutions starting from 1,000 to 0.1 ng. Different sized particles functionalised with anti-rabbit Abs were employed, including 15 nm AuNPs and shell@core 15@100 nm, 15@150 or 15@180 nm Au@Si. The bottom row represents a negative control with BSA instead of NRP. Adapted from Khlebtsov *et al.*[269] with permission from IOP Publishing.

Recently, a rapid test for the diagnosis of hyperthyroidism was developed with Ab-functionalised *ca*. 150 (15@120) nm AuNSs.[270] The functionalisation consisted of an easy-to-perform EDC/sulfo-NHS coupling of anti-thyroid stimulating hormone Ab. The test improved the LOD of traditional AuNP-based LFAs by a factor of 25 (LOD reported in activity units as 0.16 µIU/mL) (**Figure 3.12A**). The assay was also applied in human serum plasma to study the matrix effect, and although the authors claimed that the assay did perform without

complications, a clear drop in intensity is observed in the control line, which became barely visible. The methodology developed did not seem to work for the 40 nm AuNPs given the absence of a control line in the LFAs (**Figure 3.12B**), although this is not discussed by the authors.

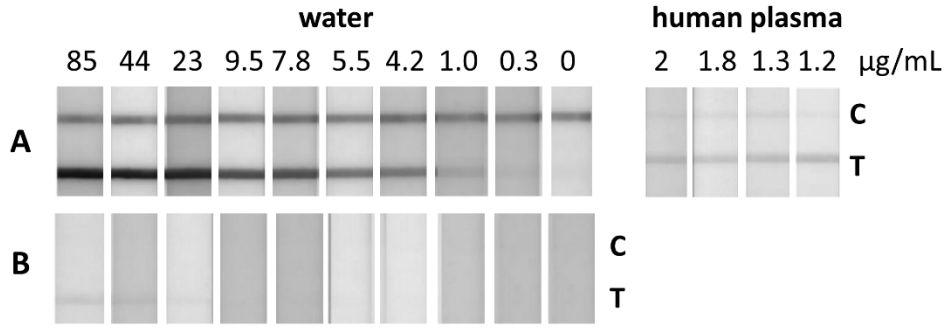

Figure 3.12 Lateral flow assays for the detection of thyroid stimulation hormone at different concentrations with (**A**) shell@core 15@120 nm AuNSs in either water or human plasma, or (**B**) 40 nm AuNPs. Adapted from Bikkarolla *et al.*[270] with permission from MDPI Publishing.

3.2. Aims

The aim of this chapter is to find the most suitable presentation of carbohydrates on a gold surface for the development of a dipstick assay for the detection of lectins, with especial interest on RCA_{120}. For this, three types of glyconanomaterials including 40 nm glyco-BSA-AuNPs, 40 nm glyco-AuNPs and 150 nm glyco-AuNSs were investigated, and their lectin-binding selectivity and sensitivity was assessed in a dipstick assay format (**Figure 3.13**). The work in this chapter will serve as the basis to establish the assay for the potential detection of the pathogenic lectin LecA from *P. aeruginosa.*

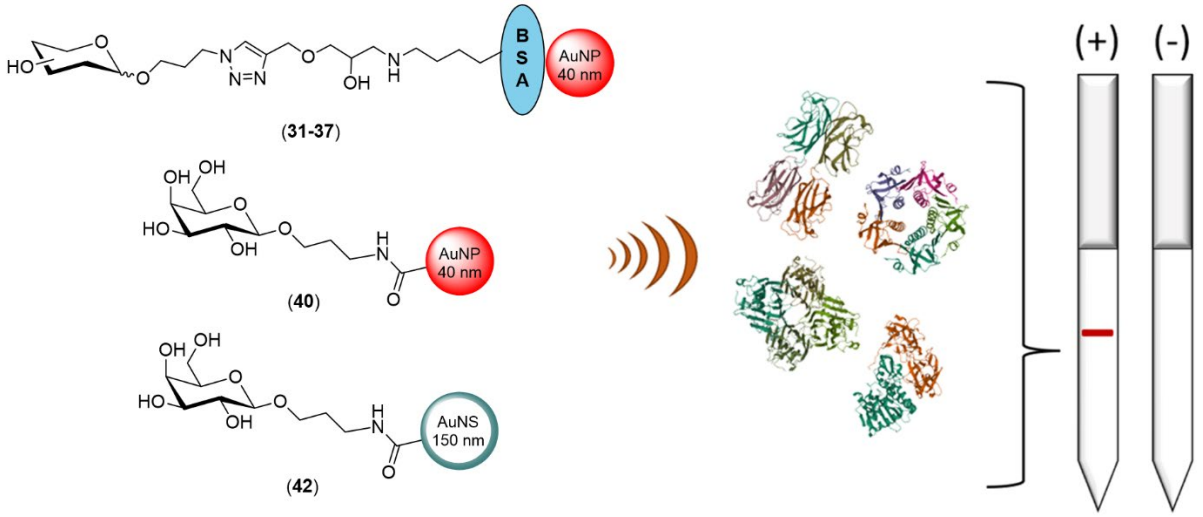

Figure 3.13. The scientific aim of *Chapter 3*. On the left, the target glyconanomaterials that will be synthesised and characterised. On the right, a schematic representation of the application of said glyconanomaterials for the detection of plant lectins in a dipstick format.

3.3. Results and discussion

3.3.1. Synthesis of glyco-BSA-AuNPs

Commercially available citrate-capped *ca.* 40 nm AuNPs (cit-AuNPs) were functionalised with the BSA conjugates **22-29** *via* passive adsorption. The methodology followed for the functionalisation of the AuNPs has been previously reported and consists in a ligand exchange process to introduce a protein on the surface of the particles, replacing the original citrate.[65,271] Therefore, BSA develops an electrostatic interaction with the surface of the particle.[64] The reaction mixture contained cit-AuNPs OD 5 and 250 µg/mL of the BSA conjugate in citrate buffer (2 mM pH 5.3) (**Scheme 3.1**). The protocol followed has been previously optimised at Iceni Glycoscience Ltd. and it results in reproducible functionalised nanoparticles.

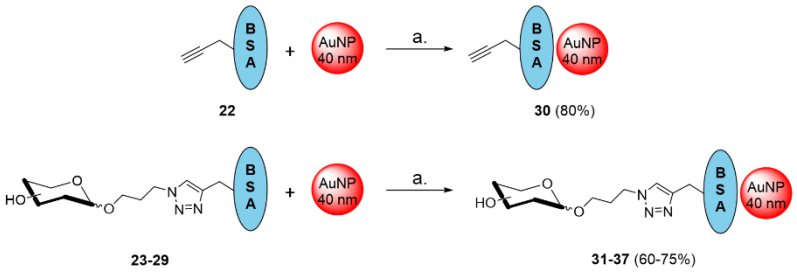

Scheme 3.1. Functionalisation of 40 nm AuNPs through passive adsorption with the propargylated BSA conjugate **22** or the BSA glycoconjugates **23-29**. This pathway yielded functionalised AuNPs **30-37**. Reagents and conditions: the reaction mixture contained citrate-capped 40 nm AuNPs OD 5 and 250 µg/mL of carbohydrate-BSA conjugate in (**a**) citrate buffer 2 mM pH 5.3, r.t., o.n.

This methodology yielded propargyl-BSA-AuNPs (**30**, 80%), Gal-BSA-AuNPs (**31**, 70%), Gal_{14}-BSA-AuNPs (**31b**, 65%), Lac-BSA-AuNPs (**32**, 70%), 2'FL-BSA-AuNPs (**33**, 70%), Glc-BSA-AuNPs (**34**, 60%), Man-BSA-AuNPs (**35**, 70%), α3α6Man-BSA-AuNPs (**36**, 75%), and 3'SL-BSA-AuNPs (**37**, 70%). AuNPs **30** and **31** were analysed through TEM to study possible post-functionalisation aggregation (**Figure 3.14A**). Some variability was found in the size measured by TEM in the AuNPs **30** (39 ± 0.5 nm) and **31** (42 ± 0.4 nm); however, this was in agreement with the specifications given by the provider of the cit-AuNPs (40 ± 4 nm). Analysis of the UV-Vis spectra of the set of gAuNPs showed a shift of the maximum of absorbance between 2 and 3 nm, except for the gAuNPs **31b** that exhibited a shift in the absorption maximum of 1 nm (data plotted in **Figure 3.14B**, tabulated in *Chapter 5*). The observed shift is an indication of the successful functionalisation, as the SPR maximum of absorbance is directly impacted by the surface of the AuNPs. The DLS data for the set showed an increase in hydrodynamic diameter between 7 and 8 nm following functionalisation, except for the gAuNPs **31b** for which the increase was 5 nm (data plotted in **Figure 3.14C**, tabulated in *Chapter 5*). It is remarkable from both the UV-Vis and the DLS data, how the whole set of particles (propargylated, and glycosylated) exhibited a relatively uniform shift in absorbance and hydrodynamic diameter. In both cases, Gal_{14}-BSA-AuNPs **31b** showed a smaller shift: 1 nm for the UV-Vis and 5 nm for the DLS. This means that the increased amount of glycan units in the BSA glycoconjugate had an impact on how the protein laid on the surface of the gAuNPs.

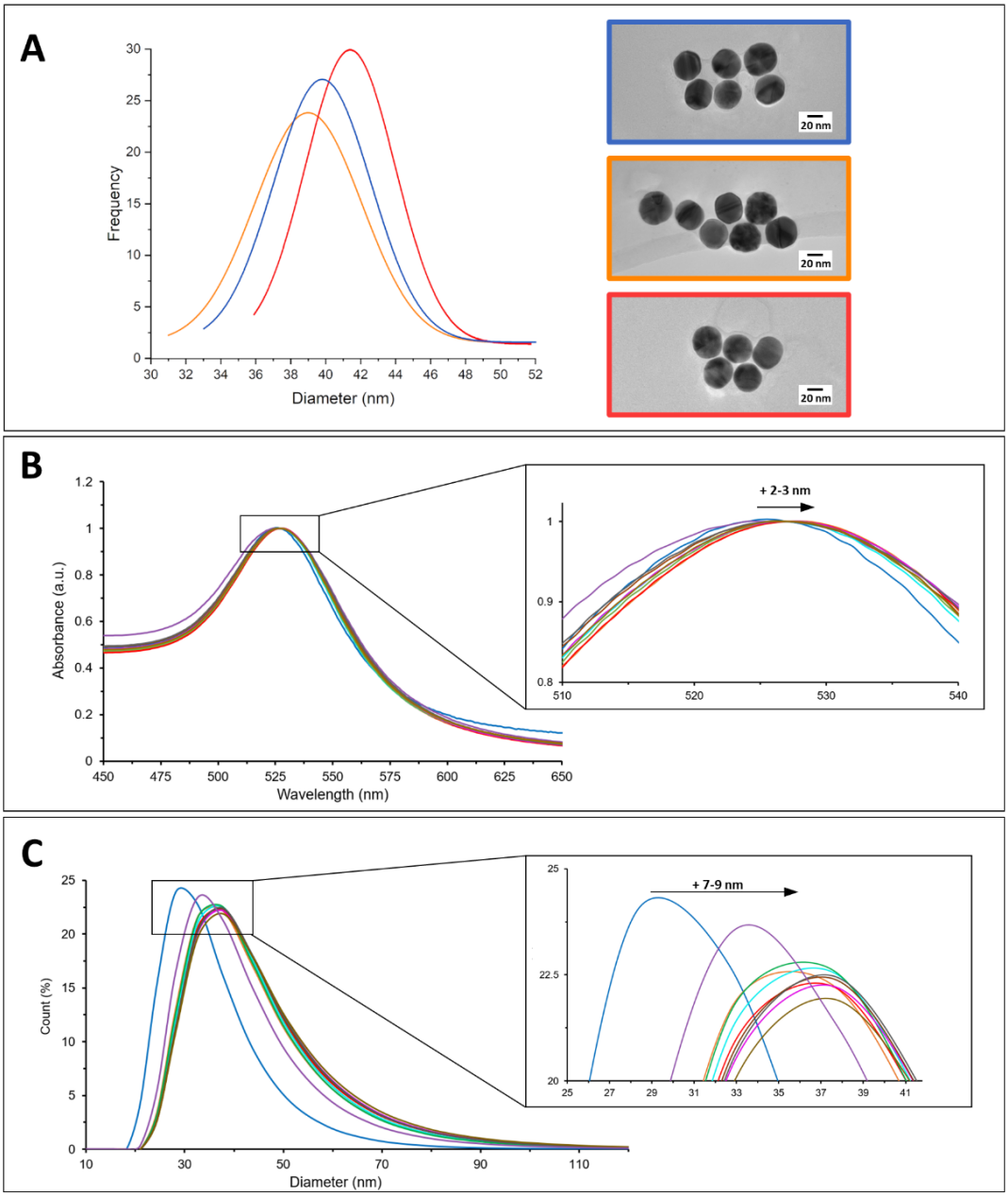

Figure 3.14. Characterisation of the 40 nm citrate-capped AuNPs and the collection of BSA-AuNPs synthesised in this work: propargyl-BSA-AuNPs (**30**), Gal-BSA-AuNPs (**31**), Gal_{14}-BSA-AuNPs (**31b**), Lac-BSA-AuNPs (**32**), 2'FL-BSA-AuNPs (**33**), Glc-BSA-AuNPs (**34**), Man-BSA-AuNPs (**35**), α3α6Man-BSA-AuNPs (**36**), and 3'SL-BSA-AuNPs (**37**). (**A**) TEM size distribution of citrate capped AuNPs, **30** and **31** (approximately 100 AuNPs of each were measured). (**B**) Normalised UV-Vis absorption spectra for all of the particles, showing an average shift of 2-3 nm for the functionalised AuNPs, except for **31b**, for which it was of 1 nm. (**C**) DLS data showing an average increase in hydrodynamic diameter of 7-9 nm after functionalisation, except for **31b**, for which it was of 5 nm.

The increase observed in hydrodynamic diameter can be explained by taking into account the reported size of BSA, 6.5 x 7.5 x 4- nm (X x Y x Z) (**Figure 3.15A**).[272] An estimation of the number of BSA units that can be located on the surface of an AuNP can be made considering the AuNP

as a sphere, and BSA as an ellipsoid (**Figure 3.15B**) forming a protein corona around the sphere. The protein corona will be formed by BSA units neighbouring by the widest point of the protein, which here is taken as its half-height. This half-height depends on the side of the BSA that lays on the surface of the 40 nm AuNP (**Figure 3.15C**), and it leads to an "outer radius" of 20 nm plus said half-height. This has a direct impact on the maximum units of BSA that can be allocated on the surface. For the upcoming calculations, we have assumed that a monolayer of BSA is formed on the surface of AuNP, and that all the BSA units lay in the same way on the AuNP.

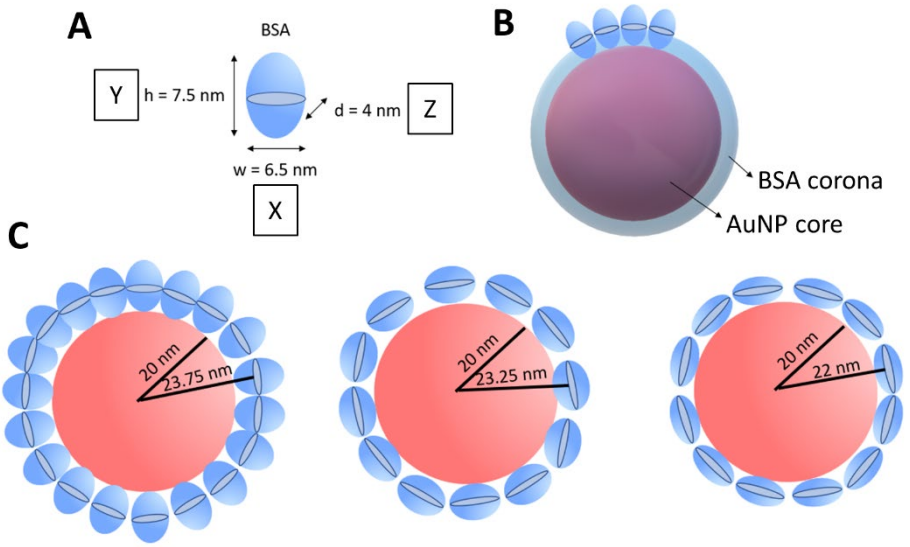

Figure 3.15. (**A**) BSA size calculated from protein database files.[272] (**B**) Schematic representation of a BSA-functionalised AuNP, where the BSA corona is estimated as thick as the half-height of BSA. (**C**) The number of BSA units per AuNP depends on the BSA face that lays on the surface of the particle.

The surface area of the BSA corona can be easily calculated following **Equation 3.1**. However, it has been reported that due to steric hindrance or electrostatic repulsion, the surface coverage of nanoparticles by BSA is rarely higher than a 50%.[273] For this reason, only half of the surface area will be considered available.

$$\text{Available surface area} = \frac{4\pi r^2}{2}, \text{where r} = 20 + \frac{\text{w}}{2}, \quad 20 + \frac{\text{h}}{2} \quad \text{or} \quad 20 + \frac{\text{d}}{2}$$

depending on which axis of BSA stands on the surface of the AuNP:

$$\text{X (w} = 6.5 \text{ nm), Y (h} = 7.5 \text{ nm) or Z (d} = 4 \text{ nm) axis}$$

$$\text{A(w)} = \frac{6793}{2} = 3397; \ \text{A(h)} = \frac{7088}{2} = 3544; \ \text{A(d)} = \frac{6082}{2} = 3041 \ \ (\text{nm}^2)$$

Equation 3.1. Calculation of the surface area of the outer sphere created by the BSA corona, where r is the radius of the sphere if BSA lays on its X-axis (w = 6.5 nm), Y-axis (h = 7.5 nm) or Z-axis (d = 4 nm), on the surface of a 40 nm AuNP.

The calculated surface areas are to be occupied by the maximum number of BSA units possible, neighbouring with one another at the wider point of the perpendicular axis. The wider section of BSA can be calculated following **Equation 3.2** as the ellipse resulting from cutting BSA at its middle point (lighter oval inside BSA in **Figure 3.15A**).

$$\text{Wider BSA section} = \pi r_{major\ axis} r_{minor\ axis} = \pi r_{maj} r_{min}$$

$$\text{If BSA stands on the X axis: } r_{maj} = \frac{\text{h}}{2}, \ \ r_{min} = \frac{\text{d}}{2} \rightarrow \text{Area}_w = 24\ nm^2$$

$$\text{If BSA stands on the Y axis: } r_{maj} = \frac{\text{w}}{2}, \ \ r_{min} = \frac{\text{d}}{2} \rightarrow \text{Area}_h = 20\ nm^2$$

$$\text{If BSA stands on the Z axis: } r_{max} = \frac{\text{h}}{2}, \ \ r_{min} = \frac{\text{w}}{2} \rightarrow \text{Area}_d = 38\ nm^2$$

Equation 3.2. Calculation of the widest section of a BSA unit, depending on which axis it stands.

Dividing the surface available [A(w,h,d)] by the widest point of a BSA unit ($\text{Area}_{\text{w,h,d}}$), the number of BSA units can be estimated (**Equation 3.3**).

$$\text{BSA units if standing on X} = \frac{\text{Area(w)}}{\text{Area}_w} = 141 \text{ BSA units}$$

$$\text{BSA units if standing on Y} = \frac{\text{Area(h)}}{\text{Area}_h} = 177 \text{ BSA units}$$

$$\text{BSA units if standing on Z} = \frac{\text{Area(d)}}{\text{Area}_d} = 80 \text{ BSA units}$$

Equation 3.3. Calculation of the minimum and the maximum number of BSA units that can be allocated on the surface of a 40 nm AuNP. The number depends on which axis the BSA unit lays.

This rough estimation leads to a range between 80 and 177 BSA units that can be allocated on the surface of 40 nm AuNPs. The actual final amount of BSA will vary depending on the ratio of BSA units standing on its X-, Y- and Z-axis. These amounts are in agreement with reported studies that quantified the maximum amount of BSA that can be passively adsorbed on the surface 40 nm AuNPs as 98 units *via* MALDI-TOF.[274]

3.3.2. The selective performance of glyco-BSA-AuNPs

To test the correct functionalisation of the gAuNPs, a dipstick assay was developed. The dipstick assay, as described in *Section 3.1.3.*, is a paper-based assay to assess the binding properties of, in this case, gAuNPs and lectins. The technical details of the method are described in *Chapter 5*. In brief, 0.5 µL of a specific concentration of lectin are deposited on a nitrocellulose strip. Then, 20 µL of a dipstick buffer composed of Tween-20 0.5% (w/v) and PVP 1% (w/v) in PBS are allowed to flow throughout the strip for conditioning and blocking. Finally, a certain concentration (usually OD 1) of functionalised AuNPs in the same buffer is allowed to flow for the particles to interact with the analyte, and, if so, develop a colorimetric line.

A preliminary experiment was performed with the Gal-BSA-AuNPs **31** and Lac-BSA-AuNPs **32** (**Figure 3.16**) to investigate the viability of assay test and possible cross-reactivities (non-specific interactions with other lectins). For this purpose, RCA_{120} (2.5 µg) was used as a model of binding to galactose whereas UEA I (2.5 µg) and WGA (2.5 µg) were used as negative controls, given their absence of interaction with terminal galactoside residues. This experiment confirmed that both **31** and **32** bound to RCA_{120}, which can be visualised by the red band that appears where the lectin has been deposited. The selectivity of such interaction was confirmed since neither of the gAuNPs interacted with the negative control lectins (UEA I, WGA). A further control was performed using the propargylated BSA-AuNPs (**30**), which did not interact with either of the lectins. These results confirmed that the binding observed between **31**/**32** and RCA_{120} was due to the selective interaction between the sugars on the particles and the lectin.

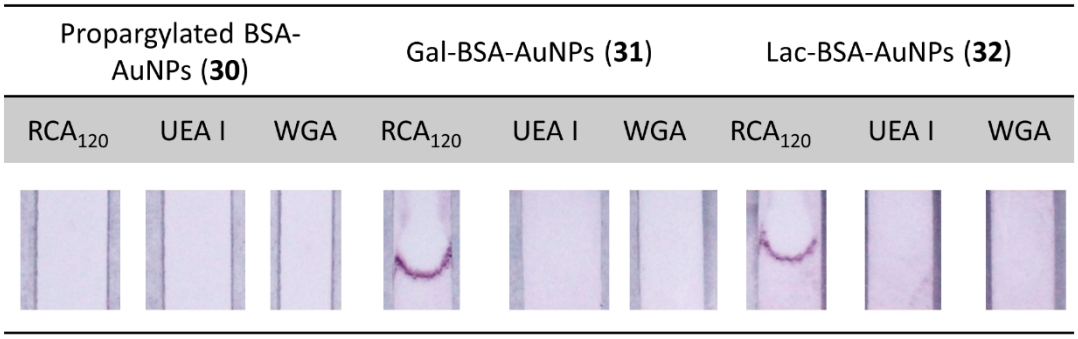

Figure 3.16. Dipstick assay for the detection of RCA_{120} (2.5 μg) with gAuNPs **31** and **32.** Negative controls include the 2'-fucoside-binding UEA I and the sialic acid-binding WGA (2.5 μg each). The AuNPs **30** were also assayed to probe the absence of non-specific interactions with either of the lectins. The assay was repeated in triplicates, obtaining similar results.

Having confirmed the viability of the assay, a systematic dipstick assay was performed testing the binding of the set of AuNPs **30-37** to the lectins RCA_{120}, UEA I, WGA and ConA (detecting 2.5 μg of each). To allow the quantification and therefore bias-free comparison of the results, the line intensities of each dipstick were quantified using a gel imager (BioRad Chemidoc). For plotting purposes, the values were normalised against the signal obtained with the Gal-BSA-AuNPs for the detection of 2.5 μg of RCA_{120} (**Figure 3.17A**). Although the selectivity observed was the expected one (except for the interaction between 2'FL-BSA-AuNPs and RCA_{120} that will be commented on in due course), the relative intensities did not match the expectation in certain cases. An example of this was the relative binding of Man-BSA-AuNPs and α3α6-Man-BSA-AuNPs to ConA, which would be expected to exhibit a tighter binding to the latter gAuNP.[111] Given that each of the gAuNPs was functionalised with a BSA glycoconjugate containing a different loading of glycan units (the glycoconjugate synthesis was discussed in *Chapter 2*), the signal intensity obtained for each dipstick was divided by said loading. The new pondered plot related better with published data, now showing a per-glycan interaction intensity (**Figure 3.17B**). It was remarkable how the intensity per glycan for the Gal_{14}-BSA-AuNP **31b** was significantly lower than the Gal-BSA-AuNP **31**, and the absolute increase of intensity is not proportional to the number of glycan units on the BSA. Another possible explanation is that at a given number of glycans, the visual signal reaches a saturation point beyond which the intensity is not further quantifiable.

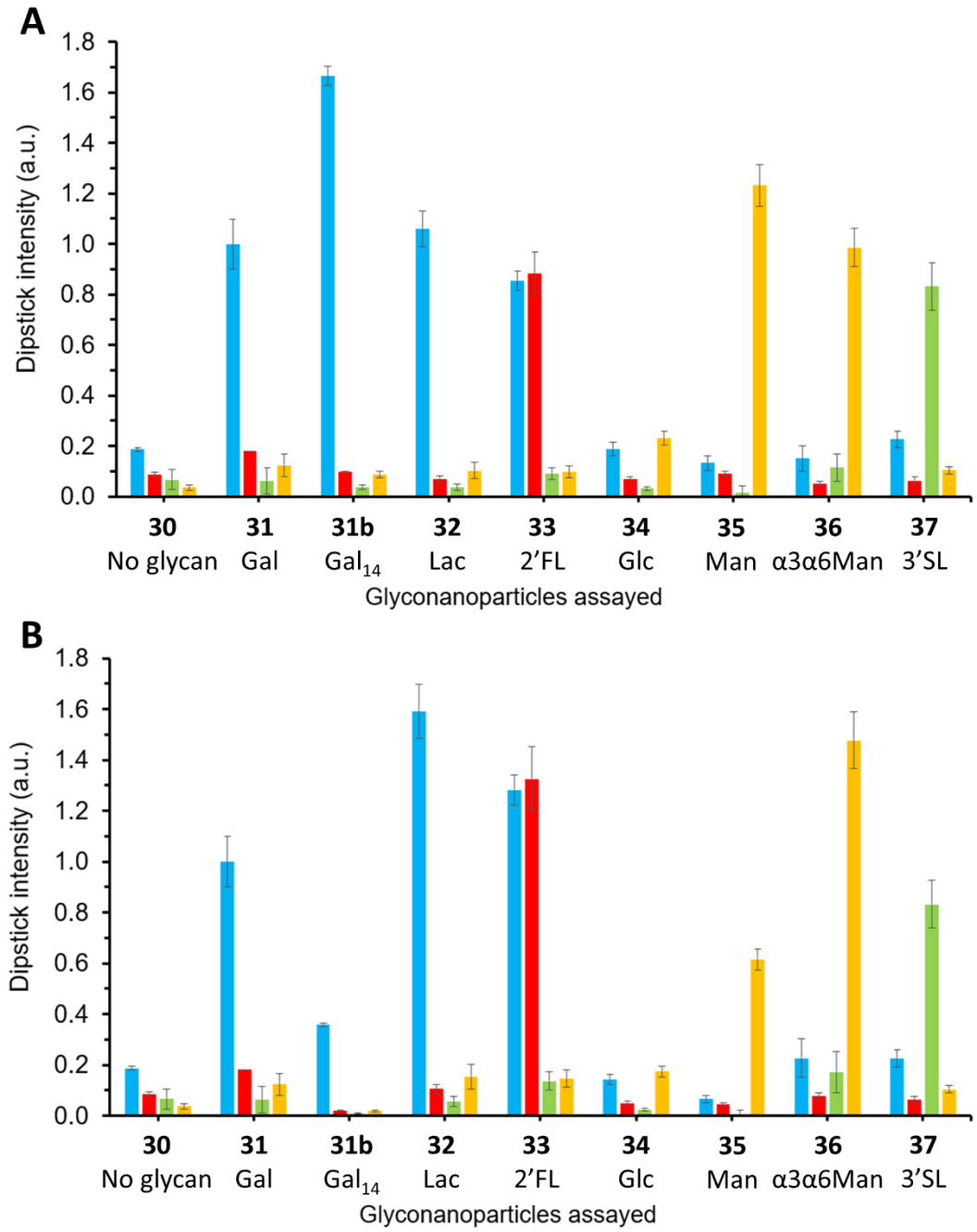

Figure 3.17. Selectivity of the gAuNPs **31-37** for the lectins RCA_{120}, UEA I, WGA and ConA. For the dipstick assay, gAuNPs at OD 1 in dipstick buffer were used to detect 2.5 µg of each lectin. A negative control was performed with propargylated BSA-AuNPs (**30**) against the respective lectins. The signal intensities were quantified with a electrophoresis gel imager Chemidoc (BioRad), and (**A**) normalised against the signal intensity of the dipstick corresponding to **31** against RCA_{120}, or (**B**) divided by the glycan loading of the respective BSA glycoconjugates and then normalised against the signal intensity of the dipstick corresponding to **31** for the detection of RCA_{120}. Error bars show the standard deviation between triplicates in the experiment.

The results obtained in the dipstick assay were compared with available literature (specificities of the lectins described in *Chapter 1*), and with a systematic ELLA performed at Iceni

Glycoscience Ltd. (*data not published*) with fluorescently labelled lectins and 37 BSA glycoconjugates including galactose, mannose, fucose and sialic acid terminal moieties with different linkages. The data related to the lectins of interest in this thesis is summarised in **Figure 3.18** (for the protocols and the rest of the data, please refer to *Appendix 2*).

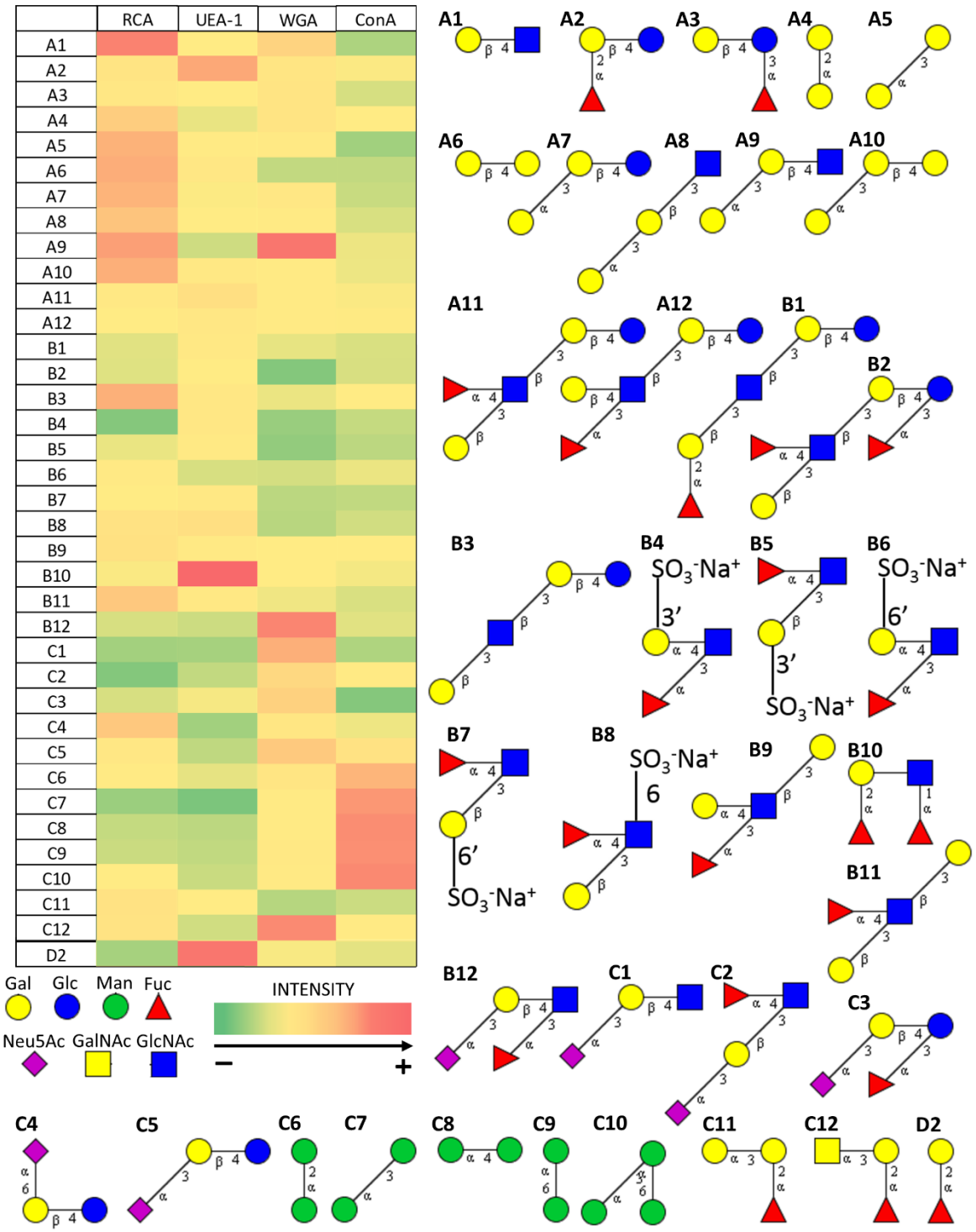

Figure 3.18. ELLA assay performed at Iceni Glycoscience Ltd (*data not published*) to screen 37 BSA glycoconjugates against fluorescently labelled RCA_{120}, UEA I, WGA and ConA.

All the gAuNPs employed in this work followed the expected binding specificities according to published literature and the ELLA assay shown above, except the 2'FL-BSA-AuNPs (**33**). It is well known that RCA_{120} does not recognise the β-galactoside residue in 2'FL due to the hindering presence of fucose, and it has been probed specifically for a BSA glycoconjugate *via* SPR.[92] Therefore, it was surprising to see such dipstick intensity for the detection of RCA_{120}, superior to the one obtained with Gal-BSA-AuNPs and nearly as high as the one of Lac-BSA-AuNPs. To further evaluate that the interaction observed was specific, a second dipstick experiment was performed (**Figure 3.19A**). The protocol was analogous to the one discussed so far, only pre-mixing RCA_{120} with lactose 10 mM before the deposition on the nitrocellulose strip, to block the lectin beforehand. This competitive assay aimed to study the replacement of lactose by either of the gAuNPs tested, to confirm the specific interaction with the lectin. Both Lac-BSA-AuNPs and 2'FL-BSA-AuNPs were tested, and in both cases, a loss of intensity in the dipstick was observed. However, the signal was still there, and it was clearly above the intensity of the control made with propargylated BSA-AuNPs. This showed that the interaction observed between the 2'FL-BSA-AuNPs was specific, but it was still in contradiction with the literature, hence the investigation continued.

It was suspected that the trisaccharide could have suffered the cleavage of the *O*-glycosidic bond from the α-fucosyl residue as a result of instability over time, leading to a lactoside that would indeed be recognised by the lectin. The hypothesis was investigated through a repetition of the ^{1}H-NMR analysis, using a higher field (500 MHz instead of 400 MHz) and a higher number of scans (1024 instead of 64). The observation of an anomeric doublet appearing at 4.53 ppm corresponding to free β-fucose and at 5.24 ppm corresponding to the α-fucose, together with the azidopropyl 2'-fucosyllactoside (**Figure 3.19B**) could explain the binding of the named 2'FL-BSA-AuNPs to RCA_{120}. This is in agreement with published literature where 2'-fucosyllactose was digested with a 2'-fucosidase and the appearance of peaks corresponding to the anomeric equilibrium of free fucopyranose was followed over time.[275] However, the cleavage must have been partial, given that the binding to UEA I did also occur in a specific manner during the dipstick assay. This is also in agreement with the ^{1}H-NMR spectra, given that the anomeric peak corresponding to fucose from the azidopropyl 2'-fucosyllactoside is still present at 5.32 ppm.

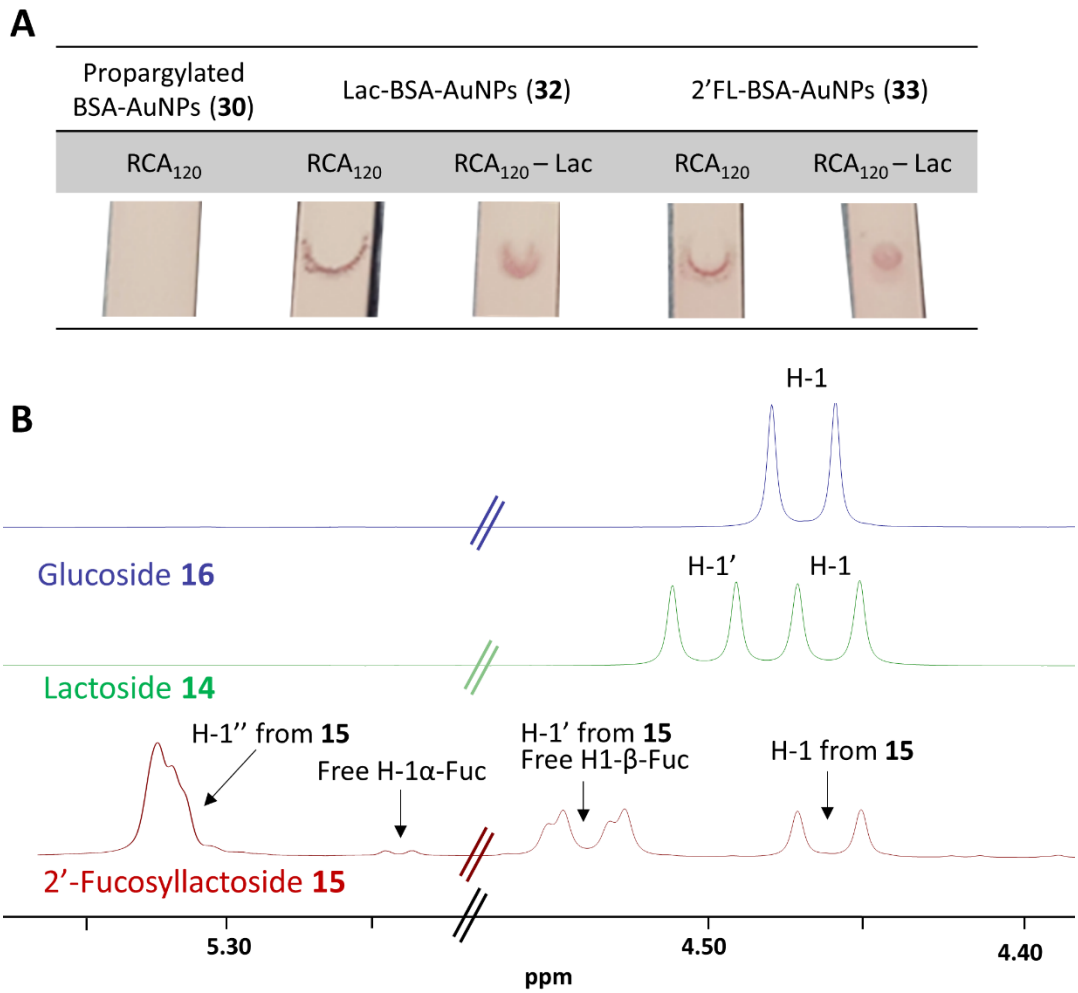

Figure 3.19. Investigation of the apparent binding of 2'FL-BSA-AuNPs **33** to RCA_{120}. (**A**) Dipsticks showing the detection of 2.5 µg of RCA_{120}, and 2.5 µg of RCA_{120} pre-mixed with lactose 10 mM (RCA_{120} – Lac) with the gAuNPs **33**. A negative control was performed with propargylated BSA-AuNPs **30**, and a positive one with Lac-BSA-AuNPs **32**. The experiment was performed in triplicates, with similar results. (**B**) Analysis of the anomeric area of the ^{1}H-NMR spectra of the azidopropyl 2-fucosyllactoside **15**, in comparison with the lactoside **14** and glucoside **16**. The cleavage of the α-fucose residue from **15** leads to the appearance of free α- and β-fucose which can be followed by NMR.

To confirm the presence of lactose in the namely 2'FL-BSA-AuNPs (**33**), the enzymatic cleavage of terminal β-galactoside residues was attempted with *Aspergillus oryzae* β-galactosidase.[276] This experiment aimed to cleave the galactoside residue from Lac in gAuNPs **33**, while leaving intact the 2'FL ligands (**Figure 3.20A**). The outcome would be analysed in a dipstick assay, ideally, observing no interaction between the modified AuNPs **33** and RCA_{120}, while still observing interaction with UEA I (due to the presence of remaining 2'FL). However, the gAuNPs aggregated immediately in the buffer suggested for the enzyme (20 mM phosphate-citrate buffer, pH 4.5). At pH 6, the gAuNPs slowly aggregated during the overnight incubation.

At pH 7, the gAuNPs did not aggregate, however, the activity of the enzyme can be compromised at this pH (pH 4.5 is the optimal as suggested by the provider). Only the sample at pH 7 was tested in a dipstick assay, and it still showed interaction with RCA_{120} (**Figure 3.20B**). A control was performed submitting Lac-BSA-AuNPs (**32**) to the enzymatic digestion with *A. oryzae* β-galactosidase, which still showed an interaction with RCA_{120} after the incubation. That result suggested an incompatibility between the gAuNPs substrate and the incubation conditions which is known in the literature, and even under optimal conditions (pH, concentration and time), β-galactosidases may not work as desired due to inaccessibility to the glycans on the surface of the gAuNPs.[38] Therefore, the enzymatic cleavage of the terminal galactoside unit from the namely 2'FL-BSA-AuNPs (**33**) was not further investigated, acknowledging the presence of lactose on the surface of the particle, which leads to an anomalous interaction of the gAuNPs with RCA_{120}.

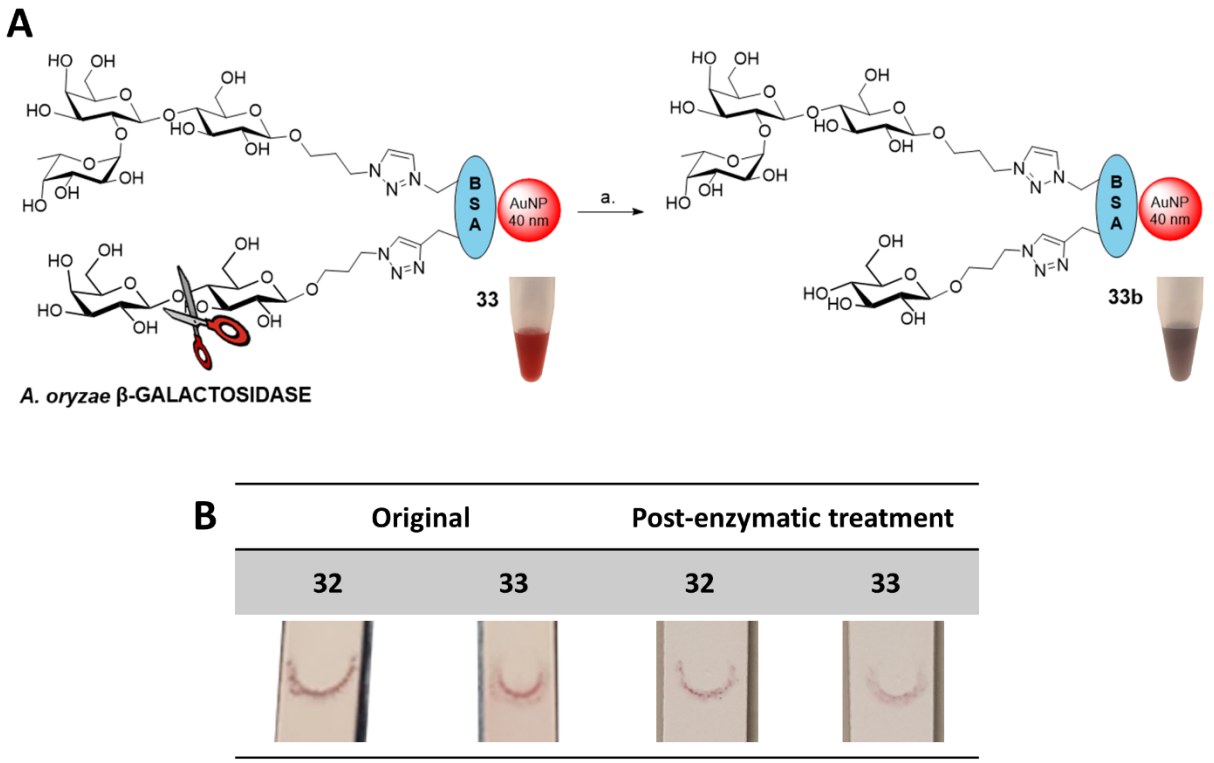

Figure 3.20. Attempted cleavage of the terminal β-galactoside residue from available lactoside ligands in the 2'FL-BSA-AuNPs **33** with *A. oryzae* β-galactosidase. (**A**) Under the enzyme's optimal conditions (20 mM phosphate-citrate buffer, pH 4.5), the particles in suspension aggregated instantly, with the characteristic colour change shown in the vials. Reagents and conditions: (**a**) phosphate-citrate buffer (20 mM, pH 4.5), 30 °C, o.n. The experiment was performed in duplicates and also with Lac-BSA-AuNPs **32**, with similar results. (**B**) Dipsticks corresponding to the detection of 2.5 μg of RCA_{120} before and after the attempted enzymatic cleavage with either gAuNPs **32** or **33**.

Summarising this subsection, a methodology for the synthesis of *ca.* 40 nm glyco-BSA-AuNPs has been developed. The protocol leads to the synthesis of gAuNPs which have been characterised through TEM, UV-Vis and DLS. The presence of the glycosides has been confirmed by testing the lectin-binding properties of the gAuNPs in a dipstick assay. This kind of gAuNPs has been proven to be selective towards the lectin of matching specificity.

As a note, the quantification of sugar loading on the surface of the different gAuNPs was attempted with the well-known anthrone test.[277,278] The final quantification was not possible, potentially due to the small percentage of glycosides present on the nanoparticles. Another technique available for this quantification is NMR, however, a similar issue would be expected.

3.3.2. Synthesis of glyco-AuNPs and glyco-AuNSs

To better understand the impact of BSA on the lectin-binding properties of gAuNPs, a method was optimised for the functionalisation of commercially available NHS ester-activated *ca*. 40 nm AuNPs through a covalent linkage (**Scheme 3.2**). For this purpose, the 3-azidopropyl galactoside **13** was reduced to 3-aminopropyl galactoside (**38**) with PPh_3 adapting a method of the classical Staudinger reaction.[279] The method discussed below yielded Gal-AuNPs (**39**) and also propyl-AuNPs (**40**) as a negative control for the dipstick assay. Encouraged by the possibility of a higher degree of glycan functionalisation, potentially resulting in better lectin-binding properties, commercially available NHS ester-activated *ca.* 150 nm shell@core Au@Si nanoshells (AuNSs) were also functionalised with the galactoside **38**. This methodology yielded Gal-AuNSs (**41**) and propyl-AuNSs (**42**).

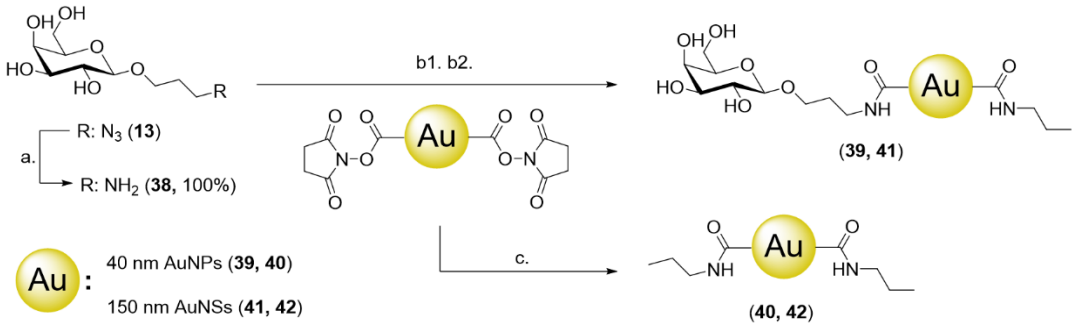

Scheme 3.2. Functionalisation of NHS ester-activated *ca*. 40 nm AuNPs and *ca*. 150 nm AuNSs. Reagents and conditions: (**a**) PPh_3, H_2O/THF, 75 °C, 3 h; (**b1**) HEPES buffer 10 mM pH 8.0, 0.5% PEG-20k, 6 h, r.t.; (**b2**) propylamine, 10 min; (**c**) propylamine, HEPES buffer 10 mM pH 8.0, 0.5% PEG-20k, 6 h, r.t.

The original approach (as suggested by the provider) for the NHS coupling consisted in the dispersion of the lyophilised AuNSs in phosphate buffer pH 7.4 containing 0.5% PEG-20k. The AuNSs were subsequently transferred to a solution of the desired sugar in the same buffer and the reaction would take place for one hour. The reaction was treated with hydroxylamine to quench the unreacted NHS esters after the reaction time. For similarity with the 3-azidopropyl glycosides synthesised in this thesis, propylamine was used for the quenching step instead of hydroxylamine. Propyl-AuNPs (**40**) and (**42**) were prepared as negative controls by quenching the particles in absence of the 3-aminopropyl glycoside, to study non-specific interactions with RCA_{120}, UEA I and WGA.

The non-specific interactions of propyl-AuNPs and propyl-AuNSs

The non-specific interactions between either AuNPs **40** or AuNSs **42**, and RCA_{120}, UEA I and WGA were studied. Whereas **40** did not exhibit any (dipsticks shown in the next section), **42** led to false positive results for both RCA_{120} and WGA that required attention (**Figure 3.21**). The composition of the dipstick buffer was optimised in a systematic way attempting to prevent the non-specific interactions observed. For this, the concentration of one component of the buffer was changed at a time to understand its effect on the improvement in terms of non-specific interaction between the propyl-AuNSs and the two lectins. Not only Tween-20 and PVP were tuned, but also Triton X100 was considered as an alternative, stronger detergent, and BSA was considered as an added blocking agent. This experiment aimed to eliminate the non-specific interactions observed with RCA_{120} and WGA. The original dipstick buffer (*Tween-20 0.05%* in **Figure 3.21**) did not prevent such non-specific interactions. Increasing the concentration of Tween-20 did not have a great impact, although a 5% did show some improvement for both RCA_{120} and WGA. However, 5% of detergent is a relatively high concentration for a detection assay and interactions with real samples would be expected. The substitution of Tween-20 for Triton X100 resulted to be more effective, at least with regards to WGA. At 1% of this detergent, the non-specific interaction with WGA practically disappeared, and the one with RCA_{120} had improved significantly.

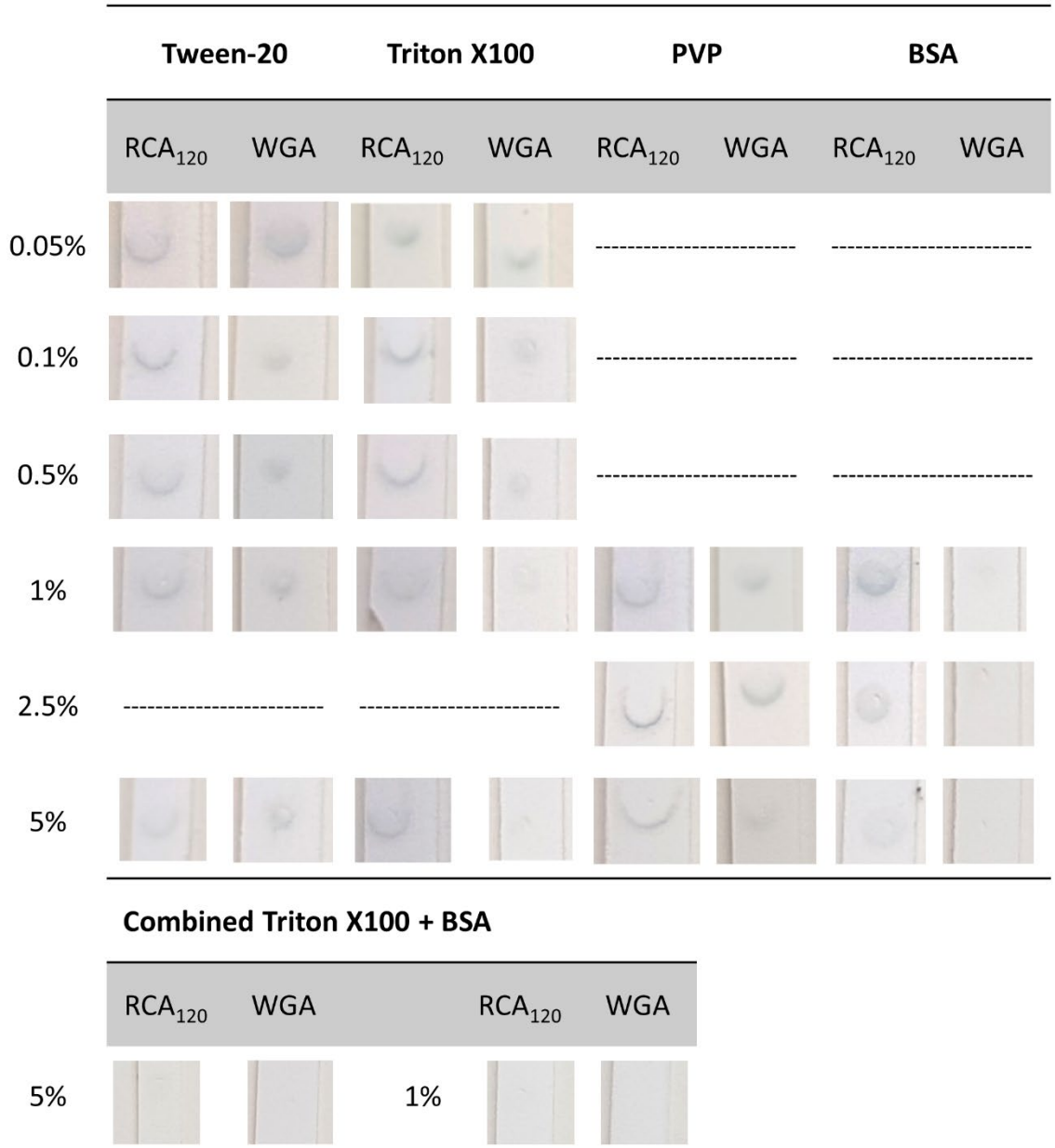

Figure 3.21. Systematic optimisation of the dipstick buffer for AuNSs. Each dipstick represents the detection of either RCA_{120} or WGA (2.5 µg) with 150 nm propyl-AuNSs (**42**) OD 1. The original composition of the running buffer was 150 nM NaCl, 10 mM PB pH 7.4, 1% (w/v) PVP, 0.05% (w/v) Tween-20, which corresponds to the 0.05% Tween-20 cells in the figure. For the set of experiments with Triton X100, Tween-20 from the original running buffer was substituted by Triton X100. For the set of experiments with BSA, this compound was added in different concentrations to the original running buffer composition. Finally, the combined effect of Triton X100 and BSA, both components simultaneously at either at 5% or 1%, was studied. *Note: unfortunately, the quality of these pictures could not be improved further. The electronic version of this figure is suggested for a better comparison of these dipsticks.*

The concentration of the blocking agent was also tuned. An increase in the concentration of PVP did not affect the observed non-specific binding, although 5% seemed to influence the

one with WGA. At that point, BSA was added to the dipstick buffer as this protein is well known to act as a blocking agent. This turned out to be more effective to prevent the non-specific binding between the AuNSs and both RCA_{120} and WGA. However, even at 5% of BSA RCA_{120} still presented some non-specific binding (which is not as apparent in a picture as it was in the actual dipstick). Given that the concentrations of detergents and blocking agents were already relatively high, the combined effect of Triton X100 and BSA was tested, as both components seemed to have a positive effect in the assay. At 5% of each component, the non-specific interactions with both RCA_{120} and WGA disappeared completely. The combined effect of 1% of each was also tested, with a similar effect, therefore the optimised composition of the dipstick buffer for AuNSs was chosen as PB 10 mM pH 7.4, 150 nM NaCl, 1% (w/v) PVP, 1% (w/v) Triton X100, 1% (w/v) BSA.

Optimisation of the functionalisation conditions for AuNPs and AuNSs with 3-aminopropyl galactoside

With the non-specific interactions between the particles and lectins minimised, the NHS coupling reaction between 3-aminopropyl galactoside (**38**) and the particles was tested. The general protocol provided by the manufacturer for the functionalisation of 150 nm AuNSs was taken as a starting point. However, that protocol was meant for Ab immobilisation on the surface of the particles. Therefore, the conditions were adapted for the coupling with galactoside **38** by exploring the pH, incubation time and concentration of the galactoside.

Following the simple mechanism of the reaction between NHS esters and primary amines (**Scheme 3.3**), the latter needs to be in a neutral state to proceed with the nucleophilic attack.

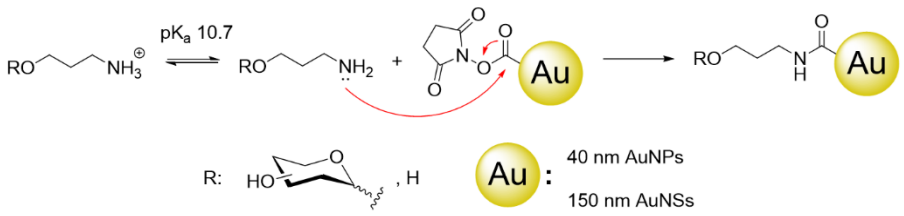

Scheme 3.3. Representation of the nucleophilic attack of primary amine to the carboxylic group of an NHS-activated AuNP/AuNS. The primary amine must have its lone pair of electrons for this step; thus, the state of its acid-base equilibria is very relevant in this process.

The buffer provided with the nanoshells was PB (10 mM, pH 7.4), however through equilibrium calculations (**Equation 3.4**) it is seen that at neutral pHs just a very reduced

fraction of the aminopropyl glycoside will be in its neutral state. For this calculation, the pKa of propylamine (10.6) is considered. Following the calculations above, higher pHs are preferred for the NHS coupling to the AuNPs and AuNSs. However, this may compromise the stability of the particles, reason why it was thought that longer reaction times would benefit the functionalisation more than an increase in pH.

$$\text{pH } 7.4 \rightarrow \frac{[NH_2][H^+]}{[NH_3^+]} = \frac{[NH_2]\,10^{-7.4}}{[NH_3^+]} = 10^{-10.6} \rightarrow \frac{[NH_2]}{[NH_3^+]} = 0.0006 \rightarrow 0.06\%\ \text{neutral}$$

$$\text{pH } 8.0 \rightarrow \frac{[NH_2][H^+]}{[NH_3^+]} = \frac{[NH_2]\,10^{-8}}{[NH_3^+]} = 10^{-10.6} \rightarrow \frac{[NH_2]}{[NH_3^+]} = 0.0025 \rightarrow 0.25\%\ \text{neutral}$$

$$\text{pH } 8.5 \rightarrow \frac{[NH_2][H^+]}{[NH_3^+]} = \frac{[NH_2]\,10^{-8.5}}{[NH_3^+]} = 10^{-10.6} \rightarrow \frac{[NH_2]}{[NH_3^+]} = 0.008 \rightarrow 0.8\%\ \text{neutral}$$

Equation 3.4. Calculations related to the acid-base equilibria of propylamine. The buffered pH directly impacts the percentage of primary amines in the neutral state.

The systematic experiment to optimise the functionalisation step started with the incubation of AuNSs with decreasing concentrations of 3-aminopropyl galactoside **38** (10, 1, 0.1, 0.01 mM), at different pHs (6.0, 7.4, 8.0) and over different incubation times (1, 6, 24h). The buffers used in this experiment included MES 10 mM pH 6.0 with 0.5% PEG-20k, PB 10 mM pH 7.4 with 0.5% PEG-20k, and HEPES 10 mM pH 8.0 with 0.5% PEG-20k (PEG-20k was included in the buffer, as suggested by the provider).

The AuNSs resulting from this experiment were applied for the detection of 2.5 µg of RCA_{120} (**Figure 3.22A**) in a dipstick assay as before, to decide the optimal conditions for the functionalisation. Analysing the information obtained in the optimisation process, the increase in incubation time has the expected positive effect on the detection, potentially indicating a greater functionalisation. This can be seen especially during the functionalisation of AuNSs with 1 mM of galactoside **38** at pH 7.4. The line corresponding to the interaction between the gAuNSs and RCA_{120} progressively increases in intensity with longer incubation times. The increase in pH has an obvious influence on the process, which agrees with the equilibria calculations indicated in **Equation 3.4**. However, longer incubations (24 h) at pH 8.0 led to more unstable particles that in some cases aggregated during the dipstick assay. The combined effect of 24 h of incubation at pH 7.4 had a very similar effect to 6 h of incubation at pH 8.0, both showing the detection of RCA_{120} when 1 mM of the galactoside **38** was used for the functionalisation. To have a shorter reaction time, the optimal conditions for the

functionalisation of AuNSs with 3-aminopropyl galactoside were chosen as 1 mM of glycoside at pH 8.0 over 6 h.

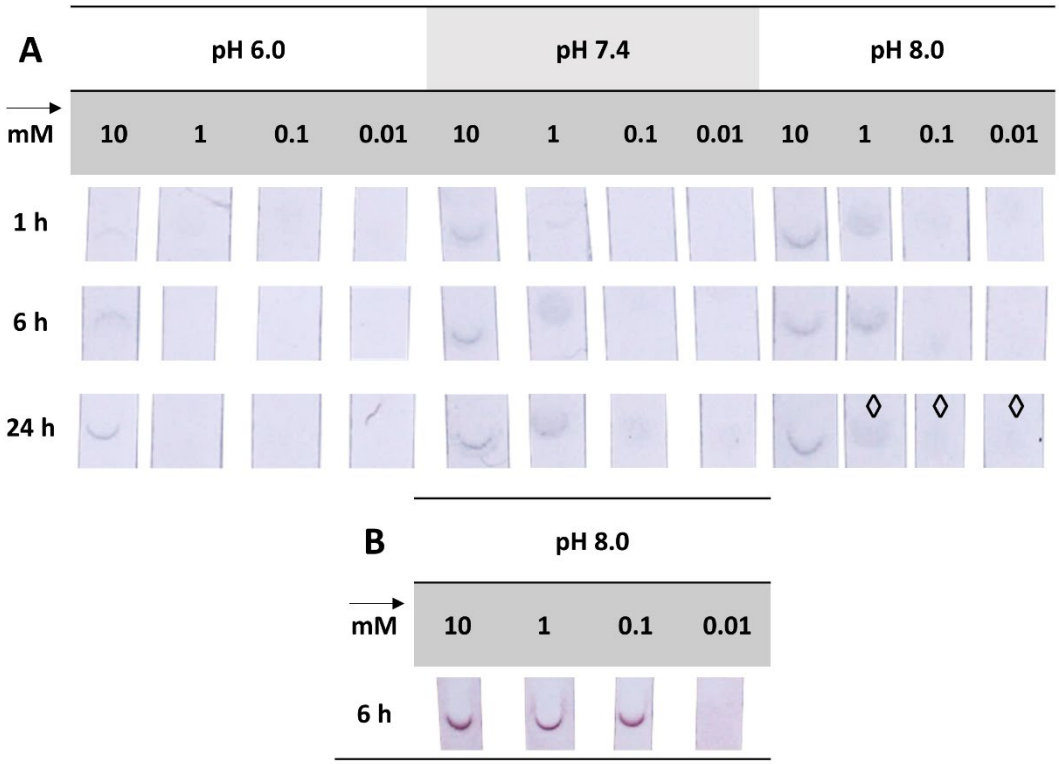

Figure 3.22. Optimisation of the NHS coupling between 3-aminopropyl galactoside (**38**) and NHS ester-activated AuNSs and AuNPs. The results of the optimisation were analysed through the detection of RCA_{120} (2.5 µg) with OD 1 of either of the gAuNSs or gAuNPs synthesised. (**A**) Dipstick signals for the detection of RCA_{120} with gAuNSs functionalised with different concentrations of **38** (10, 1, 0.1, 0.01 mM), at different pHs (6.0, 7.4, 8.0) and over different incubation times (1, 6, 24h). ◊: indicates aggregation of the gAuNSs at the bottom of the dipstick. (**B**) Dipstick signals for the detection of RCA_{120} with gAuNPs functionalised with different concentrations of **38** (10, 1, 0.1, 0.01 mM), at pH 6.0 over 6 h.

The optimal conditions (pH 8.0, 6h) were also applied for the NHS coupling of 40 nm AuNPs with glycoside **38**, given that the gold surface should be analogous, although smaller. Only the concentration of glycoside was optimised (**Figure 3.22B**). No detection of RCA_{120} was observed when the particles were functionalised with 0.1 mM of glycoside 38. However, the signal intensity of the dipsticks was saturated from 1 mM onwards. Therefore, the optimal conditions for the functionalisation of AuNSs with 3-aminopropyl galactoside were chosen as 1 mM of glycoside at pH 8.0 over 6 h.

The propyl-AuNPs **40** and propyl-AuNS **42** were characterised using UV-Vis and DLS; however, they were not distinct from unfunctionalised AuNPs or AuNSs due to the small size of the

propyl tether (data tabulated in *Chapter 5*). The Gal-AuNPs **39** and Gal-AuNSs **41** were characterised using TEM, UV-Vis and DLS.

With regards to the AuNPs, the TEM (**Figure 3.23A**) showed some variability in size (38 ± 2 nm), although it could not be compared with the manufacturer's data as the deviation was not specified. Analysis of the UV-Vis spectra of the Gal-AuNPs **39** did not show any shift in the spectrum compared with the original particles. This is not unexpected, given the small size of the glycosides in comparison with the particle (data plotted in **Figure 3.23B**, tabulated in *Chapter 5*). The DLS data of **39** showed an increase in hydrodynamic diameter of 5 nm (data plotted in **Figure 3.23C**, tabulated in *Chapter 5*). It is worth mentioning that, even though the core of the AuNPs is *ca.* 40 nm as observed in the TEM analysis, and in agreement with the UV-Vis spectrum and information from the manufacturer, the diameter obtained through DLS was originally of *ca.* 52 ± 0.4 nm. This is not necessarily an incongruence, given that DLS measures the hydrodynamic diameter and not the actual size of the core. Therefore, the discrepancy in size is assumed to be due to the linker between the activated ester and the surface of the particle, which is not disclosed by the manufacturer.

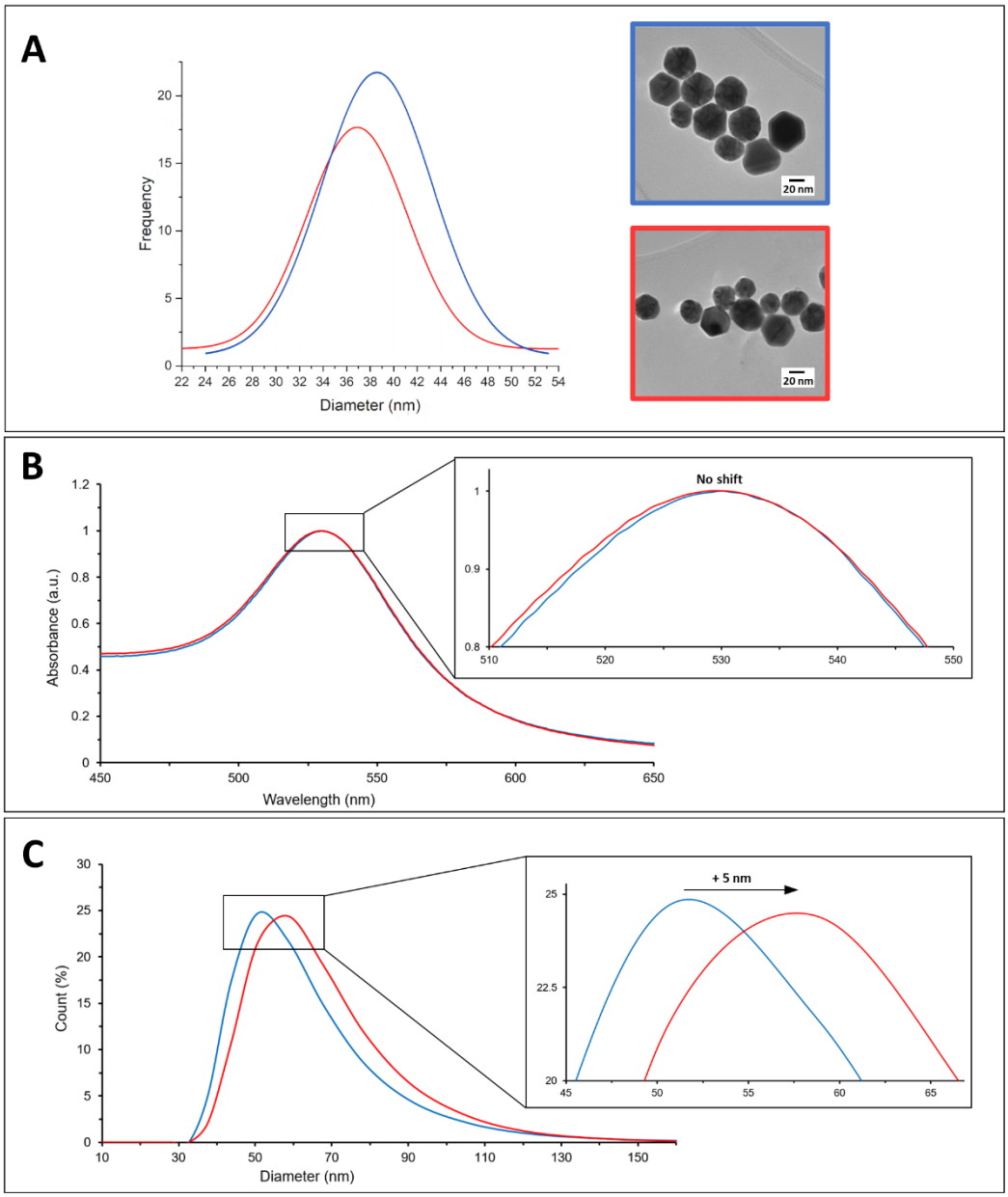

Figure 3.23. Characterisation of the 40 nm NHS ester-activated AuNPs and the Gal-AuNPs **39** synthesised in this work. (**A**) TEM size distribution of both (approximately 100 AuNPs of each were measured). (**B**) Normalised UV-Vis spectra of both particles, showing no shift for the functionalised AuNPs **39**. (**C**) DLS data showing an average increase in hydrodynamic diameter of 5 nm after functionalisation.

The Gal-AuNSs were characterised analogously. The TEM (**Figure 3.24A**) showed very little variability in sizes (149 ± 10 nm), which was in agreement with the data provided by the manufacturer (150 ± 15 nm). Analysis of the UV-Vis spectra of the Gal-AuNSs **41** did not show any shift in the spectrum compared with the original particles. This is not unexpected, given the small size of the glycosides in comparison with the particle (data plotted in **Figure 3.24B**,

tabulated in *Chapter 5*). The DLS data of **41** shows an increase in hydrodynamic diameter of 5 nm (data plotted in **Figure 3.24C**, tabulated in *Chapter 5*).

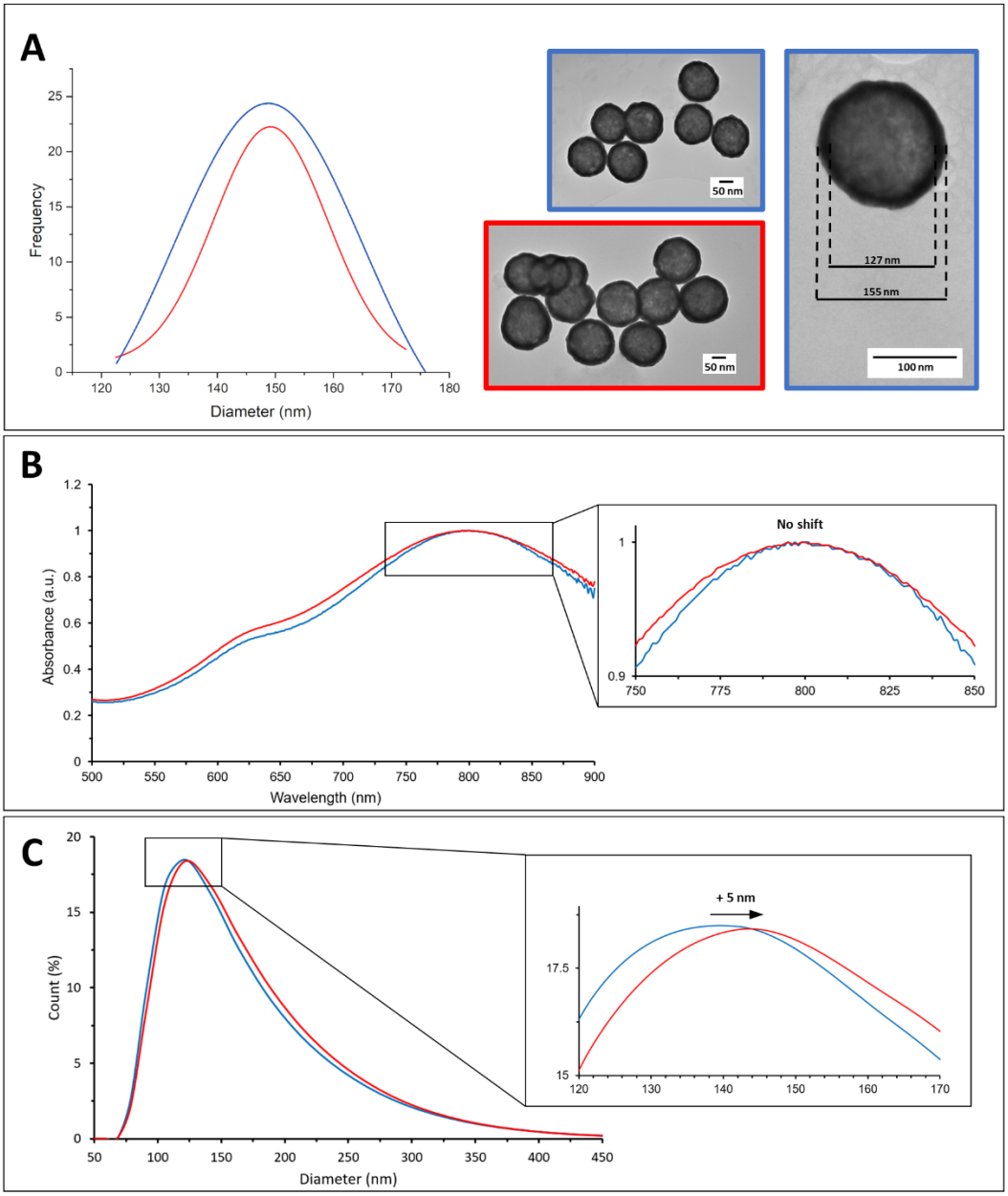

Figure 3.24. Characterisation of the 150 nm NHS ester-activated AuNSs and the Gal-AuNSs **41** synthesised in this work. (**A**) TEM size distribution of both (approximately 100 AuNPs of each were measured). (**B**) Normalised UV-Vis spectra of both particles, showing no shift for the functionalised AuNSs **41**. (**C**) DLS data showing an average increase in hydrodynamic diameter of 5 nm after functionalisation.

Summarising this section, a methodology for the covalent functionalisation of *ca*. 40 nm AuNPs and *ca.* 150 nm AuNSs with 3-aminopropyl galactoside has been developed. The synthesised particles have been characterised and have been applied in a dipstick assay for

the detection of RCA_{120}. The behaviour of the NHS-activated 40 nm AuNPs was better in terms of optimisation requirements and non-specific interactions observed than NHS-activated 150 nm AuNSs, which should be considered from the assay development point of view. The gAuNPs were applied to the dipstick assay without the observation of non-specific interactions (**Figure 3.25A**). The gAuNSs exhibited non-specific binding that required in-depth assay optimisation, although such interactions were removed using increased amounts and different types of detergent and blocking agents (**Figure 3.25B**).

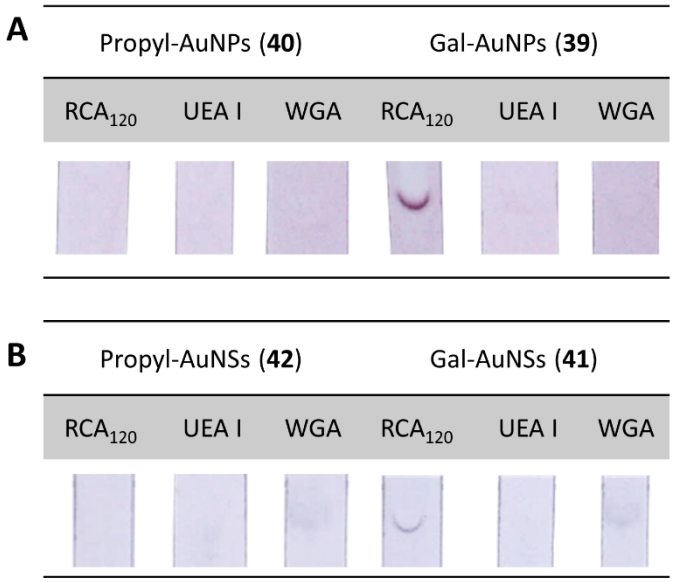

Figure 3.25. Dipstick assay under optimised conditions for the detection of RCA_{120} (2.5 µg) with (**A**) gAuNPs **39** and (**B**) gAuNSs **41**. Negative controls include the 2'-fucoside-binding UEA I and the sialic acid-binding WGA (2.5 µg each). The propyl-AuNPs **40** and propyl-AuNSs **42** were also assayed to probe the absence of non-specific interactions with either of the lectins. The assay was repeated in triplicates, obtaining similar results.

3.3.3. Sensitivity studies: comparing Gal-BSA-AuNPs, Gal-AuNPs and Gal-AuNSs.

With an optimised methodology for the synthesis of different gAuNPs and gAuNSs, the sensitivity of all of them for the detection of RCA_{120} in a dipstick assay was evaluated. In this section, the performance of Gal-BSA-AuNPs (**31**), Gal_{14}-BSA-AuNPs (**31b**), Gal-AuNPs (**39**) and Gal-AuNSs (**41**) will be compared to find the optimal presentation of sugars for the detection of RCA_{120}.

For this purpose, dipsticks were generated in triplicates with amounts of RCA_{120} ranging from 2,500 – 2.5 ng (**Figure 3.26**). In the 2,500 – 300 ng range, the four systems detected the lectin without any complication, with differences in sensitivity appearing in the 150 – 5 ng (**Figure**

3.26A). The range of interest (150 – 5 ng) was further analysed to compare the signal intensity and sensitivity of the four systems (**Figure 3.26B**).

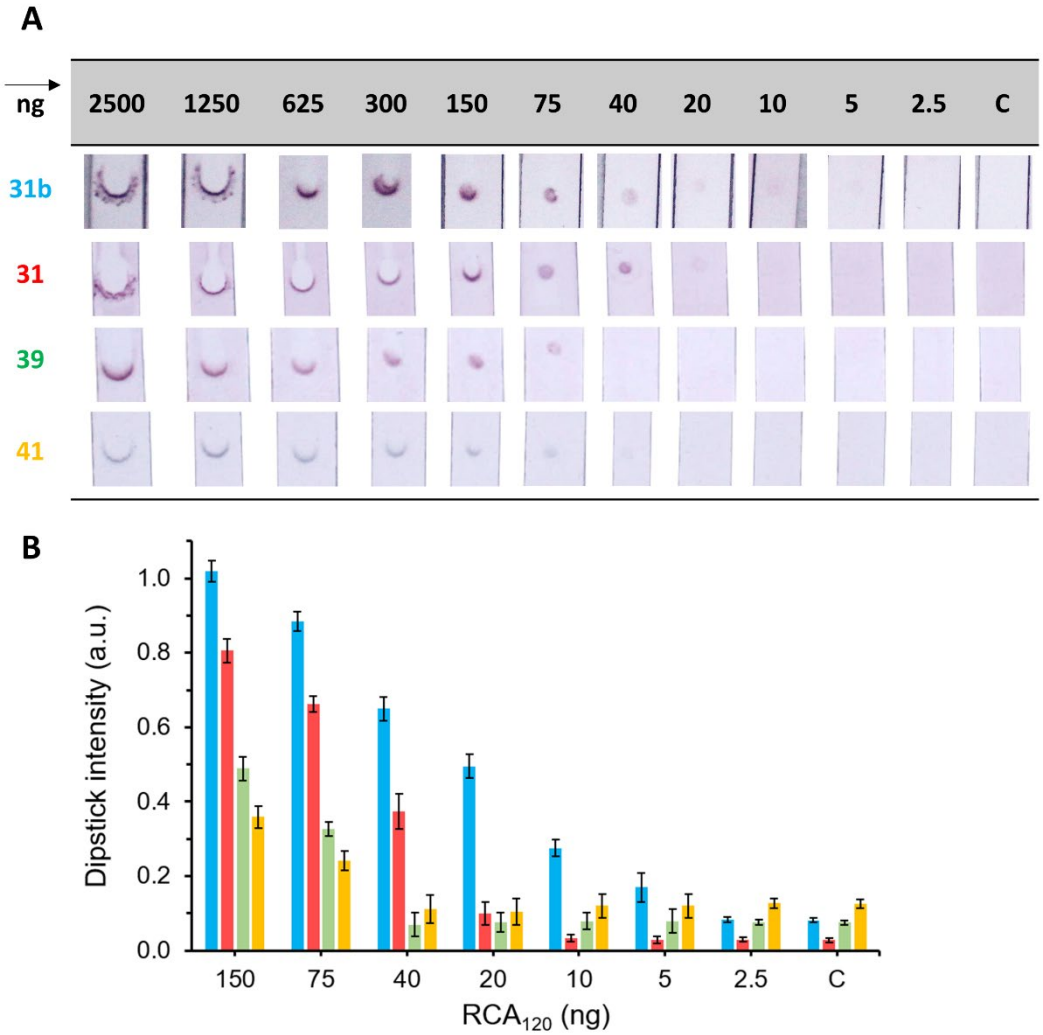

Figure 3.26. Sensitivity studies using OD 1 of either Gal_{14}-BSA-AuNPs (**31b**), Gal-BSA-AuNPs (**31**), Gal-AuNPs (**39**) or Gal-AuNSs (**41**) for the detection of RCA_{120} in a dipstick assay. (**A**) Dipstick images for the whole range of RCA_{120} tested (2,500 – 2.5 ng). (**B**) Quantification of the intensity of the dipsticks in the 150 – 2.5 ng range. Error bars show the standard deviation of triplicates in the experiment. C: negative control performed with the respective propyl-functionalised particles for the detection of 2,500 ng of RCA_{120}.

From these results, it is obvious that the glyco-BSA-AuNPs remain superior to the covalently functionalised AuNPs and AuNSs, in terms of both signal intensity and sensitivity of the assay. Contrary to certain literature in which Ab-functionalised AuNSs would improve the performance of LFAs, the Gal-AuNSs synthesised in this research work had the worst performance for the detection of RCA_{120}, with a visual LOD of 75 ng and considering the optimisation required for the assay. The Gal-AuNPs had a similar visual LOD, but the assay did

not present complications in terms of non-specific binding. The Gal-BSA-AuNPs allowed the detection of RCA_{120} in amounts ranging from 2,500 – 20 ng, with a visual LOD between 40 and 20 ng. This is lower than the values reported recently in the literature for a glycan-based LFA for the detection of RCA_{120}, which has been discussed in *Section 3.1*.[262] That work developed an assay based on 40 nm AuNPs decorated with a galactose-ending thiolated PHEA, which had a dynamic range of 5,000 – 100 ng, with a visual LOD of 500 ng.

The Gal_{14}-BSA-AuNPs reported in this work further improved the visual LOD, reaching amounts between 10 and 5 ng. The visual LOD obtained with the gAuNPs synthesised in this research was lower than the one reported for an Ab-based detection assay, which had a LOD of 9.5 ng of RCA_{120}, with a dynamic range of 70 – 0.35 ng.[280] Furthermore, the Ab-based assay was based on fluorescent latex beads functionalised with Abs, requiring a reader for the quantification of the signal.

Attempting to improve the limit of the detection, the Gal-BSA-AuNPs (**39**) and Gal-AuNSs (**41**) were tested at OD 5 instead of OD 1 for the detection of RCA_{120}. Whereas **39** did not present any particular complication, **41** aggregated at the bottom of the dipstick in every test. To solve the issue, different nitrocellulose membranes were tested for the assembly of the dipstick. Three main characteristics define the performance of a nitrocellulose strip: flow speed (s/strip), thickness (µm) and content of surfactant in the strip. A series of experiments were performed to investigate the influence of the flow speed of the nitrocellulose employed to assemble the dipstick (**Figure 3.27**). For that set of experiments, neither slow (entry 1) nor medium flow speed (entries 2-5, being 2 the one used by default in this thesis) prevented the aggregation of gAuNSs at the bottom of the dipstick. Higher speeds (entries 6-9) partially avoided the aggregation and a signal indicating the detection of the lectin could be observed, especially for entry 9. The best result was obtained when using nitrocellulose with the highest speed (entry 10), which seemed to recover the signal for the detection of RCA_{120}. Given that the type and content of surfactants in the different types of nitrocellulose are not disclosed by the manufacturers, they will not be compared in this study.

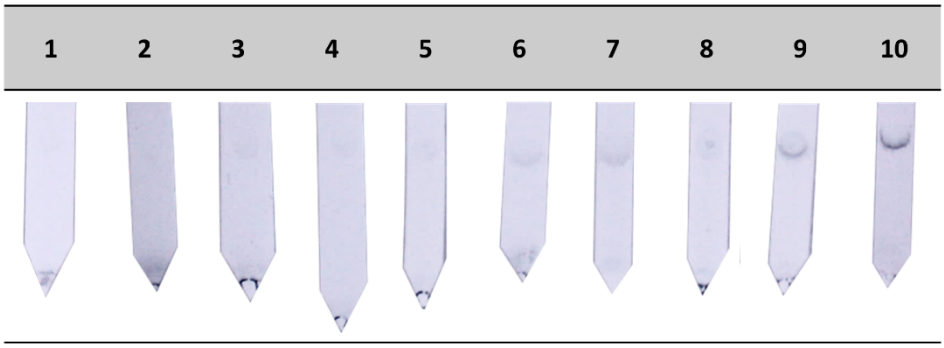

Figure 3.27. Influence of the nitrocellulose to overcome the aggregation of AuNSs at OD 5 in the dipstick assay. For the tests, Gal-AuNSs (**41**) at OD 5 were used to detect RCA_{120} (2.5 µg). The types of nitrocellulose tested included **1**: Immunopore FP (110-150 s/strip, 200 µm thick). **2**:Immunopore RP (90-150 s/strip, µm thick); **3**: FF120HP (90-150 s/strip, reduced content of surfactant, 200 µm thick); **4**: FF120HP Plus (90-150 s/strip, higher content of surfactant, 200 µm thick); **5**: FF120HP Plus Thick (90-150 s/strip, higher content of surfactant, 235 µm thick); **6**: Immunopore XP (60-100 s/strip, 200 µm thick); **7**: FF80HP (90-150 s/strip, reduced content of surfactant, 200 µm thick); **9**: FF80HP Plus (90-150 s/strip, higher content of surfactant, 200 µm thick); **9**: FF80HP Plus Thick (90-150 s/strip, higher content of surfactant, 235 µm thick); **10**: Prima40 (40 s/strip, higher content of surfactant, unknown thickness).

With the issue of aggregation solved, the sensitivity assay was repeated using the usual *Immunopore RP* nitrocellulose (entry 2) for Gal-BSA-AuNPs **39** and *Prima 40* (entry 10) for Gal-BSA-AuNSs **41** (**Figure 3.28**). A remarkable increase in the intensity of the signal could be appreciated in comparison to the dipsticks at OD 1 seen before (as seen in **Figure 3.26A**), whereas, unfortunately, the sensitivity remained unchanged.

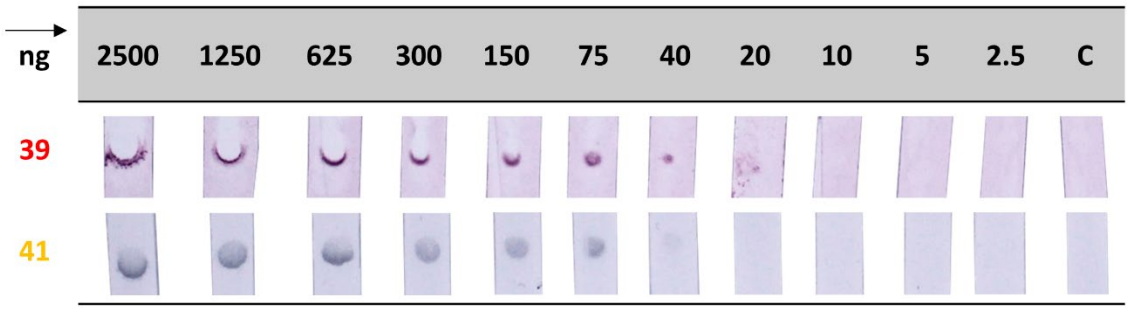

Figure 3.28. Sensitivity studies using OD 5 of either Gal-BSA-AuNPs (**39**) or Gal-AuNSs (**41**) for the detection of RCA_{120} ranging from 2500 – 2.5 ng in a dipstick assay. C: negative control performed with the respective propyl-functionalised particles for the detection of 2500 ng of RCA_{120}.

3.4. Conclusions

Representative examples of traditional Ab-based methodologies for the development of immunochromatographic assays have been discussed. A thorough literature search has been performed in this chapter to discuss every example of gAuNPs in paper-based diagnostic tools such as lateral flow and dipstick assays, understanding the current state of the field. A clear conclusion from that search is that, even though gAuNPs have shown potential for their application in detection bioassays, they have not yet been fully implemented and Abs are still dominating the field of diagnostics.

Seeking to understand the presentation of glycans on the surface of different nanomaterials and their influence on detection assays, three different types of glyconanomaterials have been successfully synthesised. Citrate-capped *ca.* 40 nm AuNPs have been functionalised with the collection of BSA conjugates **22-29**, yielding the set of BSA-AuNPs **30-37** which included propargyl, galactose, lactose, 2'-fucosyllactose, glucose, mannose, α3,6-mannotrioside and 3'-sialyllactose derivates. The set also included the BSA glycoconjugate **23b**, which contained 14 galactose residues instead of 3 as the original glycoconjugate **23**. TEM confirmed the size of the core of the AuNPs being 40 ± 2 nm, which is in agreement with the information from the manufacturer. Both UV-Vis and DLS showed an expected shift of 2-3 and 7-9 nm, respectively. The only exception to this was the gAuNPs **31b** (the ones synthesised from glycoconjugate **23b**), whose UV-Vis maximum of absorbance shifted only by 1 nm, and hydrodynamic diameter measured by DLS increased only by 5 nm. These facts are already informative of the possible surface differences that gAuNPs **31b** may present in comparison with the rest of the set. To understand the contribution of BSA as support for the carbohydrates on gAuNPs, commercially available NHS-ester activated AuNPs were covalently functionalised *via* NHS coupling with an aminopropyl galactoside, yielding the Gal-AuNPs **39**. TEM confirmed the size of the core of the AuNPs being 38 ± 2 nm, however, DLS showed a hydrodynamic diameter of 52 nm. This discrepancy is not unforeseen, given that the linker between the NHS-ester and the surface is not disclosed by the manufacturers. The UV-Vis did not show any appreciable shift, which was expected given the small size of the ligand. Finally, 150 nm AuNSs were covalently functionalised with an aminopropyl galactoside *via* NHS coupling, yielding Gal-AuNSs **41**. TEM confirmed the size of the particles as 149 ± 10 nm, and the DLS/UV-Vis showed similar shifts to the ones observed for Gal-AuNPs.

All the gAuNPs synthesised in this research work have been applied to a dipstick assay for the detection of plant lectins of well-known specificities. The glyco-BSA-AuNPs were first submitted to a specificity evaluation, which was very successful due to the very little non-specific interaction observed between the gAuNPs and the control lectins. Only the 2'FL-BSA-AuNPs **33** gave an unexpected interaction with RCA_{120}, even though that lectin should not interact with fucosylated structures. Indeed, further investigations allowed to find a certain amount of lactose in the original 2'-fucosyllactoside, which could perfectly explain the observed binding with the lectin. The results observed in the assay have been proved to be specific due to the interaction of the galactose residues exhibited on the surface. Similarly to the Gal-BSA-AuNPs, the Gal-AuNPs did not show any non-specific interactions with any lectins. However, the Gal-AuNSs required a thorough revision of the buffers used in the dipstick assay, as well as tuning the conditions for the functionalisation.

The sensitivity of all the nanoparticles against RCA_{120} has been tested and compared. In this work, gAuNPs exhibiting carbohydrates *via* a BSA glycoconjugate were found to be optimal agents for the detection of lectins. The assay has achieved a visual LOD between 10 and 5 ng of RCA_{120}, which is lower than the ones reported in the literature up to date. Efforts have been made to further improve the sensitivity of the assay, however, this remains challenging and requires more investigation.

3.5. Future work

The synthesised Gal-BSA-AuNPs and Gal_{14}-BSA-AuNPs performed differently in terms of intensity and sensitivity during the dipstick assay. A very interesting study here, linked to the future work discussed in *Chapter 2*, would involve the synthesis of a range of Gal_n-BSA-AuNPs to study the influence in the assay of the progressive increase of glycan multivalency (**Figure 3.29**). From the results obtained up to date, an increase in sugar loading on the BSA glycoconjugates has a beneficial impact on the assay. However, with high probability there is a limit to that, and. Many reports from the literature have been discussed in this chapter, where the density of glycans on gAuNPs was optimised, given that crowded surfaces may hinder the accessibility to the glycan by the targeted lectin.

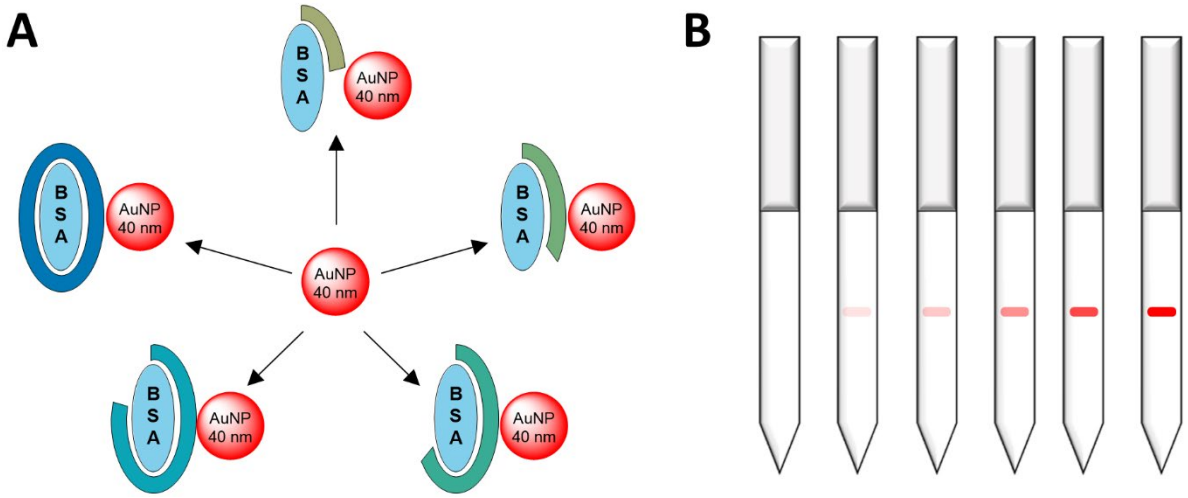

Figure 3.29. Potential future work following the results obtained in *Chapter 3*. (**A**) Schematic representation of the synthesis of a set of glyco-BSA-AuNPs covering different degrees of glycosylation, represented as an outer ring around the BSA glycoconjugate. (**B**) Potentially progressive increase of dipstick signal intensity with an increased rate of glycosylation on the surface of gAuNPs.

The comparison of AuNPs and AuNSs as colorimetric labels for the multivalent presentation of sugars in the dipstick assay was, to some extent, disappointing. The expected outcome of that research was to find a higher sensitivity coming from the larger surface area that AuNSs exhibit, however, this was not the case. The main issue were the non-specific interactions found, which were overcome with detergent and blocking agents in the dipstick buffer. It is still a question whether further assay optimisation, different buffers or even types of nitrocellulose would lead to a different outcome.

The assay developed in this research has covered a range of non-toxic lectins. A further step in this line would be the application of the assay to pathogenic lectins such as the cholera toxin from *V. cholerae* or LecA from *P. aeruginosa*, or even the whole pathogens.

CHAPTER 4

DESIGN AND SYNTHESIS OF GLYCOSIDE DIMERS FOR THE DETECTION OF BACTERIAL LECTINS

4.1. Introduction

In the previous chapters, the synthesis of carbohydrate-based ligands was designed based on the glycan-specificity of the targeted lectins. The following chapter covers the literature on the design of multivalent carbohydrate-based ligands targeting specific bacterial lectins and adhesins, with a focus on LecA from *P. aeruginosa*. With the aim of undertaking a potential case of study for LecA inhibitors, a small collection of novel galactoside dimers has been designed employing a combination of CuAAC chemistry and EDC couplings to allow a systematic combination of building blocks. The retrosynthetic pathways, the selected synthetic strategies and the key characterisation of the synthesised compounds are presented, together with the discussion of issues encountered.

In the second part of the chapter, some preliminary results with *P. aeruginosa* strain PAO1 are presented describing the growth of the bacteria, a flow cytometry (FCM) method to potentially detect bacteria–gAuNPs interactions and the detection of LecA in samples of *P. aeruginosa* through Western Blot.

4.1.1. Targeted detection of lectins: tailoring glycoside ligands

In *Chapter 2*, the importance of multivalency and glycan density in the development of sensing systems for lectins has been discussed. A critical analysis of the reported literature seems to suggest that a higher multivalency of the carbohydrate ligands tends to be beneficial for the binding to lectins. However, a higher density of glycans does not directly correlate with an improved affinity of the ligand and it needs to be evaluated for each application. The concept of multivalency covers the number of copies of a glycan within a ligand unit (**Figure 4.1A**), whereas the concept of ligand density covers the number of copies of a ligand in a given space or surface area (**Figure 4.1B**). However, the density of glycan units within a multivalent ligand, which could be named intra-ligand glycan density (**Figure 4.1C**), is also of great importance to design ligands for specific lectins.[281]

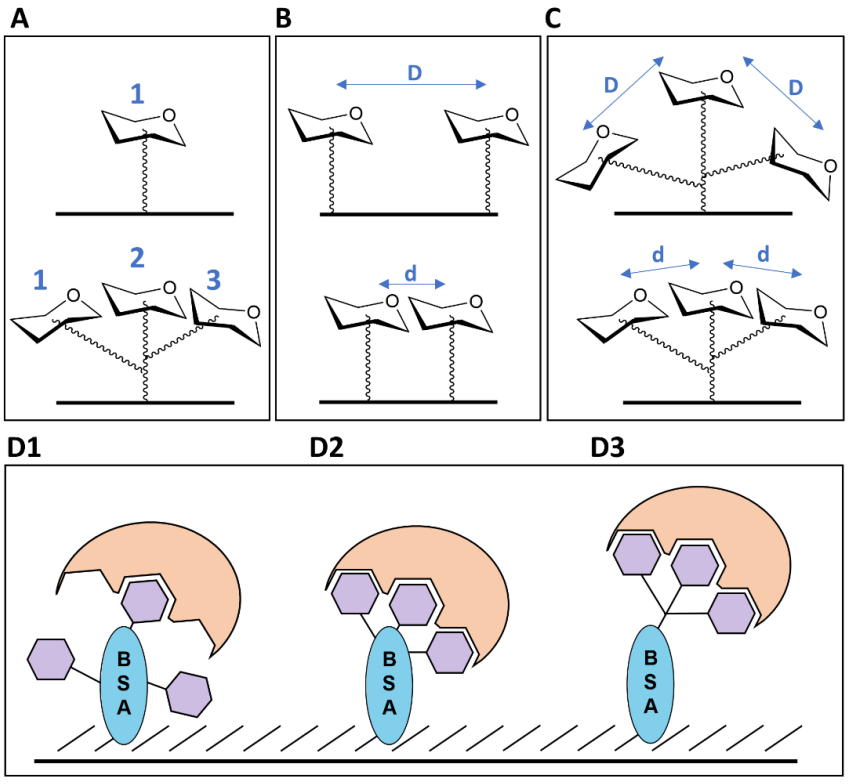

Figure 4.1. Parameters to consider while designing a carbohydrate-based ligand for a specific lectin: (**A**) the multivalency required for the target, (**B**) the optimal ligand density to allow accessibility of the glycans and (**C**) the intra-ligand glycan density, whose optimisation may turn a (**D1**) less efficient glycan-lectin binding into a (**D2**) very efficient one (adapted from Oyelaran *et al.*[282]). (**D3**) Glycodendrimers are good candidates for fine-tuning the intra-glycan density, allowing the design of ligands to measure for specific lectins. ***D*** and ***d***: longer and shorter distances between glycan units, respectively.

Glycoarray experiments have suggested that the intra-ligand glycan density is a crucial factor for the development of detection tools against specific lectins (**Figure 4.1D1,D2**).[282] BSA was decorated with different amounts of glycans (ranging from 4-37) *via* either reductive amination or EDC/NHS couplings, and subsequently bound to glass slides. A collection of 45 different neoglycoconjugates was screened against different lectins, showing that the multivalent presentation of glycans enhanced the binding with lectins in comparison with free sugars. An example of that result was given with a GalNAc-BSA glycoconjugate targeting soybean agglutinin, which exhibited a K_D value 220 times lower than the one of free GalNAc. However, the authors commented on the unprecise arrangement of carbohydrates due to the many possible binding points to the protein. The different arrangements of glycans in the neoglycoprotein may lead to combinations of equal multivalency but different distribution, thus different interaction with a targeted lectin. For an accurate, controlled and reproducible arrangement of carbohydrates, designing ligands tailored for the targeted lectins is preferred (**Figure 4.1D3**).

4.1.2. Inhibitors of Shiga and Shiga-like toxins

Shiga toxins (Stx1, Stx2) from *S. dysenteriae* and Shiga-like toxins (SLT-1, SLT-2) from *E. coli* have been the subject of intense research for more than 20 years. Stx and SLT belong to the pentameric AB_5 type of proteins with an affinity for the P^k trisaccharide Galα(1-4)Galβ(1-4)Glcβ (**Figure 4.2A**) which is found in the Gb3 glycolipid.[283] The first multivalent ligands employed as toxin inhibitors were the peptide dimers reported by Toone and collaborators (**Figure 4.2B**)[284], and the STARFISH ligands developed by the Bundle group (**Figure 4.2C-D**).[285] The work of Toone developed pentapeptide decorated with two terminal P^k units. Assessment of its binding to SLT-1 by ITC showed a K_D value of 91 µM, 14 times tighter than the binding of P^K alone (K_D 1.3 mM). Meanwhile, Bundle and co-workers looked at the crystal structure of the SLT-1 – Gb3 complex and observed that position 2' of the trisaccharide was the furthest from the protein surface, and it was selected as the optimal one where to install a tether without compromising the affinity. The designed ligand successfully targeted two binding sites of SLT-1 with the P^k dimer with a K_D value in the millimolar range. The ligand was improved to obtain a pentameric inhibitor, namely STARFISH, using a glucose unit as a five-armed core. The clustering effect of the resulting ligand was very effective, with an improvement of the K_D value to the subnanomolar range. The STARFISH ligand was assessed as an inhibitor of both

SLT-1 and SLT-2 in kidney cells, presenting for the first time an 80% of success when using submillimolar concentrations.

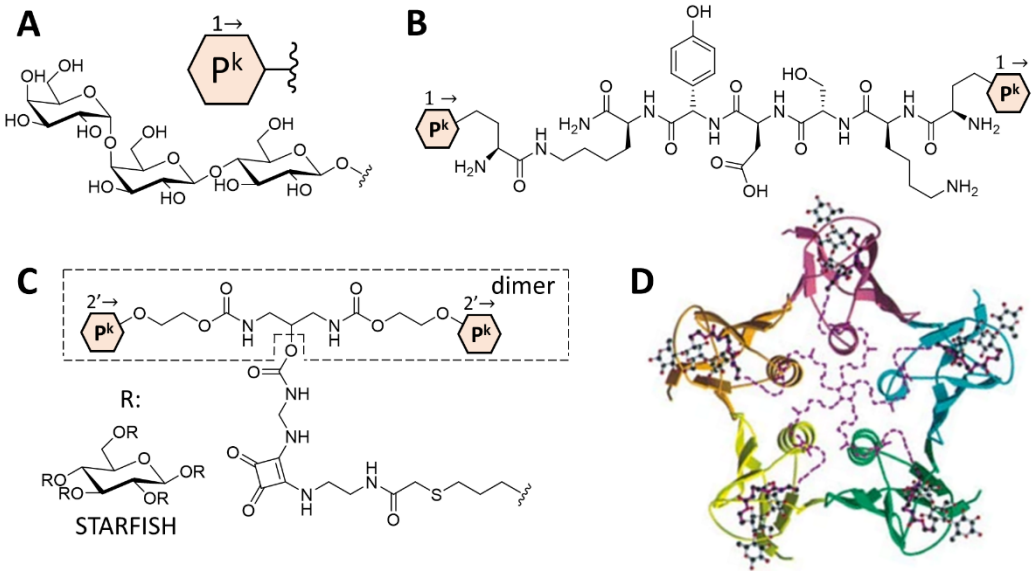

Figure 4.2. Multivalent inhibitors of STL-1. (**A**) Structure of the P^k trisaccharide found in the receptor of Shiga and Shiga-like toxins, and the symbol used for it in this thesis. (**B**) Structure of the divalent glycopeptide reported by Lundquist *et al.*[284] (**C**) Structure of the decavalent STARFISH toxin inhibitor and (**D**) crystallographic diagram of its binding to the STL-1 (for clarity, only half of the sandwich is represented). Reproduced from Kitov *et al.*[285] with permission from Springer.

A few years later, the STARFISH inhibitor was taken to the next stage, evaluating its ability to protect mice from Stx1 and Stx2.[286] Although the inhibitor was able to fully protect the mice inoculated with lethal doses of Stx1, the deadlier Stx2 presented a challenge, with a survival rate of 0% after 72 h. The structure was revised, and the tether was elongated by eight bonds in a new inhibitor, namely Daisy, granting more flexibility to the structure for better targeting of Stx2. Indeed, the modification allowed Daisy to protect mice not only from Stx1 but also from Stx2.

In the same period of time, a set of P^k-based inhibitors of Stx with a silicon core was developed under the name of SUPER TWIGs (**Figure 4.3**).[287] They were designed and applied to infected mice to probe their high cell viability and inhibitory effect on both Stx1 and Stx2, with reported K_D values in the micromolar range for all the tested compounds (reported values of 44, 1.4 and 4.2 μg/mL, respectively for SUPER TWIG 1, 2 and 3 against Stx1). The SUPER TWIG 2 was further investigated to show how its interaction with Stx not only prevented the uptake of the toxin by targeted cells but also induced its degradation by macrophages.

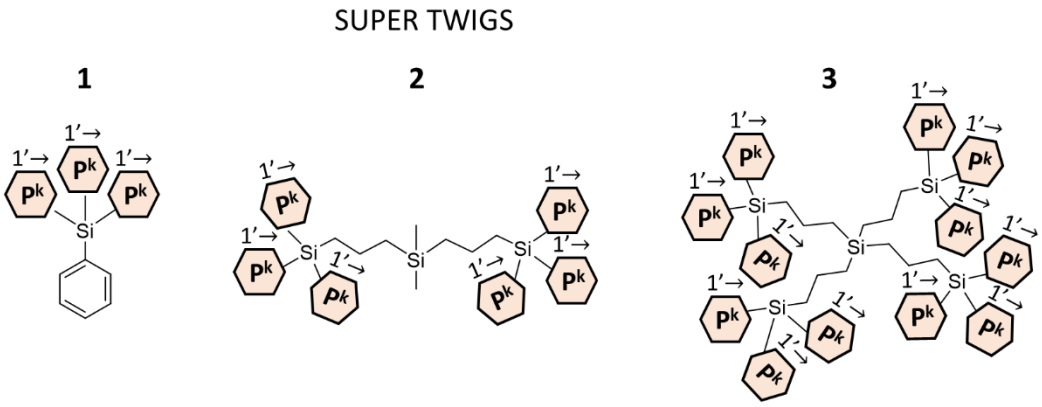

Figure 4.3. Structures of the three SUPER TWIGS developed by Nishikawa *et al*.[287] as inhibitors of Stx1 and Stx2.

In an attempt to improve the STARFISH strategy with a pentameric scaffold to direct the P^k units correctly, a trap-inhibitor ligand was developed with the name BAIT (**Figure 4.4**).[288] For the scaffold, the serum amyloid P component (SAP) was chosen as it presents a B_5 structure similar to the one of Stx. The authors had previously developed a ligand for SAP based on a cyclic pyruvate of glycerol,[289] which was incorporated into the BAIT bifunctional inhibitor. The strategy successfully directed the pentameric ligand towards the binding sites of Stx1, achieving an IC_{50} of 4 μM.

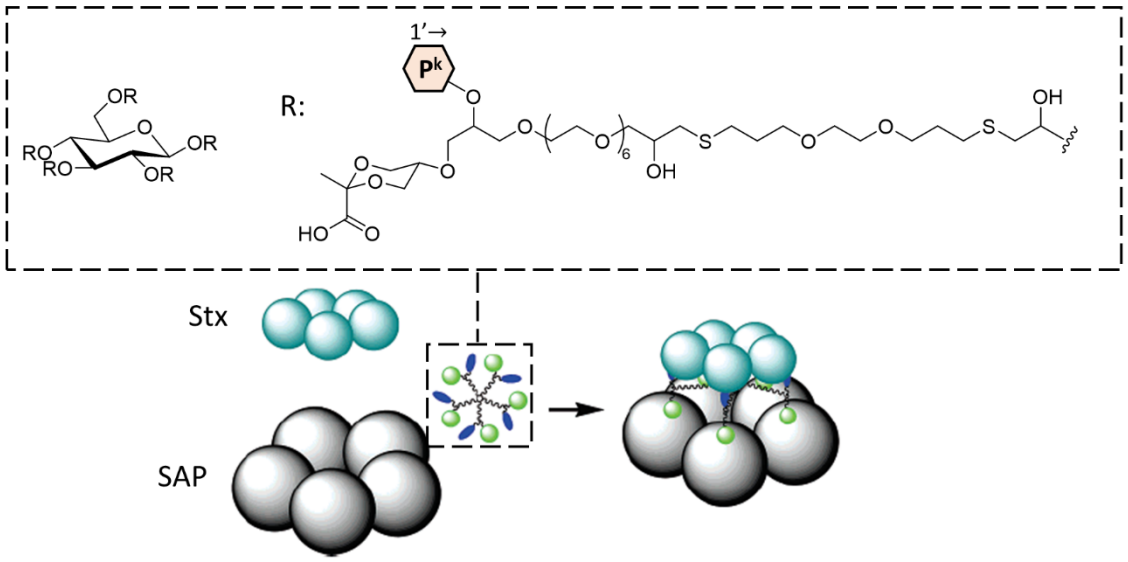

Figure 4.4. Structure of the BAIT trap-inhibitor system designed against Stx, and conceptual representation of the system. Adapted from Fan *et al.*[288] with permission from the American Chemical Society.

The Bundle group continued their work on supramolecular traps targeting STL-1 with an adaptation of the BAIT approach.[290] The developed ligand and the trap remained the same, although the multivalency relayed on a polymeric backbone for which two different assemblies were tested: a randomised polymer A (**Figure 4.5A**) and a pre-organised polymer B (**Figure 4.5B**). Polymer A was built starting from three monomers: the P^k inhibitor, the glycerol pyruvate trap, and acrylamide as spacer. Polymer B was built from two monomers: the bifunctional trap-inhibitor ligand previously synthesised, and acrylamide. Polymers A and B on their own successfully inhibited Stx1, with IC_{50} values of 0.6 and 14 µM. As the ligand units in polymer A are randomly distributed, the addition of the SAP trap to the system did not have any effect on its binding to Stx1, although it lowered the IC_{50} value of polymer B to 2.3 nM. The experiment confirmed the importance of the pre-organised arrangement of the ligands before assembling the polymeric backbone.

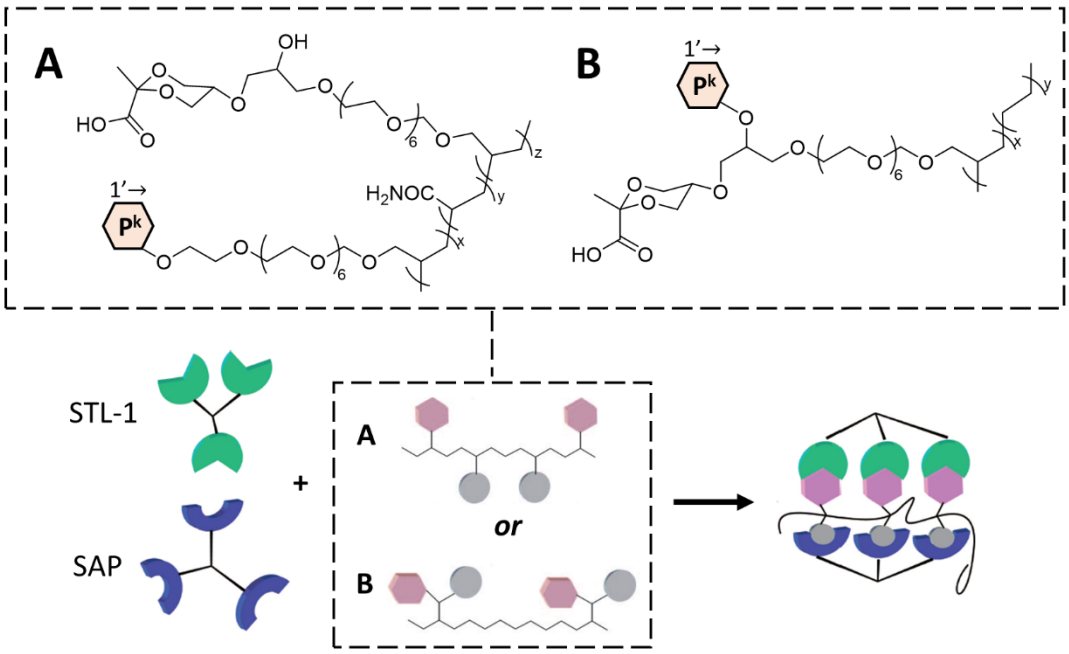

Figure 4.5. Structure of the two polymeric trap-inhibitor systems designed against Stx1, and conceptual representation of the system. Adapted from Kitov *et al.*[290] with permission from the National Academy of Sciences. Note: SAP was represented as a trivalent receptor instead of a pentavalent one, possibly for the simplification of the figure.

Years later, the polymeric approach was varied removing the trap side of the system and installing the P^k ligand on a pre-made polyacrylamide backbone through CuAAC chemistry.[291] However, the new polymer was not tested against Stx2 until a later publication, where an ELISA was developed (**Figure 4.6**).[292] The authors observed from the crystal structure of the

Stx2 complex with P^kNAc, that there was an opportunity to enhance the interaction upon derivatisation of the N-acetyl side of the molecule. They firstly tested P^kNAc and P^kNH_2 in the polymer, the latter showing no interaction with the toxin. Up to 90 different acylation reagents were screened, however, they did not seem to produce an enhancement of the inhibition of Stx2, except lysine derivatives. At that point, the authors decided to go further and use the P^kN-Lysine conjugate as a scaffold to build a collection of new polymers, from which 5-(3-nitro-phenyl)-furan-2-carboxylic acid (highlighted in the figure) improved the inhibition of a factor of 30, with an IC_{50} value of 0.26 nM.

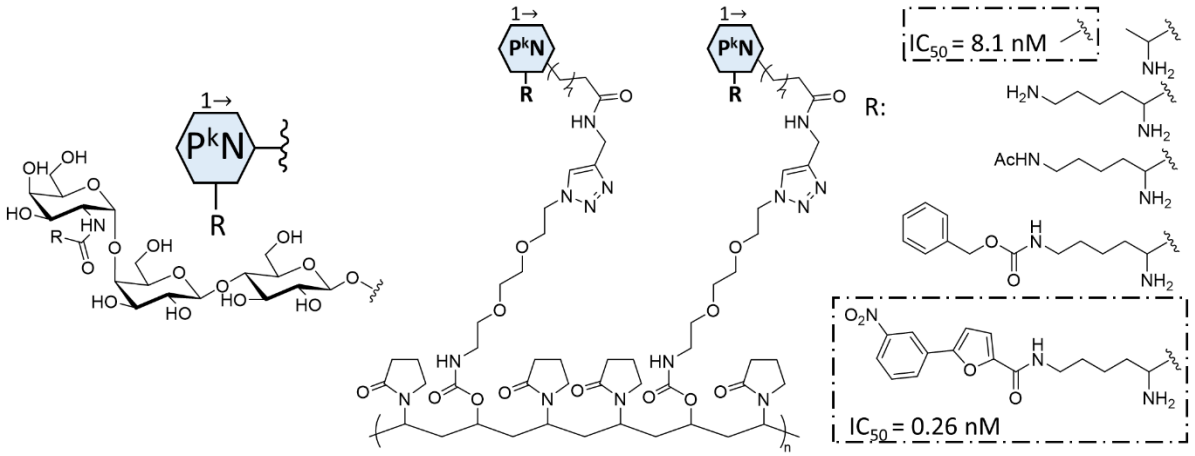

Figure 4.6. Polymers developed by Dasgupta *et al.*[292] as inhibitors of Stx2 in an ELISA.

Other polymers have been used over the years to gain multivalency against the Stx. Polymeric derivatives of the P^k trisaccharide have been developed tethering the carbohydrate with an amino acid (**Figure 4.7A**).[293] Three different amino acids (L-glycine, L-alanine and β-alanine) were used to link P^k to the polymeric backbone, and two different kinds of polymers were synthesised: a homopolymer of P^k and a copolymer with 90% of acrylamide to dilute the presence of P^k. A cytotoxicity test to study the IC_{50} against Stx1 and Stx2 showed that whereas both polymers inhibited Stx1 with values in the submicromolar range, only the homopolymers did inhibit Stx2. A homopolymer bearing L-alanine in the tether exhibited the lowest IC_{50} values, these being 0.14 and 0.8 µM for Stx1 and Stx2, respectively.

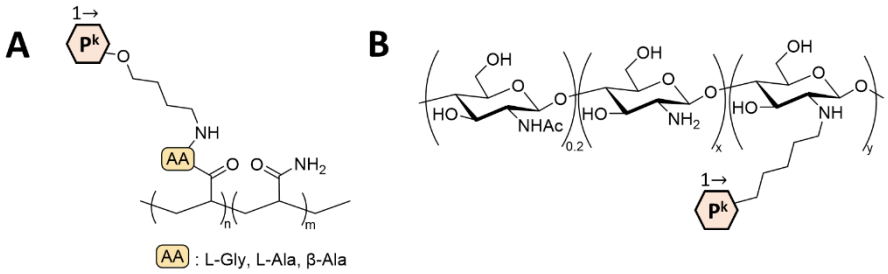

Figure 4.7. Polymers developed by (**A**) Matsuoka *et al.*[293] and (**B**) Li *et al.*[294] for the inhibition of Stx1 and Stx2.

Lastly, from synthetic to natural polymers, chitosan has also been used as a polymeric support for P^k targeting Stx1 and Stx2 (**Figure 4.7B**).[294] Four different variants were synthesised, yielding degrees of substitution of 9, 22, 38 and 59%. Their IC_{50} values against Stx1 were evaluated, showing a progressive decrease with an increasing degree of substitution from the submicromolar to nanomolar range. Likewise, IC_{50} values for Stx2 decreased from the micromolar to the submicromolar range. To test the inhibition of cytotoxicity, Stx-sensitive Vero cells were incubated with lethal doses of Stx, showing an increase of the cell viability with the increasing degree of substitution of the polymers. The polymer with a 59% of substitution, which had IC_{50} values of 50 and 430 nM for Stx1 and Stx2 respectively, inhibited the cytotoxicity of lethal doses of Stx1 and Stx2 at 10 µg/mL.

Cyclodextrins are naturally occurring multivalent scaffolds that have also been exploited as backbones to exhibit P^k as inhibitors of Stx2 (**Figure 4.8A**).[295] The radial symmetry of cyclodextrin was used as a template to install seven units of the trisaccharide *via* CuAAC chemistry. The inhibitors were tested in an ELISA assay against both Stx1 and Stx2, showing for the first time a superior affinity for the latter. The IC_{50} values obtained in this work were unprecedently low for the Stx2 toxin, approximately 9 ng/mL as reported (which translates to a concentration of approximately 1.5 nM).

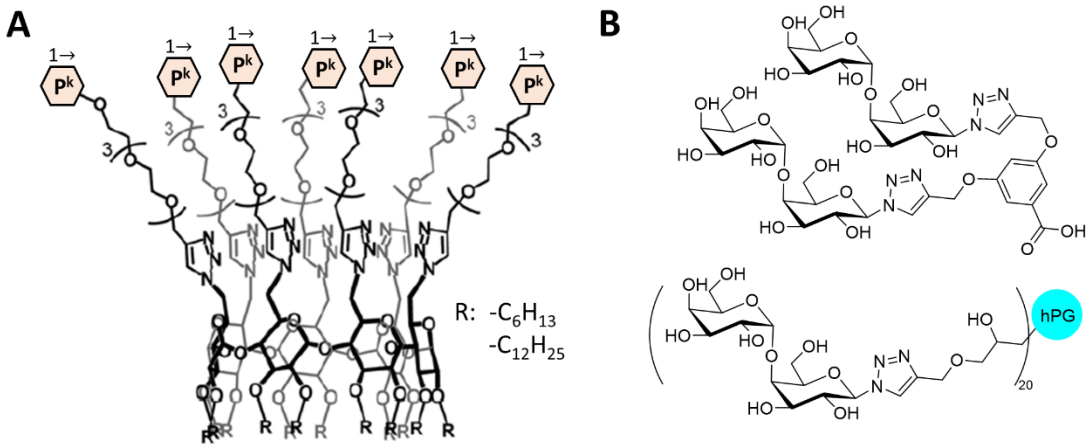

Figure 4.8. (**A**) Structure of a multivalent inhibitor of Stx2 supported on cyclodextrin developed by Zhang *et al.*[295] (**B**) Structure of multivalent ligands of Stx1 reported by Haksar *et al.*[296] bearing galabiose as a mimic of P^k: one dimer, and one cluster supported on hyperbranched polyglycerol (hPG).

Finally, galabiose was used in a recent report as a mimic of P^k for the inhibition of Stx1.[296] A dimer and a tetramer were synthesised, and lastly an icosavalent (20 glycoside units) cluster of galabiosides supported on hyperbranched polyglycerol (hPG) (**Figure 4.8B**). The compounds were applied in an ELISA to evaluate the inhibition of Stx1, showing that the increase in valency would grant lower IC_{50} values. Whereas the dimer exhibited an IC_{50} of 1070 µM, the cooperative effect of glycosides was observed in the tetramer, whose IC_{50} was 13.5 µM. A further improvement was observed for the hyperbranched polyglycerol derivative, with an IC_{50} of 8.3 nM. Not only the polymeric approach reported a potent inhibitor of the toxin, but also it was built from biocompatible materials with applicability for *in vivo* studies.

4.1.3. Inhibitors of the cholera toxin

The cholera toxin (CT) from *V. cholerae* has also attracted attention over the years towards the development of inhibitors due to the hazard that it presents to public health, especially in underdeveloped countries. Many inhibition systems have been developed taking advantage of the affinity of the lectin for the ganglioside GM1 (**Figure 4.9A**). A strategy with an analogous approach to the above-discussed BAIT inhibitor employed the actual toxin as a scaffold to build a pentavalent GM1-ending ligand (**Figure 4.9B**).[297] To build the protein scaffold, the B subunit of the toxin (CTB) was firstly modified through a tryptophan-to-glutamic acid mutation in each of the binding pockets, leading to an inactivated CTB/W88E which has been reported to lead to a loss of GM1-binding capacity.[298] A second modification was performed on the

unique threonine residues (one per binding site), whose β-aminoalcohol moiety in the side chain allowed oxidation to an aldehyde and subsequent coupling with amino-ending GM1 derivatives to form an oxime. The interaction of the neoglycoprotein with CT was confirmed by ITC and ELLA, showing a K_D of 30 nM and an IC_{50} value of 0.1 nM. As the conjugate formed was glycoprotein-protein rather than carbohydrate-protein, DLS also allowed confirmation of the binding, observing an approximate particle diameter increase from 5.5 to 9 nm.

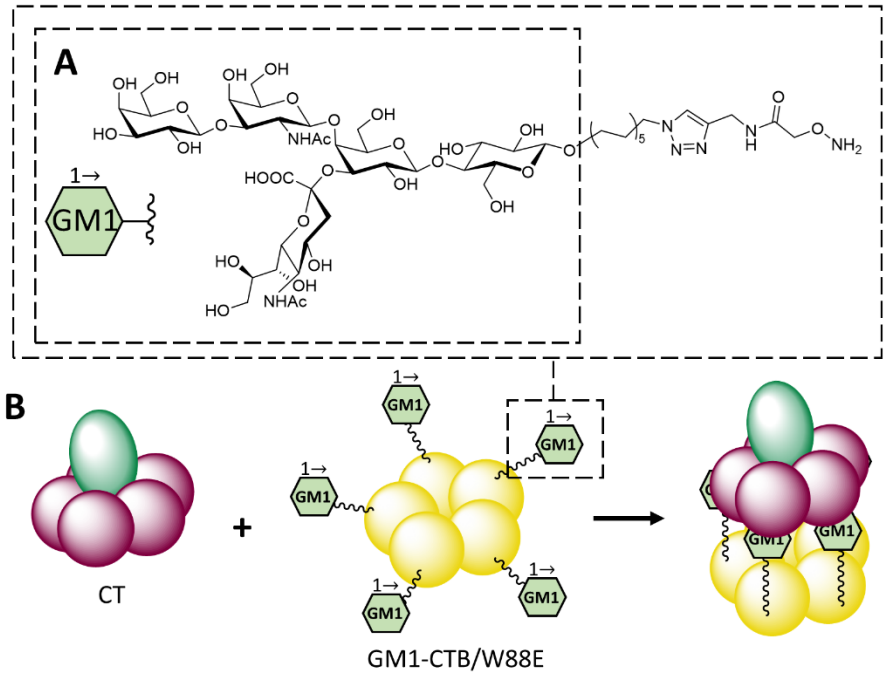

Figure 4.9. (**A**) Structure of the GM1 receptor of CT through its B subunit (CTB), and (**B**) Pentavalent CTB inhibitor using an inactivated CTB (CTB/W88E) scaffold, developed by Branson *et al.*[297]

Other works have derivatised GM1 or GM1 mimics with a tether to build glycodendrimers of first, second and third generation. In three different reports, Pieters and collaborators described the development of libraries of GM1 or GM1 mimics varying tethers and multivalency. The first of this series of works employed lactose as a mimic of the terminal galactose GM1 (**Figure 4.10A**).[299] The authors described a fluorescence titration assay where CT is titrated with ligands to quench the fluorescence of a tryptophan residue. They reported a decreasing trend in the K_D values as the multivalency increased: 235, 99, and 33 μM for the dimer, tetramer and octamer, respectively. In a following publication, they employed not only GM1 but also GM2 (which has the same structure as GM1 but lacking the terminal galactoside), to build a collection of analogous dimers, tetramers and octamers (**Figure**

4.10B).[300] An ELISA was used to test the efficiency of those compounds to inhibit the toxin, finding again that the higher multivalency correlated with a better inhibition. Those dendrimers achieved unprecedented IC_{50} values of 2, 0.2 and 0.05 nM for the dimer, tetramer and octamer of GM1, respectively, which represented up to a 380,000-fold improvement over the GM1 interaction with the toxin. As expected, the inhibitors based on the weaker binder GM2 exhibited IC_{50} values in the millimolar range. Analogous tetramers were used in a later publication to compare the inhibition of both CT and the heat-labile enterotoxin (LTBh) produced by *E. coli*.[301] Although still potent inhibitors, the IC_{50} value for the inhibition of LTBh with the tetramer was of 31 nM, with a K_D value of 7 nM found through ITC.

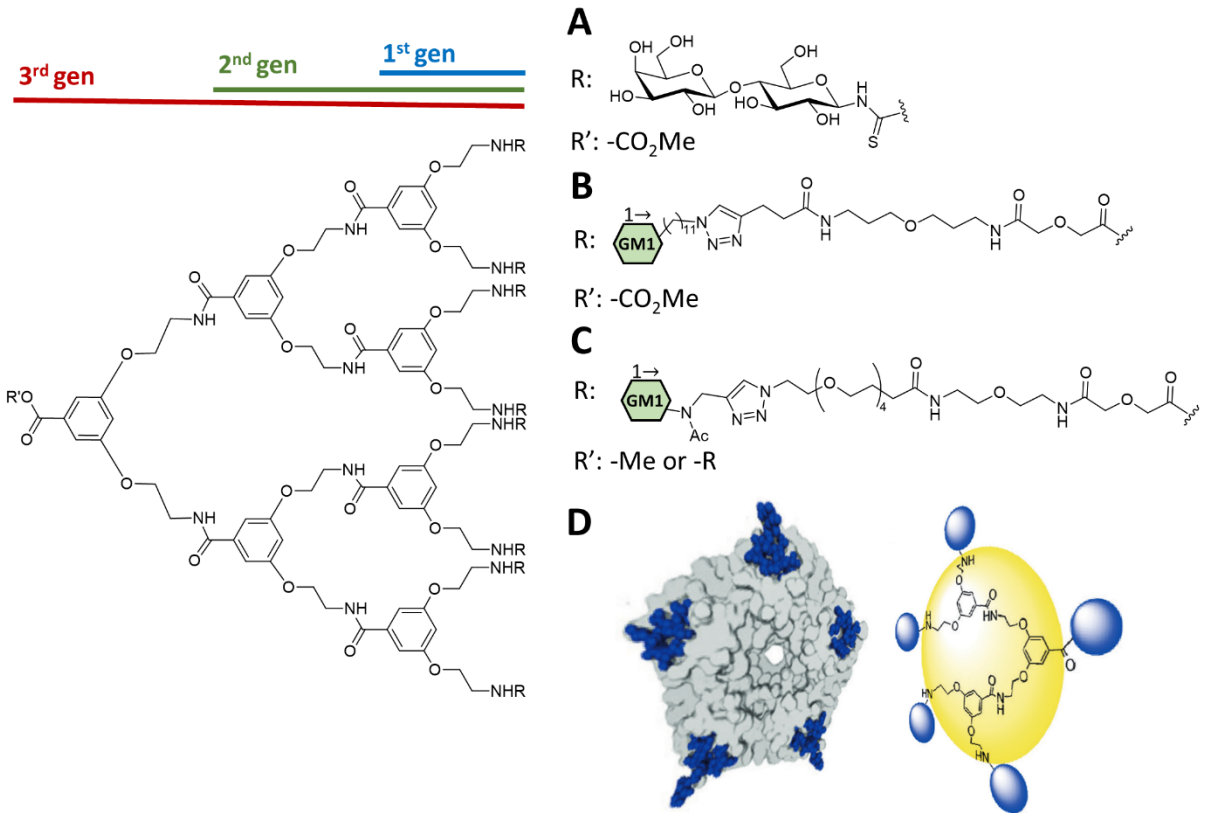

Figure 4.10. Flexible dendrimers of first, second and third generation prepared in the Pieters group for the detection of CT. (**A**) Collection of dimers, tetramers and octamers prepared by Vrasidas *et al.*[299] (**B**) Collection of dimers, tetramers and octamers prepared by Pukin *et al.*[300] (**C**) Tetra- and pentavalent ligands synthesised and (**D**) their mode of binding with CTB (PDB 3CHB), adapted from Fu *et al.*[302] (CC-BY-NC).

In a follow-up work, a comparison between tetravalent and pentavalent inhibitors of CT was published (**Figure 4.10C-D**).[302] The GM1-ending ligands were tethered with a long, PEGylated chain to attempt the simultaneous interaction with the binding pockets of the toxin. The scaffold presented in that work was more flexible than the previously reported, however, it

successfully yielded a nanomolar inhibitor of the toxin. The comparison between tetra- and pentavalent ligands showed little difference, with a slightly lower IC_{50} value for the tetravalent one (0.16 ± 0.04 nM) in comparison with the pentavalent one (0.26 ± 0.02 nM). A follow up work from the same group reported the development of a GM1 mimic following a structure-based design, keeping the terminal galactoside residue and a carboxyl group instead of the sialic acid.[303] After trials testing the IC_{50} values of the monomers, the authors presented the ligand shown in **Figure 4.11A.** To enhance the binding, the authors employed an analogous approach to the one shown in **Figure 4.10**. The dimer and tetramer synthesised in that work were assessed for the inhibition of the toxin *via* SPR, showing IC_{50} values of 13 and 0.5 µM, which are approximately 1000-fold higher than the ones obtained with analogous structures using GM1. The octamer was also tested, although the value could not be reported as they reached the lower limit of detection of the technique.

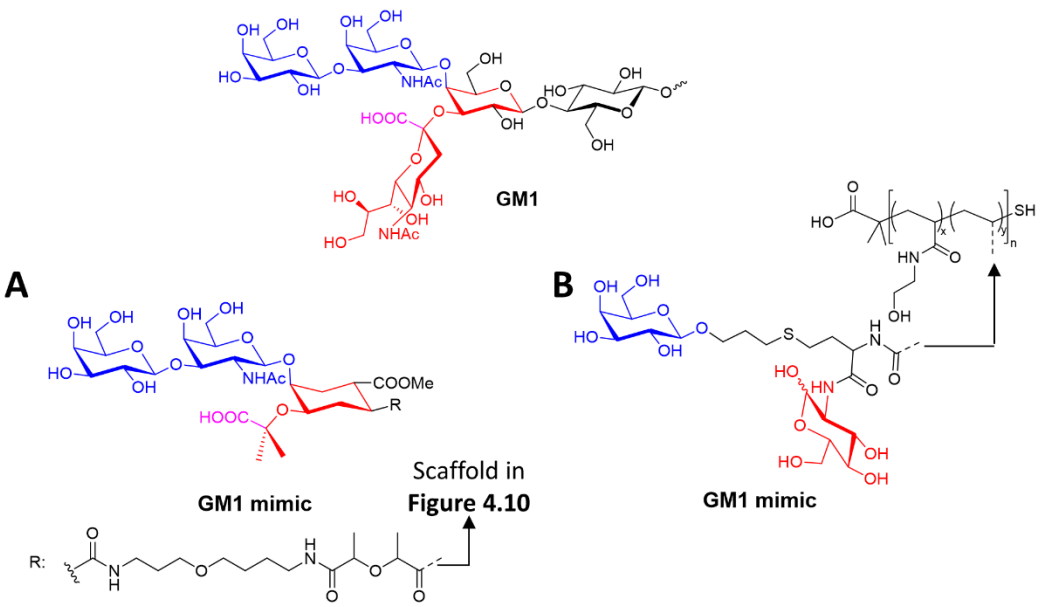

Figure 4.11. Comparison of the structures of GM1 and the GM1 mimics developed by (**A**) Arosio *et al.*[303] and (**B**) Wilking *et al.*[304]

Another GM1 mimic was developed a few years ago, combining galactose as a primary binding unit and glucosamine as a secondary one, using a polymeric backbone (**Figure 4.11B**).[304] The effect of the glycan density was investigated by synthesising polymers containing 5, 10 and 20% (mol) of the glycoside monomer. The increasing density of substitution was found to hinder the inhibition of the toxin, with IC_{50} values of 0.5, 15 and 30 µM, respectively. The length of the aglycon was also varied, comparing the original propyl with a hexyl linker

between the galactose residue and the thiolactone, which did not have a significant effect. However, the secondary binding moiety (originally GlcNAc) showed influence in the modulation of the binding. Upon substitution of the GlcNAc residue for a benzyl moiety, BLI experiments showed a lower inhibition of the toxin or even the loss of inhibition capacity.

In the context of polymeric backbones exhibiting inhibitors of CT, peptides have also been employed to yield the multivalency of galactoside ligands. Helical peptides have been designed taking into account the targeted separation between galactose units and the desired valency of the inhibitor.[305] Different sequences of amino acids were designed bearing alanine and glutamine residues to grant helicity,[306] and introducing glutamic acid residues as the reactive handle to attach the glycoside (**Figure 4.12**). The amount and distribution of glutamic acid allowed control of the multivalency and glycan density in the final peptides. The targeted distance between galactose units was of 35 Å, in agreement with the crystal structure of CTB complexed with the natural receptor GM1.[307] To probe the effect of the distance, peptides were designed leaving a 35 and a 17 Å distance between glycosides. The influence of multivalency was also investigated for the 17 Å one, by assembling a shorter version of the tether, therefore with fewer glutamic acid residues. The functionalisation of carboxylic acid moieties to glycan-bearing amides was convergent from NMR and MALDI-TOF experiments, with conversion rates of 90-97%. Inhibition of CT was evaluated in an ELLA, showing, as expected, that the longer peptide with 35 Å between glycoside units exhibited the best IC_{50}, of 160 µM. Secondly, the peptide of equal length and double the number of glycosides, separated by a 17 Å gap, exhibit an IC_{50} value of 725 µM. Not only the importance of glycan density was proven, but also of multivalency, as evidenced by the shorter peptide with 17 Å between glycosides, which had an IC_{50} value of 3340 µM.

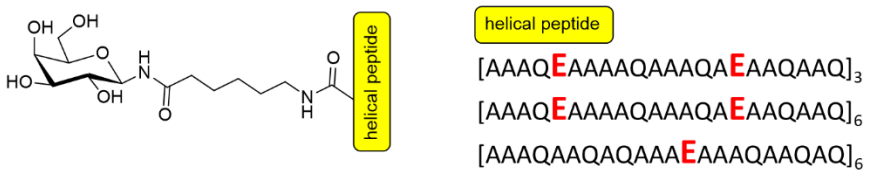

Figure 4.12. Peptide-based multivalent inhibitors of CT reported by Liu *et al.*[305] highlighting their **binding points**. Amino acids: A, L-alanine; Q, L-glutamine; **E**, L-glutamic acid.

Lastly, on the topic of bacterial toxins, the inhibition of LTBh has been addressed with a pentacyclen scaffold to direct the binding of glycan monomers (**Figure 4.13**).[308] Galactose was

used as a mimic of the natural epitope of the lectin, GM1. The inhibition of the toxin was measured through ELISA, finding an IC_{50} value of 195 μM for the monomer, and 0.9 for the pentamer. Following analysis of the crystal structures, the authors acknowledged the need for more rigid ligands that would allow simultaneous interaction with the binding sites of the toxin. This conclusion is often the case for works in CT as well.

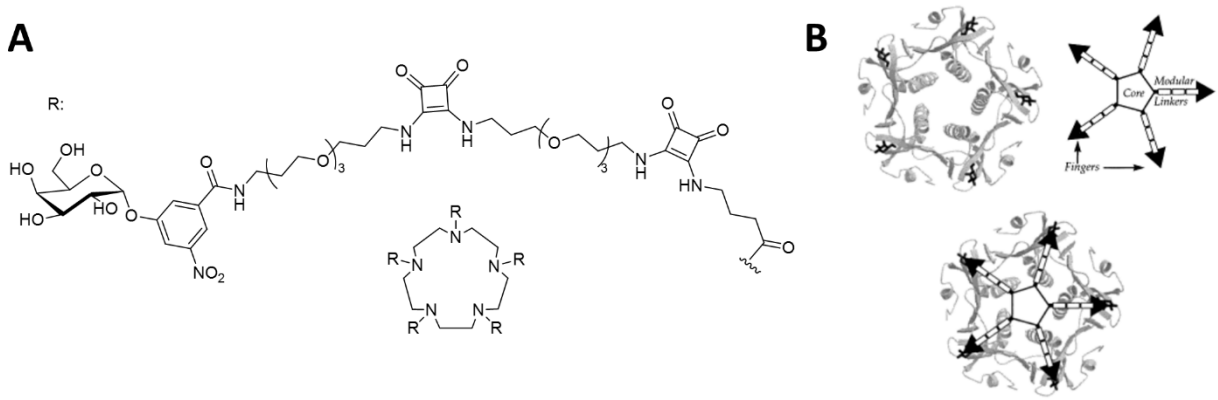

Figure 4.13. (**A**) Structure of the squaramide-linked pentavalent ligand with pentacyclen core reported and (**B**) schematic representation of its binding mode to LTBh from *E. coli.* Adapted from Merrit *et al.*[308] with permission from the American Chemical Society.

4.1.4. Inhibition of bacterial adhesins

Bacterial adhesins have been targeted for the development of anti-adhesive therapies. The *Streptococcus* genus has been targeted in different works for the development of inhibitors against its galactose-binding adhesins.[309] Targeting the P_N and P_O adhesins from the source of meningitis *Streptococcus suis*, Pieters and collaborators developed a collection of multivalent galabiose-based inhibitors.[310] Short-tethered dimers were constructed with aromatic cores differing at the relative position of the glycosides (meta and para, **Figure 4.14A**), showing little differences in terms of adhesin inhibition, with an approximate IC_{50} value of 300 nM. Longer tethers in the meta position (**Figure 4.14B**) seemed to improve the inhibition by a factor of 2, with an IC_{50} value of 159 nM. Both the tetramer and octamer inhibitors (**Figure 4.14C**) seemed to exhibit the same level of adhesin inhibition, with IC_{50} values of 7 nM. With analogous ligands, the group of Pieters also targeted the asialo-GM2-binding fimbriae[311] and the mannose-binding FimH adhesin present in *E. coli*.[312] The assessment of bacterial inhibition properties of the meta- and para-substituted ligands showed different trends if compared to the ones previously found for *S. suis*, with IC_{50} values of 376 and 159 μM respectively. The longer-armed meta-substituted dimer ligand resulted in better inhibition with an IC_{50} value of

27 μM, which worsened in the case of the tetramer, whose IC_{50} value was found to be 51 μM. This is an example of the case-by-case analysis required in the attempt to translate inhibitors from one biological system to another.

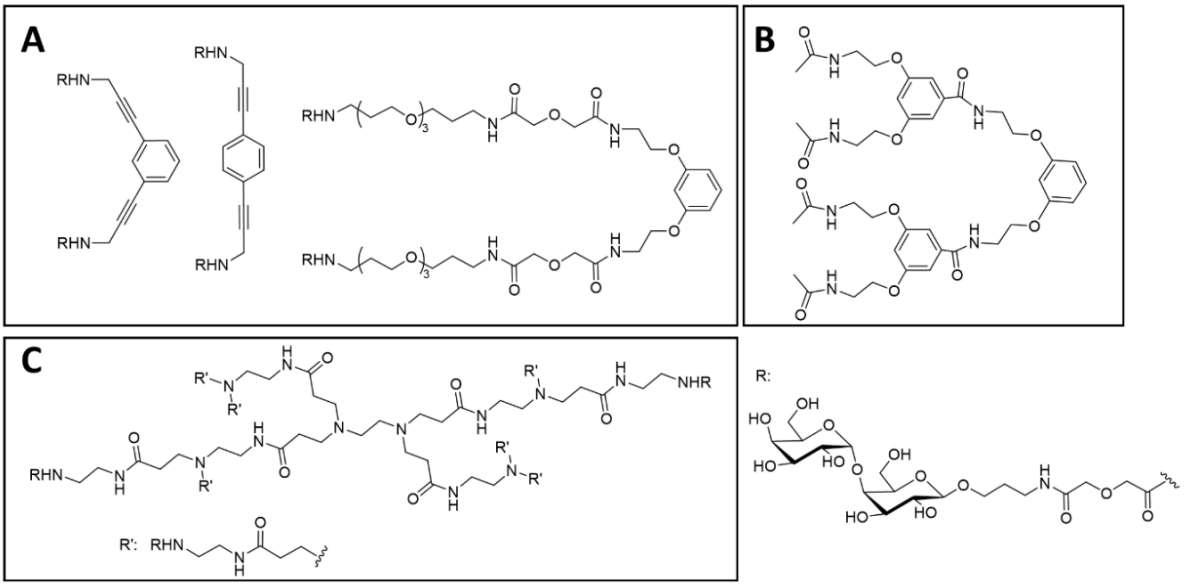

Figure 4.14. Structures of (**A**) divalent, (**B**) tetravalent and (**C**) octavalent galabiose-bearing adhesion inhibitors developed by Joosten *et al.*[310] against *S. suis.*

A very tight-binding dendrimer was developed against the *S. suis* SadP adhesin (**Figure 4.15**).[313] The adhesin is known to naturally bind to the P^k trisaccharide,[314] however modelling in that work revealed the potential for an increase in binding upon the addition of a phenylurea moiety on the terminal glycosyl unit. Indeed, the P^k dendrimer exhibited an IC_{50} value of 2.5 nM, but the phenylurea derivative proved to be 1000-fold more potent, with an IC_{50} value of 26 pM. Such value is remarkable given that high-affinity carbohydrate-based ligands (dendrimers, for example) are often in the nanomolar range.

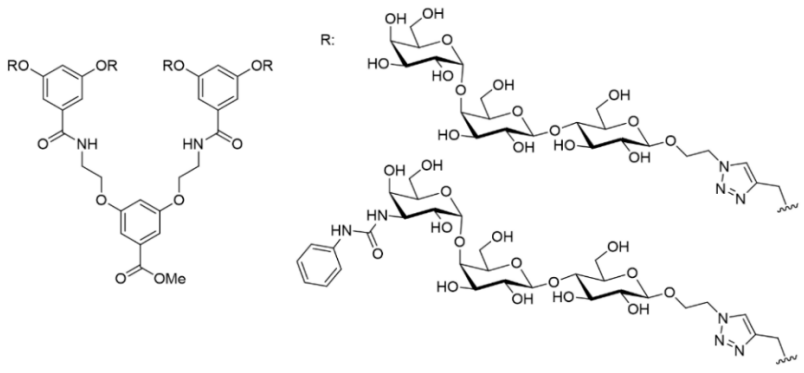

Figure 4.15. P^k and phenylurea-P^k dendrimers synthesised by Haataja *et al.*[313] targeting the SadP adhesin of *S. suis.*

The FimH adhesins from *E. coli* were again targeted using mannosylated acrylamide polymers.[315] The polymers were decorated with mannose bearing shorter (ethyl) and longer (heptyl) tethers (**Figure 4.16A**), achieving degrees of polymerisation in the 30 to 190 range. The data reported show the importance of this parameter, with a shorter tether leading to no inhibitory effects. That result confirmed that multivalency is not enough for the inhibition of adhesins, and proper design of the ligands to be accessible is required. In a follow-up work, the authors selected the same type of heptyl mannoside acrylamide polymer to explore further the possible variations to enhance its antiadhesive properties.[316] A copolymer of the heptyl mannoside methacrylate and glycidyl methacrylate was synthesised, adding to the structure an epoxide moiety for further installation of cationic, neutral and anionic polar groups (ammonium, hydroxyl and sulphonate, respectively) (**Figure 4.16B**). The copolymers were synthesised with different topologies, although they did not seem to influence the antiadhesive properties. The polymers presented in that work inhibited the adherence of *E. coli* to epithelial and carcinoma cell lines with rates of up to 80%, with the best results being obtained by the sulphonate-functionalised polymers.

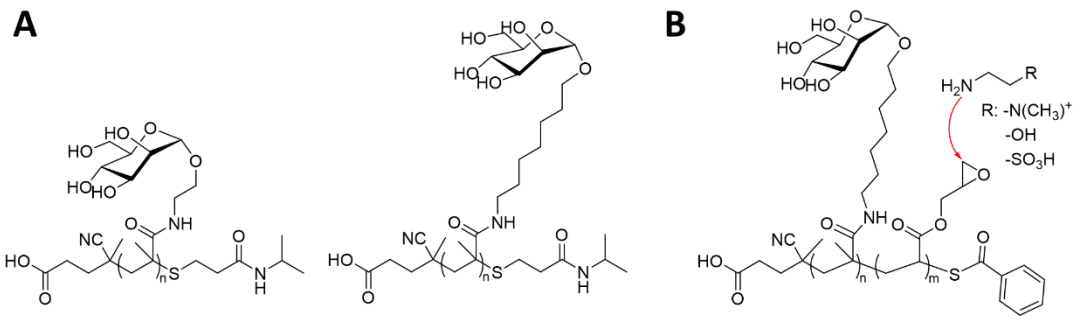

Figure 4.16. Structures of the mannosylated polymers developed by Yan *et al.*[315,316] to (**A**) optimise the length of the aglycon and (**B**) investigate the further influence of other monomers in the antiadhesive properties against *E. coli.*

4.1.5. Case of study: *Pseudomonas aeruginosa* LecA

The opportunistic respiratory pathogen *P. aeruginosa* has been targeted on many occasions seeking detection, anti-bacterial and anti-biofilm formation tools. A general description of this bacterium and its lectins LecA and LecB is given in *Chapter 1.* In this section, we will focus on the discussion of the design of ligands tailored for the enhanced binding to the galactose-binding LecA.

In the early investigations of the binding specificity of LecA, it was found that aromatic moieties on the anomeric position of β-galactose enhance the binding of ligands.[317] Many years later, it was proved that T-shaped π interactions were developed between the aromatic aglycon and the imidazole group of a neighbouring histidine residue (His50) in the binding pocket (**Figure 4.17A**).[318] Since then, libraries of LecA inhibitors have been developed to study the effect of different aromatic aglycons (**Figure 4.17B**)[319] and also the distance between the aromatic moiety and the glycan (**Figure 4.17C**).[320] A general conclusion was that the inclusion of the aromatic aglycon roughly improves by a factor of 10 the binding with LecA measured *via* ITC, reaching K_D values in the 4 – 9 μM range (as a reference, the reported K_D for galactose is 87.5 μM)[319]. However, the type of aromatic moiety or the length of the tether used to attach it to the glycan seem to have little influence on the K_D. That enhancement of interaction has been recently exploited by Titz and collaborators to improve the delivery and accumulation of the antibiotic ciprofloxacin in *P. aeruginosa* biofilms.[321,322]

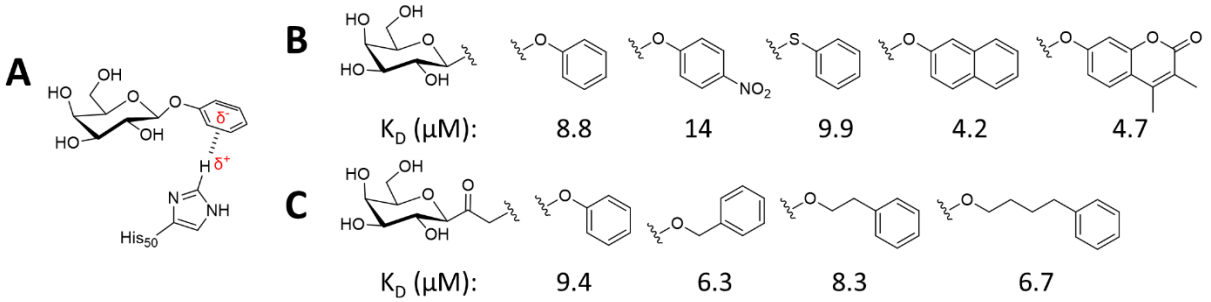

Figure 4.17. (**A**) Schematic representation of the T-shaped π interactions occurring in the binding pocket of LecA. Representative examples of aromatic glycosides synthesised to study the influence of (**B**) the type of aromatic aglycon (Kadam *et al.*[319]) and (**C**) the distance between the aromatic aglycon and the carbohydrate (Siebs *et al.*[320]).

As is the case for many other lectins as discussed above, multivalent ligands exhibit tighter interactions with LecA than monovalent ones. For fifteen years, the development of multivalent LecA inhibitors has been led by the groups of Imberty, Roy, Vidal, Pieters, Titz and their collaborations. The first publication in this line reported the synthesis of a hetero-glycodendrimer functionalised asymmetrically with D-galactose and L-fucose targeting simultaneously both LecA and LecB from *P. aeruginosa*.[323] Employing a series of amine couplings and CuAAC reactions, an octavalent ligand was synthesised (**Figure 4.18**). The ability of the dendrimer to crosslink the lectins was tested *via* turbidimetry, which measures the magnitude of scattered lighted passing through a solution due to the formation of aggregates.

Those experiments showed how the dendrimer crosslinked better LecB than it did LecA, which sounded reasonable given that the Fuc-LecB interaction is reportedly stronger than the one of Gal-LecA.[324]

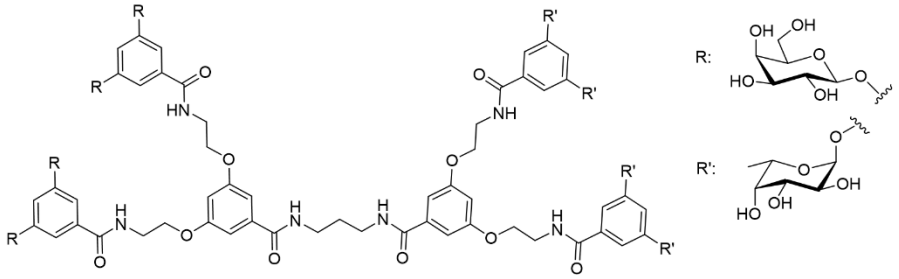

Figure 4.18. Heteroglycodendrimers functionalised with D-galactose and L-fucose for the simultaneous detection of LecA and LecB from *P. aeruginosa*, reported by Deguise *et al.*[323]

Dually functionalised dendrimers have not been published frequently, however, a recent report presented an anti-biofilm tetradecavalent glycorotaxane (**Figure 4.19A**).[325] Encouraged by previous works showing the potential of pillar[5]arenes as biofilm inhibitors,[326] the authors decided to combine a decavalent galactose-functionalised pillar[5]arene, and an axle connecting a tetravalent fucose dendrimer and a cationic module. The design was strategically thought so each of the key blocks would be independently synthesised, avoiding the need of adding protection and deprotection steps and step-wise functionalisation. The formation of the axle through the pillar[5]arene unit was ensured by performing the reactions in chloroform, which does not form an inclusion complex with the cycle, leaving space for the triazole from the axle to establish the key hydrogen bonds leading the threading of the rotaxane. The interaction of this compound with LecA and LecB was quantified through ITC resulting in 770 and 160 nM, respectively. Interestingly, the anti-biofilm properties of this compound were tested, revealing a significant drop in biomass formation (up to 80%) when micromolar concentrations of the compounds were employed. The effectiveness of the anti-biofilm agents was due to the cationic module installed on one side of the axle, which was proved by installing a second fucose dendrimer on that side (**Figure 4.19B**). That new rotaxane exhibited no anti-biofilm properties whatsoever.

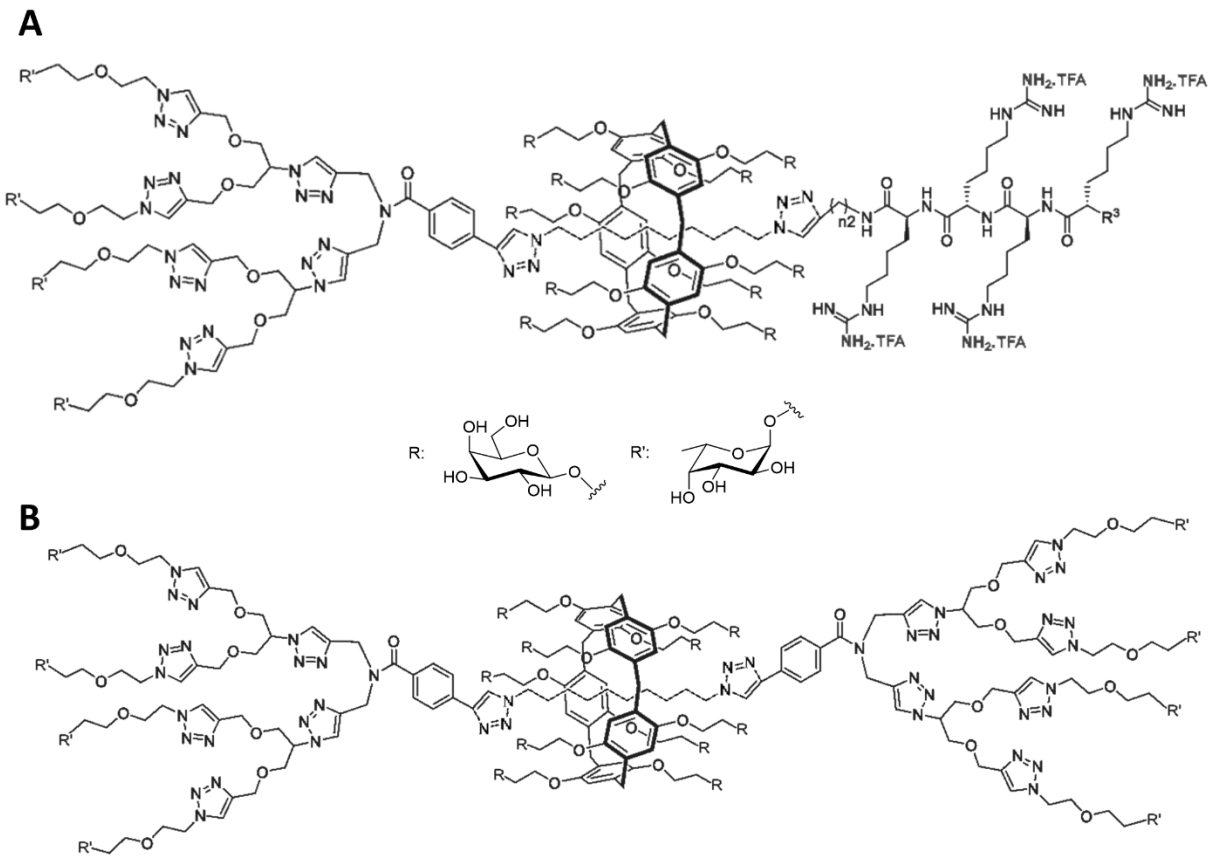

Figure 4.19. Glycorotaxanes developed by Mohy El Dine *et al.*[325] targeting LecA and LecB from *P. aeruginosa* as anti-biofilm therapy. Two types of glycorotaxanes were tested, probing that (**A**) a cationic module at the terminus of the axle was required to develop anti-biofilm properties, as these would not occur in a (**B**) rotaxane lacking the cationic module.

Structurally similar to pillar[n]arenes, homo-functionalised calix[n]arenes have been explored as scaffolds for the multivalent presentation of glycans. A thorough work was published studying the possible conformations and topologies of a series of tetravalent galactose calix[4]arenes.[327] Different synthetic approaches were adopted to install alkyne moieties, yielding calix[4]arenes varying in valency. The optimal conditions yielding tetravalent derivatives were tuned to afford calix[4]arenes differing in the conformation of the calix: cone (**Figure 4.20A**), partial cone (**Figure 4.20B**) and alternate (**Figure 4.20C**). Upon installation of galactose moieties through CuAAC chemistry, the interaction with LecA was quantified through ITC. The results showed a dramatic decrease in K_D from the free sugar to the tetravalent compounds. Between the three conformations, it was found that the cone conformation was performing the worst in terms of K_D (2 µM), while the partial cone and the alternate conformations bound tighter with the lectin (200 and 176 nM, respectively). In a follow-up work from the same group, they expanded the macrocycle to build a hexavalent

calix[6]arene (**Figure 4.20D**) whose interaction with LecA was again tested through ITC.[329] Interestingly, not only the binding was slightly tighter than the previous ones (K_D of 140 nM) but also the stoichiometry was found to be of three glycans per lectin unit.

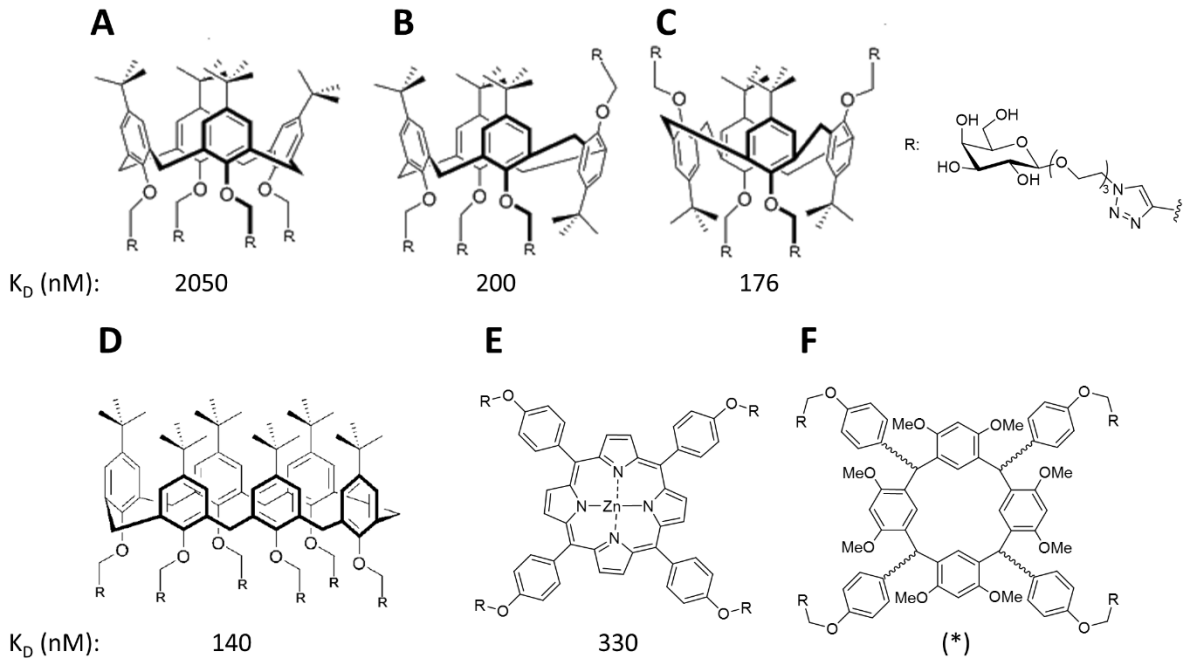

Figure 4.20. Comparison of different aromatic macrocycle-based scaffolds developed as inhibitors of LecA. Structures reported by (**A-E**) Cecioni *et al*.[328,329] and (**F**) Somro *et al.*[330] (*): K_D was not measured due to solubility issues during the ITC experiments.

To explore the effect of a planar scaffold, a tetravalent porphyrin was functionalised with galactose through CuAAC chemistry (**Figure 4.20E**).[329] The conjugate exhibited a weaker interaction with LecA than the previously reported calix[n]arenes as measured by ITC (K_D of 330 nM). That results proved the relevance of the 3-dimensional scaffold employed to present glycans, as it affects not only the strength of binding but also the stoichiometric ratios involved in the process. Resorcin, a relatively similar structure to porphyrins, has also been used as a planar scaffold for the multivalent presentation of glycans against LecA (**Figure 4.20F**).[330] That compound gave noticeable solubility problems which hindered the ITC and SPR measurements of the inhibition of LecA, which is an important factor to take into account during the design of a protein inhibitor.

Following up on the work on alternate glyco-calix[4]arenes (ligand shown in **Figure 4.20C**), the group published a very interesting study on the structures formed upon interaction with LecA.[331] Atomic-force microscopy allowed to observe discrete filaments formed by the head-

to-tail crosslinking achieved by the tetravalent ligand (**Figure 4.21**). These results are proof of the importance of strategic thinking when designing a ligand. Even though it was not tested, it sounds sensible to speculate that having used the ligand shown in **Figure 4.20A**, such filaments would not have appeared, or possibly any crosslinking at all, due to the wrong presentation of glycans to interact simultaneously with two lectins.

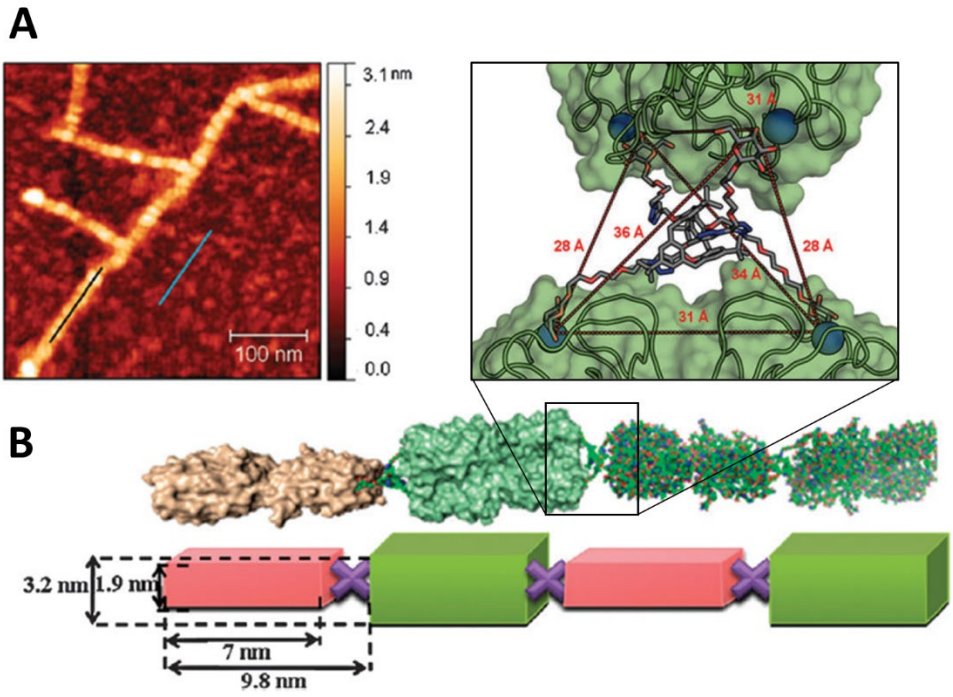

Figure 4.21. Study of the filaments formed by the alternate conformation of galactose-calix[4]arenes. (**A**) Atomic-force microscopy image showing a scan of filaments formed at the nanometric scale. The colour scale on the right indicates the depth of each point. (**B**) Modelling of the mode of crosslinking between the calix[4]arene and lectin units. Below that, a schematic representation with the observed sizes annotated. Adapted from Sicard *et al.*[331] with permission from the Royal Society of Chemistry.

Working on a different kind of macrocycles, the group developed a cyclic oligo-(1→6)-β-glucosamine scaffold to exhibit galactose in a multivalent manner (**Figure 4.22**).[332] The work focused on di- and tetravalent ligands with cyclodi- and cyclotetrasaccharides. The authors observed clear differences between ligands in terms of the strength of interaction with LecA measured by ITC, which was explained due to the distance between glycans. The smallest macrocycle, obviously more constrained, limits the ability of the ligand to interact simultaneously with two binding sites of the lectin, and a bigger K_D was observed. Importantly, two variations of the tether were employed, differing in the presence of a phenyl group close to the anomeric position. The ligands comprising that phenyl group exhibited a K_D 5 to 10-fold

smaller, an effect that has been discussed before.[320] Remarkably, the tetravalent 5-member macrocycle achieved a K_D value of 2 nM, which is the lowest one reported to date.

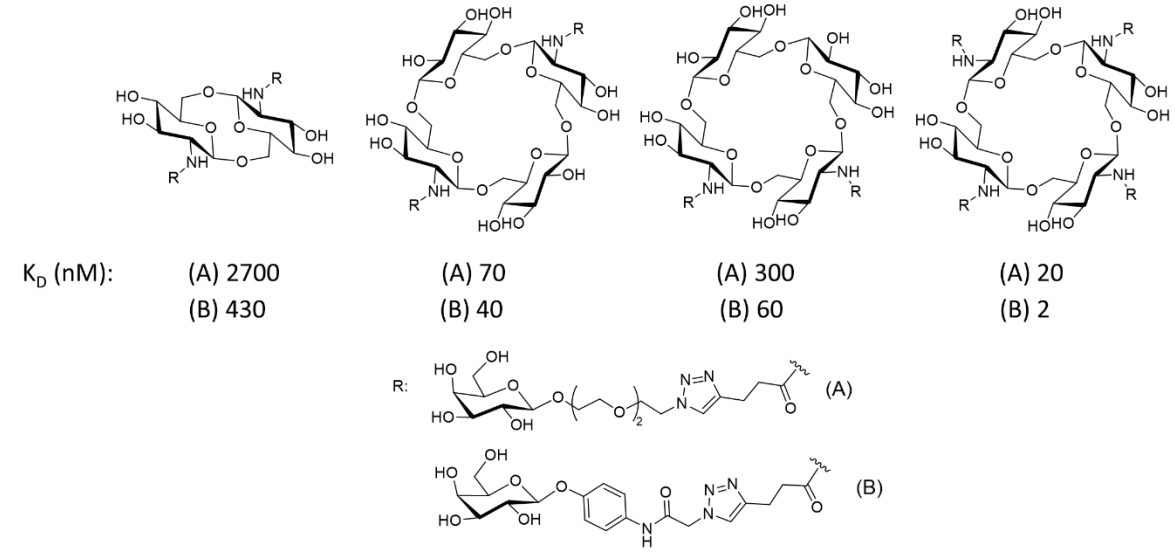

Figure 4.22. Oligo-(1→6)-β-glucosamine scaffolds developed by Gening *et al.*[332] for the detection of LecA, with their related K_D values measured by ITC.

Although macrocycles have been proven to be effective scaffolds for the multivalent presentation of carbohydrates, a major part of the literature targeting LecA has been dedicated to the development of dimers and dendrimers of galactose. An important synthetic work reported a series of ligands using *C*-galactose as a more hydrolytically stable option instead of the typical *O*-galactose.[333] Using trimesoyl chloride (1,3,5-benzenetricarbonyl chloride) as a tri-armed core, a mono-, di- and tri-functional azide-ending linker was installed to synthesise tri-, hexa- and nona-valent dendrimers. However, due to solubility issues, the retrosynthetic pathway was reviewed to install a mono-, di- and tri-functional alkyne-ending linker instead. The synthesised dendrimers (**Figure 4.23A-C**, respectively) had a better water solubility that allowed quantification of their binding with LecA through ITC, showing a decreasing K_D with increasing valency (1370, 370 and 230 nM, respectively). Encouraged by those results, the synthesis was taken further to obtain glycodendrimers exhibiting 18 and 27 glycans (the latter shown in **Figure 4.23D**). However, these also presented foreseeable solubility issues in water due to the high hydrophobicity of the structure. Overall, this work not only yielded a set of glycodendrimers with good binding properties against LecA, but it also represented a good exercise of synthetic troubleshooting.

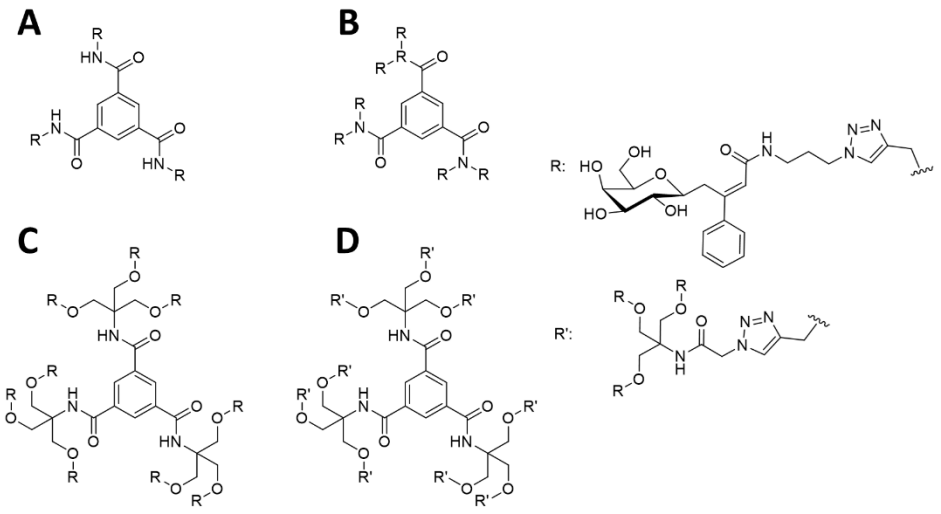

Figure 4.23. Dendrimers exhibiting (**A**) three, (**B**) six, (**C**) nine and (**D**) twenty-seven units of *C*-galactose reported by Chabre *et al*.[333] as LecA inhibitors.

An important fraction of the development of bis-galactoside dimers as inhibitors of LecA has been reported in the Pieters group over the last decade. In the first report of this series of publications, a glucose-based spacer was evaluated as a linker between galactoside residues, granting both rigidity and water solubility.[334] A series of CuAAC reactions allowed to build the spacer with either two or three glucose units, which were subsequently coupled with either an ethynyl *C*-galactoside (**Figure 4.24A**) or a 4-pentynyl *O*-galactoside (**Figure 4.24B**). The assessment of their affinity for LecA (measured as IC_{50}) revealed that the triazole formation directly on the anomeric position of galactose had a negative impact on the binding, with an unprecedented relative binding potency of 0.3 if compared to the monomer. On the other hand, the *O*-galactoside had a value of 545. Continuing in that line, the same group published the optimisation of the piece of spacer between the glucose linker and the terminal galactoside.[335] They compared linkers comprising two, three or four glucose units, leaving either a methylene or propylene piece of the linker between the glucose chain and the terminal galactose (representative example in **Figure 4.24C**). From the measurement of IC_{50}, it was clear that four glucose units in the spacer did not improve the binding as much as the others, which values were found in the 0.9-3.5 µM range. The three-glucose unit spacer had a remarkably higher improvement of the IC_{50}, especially for the propylene-linked, with a K_D of 28 nM. The successfulness of that linker was explained as a good compromise of flexibility, yet able to interact with two binding sites of LecA, which was verified through molecular dynamics.

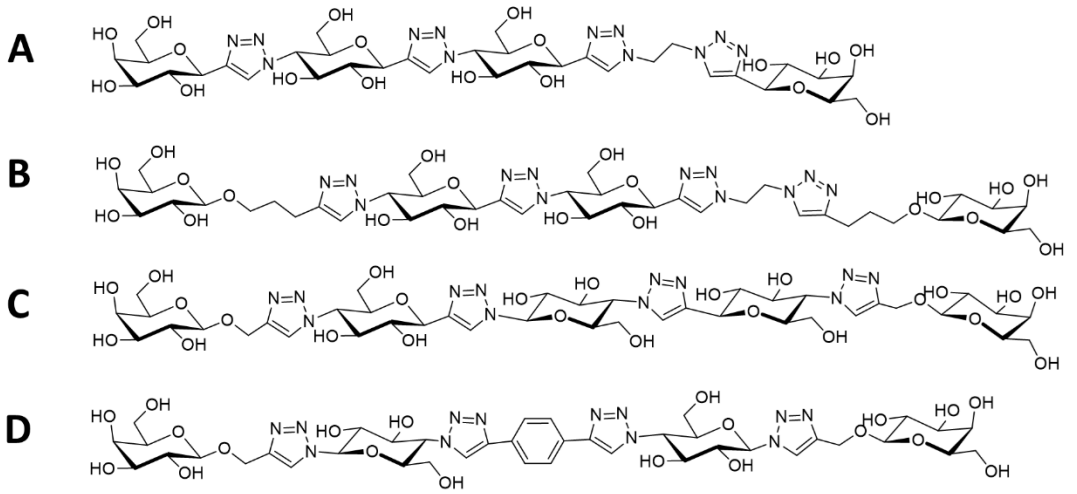

Entry	IC_{50} (μM)	K_D (μM)
A	310	-
B	0.22	-
C	0.0027	0.028
D	-	0.013

Figure 4.24. Comparison of different glucose-linked galactose dimers developed as inhibitors of LecA. Structures reported from (**A-B**) Pertici *et al*.,[334] (**C**) Yu *et al*.[335] and (**D**) Pieters *et al.*[336] (-): not reported.

A later follow-up work managed to improve the interactions with the lectin with a combination of glucose and phenyl units in the spacer (**Figure 4.24D**).[336] With an analogous synthetic approach as before, the authors reported a K_D value of 13 nM. At that point, the authors acknowledge the difficulty to improve further the avidity of these molecules and the importance to progress in the predictions through molecular dynamics. Further modifications of the spacer were attempted by introducing aromatic substituents on the 6-position of the glucose units.[337] However it did not improve upon the K_D obtained for previous derivatives. Molecular modelling did not explain accurately the reason behind the lack of improvement, since it did show the enhanced interaction as geometrically possible, but alternative conformations where the aromatic groups pointed elsewhere were also plausible. In any case, the conclusion of this work was to avoid chemical modifications on the 6-position of the glucose units of the spacer during the design of LecA inhibitors. In the latest work of this series, the interactions of the optimised compound from **Figure 4.24D** with LecA were evaluated with a selection of techniques to complement the usual ITC.[338] The compound was functionalised with a biotinylated tether to allow analysis through BLI, not only confirming the

nanomolar K_D value found through ITC but also showing slow dissociation kinetics. The presence of the biotinylated tether only led to a change of K_D from the previously reported 13 nM, to 31. Affinity capillary electrophoresis showed how the divalent ligand would competitively interact with LecA, reversing the binding formed with a monovalent ligand. Finally, TSA proved a stabilisation of LecA upon binding with the divalent ligand, increasing its unfolding temperature by 20°C. That result was easily explained, as the divalent ligand is adding a bridge between the LecA monomers, preventing them from unfolding. In a parallel work, those rigid glucose rods were compared with a peptide-based tetramer which achieved a very tight binding with LecA (**Figure 4.25**).[339] The peptide was synthesised by collaborators with a specific H-shape to allow the special distribution of galactose residues. The authors performed a thorough molecular modelling study of this and other previously synthesised multivalent ligands to assess flexibility and the distance between galactoside units. They found the reported glycopeptide to have an optimal distance of 31 Å, matching with the separation between binding sites of LecA. The addition of aromaticity and multivalency, in combination with the appropriate distribution of glycan residues, yielded a LecA inhibitor with a remarkable K_D of 2.5 nM, the second tightest up-to-date after the 2 nM reported by Gening *et al.*[332]

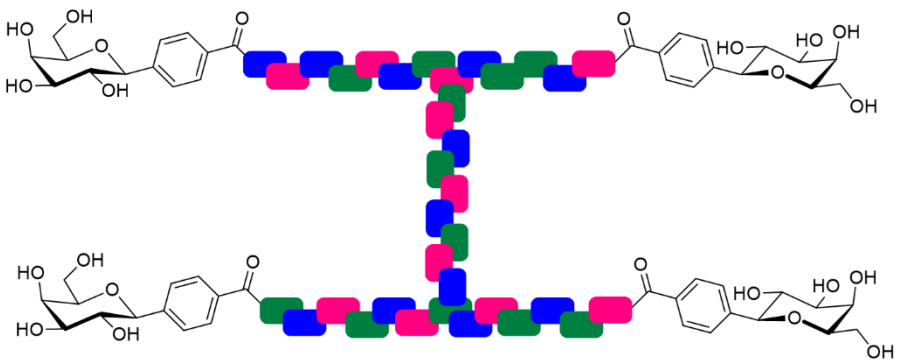

Figure 4.25. Structure of the tetravalent LecA inhibitor with an H-shaped peptide scaffold reported by Visini *et al.*[339]

Exploring a different kind of spacers, a more rigid phenylene-ethynylene was used to bridge between terminal galactoside residues (**Figure 4.26A**).[340] Even though there was an enhancement of the interaction with LecA, the IC_{50} value was in this case 0.9 µM, which was still far from the values obtained with the previous glucose-based linker. Following on the development of phenyl-based linkers, a relatively recent work reported a better binding enhancement with a divalent ligand (**Figure 4.26B**).[341] The relative position of the glycan

(meta, para) and the distance of the bridge were optimised to reach a K_D value of 11 nM measured through ITC. Importantly, this work reported a simpler structure, more easily accessible through chemical synthesis, which performed in a superior way than dimers published before.

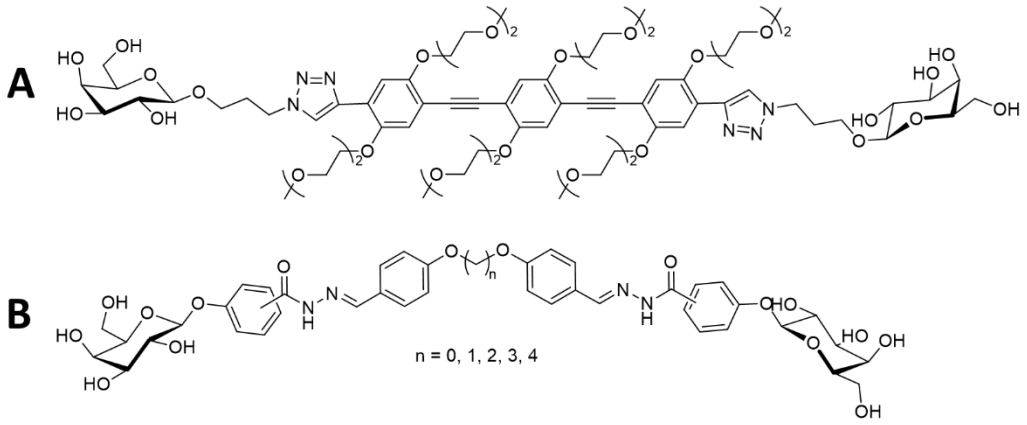

Figure 4.26. Comparison of different phenyl-linked galactose dimers developed as inhibitors of LecA. Structures reported from (**A**) Pertici *et al*.[340] and (**B**) Zahorske *et al.*[341]

4.2. Aims

The aim of the research work reported in this chapter is to design an aspartic acid-bridged galactoside dimer to target LecA from *P. aeruginosa* (**Figure 4.27**). The synthetic methodology developed here will include CuAAC and EDC-couplings to allow variability in the selection of four dimers that will offer different types of interactions, lengths and flexibilities.

The interaction of the synthesised ligands with LecA will be investigated through ITC to understand the effect of multivalency. Following the methodology developed in *Chapter 2,* the galactose dimers will be coupled to BSA and the interaction of the neoglycoproteins with LecA will be assessed through BLI. The immobilisation of the glycosyl dimers on BSA would allow the synthesis of a set of glyco-BSA-AuNPs prepared following the methodology developed in *Chapter 3*. Finally, the interaction of all the gAuNPs synthesised in this research work with *P. aeruginosa* will be assessed through FCM.

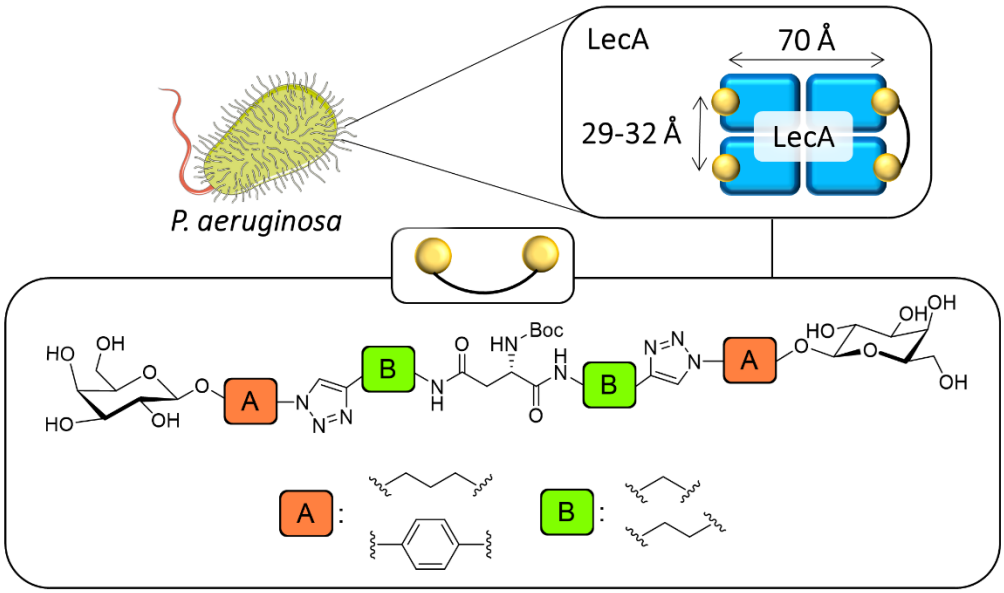

Figure 4.27. The scientific aim of *Chapter 4*. A novel selection of dimers has been designed for the enhanced interaction with LecA from *P. aeruginosa*.

4.3. Results and discussion

4.3.1. Synthetic strategy

Design of the ligand

Aspartic acid was chosen as a readily available tri-functional support to connect two terminal β-galactoside residues. Commercially available Boc-protected aspartic acid is an ideal candidate due to the two equivalent terminal carboxylic acids that allow the formation of amide bonds to bridge the glycan ends. The deprotection of the central amine will allow the formation of another amide bond, enabling further derivatisation such as the introduction of a tether for conjugation to BSA, AuNPs, or even to bridge two dimers leading to a dendrimer.

The available literature about LecA and the development of its ligands for enhanced binding highlights two main features to consider. Firstly, to assess the benefits of an aromatic structure on the anomeric position of β-galactosides, two different aglycons (**A** throughout this chapter) were employed: phenyl and propyl. Secondly, to tailor the length of the dimer for the β-galactosides to interact with two binding pockets simultaneously, two different spacers (**B** throughout this chapter) were placed in between the glycan and the aspartic acid: propyl and butyl.

With the design of the final structure of the dimer in hands, the focus was on the connectivity between the glycans, which was a combination of a bifunctional aspartic acid and two terminal spacers. To maximise the yields and to allow the potential design of a larger library of compounds, CuAAC chemistry was chosen to connect the glycan and the spacer through a 1,4-disubstituted 1,2,3-triazol ring, and EDC coupling chemistry was chosen to connect the spacer to the aspartic through an amide bond. The assembly of the different building blocks (terminal galactoside, aglycon **A**, spacer **B** and aspartic acid bridge) is shown in **Figure 4.28**.

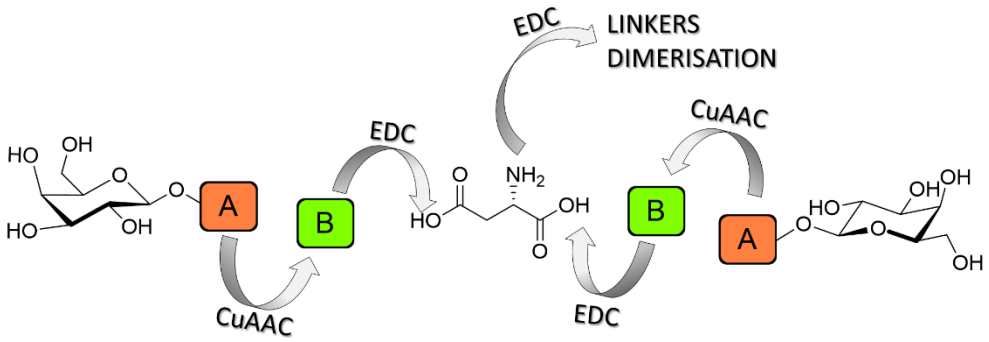

Figure 4.28. Concept of the designed prototype of a β-galactoside dimer using a central aspartic acid as tri-functional support to connect the carbohydrate moieties. The aglycon (**A**) will be used to assess the impact of aromaticity in the binding with LecA. The spacer (**B**) will allow to tune the length of the dimer to fit between the binding pockets of the lectin. The central amine group from aspartic acid can be used for further derivatisation, attachment of a linker, or dimerization of the ligand.

The galactose dimers targeted in this chapter resulting from the combination of the proposed building blocks have been analysed with Avogadro.[342] The modelling software grants a rough estimation of the linear length of the dimers, which was about 32-33 Å. The estimated distance is desirable to target the two binding pockets on the short side of LecA, which are reported to be between 29 and 32 Å apart.[343]

Retrosynthetic pathway

The retrosynthetic pathway followed in this chapter is shown in **Scheme 4.1**. It starts with a CuAAC reaction between the galactosides and the Boc-protected amines, and subsequent dimerization through EDC-coupling with Boc-protected aspartic acid.

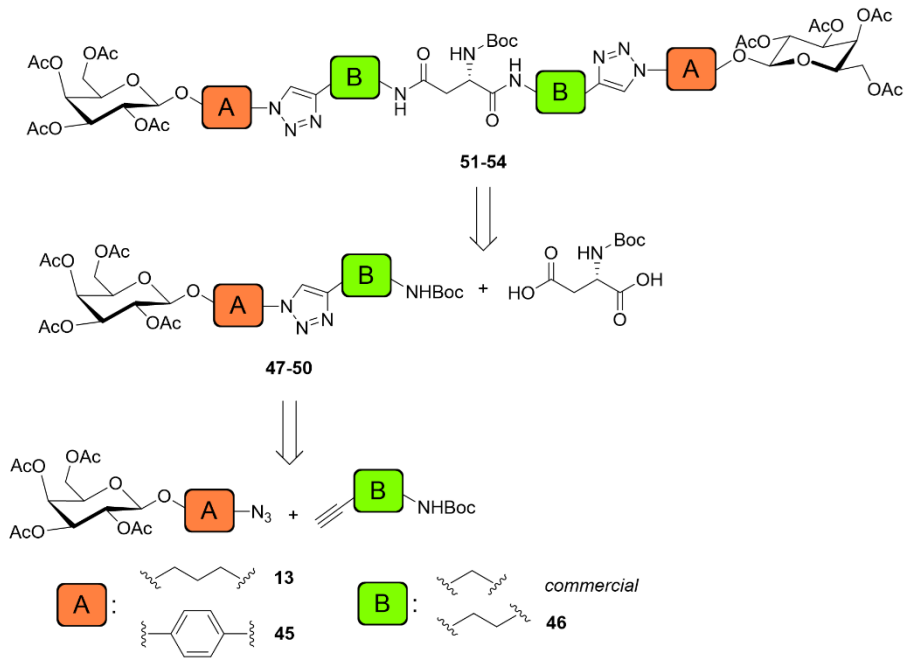

Scheme 4.1. Chosen retrosynthetic pathway for the synthesis of aspartic acid-bridged galactoside dimers **51-54**. The pathway starts with the CuAAC reaction between galactosides **13** or **45** and either commercial Boc-protected propargylamine or synthesised Boc-1-aminobut-3-yne **46**. The triazolyl compounds are finally dimerised through an EDC coupling with Boc-protected aspartic acid.

4.3.2. Synthesis of the building blocks

The peracetylated galactoside derivatives and Boc-protected alkynylated amines were synthesised following published methods.

Galactoside derivatives

The azidopropyl derivative **7** was synthesised as discussed in *Chapter 2.*

With regards to the phenyl derivative, commercially available 4-nitrophenyl galactoside was used instead of free galactose. This allowed the derivatisation of the aglycon to convert the nitro into an azide group (**Scheme 4.2**) to use the efficient CuACC reaction instead of a glycosylation step, which could have lowered the final yield. The transformation of aromatic nitro groups is very common and it is based on a first reduction of the nitro group into an amino derivative, followed by a diazotization reaction to introduce, in this case, an azide to the aromatic ring.

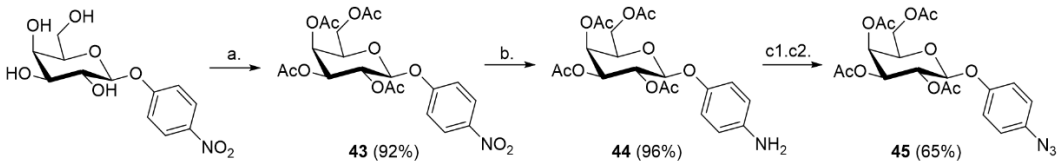

Scheme 4.2. Synthesis of peracetylated 4-azidophenyl galactoside (**45**). Reagents and conditions: **a.** Pyridine, Ac_2O, DMAP (cat.), r.t., o.n.; **b.** Pd/C (10%), MeOH, H_2, r.t., 2 h; **c1.** $NaNO_2$, HCl (aq., 1 M), 0°C, 30 min.; **c2.** NaN_3, 1 h. The yields shown here are unoptimized.

The peracetylated 4-nitrophenyl galactoside **43** was obtained by acetylation of the commercially available nitrophenyl derivative in pyridine following a standard methodology.[344] Two different strategies were attempted for the reduction of the aromatic nitro group: reduction with tin(II) chloride in acidic conditions,[345] and catalytic hydrogenation.[346] The choice was directed towards the latter, yielding the galactoside **44** with nearly quantitative yield and minimal purification required. Lastly, it was converted to the acetylated 4-azidophenyl galactoside **45** following a standard protocol.[347] The diazotisation reaction follows a well-known mechanism dependent on the presence of an acid (**Scheme 4.3**).

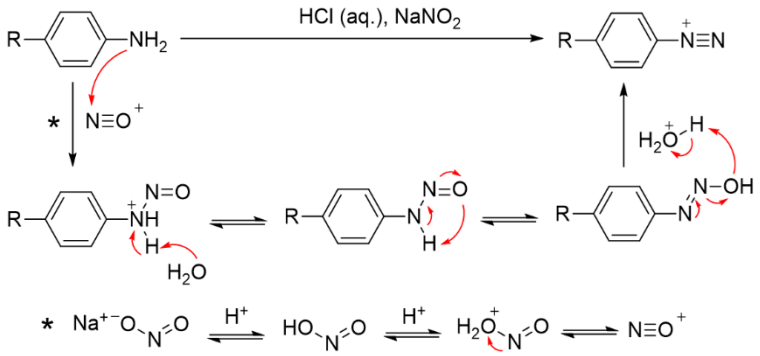

Scheme 4.3. General mechanism for the diazotization reaction of a 4-aminophenyl compound. The process starts with the formation of nitrous acid which equilibrates to release nitric oxide. The amino group from the substrate engages in a nucleophilic attack, following an acid-base equilibrium that leads to the formation of the diazo-compound.

The limited solubility of the acetylated glycoside in the aqueous reaction solvent is aided by the amine and the diazo group as the reaction progresses. With the formation of the final azide, the solubility decreases and a precipitate is rapidly observed. The difference in polarity between starting material and final compounds allows a very simple purification through silica gel flash chromatography, isolating the galactoside **45** with an overall yield of 57%.

The progress of the reaction could be easily followed using TLC, and the NMR of the products was compared with available literature (**Table 4.1**). No reported NMR was found for the acetylated azidophenyl galactoside **45**, however, the data obtained was consistent with literature for the aminophenyl and nitrophenyl derivatives. The $[\alpha]_D^{25}$ value found (+8) was in agreement with the one reported in the literature (+7),[347] and the presence of the azide group was identified by the diagnostic FT-IR signal (2117 cm^{-1}).

Table 4.1. NMR shifts of the anomeric proton ($\delta_{H\text{-}1}$, ppm) and carbon ($\delta_{C\text{-}1}$, ppm), and H1-H2 coupling constant ($J_{1,2}$, Hz) for the respective peracetylated galactosides. (*) Peak not assigned by the authors. (**) No NMR data was found in the literature.

		Nitrophenyl			**Aminophenyl**			**Azidophenyl**		
		$\delta_{H\text{-}1}$	$J_{1,2}$	$\delta_{C\text{-}1}$	$\delta_{H\text{-}1}$	$J_{1,2}$	$\delta_{C\text{-}1}$	$\delta_{H\text{-}1}$	$J_{1,2}$	$\delta_{C\text{-}1}$
Gal	lit.	Kawano *et al.*[344]			Kawano *et al.*[344]			(**)		
		5.17	8.0	98.6 (*)	4.86	7.9	101.5 (*)	--	--	--
	this work	5.17	7.9	98.6	4.86	8.0	101.2	4.98	8.0	101.1

Coupling of the galactoside derivatives to Boc-protected alkynylated amines

For better handling of the alkynylated amines, the corresponding Boc-protected derivatives were used. Boc-propargyl amine was commercially available, whereas the 1-aminobut-3-yne was protected using di-*tert*-butyl dicarbonate (**Scheme 4.4A**). The successfulness of the reaction was confirmed through ^{1}H-NMR following the appearance of a singlet at 1.42 ppm, corresponding to the *tert*-butyl group.[348]

The two azido-galactosides (propyl and phenyl) and both alkynylated amines (propargyl and butyne) were submitted to a combinatorial set of CuAAC reactions, leading to the novel triazolyl derivatives **47-50** (**Scheme 4.4B**).

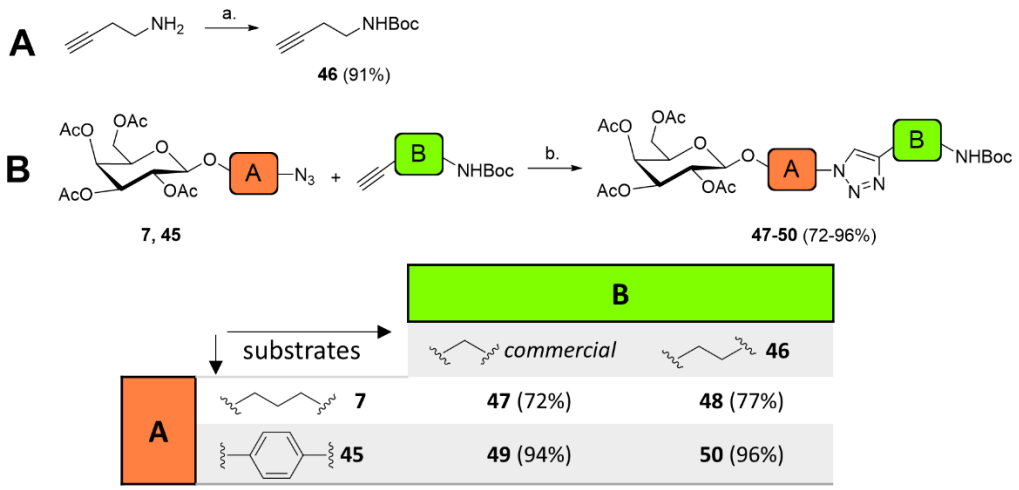

Scheme 4.4. (**A**) Synthesis of Boc-protected 1-aminobut-3-yne (**46**). (**B**) Synthesis of the triazolyl derivatives **47-50** through the CuAAC reaction between azido-galactosides **7** and **45**, and the Boc-protected propargylamine and **46**. Reagents and conditions: (**a**) TEA, DCM, Boc_2O, 0°C, o.n.; (**b**) $CuSO_4$ (MeOH, 5 mg/mL), THPTA (aq. 12 mg/mL), NaAsc (aq., 6 mg/mL), MeOH-H_2O 3:2, N_2, r.t., o.n.

The reactions set-up was similar to what was described for the synthesis of BSA glycoconjugates in *Chapter 2*, with only two adjustments. Firstly, the solvent in this case was not only water but an approximate 3:2 mixture of methanol and water to allow the substrates to solubilise. Secondly, the reaction was performed at r.t. instead of at 37 °C. The reactions worked without complication with only one product observed by TLC, affording the triazolyl derivatives **47-50** with yields ranging from 72-96%. The structure of each product was confirmed by ^{1}H-NMR using the diagnostic peak of the newly formed triazole ring as a singlet between 7.47 and 7.90 ppm depending on the substrate. A coupling was observed through ^{1}H-^{13}C HSQC between the triazole proton and the corresponding carbon between 119.9-122.5 ppm. This confirmed the 1,4-disubstitution of the triazole ring, as opposed to the carbon corresponding to the 1,5-disubstituted isomer which would appear around 133 ppm.[349] A secondary diagnostic peak used to confirm the final structure was the singlet appearing at 1.42-1.45 ppm, integrating for nine protons and corresponding to the Boc group.

4.3.3. Synthesis of galactoside dimers

The synthesised triazolyl derivatives **47-50** were deprotected with TFA and submitted to an EDC-coupling with Boc-protected aspartic acid to yield the protected galactoside dimers **51-54** (**Scheme 4.5**).

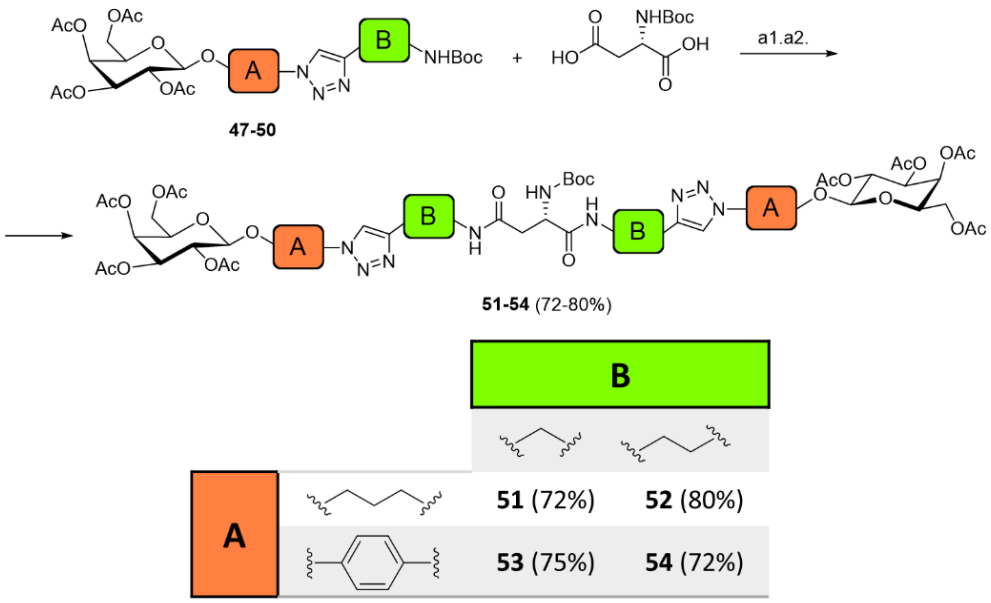

Scheme 4.5. Synthesis of the protected galactoside dimers **51-54** through the EDC coupling between the triazolyl derivatives **47-50** and Boc-protected aspartic acid. Reagents and conditions: (**a1**) TFA, DCM, r.t., 15 min.; (**a2**) EDC, TEA, DCM, r.t., o.n.

The reaction started with the cleavage of the Boc-group from the triazolyl derivatives **47-50** with TFA, which was completed in 15 minutes. The deprotection reaction could be easily followed by TLC as the R_f of the starting material decreased from approximately 0.6, to 0.2 (DCM-MeOH 95:5). Since the reaction follows a one-pot approach, it is important to neutralise the excess of TFA used in the first step with TEA before the addition of the EDC-activated Boc-protected aspartic acid (which was stirred with EDC and TEA in DCM for 45 minutes beforehand), to avoid the unwanted cleavage of its protecting group. This set of reactions led to single products, affording the protected dimers **51-54** with yields ranging from 72-80%. The overall yield for these pathways (considering the previous synthesis of the glycoside derivatives) ranges from 30-40%. An alternative approach was also attempted using HOBt (N-hydroxybenzotriazole) in addition to EDC, which works analogously as an EDC/NHS coupling (**Scheme 4.6**). However, no improvement was observed in the final yield and the two synthetic approaches were considered equivalent.

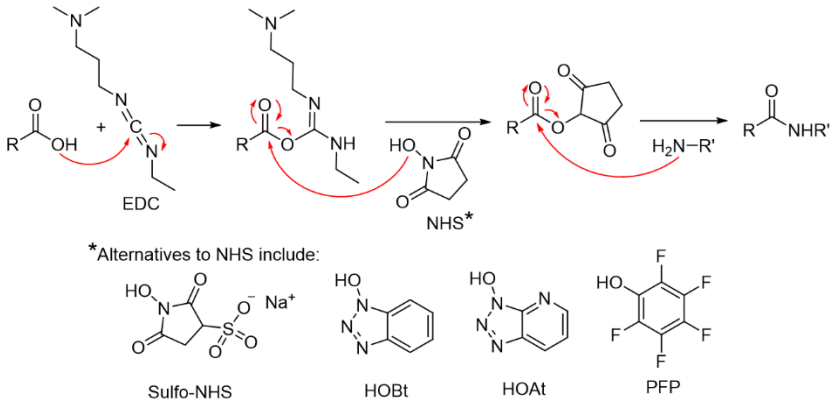

Scheme 4.6. The mechanism for the EDC/NHS coupling, and four alternatives for the NHS reagent: sulfo-NHS, HOBt, HOAt (N-hydroxylazabenzotriazole) and PFP (pentafluorophenol).

The correct structure of the products was confirmed by NMR experiments, especially for the relative integration of the peaks corresponding to the triazolyl glycoside moieties, in comparison with the peaks of the aspartic acid spacer, resulting in the expected 2:1 ratio. A key change in the ^{1}H-NMR spectra was observed for the peak corresponding to the proton of the triazole ring. That peak, which was a singlet for the triazolyl derivatives **47-50**, split into two different singlets very close to each other (**Figure 4.29**). This might be due to the restricted rotation of the two amide bonds formed in the last step of the synthesis, or perhaps to π-π staking of the triazole rings. Both cases would lead to magnetically inequivalent triazolyl protons. In future experiments, this could be evaluated following a variable temperature ^{1}H-NMR experiment to favour the rotation around the amide bonds at higher temperatures,[350] potentially leading to a single peak corresponding to the triazole ring. The addition of the triazolyl peaks integrated for two protons as expected, however, they did not integrate equally, meaning that the potential rotamers were not equally present in the equilibrium. The ratio between both varied from dimer to dimer, possibly affected by the length and flexibility of each linker.

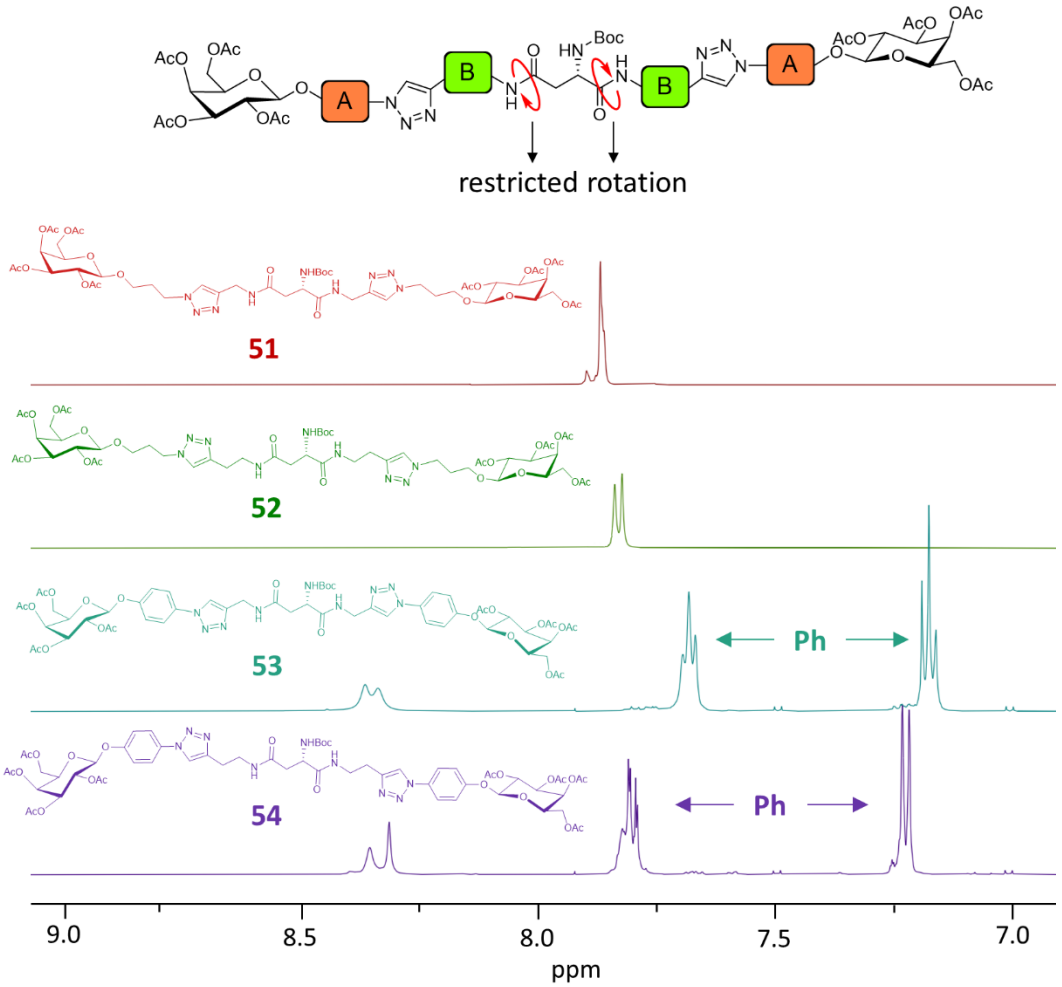

Figure 4.29. Expanded aromatic area of the ^{1}H-NMR spectrum from the protected galactoside dimers **51-54**. The peaks corresponding to the triazolyl protons are observed as two distinguished singlets, potentially corresponding to the rotamers due to the restricted rotation of the amide bonds.

In preparation for the biological evaluation of this library, the Boc-group from the aspartic acid was cleaved with standard TFA treatment, followed by EDC coupling of the free amine to the 6-azidohexanoic linker and final deacetylation of the galactoside dimer (**Scheme 4.7**). The intention was to add an azide-ending central arm to the dimer to enable CuAAC chemistry with propargylated BSA for the synthesis of glycoconjugates following the methodology developed in *Chapter 2.*

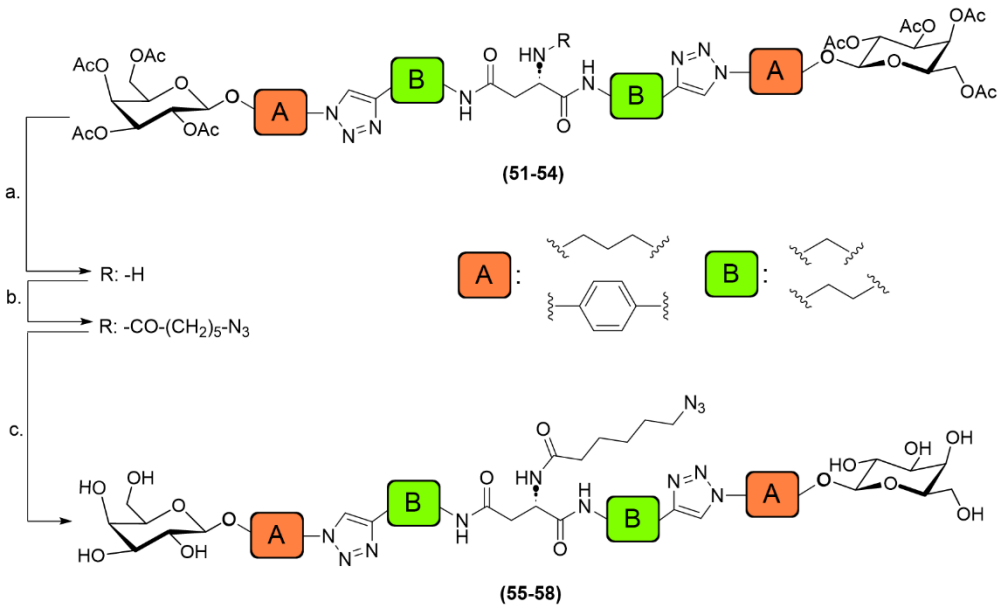

Scheme 4.7. Attempted pathway for the deprotection of the galactoside dimers **51-54** and addition of an azide-ending to obtain the *N*-L-(6-azidohexoxycarbonyl)-aspartic acid-bridged galactoside dimers **55-58**. Reagents and conditions: (**a**) TFA, DCM, r.t., 15 min.; (**b**) 6-azidohexanoic acid, EDC, TEA, DCM, r.t., o.n.; (**c**) TEA, DCM, r.t., o.n.

Similarly to the previous step, the cleavage of the Boc group worked upon the addition of TFA. 6-Azidohexanoic acid was activated with EDC as before and added to the reaction mixture. The progress of the reaction could be followed by TLC by using the usual sulfuric acid staining to detect the presence of the glycans, and a PPh_3/ninhydrin staining to detect the presence of the azide-ending tether. The latter is a two-step stain starting with a 10% solution of PPh_3 in DCM to reduce the azides to primary amines directly on the TLC plate. Secondly, the TLC is dipped in a 0.5% solution of ninhydrin in butanol-acetic acid 100:3. This allows the addition of the amine to the 1,3-dicarbonyl compound, leading to the formation of the well-known Ruhemann's purple.[351] Indeed, the spot corresponding to unreacted 6-azidohexanoic acid stained only with the PPh_3/ninhydrin stain, whereas the spot corresponding to the product was visualised with both staining solutions.

However, this reaction did not lead to only one product, and other spots could be observed by TLC when staining with sulfuric acid. Concerned about the possible partial deacetylation of the dimers during the overnight EDC coupling in the presence of TEA, the mixture was stirred longer with an increased amount of TEA (5%) to allow the full deacetylation. Several spots were observed by TLC after this, including unreacted 6-azidohexanoic acid (**Figure 4.30A**). The excess of tether was removed by washing the reaction residue with acetonitrile, however,

several glycan-related spots were still observed by TLC analysis. Hydrophobic interaction liquid chromatography (HILIC) did not succeed in the purification of the compounds, and neither did GPC. Furthermore, the solubility of these potentially deprotected *N*-L-(6-azidohexoxycarbonyl)-aspartic acid-bridged galactoside dimers turned out to be very poor in water (**Figure 4.30B**). This was thought to be due to the hexoxycarbonyl chain, which increased the hydrophobicity of the compound and could potentially lead to the observed aggregated material. Further investigation would be required to test this hypothesis and optimise the synthesis of these dimers.

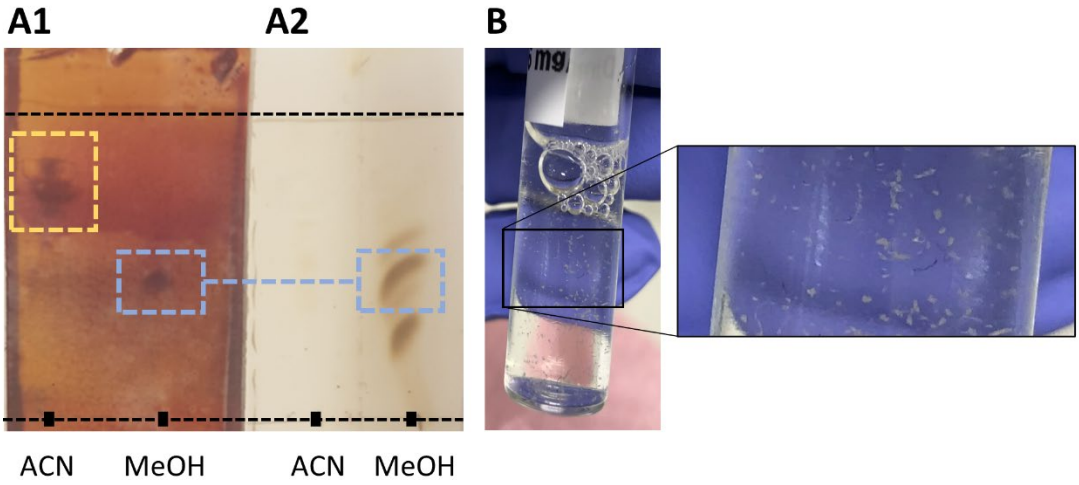

Figure 4.30. Data supporting the difficulties to isolate the deprotected dimers 55-58. (**A**) TLCs (mobile phase: IPA-NH_4OH-H-O 6:3:1) of the ACN- and MeOH -soluble fractions from the coupling and deprotection reaction. (**A1**) The TLC was stained with a PPh_3/ninhydrin staining, showing two spots: one corresponding to the 6-azidohexanoic acid linker used (highlighted in yellow), and to the deprotected product (highlighted in blue). This hypothesis is supported by (**A2**) the TLC stained with sulphuric acid, which is specific for glycans, which shows several spots, one of them coincident with an azide-containing spot (highlighted in blue). (**B**) Vial containing the product of the reaction in water (about 1 mg/mL), which precipitated.

As outlined in *Section 4.5*, the planned work to evaluate the interaction between the attempted dimers **55-58** and LecA included the use of techniques such as ITC or TSA. These techniques are highly sensitive to the concentration of ligands, therefore it is predicted that the low solubility of the targeted dimers would have caused further complications due to inaccuracy to measure the concentration of the ligands during the assay. The experiments could possibly benefit from using the amine-free dimers resulting from the deprotection of the compounds **51-54**. These would be expected to be more readily soluble in water, allowing to quantify the interaction with LecA.

4.3.4. Preliminary investigations of the effects of AuNPs on *Pseudomonas aeruginosa*

The strain PAO1 was selected to assess the use of gAuNPs developed in *Chapter 3* towards the development of a detection tool for *P. aeruginosa* targeting its lectin LecA. The multivalent presentation of Gal on the surface of the 40 nm AuNPs could potentially lead to a crosslinking process between different bacteria resulting in aggregation.[352] Although AuNPs-induced bacterial aggregation has not been explored in literature, preliminary results at Iceni Glycoscience have shown the ability of gAuNPs to aggregate *E. coli* and *P. aeruginosa* samples in a filter assay (**Figure 4.31A**).[353] Whereas the results with *E. coli* clearly showed the aggregation of bacteria upon incubation with AuNPs (**Figure 4.31B**), the results with *P. aeruginosa* were less obvious, although still positive (at bacterial OD 0.4, the filters are slightly pink) (**Figure 4.31C**).

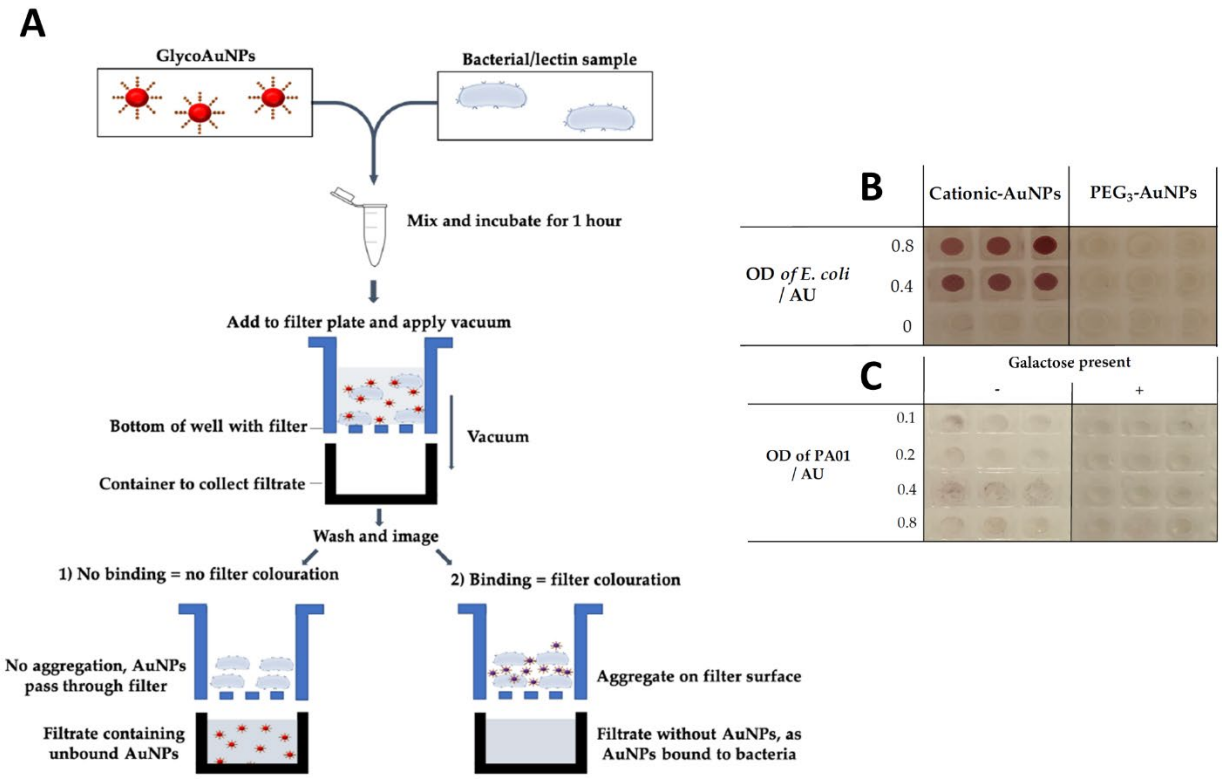

Figure 4.31. Filter plate and aggregation results from the previous work in our group by Moore *et al.*[353] (**A**) Schematic representation of the filter plate assay developed by Iceni Glycoscience for the detection of AuNPs-induced bacterial aggregation. (**B**) Image of a filter plate assay where *E. coli* strain ORN178 was incubated with cationic *N,N,N*-trimethyl(11-mercaptoundecyl)ammonium chloride-functionalised AuNPs. (**C**) Image of a filter plate assay where *P. aeruginosa* strain PAO1 was incubated with Gal-AuNPs.

Encouraged by those results, we attempted to develop a method to study bacterial aggregation through FCM. *P. aeruginosa* PAO1 strain was grown in lysogeny broth (LB media)[354] and the growth was monitored by measuring the absorbance at 600 nm. After 1 hour lag-phase, the cells grew for 5 hours in the exponential phase before entering the stationary phase (**Figure 4.32**).

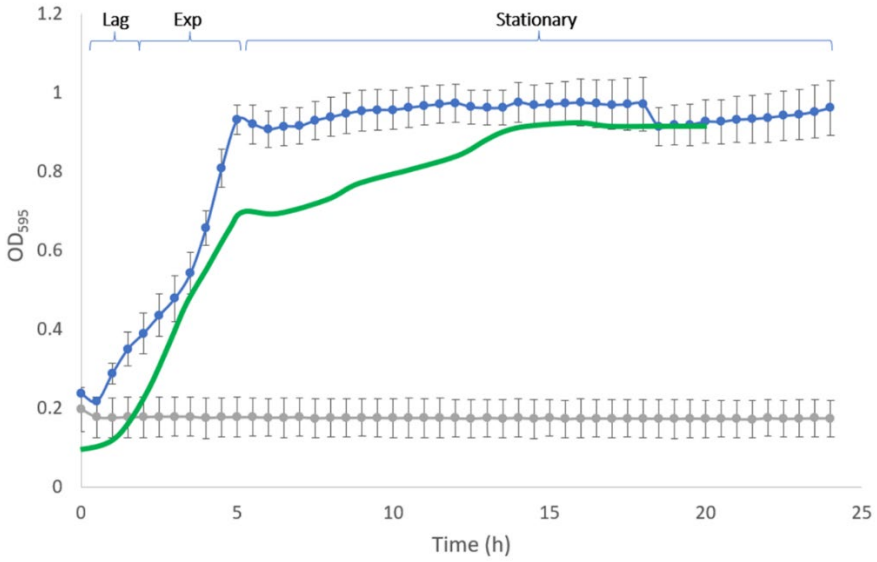

Figure 4.32. Culture of *P. aeruginosa* PA01 strain. The **growth curve** was compared with **published data**.[355] In **grey**, a blank was performed measuring the OD of the media. Error bars represent the standard deviation between triplicates.

The interaction between gAuNPs and the surface of *P. aeruginosa* was then tested by FCM. FCM-based methods often take advantage of the fluorescent properties of either ligands or cells, leading to changes in emission that inform about interactions developed between both of them.[356,357] However, to avoid potential interferences caused by the presence of a fluorophore on the cell surface of the bacteria, dynamic light scattering was used to monitor changes in cell population upon incubation with gAuNPs. Sidelight scattering (SSC) informs about the surface granularity of the cells, and forward light scattering (FSC) informs about the cellular size. The premise of this approach is to cause AuNPs-induced bacterial aggregation, leading to changes in surface and size, quantifiable by SSC and FSC respectively. To test the effect of AuNPs on the LecA-expressing cells, the culture was harvested at 16 hours and bacterial cultures were diluted at $5x10^7$ and $5x10^8$ cells/mL. FCM analysis was first used to select cell density. Bacterial populations were gated to study the differences observed in light scattering (**Figure 4.33A**). A clear population shift was observed when cells were used at $5x10^8$

cells/mL (top-right shift of the bacterial population), which may be due to bacterial aggregation. Therefore, $5x10^7$ cell/mL concentration was used in the rest of the experiments. To further confirm that the gated population corresponded to the bacteria, the cells were labelled with fluorescein isothiocyanate (FITC)-labelling using carbonate buffer (see methods in *Chapter 5*) and analysed as above. FITC targets available lysine residues on the surface of the bacteria, in a non-specific manner.[358] The FCM analysis confirmed that the gated population corresponded to bacteria (84% of cells were labelled) (**Figure 4.33B**).

The interaction between *P. aeruginosa* and either Gal-BSA-AuNPs (**31**) or propargylated BSA-AuNPs (**30**) was then tested. Briefly, bacterial samples were incubated at room temperature in cell:AuNPs ratios 1:100, 1:500, 1:1000, and analysed by FCM. However, no shift in bacterial population was observed in the presence of gAuNPs (representative data in **Figure 4.33C**). To investigate this further, the cells were incubated with a commercial FITC-labelled anti-lecA rabbit antibody (10 µg/mL). However, no fluorescence was found in the bacterial population by FCM (**Figure 4.33D**), suggesting that LecA was not present on the *P. aeruginosa* cell surface in the tested conditions.

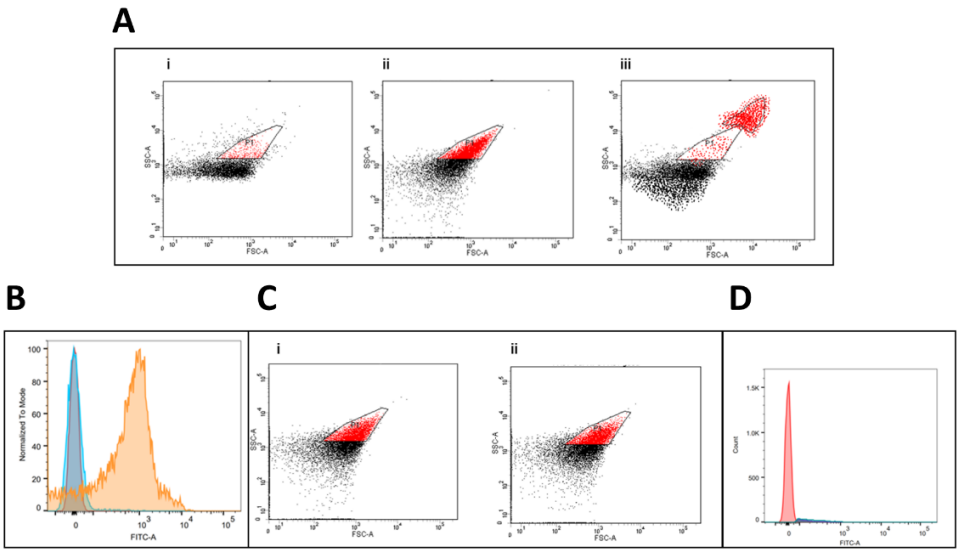

Figure 4.33. FCM analysis of the interaction between *P. aeruginosa* PA01 and 40 nm gAuNPs. (**A**) Dot plots of (**i**) AuNPs at OD 1, (**ii**) *P. aeruginosa* PAO1 at $5x10^7$ cells/mL and (**iii**) *P. aeruginosa* PAO1 at $5x10^8$ cells/mL. (**B**) Fluorescence histogram of FITC-labelled *P. aeruginosa* PAO1 at $5x10^7$ cells/mL. **Blue** corresponds to PAO1 and **yellow** to FITC-labelled PAO1 cells. (**C**) Dot plots of *P. aeruginosa* PAO1 at $5x10^7$ cells/mL incubated with (**i**) 40 nm AuNPs and (**ii**) Gal-BSA-AuNPs. No shift of the bacterial population can be observed. (**D**) Fluorescence histogram of *P. aeruginosa* PAO1 at $5x10^7$ cells/mL (**red**) incubated with FITC-labelled anti-LecA antibody (**blue**). No fluorescence shift was observed.

To determine whether LecA was produced by *P. aeruginosa* in the growth conditions, the bacterial lysates of cells harvested at 24h were analysed by western blot. Briefly, the proteins were separated by electrophoresis on SDS-PAGE and, after the transfer, the membrane was incubated with a commercial FITC-conjugated anti-LecA antibody (also used in the FCM analysis), or with a rabbit anti-LecA antibody followed by a secondary alkaline phosphatase-conjugated goat anti-rabbit antibody. The presence of LecA was then determined by colorimetric staining following the addition of nitro-blue tetrazolium and 5-bromo-4-chloro-3'-indolyphosphate (NBT/BCIP) (**Figure 4.34A-C**). Using this approach, a band of apparent molecular weight of 12 KDa was detected in the LecA control (1 µg) using the first/second antibody detection method, whereas no signal was detected with the FITC-labelled antibody. These results explain why no fluorescence was observed on the cell surface of the bacteria with the FITC-antibody in the FCM experiment. However, no discrete band corresponding to LecA was observed in the bacterial extracts with either antibody, suggesting that LecA protein may not be produced in the conditions of the growth assay or it was produced in amounts below the limit of detection. The data obtained in this thesis was compared with the one reported in a previous thesis by Dr Brydie Moore, where the expression of LecA in *P. aeruginosa* PAO1 was studied in analogous conditions, with a positive outcome (**Figure 4.34D**).[353] In those experiments, the expression of LecA was studied over time in liquid cultures where the bacteria were harvested at time points ranging from 2 to 78 h. LecA was found in the extracts from 10 hours onwards.

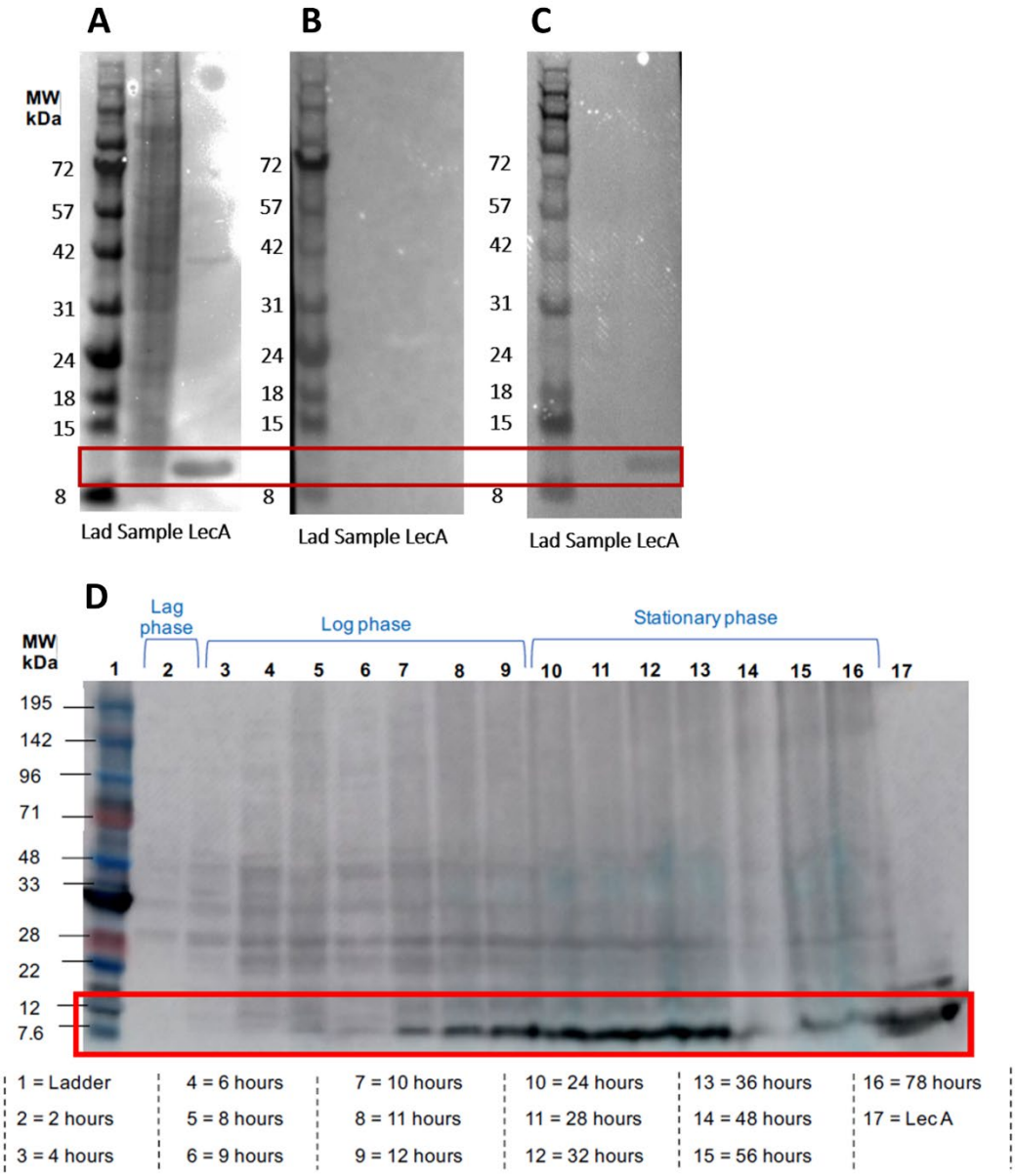

Figure 4.34. Western Blot analysis of *P. aeruginosa* LecA. Proteins were visualised in (**A**) a Coomassie Blue-stained gel, or a membrane revealed with (**B**) a FITC-conjugated anti-LecA antibody (1:500 dilution) or (**C**) a rabbit anti-LecA antibody (1:1000 dilution) with a secondary alkaline phosphatase-conjugated anti-rabbit antibody. The band corresponding to LecA (12 kDa) is highlighted in red. The left lane of each gel contained the molecular weight ladder (Lad), and the right lane contained a positive control with LecA. (**D**) Previous work in the group where LecA was observed in extracts from liquid cultures of *P. aeruginosa* PAO1 from 10 hours onwards.[353]

To further investigate the reason behind the lack of LecA detection, we checked for the presence of the LecA-encoding gene in the bacterial strain used in the growth assays by PCR. Briefly, the DNA was extracted from an overnight culture of *P. aeruginosa* following the lysis of the cells and amplified using DNA primers specific to the LecA gene. Sequencing of the PCR

product confirmed the integrity of the LecA-encoding gene by comparing the assembled genome from the sample and the reported sequence of the LecA gene (**Table 4.2**).[359] Therefore, the lack of protein may be due to a lack of expression in the conditions of the growth assays and/or to the sensitivity of the immunodetection assay.

Table 4.2. Sequencing data showing the assembled fragment highlighting in yellow the LecA gene in the PAO1 bacteria used in this thesis, which is in agreement with the genome reported by Winsor *et al*.[359]

This work
ATGCAGGAGAAAAGAGGATAATTCCGCCAGTGTATATTCAATTCACTGGCGGAATTATCCTCTTTT CTCCTGCATGAATTGGTAGGCGGTACTTCCTCGTTGCTGTGCTTTGCTAACAGGGAAGGATCGCGA ATCAGGGTTTTTCGCCTCTTTCGTTTATGAACAGGAATTCATATATCGGAGATCAATCATGGCTTGG AAAGGTGAGGTTCTGGCTAATAACGAAGCAGGGCAGGTAACGTCGATTATCTACAATCCGGGCG ATGTCATTACCATCGTCGCCGCCGGTTGGGCCAGTTACGGACCTACCCAGAAATGGGGGCCGCAG GGCGATCGGGAGCATCCGGACCAAGGGCTGATCTGCCACGATGCGTTTTGTGGTGCGCTGGTCAT GAAGATTGGCAACAGCGGAACCATTCCGGTCAATACCGGGTTGTTCCGTTGGGTTGCACCCAATA ATGTCCAGGGTGCAATCACTCTTATCTACAACGACGTGCCCGGAACCTATGGCAATAACTCCGGCT CGTTCAGTGTCAATATTGGAAAGGATCAGTCCTGATAACTTGTCTCGGAAAAAAAAAGGGCCCGA ATGGGCTCTTTTTTTAAATGCAAATAAAGTGAAGTTGCCCGTGTGGCCGTTATGAACGGACAGGCA GCGCTTCGCAGTTGCGACTACCAATGACAAGAGCTGTCTCAT
Winsor *et al*.[359]
ATGGCTTGG AAAGGTGAGGTTCTGGCTAATAACGAAGCAGGGCAGGTAACGTCGATTATCTACAATCCGGGCG ATGTCATTACCATCGTCGCCGCCGGTTGGGCCAGTTACGGACCTACCCAGAAATGGGGGCCGCAG GGCGATCGGGAGCATCCGGACCAAGGGCTGATCTGCCACGATGCGTTTTGTGGTGCGCTGGTCAT GAAGATTGGCAACAGCGGAACCATTCCGGTCAATACCGGGTTGTTCCGTTGGGTTGCACCCAATA ATGTCCAGGGTGCAATCACTCTTATCTACAACGACGTGCCCGGAACCTATGGCAATAACTCCGGCT CGTTCAGTGTCAATATTGGAAAGGATCAGTCCTGA

4.4. Conclusions

In this chapter, available literature about the rational design of ligands against bacterial lectins has been discussed. Multivalent inhibitors developed against the galactose-binding lectin LecA from *P. aeruginosa* have been reviewed aiming at better understanding the features required to increase the avidity of ligands for LecA, leading to more sensitive detection assays. Successful ligands found in literature seem to satisfy the requirements: not a higher multivalency, but a precise distance between galactosides, that should permit a tighter binding to the lectin. A combination of an aromatic aglycon and the finely tuned length and

rigidity of the spacer can lead to a 1000-fold enhancement of the K_D value between the inhibitor and LecA. A clear conclusion from the literature review is that a more complex, or more sophisticated structure accessing the presentation of six and more glycan units does not guarantee a better binding. Moreover, most of the ligands discussed in the literature review exhibited K_D values in the 10-450 nM range, regardless of their structural differences.

With this information in hand, a galactose dimer ligand has been designed employing CuAAC chemistry and EDC couplings. The envisioned pathway allows the installation of two different modules (**A** and **B**) through a 1,4-disubstituted 1,2,3-triazol ring. The designed modular approach would be ideal to create combinatorial libraries from independent building blocks, allowing access to exponential amounts of chemical compounds for biological testing.

The synthesis of four different novel galactose dimers has been attempted starting from an aspartic acid bridge, elongated by either a three or four atoms tether through an amide bond using propargylamine or aminobutyne, respectively. Two different aglycons have been incorporated, propyl and phenyl, to evaluate the reported beneficial effect of aromatic moieties at the anomeric position of LecA inhibitors. The intermediates have been fully characterised through ^{1}H- and ^{13}C-NMR, HR-MS, polarimetry and/or infrared spectroscopy when required. The completed work has afforded the four dimers in their acetylated precursors, with overall yields (from the beginning of the pathway) of 14, 18, 35 and 39% for the **51-54** set, respectively. The deprotection of such compounds and the installation of an azide-ending tether was also attempted before their biological evaluation. However, the high polarity and low water solubility of the final products complicated their purification. It is possible that the azidohexanoic tether installed is increasing the hydrophobicity making the final structure insoluble in aqueous media. Issues on insolubility have been encountered in the past and have been discussed in *Section 4.1.* Further optimisation is required to overcome the low solubility issue and to be able to evaluate the binding capacity of the synthesised ligands to LecA. A discussion on the planned work and expected outcomes had the synthesis been successful is given in *Section 4.5*.

A FCM method has been developed in a preliminary study to evaluate the binding properties of the gAuNPs synthesised in this thesis. However, the preliminary data did not show any effect of the Gal-BSA-AuNPs on the bacterial cell population, which may be due to a lack of expression of the LecA adhesin of the bacteria in the growth conditions as indicated by

Western Blot analysis. However, this does not exclude that the gAuNPs synthesised in this thesis cannot cause bacterial aggregation, underscoring the importance of using a ligand with enhanced affinity for LecA. The pathway developed in this chapter for the enhanced interaction with the lectin has the potential to provide such ligands, opening the door for the development of a AuNP-based detection system for *P. aeruginosa.*

4.5. Future work

The synthesis of the deprotected dimers needs to be revised, given the difficulties to isolate the final products. The addition of an intermediate deacetylation step would potentially allow the proper isolation of the dimers (**Scheme 4.8**) and therefore their full characterisation. Having a readily soluble set of dimers would allow their assessment as potential inhibitors of LecA. The technique of choice for it would have been ITC, to obtain the thermodynamic values and eventually, the respective K_D.

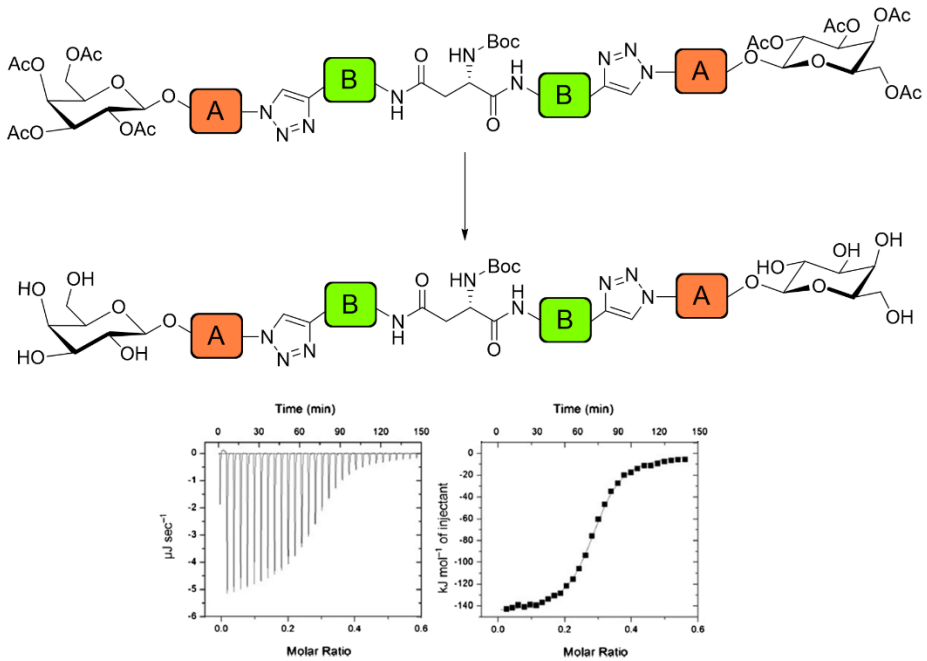

Scheme 4.8. Next step to be attempted in the synthesis of the dimers, to allow more water solubility and characterisation of the LecA binding properties of the dimer through ITC.

The installation of an azide-ending tether or other variations would still be needed to allow the functionalisation of BSA and AuNPs to develop a dipstick assay. The further development of the ligand would still be problematic due to the solubility problems of the azidohexanoic

acid tether; however, a PEGylated chain would possibly allow better solubility. The completion of those experiments and successful synthesis of a glycodimer-BSA (**Scheme 4.9**) could have potentially informed a very sensitive assay for the detection system of LecA, quantifying the interaction through BLI, as a simplified model of binding to *P. aeruginosa.*

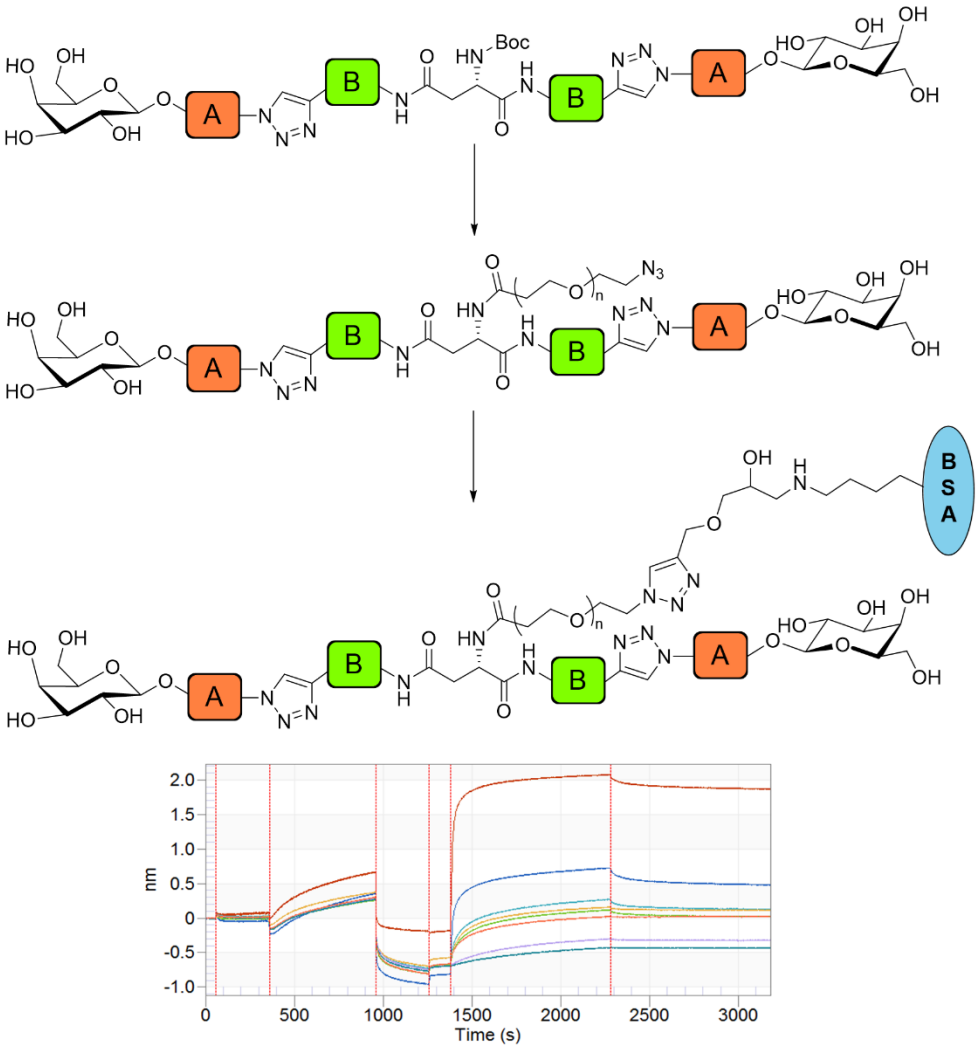

Scheme 4.9. Installation of an azide-ending PEGylated tether to improve the water solubility of the dimer concerning the original azidohexanoic version, and subsequent synthesis of a glycodimer-BSA conjugate to be evaluated through BLI.

In the long term, the synthesis of glycodimer-BSA-AuNPs for the detection of bacterial samples containing *P. aeruginosa* would be attempted. However, the approach developed in this chapter is dependent on the expression of LecA at the cell surface of *P. aeruginosa* PAO1. Previous data from the group revealed a lack of reproducibility in the expression of the lectin by the same strain.[353] Therefore, more work is required to monitor the expression and detection of LecA in *P. aeruginosa* PAO1 cultures over time. Specific objectives will be to

determine LecA protein expression throughout growth phases using the first/second antibody detection method, which we showed was effective against LecA purified protein used as a control. This work could be complemented by gene expression analysis using quantitative PCR targeted to the gene encoding LecA, to determine whether the lack of protein detection in the conditions used in our preliminary work was due to the repression of gene transcription or to the low amount of protein produced. This will also inform on whether LecA expression is constitutive or whether it would need induction. Upon confirmation of LecA expression, it will also be necessary to check that the protein is present at the cell surface by FCM using the antibody approach described above. The FCM assay described in this preliminary work will provide a new approach to study gAuNPs – bacteria interactions.

The final aim of this project would be to develop a dipstick assay for the rapid detection of *P. aeruginosa* following the methodology described in *Chapter 3*. A number of antibody-based LFAs have been published in relation to the detection of whole pathogens,[360] however the same approach has not been explored with gAuNPs. Moreover, the development of gAuNPs based assays towards the detection of LecA could not immediately translate to *P. aeruginosa*, with the related challenges discussed in Section 4.3.4.[353] The complexity of the *P. aeruginosa* detection in relation to system optimised on LecA has been reported before (**Figure 4.35A**).[361] LecA was targeted with a galactose tetramer showing a K_D value of 80 nM; however, the inhibition of the cell adhesion of *P. aeruginosa* to A549 lung epithelial cells did not succeed (**Figure 4.35B**). Unfortunately, predicting a successful translation from the model lectin LecA to the more complex full pathogen detection seems to be governed by an empirical approach.

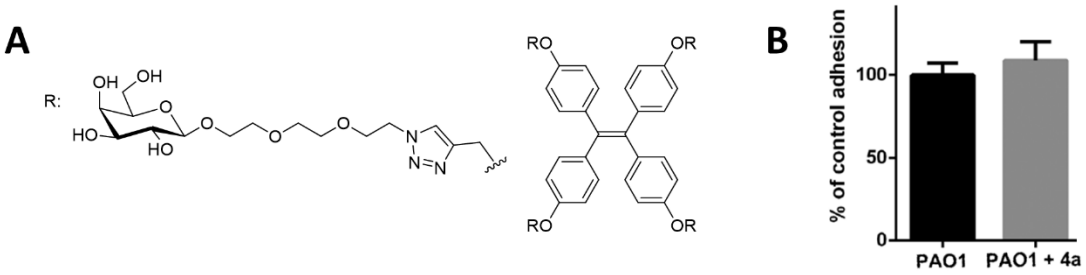

Figure 4.35. (**A**) Galactose tetramer synthesised by Donnier-Marechal *et al.* for the detection of LecA. (**B**) Percentage of *P. aeruginosa* adhesion to lung epithelial cells, with and without the developed ligand (numbered 4a).

CHAPTER 5

MATERIALS AND METHODS

The following Chapter outlines the materials and methods used in the experiments conducted in this thesis.

5.1. Materials

5.1.1. Reagents

All reagents were of analytical grade and purchased from Sigma Aldrich, Merck, Fischer Scientific, Thermo Fischer Scientific or Carbosynth unless stated otherwise. Citrate-capped 40 nm AuNPs were purchased from Expedeon, NHS-ester-activated 40 nm AuNPs were purchased from CytoDiagnostics and NHS-activated 150 nm AuNSs were purchased from NanoComposix).

5.1.2. Cells

The *Pseudomonas aeruginosa* strain PAO1 was kindly provided by Professor Mark Webber (Quadram Institute Bioscience, Norwich Research Park, Norwich, UK).

5.1.3. Buffers/media

A summary of the buffers and media used in PhD research can be found in **Table 5.1.**

Table 5.1. Buffers and media used in this thesis.

Buffer/media name	Composition
Citric acid buffer	2 mM citric acid buffer, pH 5.3
ConA buffer	10 mM HEPES, pH 8.5, 100 mM $CaCl_2$
Dipstick buffer (AuNPs)	PBS with 1% PVP
Dipstick buffer (AuNSs)	PB with 1% PVP, 1% BSA, 1% Triton-X100
HEPES-PEG reaction buffer	100 mM HEPES buffer (pH 8.0), 0.5% (w/v) PEG-20k
LecA buffer	Tris-HCl 0.1 M, pH 7.5, 25 mM $CaCl_2$
PCR reaction buffer	20 mM Tris HCl (pH 8.4), 50 mM KCl, 5 mM $MgCl_2$ (NewEngland Biolabs)
Phosphate buffer (PB)	10 mM phosphate buffer, pH 7.6
Phosphate buffer saline (PBS)	PB with 50 mM NaCl
Phosphate buffer, Tween-20 (PBT)	PB with 0.5% Tween-20
Phosphate buffer saline, Tween-20 (PBST)	PBS with 0.5% Tween-20
RCA_{120} buffer	10 mM Na_3PO_4, 150 mM NaCl, pH 7.8
UEA I buffer	10 mM HEPES, pH 7.5, 150 mM NaCl, 0.1 mM $CaCl_2$
WGA buffer	10 mM HEPES, pH 8.5, 100 mM $CaCl_2$

5.2. Instrumental techniques

A summary of the equipment used in this PhD research can be found in **Table 5.2.**

Table 5.2. Equipment and instruments used in this thesis

Equipment / technique	Instrument manufacturer / model
Centrifuge	Techne Genofuge 16M microcentrifuge
Dynamic Light Scattering	Malvern Zetasizer Nano-ZS

Flow cytometry	BD LSR Fortessa flow cytometer
Gel imaging	Bio-Rad Chemidoc
High-Performance Mass spectrometry	Bruker Daltonics autoflex speed ToF/ToF mass spectrometer
Infrared spectroscopy	Perkin Elmer Fourier Transform Infrared spectrometer
Liquid Chromatography - Mass spectrometry	Advion Expression Compact Mass Spectrometer
Nuclear Magnetic Resonance	Bruker AVIII 400 MHz and Bruker NEO 600 MHz
Plate reader	POLARstar Omega, BMG Labtech
Polarimetry	Perkin Elmer PE 341/342
Rotatory mixer	Benchtop MX-RL-E rotatory laboratory mixer
Spectrophotometer 1 (bacterial OD_{600})	Biochrom Ultrospec 10 Cell Density Meter
Spectrophotometer 2 (DNA concentration)	Thermo Scientific NanoDrop 2000
Thermocycler	Biometra T-Gradient Thermoblock
Transmission electron microscopy	FEI Tecnai F20 S/TEM
UV-Vis spectroscopy	Hitachi U-3900 spectrophotometer

Dynamic Light Scattering

For dynamic light scattering size measurements, the sample (500 µL) in PBS was added to a 1 mL Quartz cuvette. The sample was equilibrated for two minutes, and the mean average size was collected from three runs, with at least 5 measurements per run.

Infrared spectroscopy

Perkin Elmer Fourier Transform Infrared spectrometer with attenuated total reflection (ATR) attachment was used to record the IR spectra of the azide-containing compounds. If enough amount of material was available, the sample was not diluted and directly deposited on the ATR crystal. If a limited amount of compound was available, the sample was diluted in MeOH

to 10 mg/mL, from which 20 µL were deposited on the instrument glass and dried before recording the spectrum. Spectrum One software was used for data analysis.

Mass spectrometry

Electrospray ionisation mass spectrometry in positive mode was used for the characterisation of carbohydrate derivates, where necessary. A 10 µl sample at the concentration of 0.01 mg/mL were injected. Advion Mass Express software was used for data analysis.

Matrix-assisted laser desorption/ionisation time-of-flight mass spectrometry was used for the characterisation of carbohydrate-BSA conjugates. A sample containing 250 µg/mL of BSA conjugate was pre-mixed in a 1: 1 ratio with a DHB matrix. The sample was prepared depositing 1 µl of DHB matrix on an MTP AnchorChip 384 target plate and it was allowed to dry for 10 minutes. Successively, 1 µl of the pre-mixed sample-matrix sample was deposited on the plate and allowed to dry for 10 minutes. The MALDI-TOF MS equipment used a nitrogen laser, and analysis was performed in a linear 3-shot mode, with 32x gain and 70% laser intensity.

Nuclear Magnetic Resonance spectroscopy

Nuclear Magnetic Resonance equipment used a broadband BBFO probe at 400 MHz (^{1}H) and 100 MHz (^{13}C) at 298 K. Compounds were characterised using 1D-^{1}H, 1D-^{13}C, ^{1}H-^{1}H- COSY, ^{1}H-^{13}C-HSQC and ^{1}H-^{1}H-NOESY. Mestrenova software (Mestrelab Research, S.L.) was used for data analysis. For ^{13}C-NMR experiments measured in D_2O as the solvent, 10 µL of acetone were added as a reference.

Polarimetry

Perkin Elmer PE 341/342 polarimeter was used to measure optical rotation of chiral compounds. Measurements were taken at 25 ^{o}C and using the sodium D line (589 nm) as the source of light. According to the specific solubility, samples were prepared using MeOH, chloroform or water, at the indicated concentration, ranging 0 – 10 mg/mL (c = 0 – 1).

Transmission electron microscopy

For transmission electron microscopy (TEM) imaging, 400 mesh copper palladium grids with carbon-coated pyroxylin support film were used. A volume of 10 µL of the sample was adsorbed on the grid, which was allowed to dry at room temperature overnight.

The samples were submitted to the TEM facility at the University of East Anglia, where the grids were placed in the instrument, operating at 200 kV, and imaged using an AMT XR60B digital camera (Deben).

UV-Vis spectrometry

UV-Vis measurements were obtained using a UV-Vis spectrophotometer or a plate reader. For UV-Vis spectrophotometer measurements, samples (1 mL) were added to a Quartz cuvette and measured using Cary WinUV software, with a 1 cm path length. For plate reader measurements, samples (50 µL) were loaded into 384-well microtiter plates (4titude), and measurements were recorded using Omega series and MARS Data Analysis software (BMG Labtech).

5.3. Synthetic protocols

5.3.1. Glycan synthesis

5.3.1.1. 1,2,3,4,6-Penta-*O*-acetyl-α/β-D-galactopyranose (1)[189]

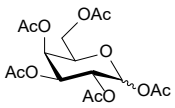

NaOAc (0.50 g, 6.1 mmol, 1.1 eq.) was suspended in Ac_2O (10 mL) and the reaction mixture was heated to 120 ^oC for 30 minutes before powdered galactose (1.0 g, 5.6 mmol) was added portion-wise with stirring together with a small crystal of DMAP. After one hour, TLC (EtOAc-Hex 1:1) showed reaction completion. The mixture was cooled to room temperature and neutralised with saturated aqueous $NaHCO_3$ solution (20 mL). The acetylated sugar product was extracted with DCM (3 x 30 mL), and the combined organic layers were dried over anhydrous $MgSO_4$, filtered and concentrated to dryness under reduced pressure to afford **1**

as a white solid (2.1 g, 98%). The compound was obtained as an α/β mixture in a 20:80 ratio. Only data for the β-anomer is reported. ratio R_f value (EtOAc-Hex 5:5): 0.31. δ_H ($CDCl_3$; 400 MHz): 5.70 (d, $J_{1,2}$ = 8.3 Hz, 1H, H-1), 5.42 (dd, $J_{3,4}$ = 3.4, $J_{4,5}$ = 1.1 Hz, 1H, H-4), 5.33 (dd, $J_{1,2}$ = 8.3, $J_{2,3}$ = 10.5 Hz, 1H, H-2), 5.08 (dd, $J_{2,3}$ = 10.5, $J_{3,4}$ = 3.4 Hz, 1H, H-3), 4.17 (dd, $J_{5,6a}$ = 7.0, $J_{6a,6b}$ = 11.2 Hz, 1H, H-6a), 4.12 (dd, $J_{5,6b}$ = 6.1, $J_{6a,6b}$ = 11.2 Hz, 1H, H-6b), 4.05 (ddd, $J_{4,5}$ = 1.1 Hz, $J_{5,6a}$ = 7.0, $J_{5,6b}$ = 6.1 Hz, 1H, H-5), 2.16 (s, 3H, CH_3), 2.12 (s, 3H, CH_3), 2.04 (s, 6H, CH_3), 1.99 (s, 3H, CH_3). δ_C (101 MHz): 170.5 (1C, C=O), 170.3 (1C, C=O), 170.01 (1C, C=O), 169.5 (1C, C=O), 169.1 (1C, C=O), 92.3 (1C, C-1), 71.8 (1C, C-5), 71.0 (1C, C-3), 68.0 (1C, C-2), 67.0 (1C, C-4), 61.2 (1C, C-6), 20.95 (1C, CH_3), 20.78 (2C, CH_3), 20.75 (1C, CH_3), 20.67 (1C, CH_3).

5.3.1.2. 4-*O*-(2,3,4,6-Tetra-*O*-acetyl-β-D-galactopyranosyl)-1,2,3,6-tetra-*O*-acetyl-α/β-D-glucopyranose (2)

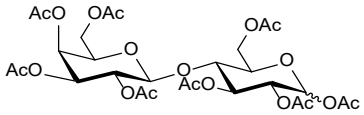

The procedure was adapted from Zhu *et al.*[189] NaOAc (0.13 g, 1.6 mmol, 1.1 eq.) was suspended in Ac_2O (2.5 mL) and the reaction mixture was heated to 120 °C for 30 minutes before powdered lactose (0.50 g, 1.5 mmol) was added portion-wise with stirring. After one hour, the reaction mixture was cooled to room temperature and pyridine (3 mL) was added together with a small crystal of DMAP. The reaction was stirred overnight at room temperature. TLC (EtOAc-Hex 3:2) showed reaction completion and the crude was diluted with DCM (10 mL). The excess of pyridine was quenched by the addition of aqueous HCl solution (15 mL, 10%). The acetylated sugar product **2** was extracted with DCM (3 x 30 mL) and the combined organic layers were dried over anhydrous $MgSO_4$, filtered and concentrated to dryness under reduced pressure (0.85 g, 1.2 mmol, 85%). The compound was obtained as an α/β mixture in a 10:90 ratio. Only data for the β-anomer is reported. R_f value (EtOAc-Hex 6:4): 0.37. δ_H ($CDCl_3$; 400 MHz): 5.67 (d, $J_{1,2}$ = 8.2 Hz, 1H, H-1), 5.35 (dd, $J_{3',4'}$ = 3.5, $J_{4',5'}$ = 1.2 Hz, 1H, H-4'), 5.24 (t, $J_{2,3}$ = $J_{3,4}$ = 9.3 Hz, 1H, H-3), 5.11 (dd, $J_{1',2'}$ = 7.9, $J_{2',3'}$ = 10.4 Hz, 1H, H-2'), 5.04 (dd, $J_{1,2}$ = 8.2, $J_{2,3}$ = 9.3 Hz, 1H, H-2), 4.95 (dd, $J_{2',3'}$ = 10.4, $J_{3',4'}$ = 3.5 Hz, 1H, H-3'), 4.47 (d, $J_{1',2'}$ = 7.9 Hz, 1H, H-1'), 4.48-4.42 (m, 1H, H-6a'), 4.19 – 4.04 (m, 3H, H-6ab, H-6b'), 3.91 – 3.82 (m, 2H, H-4, H-5´), 3.76 (m, 1H, H-5), 2.15 (s, 3H, CH_3), 2.12 (s, 3H, CH_3), 2.10 (s, 3H, CH_3), 2.07 (s, 3H, CH_3), 2.05 (s, 3H, CH_3), 2.04 (s, 3H, CH_3), 2.03 (s, 3H, CH_3), 19.97 (s, 3H, CH_3). δ_C (101 MHz):

170.5 (1C, C=O), 170.5 (1C, C=O), 170.3 (1C, C=O), 170.2 (1C, C=O), 169.8 (1C, C=O), 169.7 (1C, C=O), 169.2 (1C, C=O), 169.0 (1C, C=O), 101.1 (1C, C-1'), 91.7 (1C, C-1), 75.8 (1C, C-4), 73.6 (1C, C-5), 72.8 (1C, C-3), 71.1 (1C, C-3'), 70.9 (1C, C-5'), 70.7 (1C, C-2), 69.1 (1C, C-2'), 66.7 (1C, C-4'), 61.9 (1C, C-6'), 61.0 (1C, C-6), 20.97 (1C, CH_3), 20.95 (1C, CH_3), 20.89 (1C, CH_3), 20.78 (2C, CH_3), 20.75 (1C, CH_3), 20.74 (1C, CH_3), 20.64 (1C, CH_3). ESI-MS: found *m/z* 701.3 $[M+Na]^+$, calcd for $C_{28}H_{38}O_{19}Na$ 701.2.

5.3.1.3. 4-*O*-(2-*O*-(2,3,4-Tri-*O*-acetyl-β-L-fucopyranosyl)-3,4,6-tri-*O*-acetyl-β-D-galactopyranosyl)-1,2,3,6-tetra-*O*-acetyl-α/β-D-glucopyranose (3)

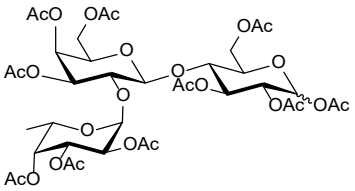

The procedure was adapted from Zhu *et al.*[189] NaOAc (35 mg, 0.34 mmol, 1.1 eq.) was suspended in Ac_2O (0.5 mL) and the reaction mixture was heated to 120 °C for 30 minutes before powdered 2'-fucosyllactose (500 mg, 1.5 mmol) was added portion-wise with stirring. After one hour, the reaction mixture was cooled to room temperature and pyridine (3 mL) was added together with a small crystal of DMAP. The reaction was stirred overnight at room temperature. TLC (EtOAc-Hex 3:2) showed reaction completion and the crude was diluted with DCM (10 mL). The excess of pyridine was quenched by the addition of aqueous HCl solution (15 mL, 10%). The acetylated product **3** was extracted with DCM (3 x 30 mL) and the combined organic layers were dried over anhydrous $MgSO_4$, filtered and concentrated to dryness under reduced pressure (850 mg, 1.2 mmol, 85%). The compound was obtained as an α/β mixture in a 40:60 ratio. Only data for the β-anomer is reported R_f value (EtOAc-Hex 6:4): 0.32. δ_H ($CDCl_3$; 400 MHz): 5.67 (d, $J_{1,2}$ = 8.0 Hz, 1 H, β-H-1), 5.34 (d, $J_{1'',2''}$ = 4.2 Hz, 1 H, H-1''), 5.20-4.95 (m, 5H, H-3, H-3'', H-2, H-2'', H-3'), 4.42 (d, $J_{1',2'}$ = 7.9 Hz, 1 H, H-1'), 4.49-4.34, 4.28-4.23, 4.17-4.03, 3.91-3.77 (4 x m, 10 H), 2.17-1.95 (10 x s, 3H, CH_3), 1.25 (d, $J_{5'',6''}$ = 7.5 Hz, 3 H, H-6''). δ_C (101 MHz): 170.9-168.8 (10 x s, 1C, C=O), 100.1 (1C, C-1'), 95.8 (1C, C-1''), 91.9 (1C, C-1), 67-74.5 (12 x s, 1C), 62.2 (1C, C-6), 61.8 (1C, C-6'), 21.0-20.6 (m, 30C, CH_3), 15.7 (1C, CH_3). ESI-MS: found *m/z* 931.8 $[M+Na]^+$, calcd for $C_{38}H_{52}O_{25}Na$ 931.3.

5.3.1.4. 1,2,3,4,6-Penta-*O*-acetyl-α/β-D-glucopyranose (4)

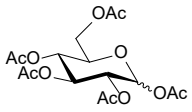

Adapted from Zhu *et al.*[189] NaOAc (0.15 g, 1.8 mmol, 1.1 eq.) was suspended in Ac_2O (3 mL) and the reaction mixture was heated to 120 °C for 30 minutes before powdered glucose (0.3 g, 0.7 mmol) was added portion-wise with stirring together with a small crystal of DMAP. After one hour, TLC (EtOAc-Hex 1:1) showed reaction completion. The mixture was cooled to room temperature and neutralised with saturated aqueous $NaHCO_3$ solution (10 mL). The acetylated product was extracted with DCM (3 x 20 mL), and the combined organic layers were dried over $MgSO_4$, filtered and concentrated to dryness under reduced pressure (0.65 g, 99%). R_f value (EtOAc-Hex 5:5): 0.43. δ_H ($CDCl_3$; 400 MHz): 6.33 (d, $J_{1,2}$ = 3.7 Hz, 0.2H, α-H-1), 5.71(d, $J_{1,2}$ = 8.1 Hz, 1H, β-H-1), 5.24 (t, $J_{2,3}$ = $J_{3,4}$ = 9.3 Hz, 1H, H-3), 5.14 (dd, $J_{3,4}$ = 9.3 Hz, $J_{4,5}$ = 9.9, 1H, H-4), 5.12 (dd, $J_{1,2}$ = 8.1 Hz, $J_{2,3}$ = 9.3 Hz, 1H, H-2), 4.29 (dd, $J_{5,6a}$ = 4.5 Hz, $J_{6a,6b}$ = 12.5, 1H, H-6a), 4.11 (dd, $J_{5,6b}$ = 12.5, $J_{6a,6b}$ = 2.3 Hz, 1H, H-6b), 3.84 (ddd, $J_{4,5}$ = 9.9, $J_{5,6a}$ = 4.5, $J_{5,6b}$ = 2.3 Hz, 1H, H-5), 2.11 (s, 3H, CH_3), 2.08 (s, 3H, CH_3), 2.03 (s, 6H, CH_3), 2.01 (s, 3H, CH_3). δ_C (101 MHz): 170.7 (1C, C=O), 170.2 (1C, C=O), 169.5 (1C, C=O), 169.4 (1C, C=O), 169.1 (1C, C=O), 91.8 (1C, β-C-1), 89.2 (0.2C, α-C-1), 72.9 (1C, C-5), 72.9 (1C, C-3), 70.4 (1C, C-4), 67.9 (1C, C-2), 61.6 (1C, C-6), 21.0 (1C, CH_3), 20.9 (1C, CH_3), 20.71 (2C, CH_3), 20.70 (1C, CH_3). IR (cm^{-1}): 3373.7 (OH), 2100.0 (N_3). ESI-MS: found *m/z* 390.8 $[M+Na]^+$, calcd for $C_{16}H_{22}O_{11}Na$ 390.1.

5.3.1.5. 1,2,3,4,6-Penta-*O*-benzoyl-D-mannopyranose (5)[198]

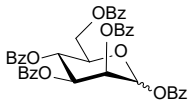

Mannose (298 mg, 1.7 mmol) was suspended in pyridine (3.3 mL). Benzoyl chloride (1.2 mL, 11.2 mmol, 6.2 eq) was added dropwise with stirring. Catalytic DMAP was added to the reaction mixture (10 mg, 0.05 eq). The reaction was stirred overnight at room temperature, at which point TLC (EtOAc-Hex 6:4) showed reaction completion. The mixture was co-evaporated several times with toluene (4 x 10 mL) to remove pyridine. The residue was dissolved in DCM (25 mL) and washed with brine (3 x 15 mL). The organic layer was dried over $MgSO_4$, filtered and concentrated to dryness under reduced pressure (**5**, 1.06 g, 92%). R_f value

(EtOAc-Hex 6:4): 0.55. δ_H ($CDCl_3$; 400 MHz): 8.23-7.83 (m, 10H, H_{meta}), 7.80-7.26 (m, 15H, H_{ortho}, H_{para}), 6.63 (d, $J_{1,2}$ = 1.9 Hz, 1H, α-H-1), 6.28 (app t, $J_{3,4}$ = $J_{4,5}$ = 10.3 Hz, 1H, H-4), 6.07 (dd, $J_{2,3}$ = 3.2, $J_{3,4}$ = 10.3 Hz, 1H, H-3), 5.91 (dd, $J_{1,2}$ = 2.0, $J_{2,3}$ = 3.2 Hz, 1H, H-2), 4.70 (dd, $J_{5,6a}$ = 2.7, $J_{6a,6b}$ = 11.8 Hz, 1H, H-6a), 4.59-4.53 (m, 1H, H-5), 4.50 (dd, $J_{5,6b}$ = 2.7, $J_{6a,6b}$ = 11.8 Hz, 1H, H-6b). δ_C (101 MHz): 166.2 (1C, C=O), 165.6 (1C, C=O), 165.3 (1C, C=O), 165.2 (1C, C=O), 165.0 (1C, C=O), 134.1-128.0 (15 x s, 30C, C_{Ar}), 91.5 (1C, α-C-1), 71.2 (1C, C-5), 70.2 (1C, C-3), 69.6 (1C, C-2), 66.2 (1C, C-4), 62.3 (1C, C-6). The anomeric proton was assigned according to literature ($H_{1\alpha}$ 6.61 ppm)[362]. ESI-MS: found *m/z* 700.5 $[M+Na]^+$, calcd for $C_{41}H_{32}O_{11}Na$ 700.2.

5.3.1.6. 3-Azidopropanol (6)[363]

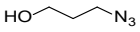

Due to the large amount of NaN_3 used in this process, a protective shield was placed around the reaction vessel when the reaction was left overnight. NaN_3 (7.5 g, 92 mmol, 4 eq.) was dissolved in water (50 mL) and 3-bromopropanol (2.2 mL, 24 mmol, 1 eq.) was added. The mixture was heated at 90 ^oC overnight with stirring. The reaction mixture was then allowed to cool to room temperature and extracted with EtOAc (3 x 15 mL). The combined organic extracts were dried over $MgSO_4$, filtered and the organic solvent was removed under reduced pressure. No further purification was needed to yield compound **5** as a colourless oil (2.2 mg, 22 mmol, 91%). R_f value (EtOAc-Hex 6:4): 0.49. δ_H ($CDCl_3$, D_2O; 400 MHz): 3.76 (t, $J_{1,2}$ = 6.3 Hz, 2H, H-1), 3.46 (t, $J_{2,3}$ = 6.3 Hz, 2H, H-3), 1.84 (p, $J_{1,2}$ = $J_{2,3}$ = 6.3 Hz, 2H, H-2). Using $CDCl_3$ only, OH was found at 1.54 – 1.47. δ_C (101 MHz): 60.1 (1C, C-1), 48.7 (1C, C-3), 31.6 (1C, C-2). IR (cm^{-1}): 2093.1 (N_3).

5.3.1.7. 3-Azidopropyl 2,3,4,6-tetra-*O*-acetyl-β-D-galactopyranoside (7)[205]

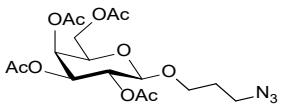

Peracetylated galactose (**1**, 0.15 g, 0.4 mmol) was dried under high vacuum overnight to remove residual moisture. The acetate was dissolved in DCM (3 mL) under nitrogen atmosphere. After cooling down in an ice bath, 3-azidopropanol (**5**, 0.07 mL, 0.8 mmol, 2 eq.) was added. Finally, boron trifluoride diethyl etherate (0.1 mL, 0.81 mmol, 2.1 eq.) was added dropwise over a period of 15 minutes. After additional 15 minutes, the ice bath was removed

and the reaction was stirred overnight at room temperature, at which point TLC (EtOAc-Hex 1:1 eluted two times) showed completion of the reaction. The reaction mixture was then diluted with DCM (5 mL), neutralised with saturated aqueous $NaHCO_3$ solution (15 mL) and extensively washed with brine (6 x 15 mL) to remove the remaining 3-azidopropanol. The organic layers were combined, dried over $MgSO_4$ and concentrated under reduced pressure. Silica gel chromatography (EtOAc-Hex 20:80 to 80:20) afforded the desired product **7** (63 mg, 42%) as a white solid. R_f value (EtOAc-Hex 1:1 run twice): 0.69. $[\alpha]_D^{25}$ - 3.0 (*c* 0.11, $CHCl_3$)[lit.,[205] - 4.4]. δ_H ($CDCl_3$; 400 MHz): 5.39 (dd, $J_{3,4}$ = 3.5, $J_{4,5}$ = 1.3 Hz, 1H, H-4), 5.20 (dd, $J_{1,2}$ = 8.0, $J_{2,3}$ = 10.5 Hz, 1H, H-2), 5.02 (dd, $J_{2,3}$ = 10.5, $J_{3,4}$ = 3.5 Hz, 1H, H-3), 4.47 (d, $J_{1,2}$ = 8.0 Hz, 1H, H-1), 4.23 – 4.13 (m, 2H, H-5, H-6a), 3.96 (m, 1H, H-7a), 3.91 (m, 1H, H-6b), 3.60 (m, 1H, H-7b), 3.37 (m, 2H, H-9), 2.15 (s, 3H, CH_3), 2.07 (s, 3H, CH_3), 2.05 (s, 3H, CH_3), 2.04 (s, 3H, CH_3), 1.98 (s, 3H, CH_3), 1.94 – 1.77 (m, 2H, H-8). δ_C (101 MHz): 170.4 (1C, C=O), 170.2 (1C, C=O), 170.1 (1C, C=O), 169.0 (1C, C=O), 101.5 (1C, C-1), 71.0 (1C, C-3), 70.9 (1C, C-5), 69.0 (1C, C-2), 67.2 (1C, C-4), 66.6 (1C, C-7), 61.4 (1C, C-6), 48.1 (1C, C-9), 31.6 (1C, C-8), 21.20 (1C, CH_3), 20.91 (1C, CH_3), 20.82 (1C, CH_3), 20.74 (1C, CH_3). IR (cm^{-1}): 2097.9 (N_3), 1745.0 (AcO).

5.3.1.8. 3-Azidopropyl 4-*O*-(2,3,4,6-tetra-*O*-acetyl-β-D-galactopyranosyl)-2,3,6-tri-*O*-acetyl-β-D-glucopyranose (8)[199]

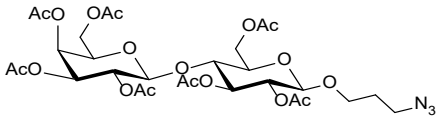

Peracetylated lactose (**2**, 0.40 g, 0.60 mmol, 1 eq.) was dried overnight under high vacuum to remove residual moisture and dissolved in DCM (7 mL) under nitrogen atmosphere. After the reaction mixture was cooled to 0 °C in an ice bath, 3-azidopropanol (**6**, 0.2 mL, 2.2 mmol, 3.6 eq.) was added. Finally, boron trifluoride diethyl etherate (0.15 mL, 1.2 mmol, 2.0 eq.) was added dropwise over a period of 15 minutes. After additional 15 minutes, the ice bath was removed and the reaction was stirred overnight at room temperature, at which point TLC (EtOAc-Hex 6:4) showed completion of the reaction. The reaction mixture was diluted with DCM (10 mL), neutralised with saturated aqueous $NaHCO_3$ solution (20 mL) and extensively washed with brine (6 x 15 mL) to remove the remaining 3-azidopropanol. The organic layers were combined, dried over $MgSO_4$ and concentrated under reduced pressure. Silica gel chromatography (EtOAc-Hex 20:80 to 50:50) afforded the desired compound **8** (102 mg, 34%).

R_f value (EtOAc-Hex 6:4): 0.59. $[\alpha]_D^{25}$ + 5.0 (*c* 0.81, $CHCl_3$)[lit.,[208] -4.7]. δ_H ($CDCl_3$; 400 MHz): 5.34 (dd, $J_{3',4'}$ = 3.5, $J_{4',5'}$ = 1.2 Hz, 1H, H-4'), 5.19 (dd, $J_{2,3}$ = 9.6, $J_{3,4}$ = 9.0 Hz, 1H, H-3), 5.10 (dd, $J_{1',2'}$ = 7.9, $J_{2',3'}$ = 10.4 Hz, 1H, H-2'), 4.95 (dd, $J_{2',3'}$ = 10.4, $J_{3',4'}$ = 3.5 Hz, 1H, H-3'), 4.88 (dd, $J_{1,2}$ = 7.9, $J_{2,3}$ = 9.6 Hz, 1H, H-2), 4.50 (dd, $J_{5,6a}$ = 2.2, $J_{6a,6b}$ = 12.0 Hz, 1H, H-6a), 4.48 (d, $J_{1',2'}$ = 7.9 Hz, 1H, H-1'), 4.46 (d, $J_{1,2}$ = 7.9 Hz, 1H, H-1), 4.16 – 4.04 (m, 3H, H-6b, H-6a'b'), 3.94 – 3.84 (m, 2H, H-7a, H-5'), 3.79 (dd, $J_{3,4}$ = 9.0, $J_{4,5}$ = 9.9 Hz, 1H, H-4), 3.59 (m, 2H, H-5, H-7), 3.35 (t, $J_{8,9}$ = 6.4 Hz, 2H, H-9), 2.15 (s, 3H, CH_3), 2.12 (s, 3H, CH_3), 2.06 (s, 3H, CH_3), 2.04 (s, 3H, CH_3), 2.04 (s, 6H, CH_3), 1.96 (s, 3H, CH_3), 1.90 – 1.77 (p, $J_{7,8}$ = $J_{8,9}$ = 6.4, 2H, H-8). δ_C (101 MHz): 170.50 (1C, C=O), 170.49 (1C, C=O), 170.3 (1C, C=O), 170.2 (1C, C=O), 169.9 (1C, C=O), 169.8 (1C, C=O), 169.2 (1C, C=O), 101.2 (1C, C-1), 100.7 (1C, C-1'), 76.4 (1C, C-4), 72.9 (1C, C-3 or C-5), 72.8 (1C, C-3 or C-5), 71.8 (1C, C-2), 71.1 (1C, C-3'), 70.8 (1C, C-5'), 69.3 (1C, C-2'), 66.7 (1C, C-4' or C-7), 66.6 (1C, C-4' or C-7), 62.1 (1C, C-6), 60.9 (1C, C-6'), 48.1 (1C, C-9), 29.1 (1C, C-8), 20.99 (1C, CH_3), 20.95 (1C, CH_3), 20.84 (1C, CH_3), 20.77 (3C, CH_3), 20.65 (1C, CH_3). IR (cm^{-1}): 2099.7. ESI-MS: found *m/z* 741.8 $[M+Na]^+$, calcd for $C_{29}H_{41}N_3O_{18}Na$ 742.2.

5.3.1.9. 3-Azidopropyl 4-*O*-(2-*O*-(2,3,4-tri-*O*-acetyl-α-L-fucopyranosyl)-3,4,6-tri-*O*-acetyl-β-D-galactopyranosyl)-2,3,6-tri-*O*-acetyl-β-D-glucopyranoside (9)

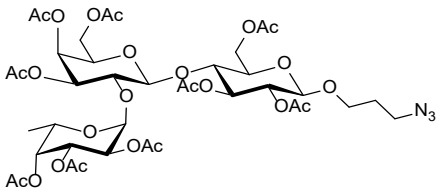

The procedure was adapted from Lee *et al.*[199] Peracetylated 2'-fucosyllactose (**3**, 184 mg, 0.20 mmol) was dried under high-vacuum and dissolved in DCM (3.5 mL) under nitrogen atmosphere. After the reaction mixture was cooled to 0 °C in an ice bath, 3-azidopropanol (0.1 mL, 1.0 mmol, 5.4 eq.) was added. Finally, boron trifluoride diethyl etherate (0.13 mL, 1.0 mmol, 5.2 eq.) was added dropwise over a period of 15 minutes. After a further 15 minutes, the ice bath was removed and the reaction was stirred overnight at room temperature, at which point TLC (EtOAc-Hex 6:5) showed completion of the reaction. The reaction mixture was diluted with DCM (10 mL), neutralised with saturated aqueous $NaHCO_3$ solution (20 mL) and extensively washed with brine (6 x 15 mL) to remove the unreacted 3-azidopropanol. The organic layers were combined, dried over $MgSO_4$ and concentrated under reduced pressure. Silica gel chromatography (EtOAc-Hex 50:50) afforded the desired compound **9** (50 mg, 25%).

R_f value (EtOAc-Hex 6:4): 0.40. $[\alpha]_D^{25}$ - 16.0 (*c* 1.0, $CHCl_3$)[no lit.]. δ_H ($CDCl_3$; 400 MHz): 5.37 (d, $J_{1'',2''}$ = 3.9 Hz, 1H, H-1''), 5.20-4.8 (m, 5H, H-3, H-3'', H-2, H-2'', H-3'), 4.47 (d, $J_{1,2}$ = 8.0 Hz, 1 H, H-1), 4.40 (d, $J_{1',2'}$ = 7.7 Hz, 1 H, H-1'), 4.33-4.21 (m, 1H, H-7a), 4.18-4.03 (m, 5H), 3.98-3.90 (m, 1H, H-7b), 3.88-3.75 (m, 5H), 3.66-3.58 (m, 2H, H-9), 2.16-1.94 (9 x s, 3H, CH_3), 1.92-1.80 (m, 2H, H-8), 1.20 (d, $J_{5'',6''}$ = 6.8 Hz, 3 H, H-6''). δ_C (101 MHz): 170.9-169.5 (m, 9C, C=O), 101.0 (1C, C-1), 100.4 (1C, C-1'), 95.8 (1C, C-1''), 64.5-75 (12 x s, 1C), 66.7 (1C, C-7), 62.3 (1C, C-6), 60.9 (1C, C-6'), 48.1 (1C, C-9), 29.2 (1C, C-8), 21.0-20.6 (m, 30C, 10 x AcO), 15.7 (1C, CH_3). IR (cm^{-1}): 2099.7 (N_3). MALDI-TOF: found *m/z* 972.3086 $[M+Na]^+$, calcd for $C_{39}H_{55}N_3O_{24}Na$ 972.3068.

5.3.1.10. 3-Azidopropyl 2,3,4,6-tetra-*O*-acetyl-β-D-glucopyranoside (10)[199]

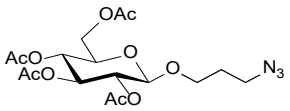

Peracetylated glucose (**4**, 0.65 g, 1.7 mmol) was dried under high-vacuum and dissolved in DCM (12 mL) under nitrogen atmosphere. After cooling down in an ice bath, 3-azidopropanol (0.75 mL, 8.1 mmol, 5 eq.) was added. Finally, boron trifluoride diethyl etherate (0.8 mL, 6.5 mmol, 4 eq.) was added dropwise over 15 minutes. After a further 15 minutes, the ice bath was removed and the reaction was stirred overnight at room temperature, at which point TLC (EtOAc-Hex 6:4) showed completion of the reaction. The reaction mixture was then diluted with DCM (15 mL), neutralised with saturated aqueous $NaHCO_3$ solution (20 mL) and washed with brine (3 x 15 mL) to remove the unreacted 3-azidopropanol. The organic layers were combined, dried over $MgSO_4$ and concentrated under reduced pressure. Silica gel chromatography (Hex-EtOAc 100:0 to 40:60) afforded the desired product **10** (135 mg, 27%) as a white solid. R_f value (EtOAc-Hex 6:4): 0.49. $[\alpha]_D^{25}$ + 15 (*c* 0.3, $CHCl_3$)[no lit.]. δ_H ($CDCl_3$; 400 MHz): 5.16 (t, $J_{2,3}$ = $J_{3,4}$ = 9.5 Hz, 1H, H-3), 5.02 (t, $J_{3,4}$ = $J_{4,5}$ = 9.5 Hz, 1H, H-4), 4.93 (dd, $J_{1,2}$ = 7.8 Hz, $J_{2,3}$ = 9.5, 1H, H-2), 4.47 (d, $J_{1,2}$ = 7.8 Hz, 1H, H-1), 4.20 (dd, $J_{5,6a}$ = 3.2 Hz, $J_{6a,6b}$ = 5.0 Hz, 1H, H-6a), 4.10 (dd, $J_{5,6b}$ = 2.4 Hz, $J_{6a,6b}$ = 5.0 Hz, 1H, H-6b), 3.90 (dt, $J_{7a,7b}$ = 9.7, $J_{7a,8}$ = 5.6 Hz, 1H, H-7a), 3.66 (ddd, $J_{4,5}$ = 9.5, $J_{5,6a}$ = 3.2, $J_{5,6b}$ = 2.4 Hz 1H, H-5), 3.56 (m, 1H, H-7a), 3.32 (m, 2H, H-9), 2.04 (s, 3H, CH_3), 2.03 (s, 3H, CH_3), 2.00 (s, 3H, CH_3), 1.99 (s, 3H, CH_3), 1.94 – 1.77 (m, 2H, H-8). δ_C (101 MHz): 170.7 (1C, C=O), 170.4 (1C, C=O), 169.6 (1C, C=O), 169.5 (1C, C=O), 100.9 (1C, C-1), 72.9 (1C, C-3), 71.9 (1C, C-5), 71.4 (1C, C-2), 68.5 (1C, C-4), 66.6 (1C, C-7), 62.0 (1C, C-6), 48.0 (1C, C-9), 29.0 (1C, C-8), 20.80 (1C, CH_3), 20.75 (1C, CH_3), 20.70 (C, CH_3), 20.68 (1C,

CH_3). IR (cm^{-1}): 2099.0 (N_3), 1746.7 (AcO). ESI-MS: found *m/z* 431.8 $[M+Na]^+$, calcd for $C_{17}H_{25}N_3O_{10}Na$ 431.2.

5.3.1.11. 2,3,4,6-Tetra-*O*-benzoyl-α-D-mannopyranosyl bromide (11)[365]

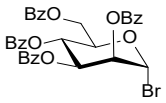

Perbenzoylated mannose (**5**, 1.06 g, 1.5 mmol) was dissolved in DCM (15 mL) and the reaction mixture was stirred at 0 °C in an ice bath. Hydrogen bromide (8.9 mL, 36 mmol, 33% solution in acetic acid) was added to the mixture, dropwise, over a period of 25 minutes at 0 °C. The reaction was stirred for further 90 minutes, at which point TLC (Hex-EtOAc 4:6) showed complete conversion of the starting material to single compound with an R_f value of 0.57. The reaction mixture was neutralised with a saturated solution of $NaHCO_3$ (10 mL) and then washed with brine (3x15 mL or until the aqueous phase was colourless). The organic solvent was evaporated under reduced pressure and product **11** was obtained as a pale-yellow oil (944 mg, 95%), which was used for the synthesis of compounds **12** and **19** without further purification.

5.3.1.12. 3-Azidopropyl 2,3,4,6-tetra-*O*-benzoyl-β-D-mannopyranoside (12)

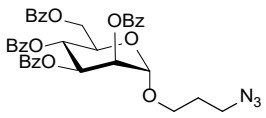

Adapted from Lee *et al.*[199] Perbenzoylated mannosyl bromide (**11**, 930 mg, 1.4 mmol) was dried under high vacuum to remove residual moisture. The benzoate was dissolved in anhydrous toluene (10 mL) in a round bottom flask equipped with crashed molecular sieves under nitrogen atmosphere . Upon addition of 3-azidopropanol (0.2 mL, 2.1 mmol, 1.5 eq.), the mixture was stirred in an acetone-dry ice bath at -20°C. In a separate round bottom flask, silver triflate (442 mg, 1.7 mmol, 1.2 eq.) was dissolved in anhydrous toluene (2 mL) under nitrogen atmosphere and transferred dropwise to the reaction flask using a syringe. The mixture was stirred overnight, at which point TEA (0.2 mL) was added to quench the unreacted promotor. The solid was filtered and the organic solvent was evaporated under reduced pressure. Silica gel flash chromatography (Tol-EtOAc 9:1) afforded the desired product **12** (597

mg, 62%) as a colourless oil. R_f value (Tol-EtOAc 9:1): 0.55. $[\alpha]_D^{25}$ – 19.7 (*c* 1.0, $CHCl_3$)[no lit.]. δ_H ($CDCl_3$; 400 MHz): 8.13-7.81 (4 x m, 8H, H_{meta}), 7.63-7.25 (m, 12H, H_{ortho}, H_{para}), 6.10 (app t, $J_{3,4}$ = $J_{4,5}$ = 10.3 Hz, 1H, H-4), 5.89 (dd, $J_{2,3}$ = 3.1, $J_{3,4}$ = 10.3 Hz, 1H, H-3), 5.701 (dd, $J_{1,2}$ = 1.8, $J_{2,3}$ = 3.1 Hz, 1H, H-2), 5.11 (d, $J_{1,2}$ = 1.8 Hz, 1H, H-1), 4.71 (dd, $J_{5,6a}$ = 2.7, $J_{6a,6b}$ = 12.0 Hz, 1H, H-6a), 4.50 (dd, $J_{5,6b}$ = 2.7, $J_{6a,6b}$ = 12.0 Hz, 1H, H-6b), 4.59-4.53 (m, 1H, H-5), 3.97 (dt, $J_{7a,7b}$ = 9.8, $J_{7a,8}$ = 6.1 Hz, 1H, H-7a), 3.65 (dt, $J_{7a,7b}$ = 9.8, $J_{7a,8}$ = 6.1 Hz, 1H, H-7a), 3.5 (t, $J_{8,9}$ = 6.1 Hz, 2H, H-9), 1.99 (m, 2H, H-8). δ_C (101 MHz): 166.7 (1C, C=O), 165.65 (1C, C=O), 165.60 (2C, C=O), 130.2-128.4 (10 x s, 24C, C_{Ar}), 97.9 (1C, C-1), 70.6 (1C, C-2), 70.2 (1C, C-3), 69.2 (1C, C-5), 67.0 (1C, C-4), 65.2 (1C, C-7), 63.1 (1C, C-6), 48.4 (1C, C-9), 28.9 (1C, C-8). IR (cm^{-1}): 2097.0 (N_3). ESI-MS: found *m/z* 702.4 $[M+Na]^+$, calcd for $C_{37}H_{33}N_3O_{10}Na$ 702.2.

5.3.1.13. 3-Azidopropyl β-D-galactopyranoside (13)[209]

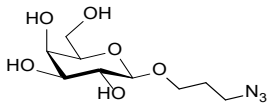

Peracetylated 3-azidopropyl galactoside (**7**, 38 mg, 0.1 mmol) was dried under high vacuum. Absolute MeOH (0.9 mL) and NaOMe (0.1 mL, 0.1 M) were added under nitrogen atmosphere. After 45 minutes, TLC (EtOAc-Hex 7:3) showed completion of the reaction. To investigate the possible presence of intermediate deprotected species, a more polar mobile phase was employed, consisting of DCM-MeOH 8:2. The reaction was neutralised using acidic DOWEX resin, the resin was filtered, and the organic solvent was evaporated under reduced pressure. The deprotected compound **13** was isolated as a white solid (14.6 mg, 63%). R_f value (DCM-MeOH 8:2): 0.35. $[\alpha]_D^{25}$ - 11.0 (*c* 1.00, MeOH)[lit.,[206] -15.9]. δ_H (D_2O; 400 MHz): 4.41 (d, $J_{1,2}$ = 8.0 Hz, 1H, H-1), 4.02 (dt, $J_{7a,7b}$ = 10.4, $J_{7a,8}$ = 6.5 Hz, 1H, H-7a), 3.94 (dd, $J_{3,4}$ = 3.5, $J_{4,5}$ = 1.0 Hz, 1H, H-4), 3.83 – 3.73 (m, 3H, H-6ab, H-7b), 3.70 (ddd, $J_{4,5}$ = 1.0, $J_{5,6a}$ = 7.8, $J_{5,6b}$ = 4.5 Hz, 1H, H-5), 3.66 (dd, $J_{2,3}$ = 9.9, $J_{3,4}$ = 3.5 Hz, 1H, H-3), 3.52 (dd, $J_{1,2}$ = 8.0, $J_{2,3}$ = 9.9 Hz, 1H, H-2), 3.48 (t, $J_{8,9}$ = 6.5 Hz, 2H, H-9), 1.93 (p, $J_{7,8}$ = $J_{8,9}$ = 6.5 Hz, 2H, H-8). δ_C (101 MHz): 102.9 (1C, C-1), 75.1 (1C, C-5), 72.7 (1C, C-3), 70.7 (1C, C-2), 68.6 (1C, C-4), 67.2 (1C, C-7), 60.9 (1C, C-6), 47.9 (1C, C-9), 28.2 (1C, C-8). IR (cm^{-1}): 2099.3 (N_3).

5.3.1.14. 3-Azidopropyl 4-*O*-(β-D-galactopyranosyl)-β-D-glucopyranoside (14)[209]

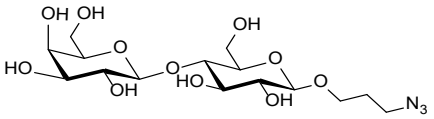

Peracetylated 3-azidopropyl lactoside (**5**, 100 mg, 0.14 mmol) was dried under high-vacuum. Absolute MeOH (4 mL) and NaOMe (0.45 mL, 0.1 M) were added under nitrogen atmosphere. After 45 minutes, TLC (EtOAc-Hex 7:3) showed completion of the reaction. To investigate the presence of intermediate deprotected species, a more polar mobile phase was employed, consisting of IPA-NH_4OH-H_2O 6:3:1. The reaction was neutralised using acidic DOWEX resin, the resin was filtered and the organic solvent was evaporated under reduced pressure. Gel permeation chromatography (0.5 mL/min, RT_o = 541, RT_f = 597) afforded the deprotected product **14** as a white solid (50 mg, 95%). R_f value (DCM-MeOH-H_2O 8:1.5:0.5): 0.49. $[\alpha]_D^{25}$ -3.3 (*c* 0.37, MeOH)[no lit]. δ_H (D_2O; 400 MHz): 4.50 (d, $J_{1',2'}$ = 8.0 Hz, 1H, H-1'), 4.46 (d, $J_{1,2}$ = 7.8 Hz, 1H, H-1), 4.04 – 3.97 (m, 2H, H-7a, H-6a'), 3.94 (d, $J_{3',4'}$ = 3.4 Hz, 1H, H-4'), 3.85 – 3.71 (m, 6H, H-5, H-6a, H-6b, H-6b', H-7b), 3.70 – 3.64 (m, 3H, H-3, H-3', H-5'), 3.64 – 3.59 (m, 1H, H-4), 3.55 (dd, $J_{1,2}$ = 7.8, $J_{2,3}$ = 10.0 Hz, 1H, H-2), 3.47 (t, $J_{8,9}$ = 6.7 Hz, 2H, H-9), 3.38 (td, $J_{1',2'}$ = 8.0 Hz, 1H, H-2'), 1.93 (p, $J_{7,8}$ = $J_{8,9}$ = 6.7 Hz, 2H, H-8). δ_C (101 MHz): 102.9 (1C, C-1), 102.1 (1C, C-1'), 78.4 (1C, C-3 or C-3' or C-5'), 75.3 (1C, C-5), 74.8 (1C, C-4), 74.4 (1C, C-3 or C-3' or C-5'), 72.8 (1C, C-2'), 72.5 (1C, C-3 or C-3' or C-5'), 70.9 (1C, C-2), 68.5 (1C, C-4'), 67.4 (1C, C-7), 61.0 (1C, C-6), 60.1 (1C, C-6'), 47.9 (1C, C-9), 28.2 (1C, C-8). IR (cm^{-1}): 2092.2 (N_3). ESI-MS: found *m/z* 448.0 $[M+Na]^+$, calcd for $C_{15}H_{27}N_3O_{11}Na$ 448.2.

5.3.1.15. 3-Azidopropyl 4-*O*-(2-*O*-α-L-fucopyranosyl)-β-D-galactopyranosyl)-β-D-glucopyranoside (15)

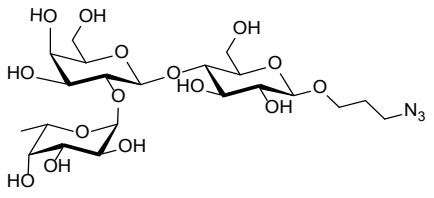

Adapted from Yu *et al.*[209] Peracetylated 3-azidopropyl 2'-fucosyllactoside (**9**, 10 mg, 0.14 mmol) was dried under high-vacuum. Absolute MeOH (1.5 mL) and NaOMe (0.15 mL, 0.1 M) were added under nitrogen atmosphere. After 45 minutes, TLC (EtOAc-Hex 7:3) showed completion of the reaction. To investigate the presence of intermediate deprotected species,

a more polar mobile phase was employed, consisting of IPA-NH_4OH-H_2O 6:3:1. The reaction was neutralised using acidic DOWEX resin, the resin was filtered and the organic solvent was evaporated under reduced pressure. Reverse phase silica gel chromatography (C8-functionalised silica gel, MeOH-H_2O 40:60) afforded the deprotected product **15** as a white solid (5.6 mg, 93%). R_f value (IPA-NH_4OH-H_2O 6:3:1): 0.38. $[\alpha]_D^{25}$ - 26.8 (*c* 0.8, H_2O)[no lit.]. δ_H (D_2O; 400 MHz): 5.23 (d, $J_{1'',2''}$ = 4.0 Hz, 1H, H-1''), 4.45 (d, $J_{1,2}$ = 7.7 Hz, 1 H, H-1), 4.37 (d, $J_{1',2'}$ = 7.8 Hz, 1 H, H-1'), 4.2-4.1 (m, 1H, H-5'), 3.95-3.96 (m, 1H, H-7a), 3.76-3.70 (m, 1H, H-7b), 3.85-3.37 (m, 17H), 3.41-3.34 (m, 2H, H-9), 3.25 (dd, $J_{1',2'}$ = 7.7, $J_{2',3'}$ = 9.0 Hz, 1 H, H-2'). 1.83 (p, $J_{7,8}$ = $J_{8,9}$ = 6.4 Hz, 2 H, H-8), 1.16 (d, $J_{5'',6''}$ = 6.4 Hz, 3H, H-6''). δ_C (101 MHz): 102.3 (1C, C-1), 100.3 (1C, C-1'), 99.3 (1C, C-1''), 76.5-66.5 (12 x s, 1C), 66.4 (1C, C-7), 61.0 (1C, C-6), 60.1 (1C, C-6'), 47.9 (1C, C-9), 28.2 (1C, C-8), 15.3 (1C, CH_3). MALDI-TOF: found *m/z* 594.2122 $[M+Na]^+$, calcd for $C_{21}H_{37}N_3O_{15}Na$ 594.2117.

5.3.1.16. 3-Azidopropyl β-D-glucopyranoside (16)

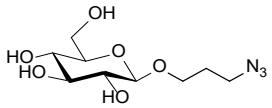

Adapted from Yu *et al.*[209] Peracetylated 3-azidopropyl glucoside (**10**, 225 mg, 0.1 mmol) was dried under high vacuum. Absolute MeOH (5 mL) and NaOMe (0.05mL, 1 M) were added under nitrogen atmosphere. After 45 minutes, TLC (EtOAc-Hex 7:3) showed completion of the reaction. To investigate the presence of intermediate deprotected species, a more polar mobile phase was employed, consisting of DCM-MeOH 8:2. The reaction was neutralised using acidic DOWEX resin, the resin was filtered and the organic solvent was evaporated under reduced pressure. The reaction mixture was purified by flash chromatography (DCM-MeOH 100:0 to 80:20). Accordingly, the deprotected compound **16** was isolated as a colourless oil (51 mg, 38%). R_f value (DCM-MeOH 8:2): 0.48. $[\alpha]_D^{25}$ - 33.0 (*c* 1.0, MeOH)[lit.,[206] -26]. δ_H (D_2O; 400 MHz): 4.47 (d, $J_{1,2}$ = 8.1 Hz, 1H, H-1), 4.01 (dt, $J_{7a,\ 7b}$ = 10.3, $J_{7a,8}$ = 6.4 Hz, 1H, H-7a), 3.93 (dd, $J_{5,6a}$ = 2.3 Hz, $J_{6a,6b}$ = 12.3 Hz, 1H, H-6a), 3.77 (dt, $J_{7a,\ 7b}$ = 10.3, $J_{7b,8}$ = 6.4 Hz, 1H, H-7b), 3.73 (dd, $J_{5,6b}$ = 5.9, $J_{6a,6b}$ = 12.3 Hz, 1H, H-6b), 3.50 (dd, $J_{2,3}$ = 9.2, $J_{3,4}$ = 12.7 Hz, 1H, H-3), 3.48 (t, $J_{8,9}$ = 6.4 Hz, 2H, H-9), 3.28 (dd, $J_{1,2}$ = 8.1, $J_{2,3}$ = 9.2 Hz, 1H, H-2), 1.93 (p, $J_{7,8}$ = $J_{8,9}$ = 6.4 Hz, 2H, H-8). δ_C (101 MHz): 102.9 (1C, C-1), 75.1 (1C, C-5), 72.7 (1C, C-3), 70.7 (1C, C-2), 68.6 (1C, C-4),

67.2 (1C, C-7), 60.9 (1C, C-6), 47.9 (1C, C-9), 28.2 (1C, C-8). IR (cm^{-1}): 3389.8 (OH), 2101.1 (N_3). ESI-MS: found *m/z* 263.3 $[M+Na]^+$, calcd for $C_9H_{17}N_3O_6Na$ 263.1.

5.3.1.17. 3-Azidopropyl α-D-mannopyranoside (17)

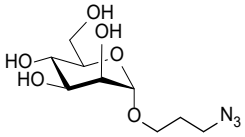

Adapted from Yu *et al.*[209] Perbenzoylated 3-azidopropyl mannoside (**12**, 597 mg, 0.9 mmol) was dried under high-vacuum. Absolute MeOH (14 mL) and NaOMe (1.4 mL, 1 M) was added under nitrogen atmosphere. After 45 minutes, TLC (EtOAc-Hex 7:3) showed completion of the reaction. To investigate the presence of intermediate deprotected species, a more polar mobile phase was employed, consisting of DCM-MeOH 8:2. The reaction was neutralised using acidic DOWEX resin, the resin was filtered and the organic solvent was evaporated under reduced pressure. The reaction mixture was purified by flash chromatography (DCM-MeOH 100:0 to 80:20). Accordingly, the deprotected compound **17** was isolated as a colourless oil (231 mg, 95%). R_f value (DCM-MeOH 8:2): 0.40. $[\alpha]_D^{25}$ + 79.4 (*c* 1.0, MeOH)[no lit.]. δ_H (D_2O; 400 MHz): 4.88 (d, $J_{1,2}$ = 1.6 Hz, 1H, H-1), 3.96 (dd, $J_{1,2}$ = 1.6 Hz, $J_{2,3}$ = 3.4, 1H, H-2), 3.90 (dd, $J_{5,6a}$ = 1.7, $J_{6a,6b}$ = 12.3 Hz, 1H, H-6a), 3.80 – 3.86 (m, 2H, H-3, H-7a), 3.77 (dd, $J_{5,6b}$ = 5.6, $J_{6a,6b}$ = 12.3 Hz, 1H, H-6b), 3.64 – 3.67 (m, 2H, H-4, H-5), 3.59 – 3.64 (m, 1H, H-7b), 3.46 (t, $J_{8,9}$ = 6.5 Hz, 1H, H-9), 1.92 (p, $J_{7a,8} = J_{7b,8} = J_{8,9}$ = 6.5 Hz, 2H, H-8). δ_C (101 MHz): 99.8 (1C, C-1), 72.8 (1C, C-4), 70.6 (1C, C-3), 70.0 (1C, C-2), 66.7 (1C, C-5), 64.8 (1C, C-7), 60.9 (1C, C-6), 48.2 (1C, C-9), 27.8 (1C, C-8). IR (cm^{-1}): 3373.7 (OH), 2100.0 (N_3). ESI-MS: found *m/z* 285.7 $[M+Na]^+$, calcd for $C_9H_{17}N_3O_6Na$ 286.1.

5.3.1.18. 3-Azidopropyl 2,4-di-*O*-benzoyl-α-D-mannopyranoside (18)

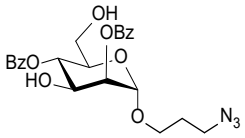

Adapted from Oscarson *et al.*[203] 3-Azidopropyl mannoside (**17**, 100 mg, 0.4 mmol) was dissolved in acetonitrile (10 mL). Triethyl orthobenzoate (0.8 mL, 2.7 mmol, 11.5 eq.) was added and the solution was stirred at room temperature. Catalytic p-toluene sulfonic acid (80

µL, 5% solution in acetonitrile) and TFA (3 µL) were added slowly under stirring. The reaction mixture was stirred for further 25 minutes, at which point TLC (Tol-EtOAc 8/2) showed complete conversion of the starting material and formation of the orthoester intermediate. R_f value (Tol-EtOAc 8:2): 0.55. ESI-MS: found *m/z* 522.2 $[M+Na]^+$, calcd for $C_{25}H_{25}N_3O_8Na$ 522.2. The reaction mixture was dried under reduced pressure and the residue was redissolved in acetonitrile (7.5 mL). TFA (0.2 mL, 90% aqueous solution) was added and the mixture was stirred for 15 min. TLC (Tol-EtOAc 8:2) showed complete conversion of the starting material. The reaction mixture was dried under reduced pressure. Purification by flash chromatography (Tol-EtOAc 100:0 to 90:10) gave compound **19** as a white solid (77 mg, 43%). R_f value (Tol-EtOAc 8:2): 0.31. $[\alpha]_D^{25}$ + 21.0 (*c* 1.0, MeOH)[no lit.]. δ_H ($CDCl_3$; 400 MHz): 8.08 (tt, $J_{ortho,para}$ = 8.0, $J_{ortho,meta}$ = 1.4 Hz, 4H, H_{ortho}-OBz), 7.60 (tt, $J_{ortho,para}$ = 8.0, $J_{meta,para}$ = 4.0 Hz, 2H, H_{para}-OBz), 7.47 (td, $J_{meta,para}$ = 4.0, $J_{ortho,meta}$ = 1.4 Hz, 4H, H_{meta}-OBz), 5.51 (app t, $J_{3,4}$ = 9.9 Hz, 1H, H-4), 5.40 (dd, $J_{1,2}$ = 1.5, $J_{2,3}$ = 3.4 Hz, 1H, H-2), 5.05 (d, $J_{1,2}$ = 1.5 Hz, 1H, H-1), 4.41 (dd, $J_{2,3}$ = 3.4, $J_{3.4}$ = 9.9 Hz, 1H, H-3), 3.93 (ddd, $J_{4.5}$ = 2.0, $J_{5,6a}$ = 10.0, $J_{5,6b}$ = 4.0 Hz, 1H, H-5), 3.87 (dt, $J_{7a,7b}$ = 11.9, $J_{7a,8}$ = 4.5 Hz, 1H, H-7a), 3.81 (dd, $J_{5,6a}$ = 2.4, $J_{6a,6b}$ = 12.6 Hz, 1H, H-6a), 3.74 (dd, $J_{5,6b}$ = 4.3, $J_{6a,6b}$ = 12.6 Hz, 1H, H-6b), 3.58 (dt, $J_{7a,7b}$ = 11.9, $J_{7b,8}$ = 4.5 Hz, 1H, H-7b), 3.46 (t, $J_{8,9}$ = 6.6 Hz, 2H, H-9), 1.93 (m, 2H, H-8). ESI-MS: found *m/z* 493.8 $[M+Na]^+$, calcd for $C_{23}H_{25}N_3O_8Na$ 494.2. IR (cm^{-1}): 3373.7 (OH), 2099.8 (N_3).

5.3.1.19. 3-Azidopropyl 2,4-di-*O*-benzoyl-3,6-di-*O*-(2,3,4,6-penta-*O*-benzoyl-α-D-mannopyranosyl)-α-D-mannopyranoside (19)

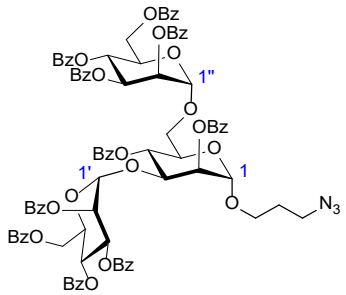

Adapted from Oscarson *et al.*[203] 3-Azidopropyl 2,4-di-*O*-benzoyl-α-D-mannopyranoside (**18**, 98 mg, 0.2 mmol) and perbenzoylated mannopyranosyl bromide (**11**, 502 mg, 0.68 mmol, 3.7 eq.) were dissolved in anhydrous toluene (5 mL) at -20 °C. Silver triflate (212 mg, 0.54 mmol, 4 eq.) was dissolved in anhydrous toluene (5 mL) and added dropwise to the acceptor-donor mixture. The mixture was allowed to room temperature and stirred overnight, at which point

TLC (Hex-EtOAc 7:3) showed complete conversion of the acceptor. TEA (0.3 mL) was added and the mixture was stirred for 20 minutes. The black precipitate was filtrated over celite and the solvent was evaporated under reduced pressure. Purification by flash chromatography (Hex-EtOAc 100:0 to 70:30) gave compound **19** as a white solid (114 mg, 34%). R_f value (Hex-EtOAc 7:3): 0.40. $[\alpha]_D^{25}$ – 42.5 (*c* 1.0, $CHCl_3$)[no lit.] (see note at the end of the paragraph). δ_H ($CDCl_3$; 400 MHz): 8.33-7.20 (m, 50 H, H_{Ar}), 6.16-5.94 (m, 4H, H-4', H-4'', H-3', H-3''), 5.75-5.67 (m, 4H, H-4, H-2, H-2', H-2''), 5.37 (d, $J_{1,2}$ = 2.1 Hz, 1 H, H-1), 5.14 (app s, 2 H, H-1', H-1''), 4.64-4.57 (m, 4 H, H-6a', H-6a''), 4.52 (dt, $J_{4,5}$ = 3.0, $J_{5,6a}$ = $J_{5,6b}$ = 10.0 Hz, 1 H, H-5), 4.46 (dt, $J_{4',5'}$ = 2.7, $J_{5',6a'}$ = $J_{5',6b'}$ = 10.0 Hz, 1 H, H-5'), 4.41-4.31 (m, 4 H, H-6b', H-6b''), 4.31-4.24 (m, 1 H, H-5''), 4.17 (dd, $J_{5,6a}$ = 6.6, $J_{6a,6b}$ = 10.4 Hz, 1 H, H-6a), 4.04 (dt, $J_{7a,7b}$ = 9.7, $J_{7a,8}$ = 6.1 Hz, 1 H, H-7a), 3.78 (dd, $J_{5,6a}$ = 1.9, $J_{6a,6b}$ = 10.4 Hz, 1 H, H-6b), 3.7 (dt, $J_{7a,7b}$ = 9.7, $J_{7a,8}$ = 6.1 Hz, 1 H, H-7b), 3.56-3.46 (m, 2H, H-9), 2.06-1.96 (m, 2 H, H-8). δ_C ($CDCl_3$; 400 MHz): 166.4 (1C, C=O), 166.24 (1C, C=O), 166.24 (1C, C=O), 165.8 (1C, C=O), 165.6 (1C, C=O), 165.44 (1C, C=O), 165.42 (1C, C=O), 165.3 (1C, C=O), 164.9 (1C, C=O), 164.8 (1C, C=O), 133.—128.0 (34 x s, 60 C, C_{Ar}), 99.9 (1C, C-1), 97.8 (1C, C-1'), 97.5 (1C, C-1''), 77.0 (s, 1C, C-5), 72.1, 70.5, 70.4, 70.2, 70.0, 69.8, 69.5, 69.1, 68.6 (9 x s, 9 C, H-2, H-2', H-2'', H-3', H-3'', H-4, H-4'', H-5', C-H5''), 67.0 (s, 1 C, C-6), 66.8 (s, 1 C, C-H-4'), 66.5 (s, 1 C, H-3), 65.5 (s, 1 C, H-7), 62.8 (s, 1 C, C-H-6'), 62.5 (s, 1 C, H-6''), 48.5 (s, 1 C, C-9), 28.9 (s, 1 C, C-8). IR (cm^{-1}): 2098.4 (N_3). MALDI-TOF: found *m/z* 1650.4656 $[M+Na]^+$, calcd for $C_{91}H_{77}N_3O_{26}Na$ 1650.4685. The $[\alpha]_D^{25}$ values reported for similar mannotriosides by Oscarson *et al.*[203] are in the -17 to -52 range, which is in agreement with the data hereby reported.

5.3.1.20. 3-Azidopropyl 3,6-di-*O*-α-D-mannopyranosyl-α-D-mannopyranoside (20)

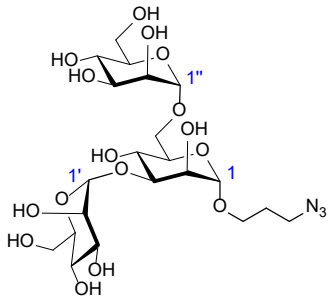

Adapted from Yu *et al.*[209] Benzoylated 3-azidopropyl mannotrioside (**19**, 90 mg, 0.06 mmol) was dried under high-vacuum. Absolute MeOH (2 mL) and NaOMe (0.2 mL, 1 M) was added under nitrogen atmosphere. After 45 minutes, TLC (EtOAc-Hex 7:3) showed completion of the

reaction. To investigate the presence of intermediate deprotected species, a more polar mobile phase was employed, consisting of IPA-NH_4OH-H_20 6:4:1. The reaction was neutralised using acidic DOWEX resin, the resin was filtered and the organic solvent was evaporated under reduced pressure. The reaction mixture was purified by gel permeation chromatography (0.5 mL/min, RT_o = 450, RT_f = 580). Accordingly, the deprotected compound **20** was isolated as a white powder (30 mg, 93%). R_f value (IPA-NH_4OH-H_20 6:4:1): 0.27. $[\alpha]_D^{25}$ – 78.2 (*c* 1.0, H_2O)[no lit.] (see note at the end of the paragraph). δ_H (D_2O; 400 MHz): 5.32(d, $J_{1'',2''}$ = 3.1 Hz, 1H, H-1''), 4.83 (d, $J_{1',2'}$ = 1.4 Hz, 1H, H-1'), 4.45 (d, $J_{1,2}$ = 7.7 Hz, 1H, H-1),4.05-3.89 (m, 3H, H-2, H-2', H-2''), 3.49-3.90 (m, 17 H, H-3, H-3', H-3'', H-4, H-4', H-4'', H-5, H-5', H-5'', H-6, H-6', H-6'', H-7), 3.41-3.35 (m, 2H, H-9), 1.88-1.79 (m, 2H, H-8). δ_C (101 MHz): 102.3 (1C, C-1), 99.9 (1C, C-1'), 99.4 (1C, C-1''), 78.4, 73.3, 72.7, 71.1, 70.6, 70.3, 66.8, 66.7, 65.7 (9 x s, 9C, H-3, H-3', H-3'', H-4, H-4', H-4'', H-5, H-5', H-5''), 70.03, 69.95, 69.7 (3 x s, 3C, C-2, C-2', C-2''), 65.3 (s, 1C, C-6), 64.9 (1C, C-7), 60.97 (1C, C-6'), 60.92 (1C, C-6''), 48.1 (1C, C-9), 27.8 (1C, C-8). IR (cm^{-1}): 2098.2 (N_3). MALDI-TOF: found m/z 610.2057 $[M+Na]^+$, calcd for $C_{21}H_{37}N_3O_{16}Na$ 610.2026. For the ^{1}H-NMR assignment of anomeric peaks, the spectra were compared with published aminoethyl 3,6-di-*O*-α-D-mannopyranosyl-α-D-mannopyranoside: $\delta_{H\text{-}1}$: 5.05 ($J_{1,2}$ = 1.6 Hz), $\delta_{H\text{-}1'}$: 4.84 ($J_{1',2'}$ = 1.6 Hz), $\delta_{H\text{-}1''}$: 4.79 (app s).[218] The corresponding ^{13}C signals were assigned through heteronuclear coupling obtained by HSQC NMR experiment. Regarding the measurement of the $[\alpha]_D^{25}$, reported values for similar mannotriosides by Oscarson *et al.*[203] are in the +86 to +100cross range, which is in agreement with the value but disagreement with the sign of the data hereby reported. More literature is needed to have a more conclusive comparison, however, these are the only examples of published mannotriosides.

5.3.1.21. 3-Azidopropyl 4-*O*-((3-*O*-(5-acetamido-3,5-dideoxy-D-glycero-α-D-galacto-2-nonulopyranosyl))-β-D-galactopyranosyl))-β-D-glucopyranoside (21)

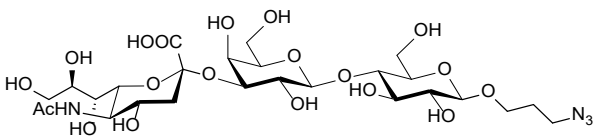

Adapted from Field *et al*.[222] *Trypanosoma cruzi* trans-sialidase was kindly expressed and purified by Dr Simona Chessa (Iceni Glycoscience Ltd.). Full details can be found in *Appendix 1.* In brief, the protein was transformed in *E. coli* with an ampicillin-resistant plasmid and

expression was induced with isopropyl β-D-1-thiogalactopyranoside (IPTG).[223] The cells were lysed and the expressed enzyme was purified *via* metal ion affinity chromatography (Ni(II) column). The solution of enzyme in water was aliquoted and stored at -20 °C. Before the reaction, the enzyme (400 µL, 1.3 µg/µL) was dialysed overnight in the reaction buffer, Tris/HCl buffer (50 mM, pH 8.4 at 25 °C). Fetuin (230 mg, equal to 2.5 eq. of α(2,3')-sialic acid) was dissolved in Tris/HCl buffer (600 µL) and 3-azidopropyl lactoside (**11**, 4 mg, 1 eq.) was added. The dialysed enzyme was then transferred to the vial containing the 3-azidopropyl lactoside and fetuin and the reaction was incubated at 37 °C overnight, at which point TLC ($CHCl_3$-MeOH-H_2O 10:6:1) showed nearly full conversion of the starting material. The reaction was diluted with MeOH (4 mL) and the proteins were precipitated at 100 °C for 2 minutes. Centrifugation and collection of supernatant allowed the removal of proteins. MeOH was evaporated under reduced pressure, and the residue was diluted with water to a final volume of 5 mL. Upon addition of an aqueous solution of NaOH (3 drops, 10 mM), the solution was loaded to an anion exchange High-Q pre-packed cartridge (Bio-Rad, 2 mL). The column was washed with water (10 mL) followed by aqueous NH_4HCO_3 (50 mM, 6 x 5 mL, 6 fractions) with the application of a limited pressure to obtain approximatively a flow of one drop per second to afford the final siallyllactoside **19** as a white powder (4 mg, 55%). R_f value ($CHCl_3$-MeOH-H_2O 10:6:1): 0.2. $[\alpha]_D^{25}$ + 2.8 (*c* 0.25, H_2O)[lit.,[226] + 4.9.]. δ_H (D_2O; 400 MHz): 4.54 (d, $J_{1',2'}$ = 7.7 Hz, 1H, H-1'), 4.50 (d, $J_{1,2}$ = 7.9 Hz, 1H, H-1), 4.21-3.42 (m, 24H), 2.77 (dd, $J_{7',8'}$ = 12.2, $J_{8',9'}$ = 4.7 Hz, 1H, H-8'), 2.04 (s, 3H, HNAc), 1.93 (p, $J_{7a,8}$ = $J_{7b,8}$ = $J_{8,9}$ = 6.4 Hz, 1H, H-8), 1.81 (t, $J_{6',7'}$ = $J_{7',8'}$ = 12.2 Hz, 1H, H-7'). δ_C (101 MHz): 175.0 (1C, COOH), 173.9 (1C, NHAc), 102.6 (1C, C-1'), 102.1 (1C, C-1), 99.8 (1C, C-2''), 78.2, 75.5, 75.1, 74.7, 74.4, 73.6, 72.8, 71.7, 68.3, 68.2, 67.4, 67.3, 63.0 (2C), 62.6, 61.0, 56.4, 39.9 (1C, C-8'), 28.3 (1C, C-8), 28.0 (1 C, C-7'), 22.0 (1C, NHAc). MALDI-TOF: found *m/z* 739.2493 $[M+Na]^+$, calcd for $C_{26}H_{44}N_4O_{19}Na$ 739.2492. Chemical shift assignment of anomeric peak signals were in agreement with literature: $\delta_{H\text{-}1}$: 4.49 ($J_{1,2}$ = 8.0 Hz), $\delta_{H\text{-}1'}$: 4.53 ($J_{1',2'}$ = 7.9 Hz).[226]

5.3.1.22. 3-Aminopropyl β-D-galactopyranoside (38)

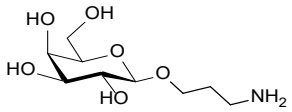

Adapted from Nyffeler *et al.*[280] 3-Azidopropyl galactoside **13** (22 mg, 0.08 mmol, 1 eq.) was dissolved in water (100 µL) in a 10 mL round bottom flask. Triphenylphosphine (46 mg, 17 mmol, 1.5 eq.) was dissolved in THF (400 µL) and then added to the previous sugar solution. The mixture was heated to 60 °C for three hours. After this time, TLC showed total conversion of the starting material, and ninhydrin staining was used to confirm the presence of the amino group. The crude mixture was cooled to room temperature and concentrated to dryness under reduced pressure. The mixture was re-dissolved in water (3 mL), filtered and the filtrate was rinsed with water (3 mL). The clear solution was concentrated again to dryness under reduced pressure to obtain the desired product **38** as a pale-yellow oil (20 mg, 0.08 mmol, 100%). R_f value (IPA-NH_4OH-H_20 6:3:1): 0.2. $[\alpha]_D^{25}$ -12 (*c* 1.0, MeOH)[lit.,[366] -14.5]. δ_H (D_2O; 400 MHz): 4.41 (d, $J_{1,2}$ = 7.9 Hz, 1H, H-1), 4.01 (dt, $J_{7a,7b}$ = 10.3, $J_{7a,8}$ = 6.6 Hz, 1H, H-7a), 3.93 (dd, $J_{3,4}$ = 3.5, $J_{4,5}$ = 1.0 Hz, 1H, H-4), 3.8 – 3.73 (m, 3H, H-6ab, H-7b), 3.70 (ddd, $J_{4,5}$ = 1.0, $J_{5,6a}$ = 7.8, $J_{5,6b}$ = 4.4 Hz, 1H, H-5), 3.65 (dd, $J_{2,3}$ = 9.9, $J_{3,4}$ = 3.5 Hz, 1H, H-3), 3.52 (dd, $J_{1,2}$ = 7.9, $J_{2,3}$ = 9.9 Hz, 1H, H-2), 2.83 (t, $J_{8,9}$ = 6.6 Hz, 2H, H-9), 1.85 (q, $J_{7,8}$ = $J_{8,9}$ = 6.6 Hz, 2H, H-8). δ_C (D_2O, 101 MHz): 102.8 (1C, C-1), 75.1 (1C, C-5), 72.8 (1C, C-3), 70.7 (1C, C-2), 68.6 (1C, C-4), 67.2 (1C, C-7), 61.0 (1C, C-6), 37.5 (1C, C-9), 30.3 (1C, C-8). ESI-MS: found *m/z* 238.5 $[M+H]^+$, calcd for $C_9H_{19}NO_6$ 237.2.

5.3.1.23. p-Nitrophenyl 2,3,4,6-tetra-*O*-acetyl-β-D-galactopyranoside (43)[345]

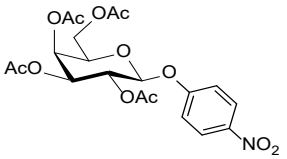

p-Nitrophenyl galactoside (500 mg, 1.7 mmol) was suspended in pyridine (5 mL). Acetic anhydride (3 mL, 35 mmol, 20 eq) was added dropwise with stirring. Catalytic DMAP was added to the reaction mixture (10 mg, 0.1 eq). The reaction was stirred overnight, at which point TLC (EtOAc-Hex 6:4) showed reaction completion. The mixture was co-evaporated several times with toluene (4 x 10 mL) to remove pyridine. The residue was dissolved in DCM (25 mL) and washed with brine (3 x 15 mL). The organic layer was dried over $MgSO_4$, filtered

and concentrated to dryness under reduced pressure to obtain the acetylated galactoside (**43**, 712 mg, 92%). R_f value (EtOAc-Hex 6:4): 0.47. $[\alpha]_D^{25}$ -7.8 (*c* 0.8, $CHCl_3$)[lit.,[343] -12]. δ_H ($CDCl_3$; 400 MHz): 8.23-8.19 (m, 2H, H_{ortho}), 7.11-7.06 (m, 2H, H_{meta}), 5.52 (dd, $J_{1,2}$ = 7.9, $J_{2,3}$ = 10.4 Hz, 1H, H-2), 5.48 (dd, $J_{3.4}$ = 3.4, $J_{4,5}$ = 0.7 Hz, 1H, H-4), 5.17 (d, $J_{1,2}$ = 7.9 Hz, 1H, H-1), 5.14 (dd, $J_{2,3}$ = 10.4, $J_{3,4}$ = 3.4 Hz, 1H, H-3), 4.25-4.15 (m, 2H, H-6ab), 4.15-4.10 (m, 1H, H-5), 2.19 (s, 3H, CH_3), 2.08 (s, 3H, CH_3), 2.07 (s, 3H, CH_3), 2.02 (s, 3H, CH_3). δ_C (101 MHz): 170.3 (1C, C=O), 170.1 (1C, C=O), 170.0 (1C, C=O), 169.4 (1C, C=O), 161.2 (1C, $C_{Ar\text{-}1}$), 143.2 (1C, C_{para}), 125.8 (2C, C_{ortho}), 116.6 (2C, C_{meta}), 98.6 (1C, C-1), 71.5 (1C, C-5), 70.6 (1C, C-3), 68.3 (1C, C-2), 66.7 (1C, C-4), 61.3 (1C, C-6), 20.72 (1C, CH_3), 20.69 (1C, CH_3), 20.65 (1C, CH_3), 20.6 (1C, CH_3). IR (cm^{-1}): 1749.8 (C=O), 1519.0+1345.1 (NO_2). ESI-MS: found *m/z* 492.8 $[M+Na]^+$, calcd for $C_{20}H_{23}NO_{12}Na$ 492.1.

5.3.1.24. p-Aminophenyl 2,3,4,6-tetra-*O*-acetyl-β-D-galactopyranoside (44)[345]

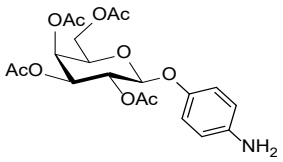

Acetylated p-nitrophenyl galactoside **43** (470 mg, 1.0 mmol) was dissolved in MeOH (10 mL). Carbon-supported palladium (Pd/C, 50 mg, 0.05 mmol, 0.05 eq) was added under nitrogen. The sealed round bottom flask was purged with hydrogen three times and the reaction was stirred together with a gently bubbling of hydrogen for two hours, at which point TLC (DCM-MeOH 95:5) showed reaction completion. The mixture was filtered over celite and concentrated to dryness under reduced pressure to obtain the acetylated galactoside **44** (420 mg, 96%). R_f value (DCM-MeOH 95:5): 0.69. $[\alpha]_D^{25}$ +8.5 (*c* 1.1, $CHCl_3$)[lit.,[343] +12]. δ_H ($CDCl_3$; 400 MHz): 6.85-6.80 (m, 2H, H_{ortho}), 6.62-6.57 (m, 2H, H_{meta}), 5.43 (dd, $J_{1,2}$ = 8.0, $J_{2,3}$ = 10.5 Hz, 1H, H-2), 5.42 (dd, $J_{3,4}$ = 3.4, $J_{4,5}$ = 1.0 Hz, 1H, H-4), 5.07 (dd, $J_{2,3}$ = 10.5, $J_{3,4}$ = 3.4 Hz, 1H, H-3), 4.86 (d, $J_{1,2}$ = 8.0 Hz, 1H, H-1), 4.22 (dd, $J_{5,6a}$ = 6.7, $J_{6a,6b}$ = 11.2 Hz, 1H, H-6a), 4.14 (dd, $J_{5,6b}$ = 6.7, $J_{6a,6b}$ = 11.2 Hz, 1H, H-6b), 3.98 (dt, $J_{4,5}$ = 1.0, $J_{5,6}$ = 6.7 Hz, 1H, H-5), 3.5 (s, 1H, NH_2), 2.17 (s, 3H, CH_3), 2.08 (s, 3H, CH_3), 2.04 (s, 3H, CH_3), 2.00 (s, 3H, CH_3). δ_C (101 MHz): 170.4 (1C, C=O), 170.3 (1C, C=O), 170.2 (1C, C=O), 169.4 (1C, C=O), 150.0 (1C, $C_{Ar\text{-}1}$), 142.3 (1C, C_{para}), 118.9 (2C, C_{ortho}), 115.9 (2C, C_{meta}), 101.2 (1C, C-1), 70.9 (1C, C-5), 70.8 (1C, C-3), 68.8 (1C, C-2), 67.0 (1C, C-4), 61.3 (1C, C-6), 20.8 (1C, CH_3), 20.68 (1C, CH_3), 20.67 (1C, CH_3), 20.60 (1C, CH_3). IR (cm^{-1}): 3340.0 (d, NH_2), 1747.2 (C=O). ESI-MS: found *m/z* 440.6 $[M+H]^+$, calcd for $C_{20}H_{25}NO_{10}$ 439.2.

5.3.1.25. p-Azidophenyl 2,3,4,6-tetra-*O*-acetyl-β-D-galactopyranoside (45)[346]

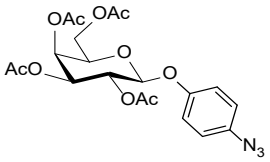

Acetylated p-aminophenyl galactoside (**44**, 470 mg, 1.0 mmol) was dissolved in aqueous HCl (10 mL, 1M) and the round bottom flask was placed in an ice bath. Under vigorous stirring, aqueous $NaNO_2$ (100 mg in 1 mL, 1.3 mmol, 1.3 eq.) was added dropwise and stirred for thirty minutes at 0°C. Aqueous NaN_3 (80 mg in 1 mL, 1.3 mmol, 1.3 eq) was added dropwise and the mixture was stirred vigorously. A precipitate started to appear, and the mixture was stirred further for one hour, at which point TLC (Hex-EtOAc 5:5) showed reaction completion. The mixture was diluted with DCM (10 mL) and washed with saturated aqueous $NaHCO_3$ solution (3 x 10 mL) and brine (10 mL). Silica gel chromatography (Hex-EtOAc 0:100 to 50:50) afforded the desired product (**45**, 321 mg, 65%) as a yellow solid. R_f value (Hex-EtOAc 5:5): 0.51. $[\alpha]_D^{25}$ +8 (*c* 1.0, $CHCl_3$) [lit.,[346] +7]. δ_H ($CDCl_3$; 400 MHz): 7.03-6.98 (m, 2H, H_{ortho}), 6.98-6.93 (m, 2H, H_{meta}), 5.47 (dd, $J_{1,2}$ = 8.0, $J_{2,3}$ = 10.5 Hz, 1H, H-2), 5.46 (d, $J_{3,4}$ = 3.4, 1H, H-4), 5.10 (dd, $J_{2,3}$ = 10.5, $J_{3,4}$ = 3.4 Hz, 1H, H-3), 4.98 (d, $J_{1,2}$ = 8.0 Hz, 1H, H-1), 4.23 (dd, $J_{5,6a}$ = 6.7, $J_{6a,6b}$ = 11.2 Hz, 1H, H-6a), 4.16 (dd, $J_{5,6b}$ = 6.7, $J_{6a,6b}$ = 11.2 Hz, 1H, H-6b), 4.04 (dt, $J_{4,5}$ = 1.1 Hz, $J_{5,6}$ = 6.7 Hz, 1H, H-5), 2.19 (s, 3H, CH_3), 2.08 (s, 3H, CH_3), 2.06 (s, 3H, CH_3), 2.02 (s, 3H, CH_3). δ_C (101 MHz): 170.4 (1C, C=O), 170.3 (1C, C=O), 170.2 (1C, C=O), 169.4 (1C, C=O), 154.2 (1C, $C_{Ar\text{-}1}$), 135.2 (1C, C_{para}), 120.1 (2C, C_{ortho}), 118.7 (2C, C_{meta}), 101.1 (1C, C-1), 71.2 (1C, C-5), 70.9 (1C, C-3), 68.7 (1C, C-2), 66.9 (1C, C-4), 61.4 (1C, C-6), 20.83 (1C, CH_3), 20.76 (2C, CH_3), 20.67 (1C, CH_3). IR (cm^{-1}): 2116.7 (N_3), 1747.2 (C=O). ESI-MS: found *m/z* 488.7$[M+H]^+$, calcd for $C_{20}H_{23}N_3O_{10}Na$ 488.1.

5.3.1.26. *tert*-Butyl *N*-(3-butyne)carbamate (46)[347]

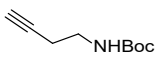

1-Amino-3-butyne (0.65 mL, 521 mg, 7.5 mmol) and TEA (2 mL) were dissolved in DCM (15 mL) and cooled in an ice bath for fifteen minutes. Boc_2O (1.71 g in 10 mL, 7.2 mmol, 1 eq) was added dropwise and the mixture was stirred overnight. TLC (Hex-EtOAc 7:3) showed reaction completion and the mixture was washed with saturated aqueous $NaHCO_3$ solution (3 x 10 mL). The organic layer was dried over $MgSO_4$, filtered and concentrated to dryness under reduced

pressure to obtain the protected amine **46** (1.15 g, 91%) as a white solid. R_f value (Hex-EtOAc 7:3): 0.53. δ_H ($CDCl_3$; 400 MHz): 3.23 (t, $J_{1,2}$ = 6.5 Hz, 2H, H-1), 2.36 (td, $J_{1,2}$ = 6.5, $J_{2,4}$ = 2.5 Hz, 2H, H-2), 1.98 (t, $J_{2,4}$ = 2.5 Hz, 1H, H-4), 1.42 (s, 9H, Boc). δ_C (101 MHz): 154.7 (1C, C=O), 80.6 (1C, C-3), 78.5 (1C, C-$(CH_3)_3$), 68.8 (1C, C-4), 38.3 (1C, C-2), 27.4 (3C, Boc), 19.0 (1C, C-1). IR (cm^{-1}): 1694.04 (Boc-C=O), 1519.8 (Boc-NH), 1392.8+1366.6 (Boc), ESI-MS: found *m/z* 170.2 $[M+H]^+$, calcd for $C_9H_{15}NO_2$ 169.1.

5.3.1.27. *tert*-Butyl *N*-([1-(3-(2,3,4,6-tetra-O-acetyl-β-D-galactopyranosyl)-propyl)-1H-1,2,3-triazol-4-yl]-methyl)carbamate (47)

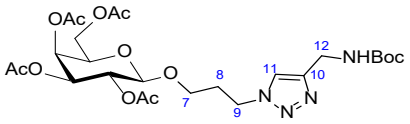

Adapted from Gao *et al.*[365] Stock solutions of $CuSO_4$ (20 mg/mL in degassed MeOH), THPTA (60 mg/mL in degassed water) and NaAsc (30 mg/mL in degassed water) were prepared. Acetylated p-azidopropyl galactoside (**7**, 50 mg, 0.1 mmol) was dissolved in degassed MeOH (0.4 mL) and mixed with *tert*-butyl *N*-(2-propyne)carbamate (20 mg in 0.4 mL of degassed MeOH, 0.1 mmol, 1.1 eq). $CuSO_4$ (0.4 mL, 6 mg, 0.04 mmol, 0.3 eq) and THPTA (0.4 mL, 17 mg, 0.04 mmol, 0.3 eq) were premixed and added to the reaction vial, and finally NaAsc (0.4 mL, 8 mg, 0.04 mmol, 0.3 eq)) was added to the mixture. The vial was purged with nitrogen, sealed, and left at room temperature overnight. TLC (Hex-EtOAc 4:6) showed reaction completion, at which point the solvents were evaporated under reduced pressure. The residue was redissolved in DCM and washed with brine (3 x 10 mL). The organic solvent was evaporated under reduced pressure. Silica gel chromatography (Hex-EtOAc 0:100 to 20:80) afforded the desired product (**47**, 49 mg, 72%) as a white solid. R_f value (Hex-EtOAc 4:6): 0.35. $[\alpha]_D^{25}$ +3.8 (*c* 1.0, $CHCl_3$). δ_H ($CDCl_3$; 400 MHz): 7.59 (s, 1H, H-11), 5.36 (dd, $J_{2,3}$ = 10.6, $J_{3,4}$ = 4.2 Hz, 1H, H-3), 5.25 (app. s, 1H, NH), 5.21 (dd, $J_{2,3}$ = 10.6, $J_{1,2}$ = 7.6 Hz, 1H, H-2), 5.03 (dd, $J_{3,4}$ = 4.2, $J_{4,5}$ = 2.1 Hz, 1H, H-4), 5.00 (d, $J_{1,2}$ = 7.6 Hz, 1H, H-1), 4.51-4.42 (m, 2H, H-9), 4.39 (s, 2H, H-12), 4.36-4.16 (m, 3H, H-6ab, H-5), 3.63-3.65 (m, 1H, H-7a), 3.37-3.30 (m, 1H, H-7b), 2.23-2.16 (m, 2H, H-8), 2.16 (s, 3H, CH_3), 2.13 (s, 3H, CH_3), 2.11 (s, 3H, CH_3), 2.09 (s, 3H, CH_3), 1.43 (s, 9H, Boc). δ_C (101 MHz): 170.4 (1C, AcO-C=O), 170.3 (1C, AcO-C=O), 170.2 (1C, AcO-C=O), 169.4 (1C, AcO-C=O), 159.5 (1C, Boc-C=O), 153.4 (1C, C-10), 122.5 (1C, C-11), 105.5 (1C, C-1), 80.1 (1C, C-5), 70.8 (1C, C-4), 68.9 (1C, C-3), 68.8 (1C, C-2), 63.5 (1C, C-7), 62.5 (1C, C-6), 46.9 (1C, C-9), 36.0 (1C,

C-12), 29.8 (1C, C-8), 28.3 (1C, Boc), 20.89 (1C, CH_3), 20.84 (1C, CH_3), 20.82 (1C, CH_3), 20.75 (1C, CH_3). IR (cm^{-1}): 1747.1 (AcO-C=O), 1703.0 (Boc-C=O), 1508.5 (Boc-NH), 1368.8+1368.5 (Boc). MALDI-TOF: found *m/z* 587.2588 $[M+H]^+$, calcd for $C_{25}H_{38}N_4O_{12}$ 586.2486.

5.3.1.28. *tert*-Butyl *N*-([1-(3-(2,3,4,6-tetra-O-acetyl-β-D-galactopyranosyl)-propyl)-1H-1,2,3-triazol-4-yl]-ethyl)carbamate (48)

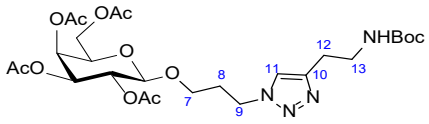

The procedure was adapted from Gao *et al.*[365] Stock solutions of $CuSO_4$ (20 mg/mL in degassed water), THPTA (60 mg/mL in degassed water) and NaAsc (30 mg/mL in degassed water) were prepared. Acetylated p-azidopropyl galactoside (**7**, 50 mg, 0.1 mmol) was dissolved in degassed MeOH (0.4 mL) and mixed with *tert*-butyl *N*-(2-butyne)carbamate (**48**, 22 mg in 0.4 mL of degassed MeOH, 0.1 mmol, 1.1 eq). $CuSO_4$ (0.4 mL, 6 mg, 0.04 mmol, 0.3 eq) and THPTA (0.4 mL, 17 mg, 0.04 mmol, 0.3 eq) were premixed and added to the reaction vial, and finally NaAsc (0.4 mL, 8 mg, 0.04 mmol, 0.3 eq) was added to the mixture. The vial was purged with nitrogen, sealed, and left at room temperature overnight. TLC (Hex-EtOAc 4:6) showed reaction completion, at which point the solvents were evaporated under reduced pressure. The residue was redissolved in DCM and washed with brine (3 x 10 mL). The organic solvent was evaporated under reduced pressure. Silica gel chromatography (Hex-EtOAc 0:100 to 20:80) afforded the desired product (**50**, 54 mg, 77%) as a white solid. R_f value (Hex-EtOAc 4:6): 0.35. $[\alpha]_D^{25}$ +4.2 (*c* 1.1, $CHCl_3$). δ_H ($CDCl_3$; 400 MHz): 7.47 (s, 1H, H-11), 5.36 (dd, $J_{2,3}$ = 10.4, $J_{3,4}$ = 4.2 Hz, 1H, H-3), 5.21 (dd, $J_{1,2}$ = 7.8, $J_{2,3}$ = 10.4 Hz, 1H, H-2), 5.06 (app. s, 1H, NH), 5.03 (dd, $J_{3,4}$ = 4.2, $J_{4,5}$ = 2.1 Hz, 1H, H-4), 5.00 (d, $J_{1,2}$ = 7.8 Hz, 1H, H-1), 4.50-4.42 (m, 2H, H-9), 4.40-4.14 (m, 3H, H-6ab, H-5), 3.75-3.68 (m, 1H, H-7a), 4.47 (app. s, 2H, H-12), 3.38-3.31 (m, 1H, H-7b), 2.92 (t, $J_{11,12}$ = 6.7 Hz, 2H, H-12), 2.27-2.16 (m, 2H, H-8), 2.16 (s, 3H, CH_3), 2.13 (s, 3H, CH_3), 2.10 (s, 3H, CH_3), 2.09 (s, 3H, CH_3), 1.42 (s, 9H, Boc). δ_C (101 MHz): 170.4 (1C, AcO-C=O), 170.3 (1C, AcO-C=O), 170.2 (1C, AcO-C=O), 169.4 (1C, AcO-C=O), 159.5 (1C, Boc-C=O), 152.3 (1C, C-10), 121.5 (1C, C-11), 105.8 (1C, C-1), 80.2 (1C, C-5), 76.2 (1C, C-4), 69.3 (1C, C-3), 68.8 (1C, C-2), 63.8 (1C, C-7), 62.8 (1C, C-6), 47.0 (1C, C-9), 39.9 (1C, C-12), 29.8 (m, 1C, C-8), 28.2 (1C, Boc), 25.8 (1C, C-13), 20.89 (1C, CH_3), 20.83 (1C, CH_3), 20.82 (1C, CH_3), 20.74 (1C, CH_3). IR (cm^-

[1]): 1745.6 (AcO-C=O), 1699.2 (Boc-C=O), 1521.8 (Boc-NH), 1368.9+1368.3 (Boc). MALDI-TOF: found *m/z* 601.2720 $[M+H]^+$, calcd for $C_{26}H_{40}N_4O_{12}$ 600.2643.

5.3.1.29. *tert*-Butyl *N*-([1-(p-(2,3,4,6-tetra-*O*-acetyl-β-D-galactopyranosyl)-phenyl)-1H-1,2,3-triazol-4-yl]-methyl)carbamate (49)

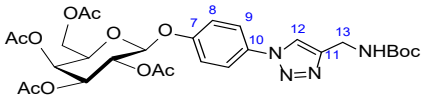

The procedure was adapted from Gao *et al.*[365] Stock solutions of $CuSO_4$ (20 mg/mL in degassed MeOH), THPTA (60 mg/mL in degassed water) and NaAsc (30 mg/mL in degassed water) were prepared. Acetylated p-azidophenyl galactoside (**45**, 125 mg, 0.3 mmol) was dissolved in degassed MeOH (0.8 mL) and mixed with *tert*-butyl *N*-(2-propyne)carbamate (46 mg in 0.8 mL of degassed MeOH, 0.3 mmol, 1.1 eq). $CuSO_4$ (0.8 mL, 13 mg, 0.08 mmol, 0.3 eq) and THPTA (0.8 mL, 35 mg, 0.08 mmol, 0.3 eq) were premixed and added to the reaction vial, and finally NaAsc (0.8 mL, 16 mg, 0.08 mmol, 0.3 eq)) was added to the mixture. The vial was purged with nitrogen, sealed, and left at room temperature overnight. TLC (Hex-EtOAc 4:6) showed reaction completion, at which point the solvents were evaporated under reduced pressure. The residue was redissolved in DCM and washed with brine (3 x 10 mL). The organic solvent was evaporated under reduced pressure. Silica gel chromatography (Hex-EtOAc 0:100 to 20:80) afforded the desired product (**49**, 156 mg, 94%) as a white solid. R_f value (Hex-EtOAc 4:6): 0.35. $[\alpha]_D^{25}$ +3.8 (*c* 1.2, $CHCl_3$). δ_H ($CDCl_3$; 400 MHz): 7.90 (s, 1H, H-12), 7.67-7.62 (m, 2H, H-8), 7.16-7.12 (m, 2H, H-9), 5.51 (dd, $J_{1,2}$ = 7.8, $J_{2,3}$ = 10.5 Hz, 1H, H-2), 5.46 (dd, $J_{3,4}$ = 3.3, $J_{4,5}$ = 0.7 Hz, 1H, H-4), 5.17 (app. s, 1H, NH), 5.13 (dd, $J_{2,3}$ = 10.5, $J_{3.4}$ = 3.3 Hz, 1H, H-3), 5.10 (d, $J_{1,2}$ = 7.8 Hz, 1H, H-1), 4.47 (d, $J_{13,NH}$ = 5.2 Hz, 2H, H-13), 4.27-4.15 (m, 2H, H-6ab), 4.15-4.10 (m, 1H, H-5), 2.19 (s, 3H, CH_3), 2.09 (s, 3H, CH_3), 2.07 (s, 3H, CH_3), 2.02 (s, 3H, CH_3), 1.45 (s, 9H, Boc). δ_C (101 MHz): 170.4 (1C, AcO-C=O), 170.3 (1C, AcO-C=O), 170.2 (1C, AcO-C=O), 169.4 (1C, AcO-C=O), 159.5 (1C, Boc-C=O), 151.5 (1C, C-7), 150.5 (1C, C-11), 147.3 (1C, C-10), 122.1 (1C, C-8), 120.4 (1C, C-12), 117.9 (1C, C-9), 99.5 (1C, C-1), 71.3 (1C, C-5), 70.7 (1C, C-3), 68.5 (1C, C-2), 66.8 (1C, C-4), 61.4 (1C, C-6), 36.0 (1C, C-13), 28.4 (1C, Boc), 20.75 (1C, CH_3), 20.69 (1C, CH_3), 20.67 (1C, CH_3), 20.58 (1C, CH_3). IR (cm^{-1}): 1750.0 (AcO-C=O), 1699.9 (Boc-C=O), 1515.9 (Boc-NH), 1369.0+1368.1 (Boc). MALDI-TOF: found *m/z* 621.2402 $[M+H]^+$, calcd for $C_{28}H_{36}N_4O_{12}$ 620.2330.

5.3.1.30. *tert*-Butyl *N*-([1-(p-(2,3,4,6-tetra-O-acetyl-β-D-galactopyranosyl)-phenyl)-1H-1,2,3-triazol-4-yl]-ethyl)carbamate (50)

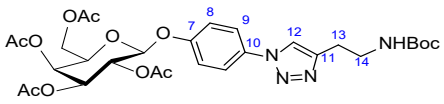

The procedure was adapted from Gao *et al.*[365] Stock solutions of $CuSO_4$ (20 mg/mL in degassed MeOH), THPTA (60 mg/mL in degassed water) and NaAsc (30 mg/mL in degassed water) were prepared. Acetylated p-azidophenyl galactoside (**45**, 125 mg, 0.3 mmol) was dissolved in degassed MeOH (0.8 mL) and mixed with *tert*-Butyl *N*-(3-butyne)carbamate (**46**, 50 mg in 0.8 mL of degassed MeOH, 0.3 mmol, 1.1 eq). $CuSO_4$ (0.8 mL, 13 mg, 0.08 mmol, 0.3 eq) and THPTA (0.8 mL, 35 mg, 0.08 mmol, 0.3 eq) were premixed and added to the reaction vial, and finally NaAsc (0.8 mL, 16 mg, 0.08 mmol, 0.3 eq)) was added to the mixture. The vial was purged with nitrogen, sealed, and left at room temperature overnight. TLC (Hex-EtOAc 4:6) showed reaction completion, at which point the solvents were evaporated under reduced pressure. The residue was redissolved in DCM and washed with brine (3 x 10 mL). The organic solvent was evaporated under reduced pressure. Silica gel chromatography (Hex-EtOAc 0:100 to 20:80) afforded the desired product **50** (167 mg, 96%) as a white solid. R_f value (Hex-EtOAc 4:6): 0.35. $[\alpha]_D^{25}$ +3.7 (*c* 1.3, $CHCl_3$). δ_H ($CDCl_3$; 400 MHz): 7.76 (s, 1H, H-12), 7.67-7.61 (m, 2H, H-8), 7.17-7.12 (m, 2H, H-9), 5.52 (dd, $J_{1,2}$ = 7.9, $J_{2,3}$ = 10.3 Hz, 1H, H-2), 5.48 (dd, $J_{3,4}$ = 3.4, $J_{4,5}$ = 0.7 Hz, 1H, H-4), 5.14 (dd, $J_{2,3}$ = 10.3, $J_{3.4}$ = 3.4 Hz, 1H, H-3), 5.10 (d, $J_{1,2}$ = 7.9 Hz, 1H, H-1), 5.00 (app. s, 1H, NH), 4.27-4.15 (m, 2H, H-6ab), 4.15-4.10 (m, 1H, H-5), 3.54 (app. s, 2H, H-14), 3.00 (t, $J_{13,14}$ = 6.5 Hz) 2.209 (s, 3H, CH_3), 2.09 (s, 3H, CH_3), 2.07 (s, 3H, CH_3), 2.03 (s, 3H, CH_3), 1.43 (s, 9H, Boc). δ_C (101 MHz): 170.3 (1C, AcO-C=O), 170.2 (1C, AcO-C=O), 170.1 (1C, AcO-C=O), 169.3 (1C, AcO-C=O), 156.8 (1C, Boc-C=O), 156.2 (1C, C-7), 152.7 (1C, C-11), 132.5 (1C, C-10), 122.0 (1C, C-8), 119.9 (1C, C-12), 118.0 (1C, C-9), 99.6 (1C, C-1), 71.4 (1C, C-5), 70.7 (1C, C-3), 68.6 (1C, C-2), 66.8 (1C, C-4), 61.2 (1C, C-6), 39.5 (1C, C-13), 28.5 (1C, Boc), 26.04 (1C, C-14), 20.75 (1C, CH_3), 20.69 (1C, CH_3), 20.66 (1C, CH_3), 20.58 (1C, CH_3). IR (cm^{-1}): 1750.2 (AcO-C=O), 1699.5 (Boc-C=O), 1516.2 (Boc-NH), 1368.7+1368.0 (Boc). MALDI-TOF: found *m/z* 635.2576 $[M+H]^+$, calcd for $C_{29}H_{38}N_4O_{12}$ 634.2486.

5.3.1.31. *tert*-Butyl *N*-[(2S)-1,4-bis([3-(2,3,4,6-tetra-O-acetyl-β-D-galactopyranosyl)-prop-1-yl)-1H-1,2,3-triazol-4-yl]-methylamino)-1,4-dioxobutan-2-yl)carbamate (51)

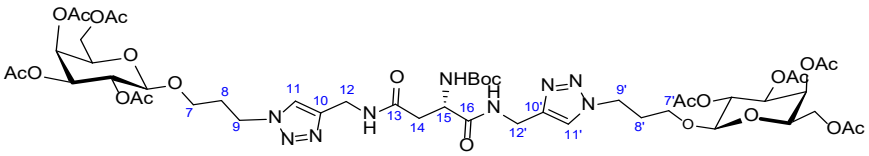

The procedure was adapted from Gao *et al.*[365] A solution of Boc-protected aspartic acid (11.4 mg, 0.05 mmol, 1 eq) in DCM (1 mL) and TEA (one drop) was stirred with EDC (20.6 mg, 0.11 mmol, 2.2 eq) for 45 minutes. Meanwhile, the peracetylated Boc-protected triazolyl phenyl galactoside **47** (62 mg, 0.11 mmol, 2.1 eq) was dissolved in DCM (1 mL) and TFA (0.1 mL, 1.3 mmol, 10 eq) was added dropwise. The mixture was stirred for thirty minutes, at which point TLC (DCM-MeOH 95:5) showed complete cleavage of the Boc group (single spot shifted from R_f 0.60 to R_f 0.20). The mixture was neutralised with TEA (0.2 mL). The EDC-activated aspartic acid was transferred to the flask and further stirred at room temperature overnight, and the TLC (DCM-MeOH 95:5) showed reaction completion (single spot shifted from R_f 0.20 to R_f 0.52). The mixture was co-evaporated several times with toluene (3 x 10 mL) to remove the TEA. The residue was dissolved in DCM (10 mL) and washed with brine (3 x 10 mL). The organic layer was dried over $MgSO_4$, filtered and concentrated to dryness under reduced pressure. Silica gel chromatography (DCM-MeOH 100:0 to 80:20) afforded the acetylated galactoside **51** (36.5, 72%) as a white solid. R_f value (DCM-MeOH 95:5): 0.52. $[\alpha]_D^{25}$ +3.5 (*c* 1.0, $CHCl_3$). δ_H (CD_3OD; 600 MHz): 7.87 (s, 2H, H-11, H-11'), 5.42 (d, $J_{3,4} = J_{3',4'}$ = 3.6 Hz, 2H, H-4, H-4'), 5.19-5.17 (m, 2H, H-3, H-3'), 5.15 (dd, $J_{2,3} = J_{2',3'}$ = 10.5 Hz, $J_{1,2} = J_{1',2'}$ = 7.7 Hz, 2H, H-2, H-2'), 4.67 (d, $J_{1,2} = J_{1',2'}$ = 7.7 Hz, 2H, H-1, H-1'), 4.51-4.43 (m, 9H, H-9, H-9', H-12, H-12', H-15, H-16), 4.21-4.16 (m, 4H, H-6, H-6'), 4.16-4.12 (m, 2H, H-5, H-5'), 3.92-3.87 (m, 2H, H-7a, H-7'a), 3.58-3.52 (m, 2H, H-7b. H-7'b), 2.76-2.66 (m, 2H, H-14), 2.21-2.15 (m, 4H, H-8, H-8'), 2.18 (s, 6H, CH_3), 2.11 (s, 6H, CH_3), 2.04 (s, 6H, CH_3), 1.98 (s, 6H, CH_3), 1.46 (s, 9H, Boc). δ_C (101 MHz): 173.9 (2C, C-13, c-16), 172.2 (2C, AcO-C=O), 172.0 (2C, AcO-C=O), 171.9 (2C, AcO-C=O), 171.4 (2C, AcO-C=O), 157.5 (1C, Boc-C=O), 146.3 (2C, C-10, C-10'), 124.3 (2C, C-11, C-11'), 102.2 (2C, C-1, C-1'), 72.3 (2C, C-5, C-5'), 71.8 (2C, C-2, C-2'), 70.4 (2C, C-3, C-3'), 68.8 (2C, C-4, C-4'), 67.15 (1C, C-7), 67.14 (1C, C-7'), 62.6 (2C, C-6, C-6'), 53.1 (1C, C-15), 48.1 (2C, C-9, C-9'), 38.6 (1C, C-14), 35.9 (2C, C-12), 35.7 (1C, C-12'), 31.4 (2C, C-8, C-8'), 28.7 (1C, Boc), 20.9 (2C, CH_3), 20.61 (2C, CH_3), 20.56 (2C, CH_3), 20.53 (2C, CH_3). IR (cm^{-1}): 1748.4 (AcO-C=O), 1654.3 (Boc-C=O), 1522.5

(Boc-NH), 1368.8 (Boc). MALDI-TOF: found *m/z* 1170.4716 $[M+H]^+$, calcd for $C_{49}H_{71}N_9O_{24}$ 1169.4612.

5.3.1.32. *tert*-Butyl *N*-[(2S)-1,4-bis([3-(2,3,4,6-tetra-*O*-acetyl-β-D-galactopyranosyl)-prop-1-yl)-1H-1,2,3-triazol-4-yl]-ethylamino)-1,4-dioxobutan-2-yl)carbamate (52)

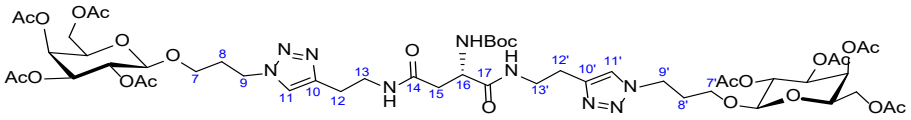

The procedure was adapted from Gao *et al.*[365] A solution of Boc-protected aspartic acid (13.2 mg, 0.06 mmol, 1 eq) in DCM (1 mL) and TEA (one drop) was stirred with EDC (20.6 mg, 0.11 mmol, 2.2 eq) for 45 minutes. Meanwhile, the peracetylated Boc-protected triazolyl phenyl galactoside **48** (58 mg, 0.10 mmol, 2.1 eq) was dissolved in DCM (1 mL) and TFA (0.1 mL, 1.3 mmol, 10 eq) was added dropwise. The mixture was stirred for thirty minutes, at which point TLC (DCM-MeOH 95:5) showed complete cleavage of the Boc group (single spot shifted from R_f 0.60 to R_f 0.20). The mixture was neutralised with TEA (0.2 mL). The EDC-activated aspartic acid was transferred to the flask and further stirred at room temperature overnight, and the TLC (DCM-MeOH 95:5) showed reaction completion (single spot shifted from R_f 0.20 to R_f 0.50. The mixture was co-evaporated several times with toluene (3 x 10 mL) to remove the TEA. The residue was dissolved in DCM (10 mL) and washed with brine (3 x 10 mL). The organic layer was dried over $MgSO_4$, filtered and concentrated to dryness under reduced pressure. Silica gel chromatography (DCM-MeOH 100:0 to 80:20) afforded the acetylated galactoside **52** (55 mg, 80%) as a white solid. R_f value (DCM-MeOH 95:5): 0.50. $[\alpha]_D^{25}$ +6.5 (*c* 1.0, $CHCl_3$). δ_H (CD_3OD; 600 MHz): 7.82 (s, 2H, H-11, H-11'), 5.42 (d, $J_{3,4} = J_{3',4'}$ = 3.4 Hz, 2H, H-4, H-4'), 5.17 (dd, $J_{2,3} = J_{2',3'}$ = 10.5 Hz, $J_{3,4} = J_{3',4'}$ = 3.4 Hz, 2H, H-3, H-3'), 5.12 (dd, $J_{2,3} = J_{2',3'}$ = 10.5 Hz, $J_{1,2} = J_{1',2'}$ = 7.5 Hz, 2H, H-2, H-2'), 4.68 (d, $J_{1,2} = J_{1',2'}$ = 7.5 Hz, 2H, H-1, H-1'), 4.55-4.43 (m, 4H, H-9, H-9'), 4.40-4.37 (m, 1H, H-16), 4.21-4.16 (m, 4H, H-6, H-6'), 4.16-4.12 (m, 2H, H-5, H-5'), 3.92-3.87 (m, 2H, H-7a, H-7'a), 3.60-3.54 (m, 2H, H-7b. H-7'b), 3.53-3.45 (m, 4H, H-13, H-13'), 2.95-2.87 (m, 4H, H-12, H-12'), 2.65-2.53 (m, 3H, H-15), 2.23-2.16 (m, 4H, H-8, H-8'), 2.18 (s, 6H, CH_3), 2.12 (s, 3H, CH_3), 2.11 (s, 3H, CH_3), 2.04 (s, 6H, CH_3), 1.98 (s, 6H, CH_3), 1.47 (s, 9H, Boc). δ_C (101 MHz): 173.9 (2C, C-14, c-17), 172.00 (2C, AcO-C=O), 171.97 (2C, AcO-C=O), 171.49 (2C, AcO-C=O), 171.46 (2C, AcO-C=O), 157.4 (1C, Boc-C=O), 146.2 (2C, C-10, C-10'), 124.0 (2C, C-11, C-11'), 102.2 (2C, C-1, C-1'), 72.3 (2C, C-5, C-5'), 71.8 (2C, C-2, C-2'), 70.4 (2C, C-3, C-3'), 68.8 (2C, C-4,

C-4'), 67.2 (2C, C-7, C-7'), 62.6 (2C, C-6, C-6'), 53.2 (1C, C-16), 48.0 (2C, C-9, C-9'), 40.2 (1C, C-13), 40.2 (1C, C-13'), 38.9 (1C, C-15), 31.4 (2C, C-8, C-8'), 28.7 (1C, Boc), 26.5 (1C, C-12), 26.4 (1C, C-12'), 20.86 (1C, CH_3), 20.85 (1C, CH_3), 20.60 (2C, CH_3), 20.55 (2C, CH_3), 20.52 (2C, CH_3). IR (cm^{-1}): 1747.6 (AcO-C=O), 1654.3 (Boc-C=O), 1553.5 (Boc-NH), 1368.7 (Boc). MALDI-TOF: found *m/z* 1198.5033 $[M+H]^+$, calcd for $C_{51}H_{75}N_9O_{24}$ 1197.4925.

5.3.1.33. *tert*-Butyl *N*-[(2S)-1,4-bis([4-(2,3,4,6-tetra-O-acetyl-β-D-galactopyranosyl)-phen-1-yl)-1H-1,2,3-triazol-4-yl]-methylamino)-1,4-dioxobutan-2-yl)carbamate (53)

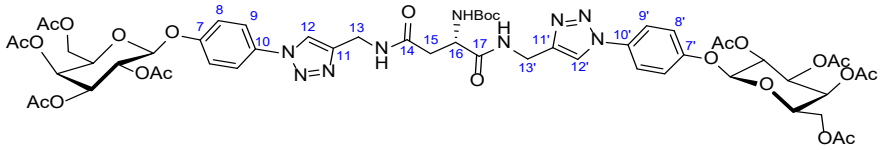

The procedure was adapted from Gao *et al.*[365] A solution of Boc-protected aspartic acid (13.4 mg, 0.06 mmol, 1 eq) in DCM (1 mL) and TEA (one drop) was stirred with EDC (24.3 mg, 0.13 mmol, 2.2 eq) for 45 minutes. Meanwhile, the peracetylated Boc-protected triazolyl phenyl galactoside **49** (76 mg, 0.12 mmol, 2.1 eq) was dissolved in DCM (1 mL) and TFA (0.1 mL, 1.3 mmol, 10 eq) was added dropwise. The mixture was stirred for thirty minutes, at which point TLC (DCM-MeOH 95:5) showed complete cleavage of the Boc group (single spot shifted from R_f 0.60 to 0.20). The mixture was neutralised with TEA (0.2 mL). The EDC-activated aspartic acid was transferred to the flask and further stirred at room temperature overnight, and the TLC (DCM-MeOH 95:5) showed reaction completion (single spot shifted from R_f 0.20 to 0.55. The mixture was co-evaporated several times with toluene (3 x 10 mL) to remove the TEA. The residue was dissolved in DCM (10 mL) and washed with brine (3 x 10 mL). The organic layer was dried over $MgSO_4$, filtered and concentrated to dryness under reduced pressure. Silica gel chromatography (DCM-MeOH 100:0 to 80:20) afforded the acetylated galactoside **53** (53.4 mg, 75%) as a white solid. R_f value (DCM-MeOH 95:5): 0.55. $[\alpha]_D^{25}$ +5.5 (*c* 1.0, $CHCl_3$). δ_H (CD_3OD; 600 MHz): 8.32 (s, 2H, H-12, H-12'), 7.71-7.65 (m, 4H, H-8, H-8'), 7.20-7.15 (m, 4H, H-9, H-9'), 5.50 (dd, $J_{3,4}$ = $J_{3',4'}$ = 3.4, $J_{4,5}$ = $J_{4',5'}$ = 1.2 Hz, 2H, H-4, H-4'), 5.44-5.39 (m, 4H, H-1,H-1', H-3, H-3'), 5.33-5.30 (m, 2H, H-2, H-2'), 4.59-4.48 (m, 5H, H-13, H-13', H-16), 4.40-4.35 (m, 2H, H-5, H-5'), 4.23-4.19 (m, 4H, H-6, H-6'), 2.80 (s, 2H, H-15), 2.21 (s, 6H, CH_3), 2,10 (s, 6H, CH_3), 2.05 (s, 6H, CH_3), 2.01 (s, 6H, CH_3), 1.43 (s, 9H, Boc). δ_C (101 MHz): 174.2 (2C, C-14, c-17), 172.0 (2C, AcO-C=O), 171.9 (2C, AcO-C=O), 171.4 (2C, AcO-C=O), 171.3 (2C, AcO-C=O), 158.3

(1C, Boc-C=O), 157.5 (2C, C-11, C-11'), 133.05 (2C, C-7, C-7'), 133.07 (2C, C-10, C-10'), 122.8 (2C, C-8, C-8'), 122.7 (2C, C-12C-12'), 118.8 (2C, C-9, C-9'), 100.0 (2C, C-1, C-1'), 72.3 (2C, C-5, C-5'), 72.2 (2C, C-2, C-2'), 70.1 (2C, C-3, C-3'), 68.7 (2C, C-4, C-4'), 62.6 (2C, C-6, C-6'), 53.2 (1C, C-16), 38.9 (1C, C-15), 36.1 (1C, C-13), 35.9 (1C, C-13'), 28.7 (1C, Boc), 20.67 (2C, CH_3), 20.66 (2C, CH_3), 20.52 (2C, CH_3), 20.51 (2C, CH_3). IR (cm^{-1}): 1749.4 (AcO-C=O), 1654.3 (Boc-C=O), 1504.7 (Boc-NH), 1368.5 (Boc). MALDI-TOF: found *m/z* 1246.4202 $[M-H]^-$, calcd for $C_{55}H_{67}N_9O_{24}$ 1237.4299.

5.3.1.34. *tert*-Butyl *N*-[(2*S*)-1,4-bis([4-(2,3,4,6-tetra-*O*-acetyl-β-D-galactopyranosyl)-phen-1-yl)-1H-1,2,3-triazol-4-yl]-ethylamino)-1,4-dioxobutan-2-yl)carbamate (54)

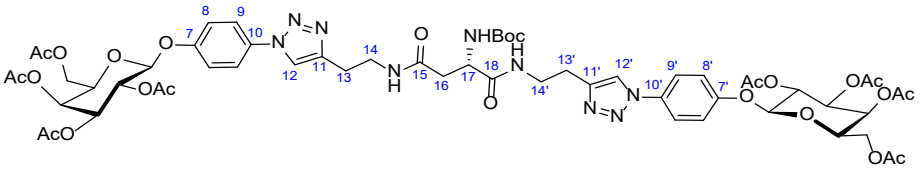

The procedure was adapted from Gao *et al.*[365] A solution of Boc-protected aspartic acid (10.5 mg, 0.05 mmol, 1 eq) in DCM (1 mL) and TEA (one drop) was stirred with EDC (19.6 mg, 0.10 mmol, 2.2 eq) for 45 minutes. Meanwhile, the peracetylated Boc-protected triazolyl phenyl galactoside **50** (62 mg, 0.10 mmol, 2.1 eq) was dissolved in DCM (1 mL) and TFA (0.1 mL, 1.3 mmol, 10 eq) was added dropwise. The mixture was stirred for thirty minutes, at which point TLC (DCM-MeOH 95:5) showed complete cleavage of the Boc group (single spot shifted from R_f 0.60 to 0.20). The mixture was neutralised with TEA (0.2 mL). The EDC-activated aspartic acid was transferred to the flask and further stirred at room temperature overnight, and the TLC (DCM-MeOH 95:5) showed reaction completion (single spot shifted from R_f 0.20 to 0.52. The mixture was co-evaporated several times with toluene (3 x 10 mL) to remove the TEA. The residue was dissolved in DCM (10 mL) and washed with brine (3 x 10 mL). The organic layer was dried over $MgSO_4$, filtered and concentrated to dryness under reduced pressure. Silica gel chromatography (DCM-MeOH 100:0 to 80:20) afforded the acetylated galactoside **54** (35.2 mg, 72%) as a white solid. R_f value (DCM-MeOH 95:5): 0.52. $[\alpha]_D^{25}$ +7.6 (*c* 1.0, $CHCl_3$). δ_H (CD_3OD; 600 MHz): 8.32 (s, 2H, H-12, H-12'), 7.85-7.77 (m, 4H, H-8, H-8'), 7.25-7.205 (m, 4H, H-9, H-9'), 5.51 (app. d, $J_{3,4} = J_{3',4'}$ = 4.0, Hz, 2H, H-4, H-4'), 5.44-5.41 (m, 4H, H-1,H-1', H-3, H-3'), 5.34-5.30 (m, 2H, H-2, H-2'), 4.41 (t, $J_{16,17}$ = 5.0 Hz, 1H, H-17), 4.38 (app. t, $J_{5,6} = J_{5',6'}$ = 6.7 Hz, 2H, H-5, H-5'), 4.23-4.19 (m, 4H, H-6, H-6'), 3.56-3.49 (m, 4H, H-14, H-14'), 3.00-2.94 (m,

4H, H-13, H-13'), 2.68-2.58 (m, 2H, H-16), 2.21 (s, 6H, CH_3), 2,10 (s, 6H, CH_3), 2.05 (s, 6H, CH_3), 2.02 (s, 6H, CH_3), 1.41 (s, 9H, Boc). δ_C (101 MHz): 173.9 (1C, C-18), 172.4 (1C, c-15), 171.97 (2C, AcO-C=O), 171.94 (2C, AcO-C=O), 171.4 (2C, AcO-C=O), 171.3 (2C, AcO-C=O), 158.3 (1C, Boc-C=O), 157.4 (2C, C-11, C-11'), 133.68 (2C, C-7, C-7'), 133.67 (2C, C-10, C-10'), 123.1 (2C, C-8, C-8'), 122.4 (2C, C-12C-12'), 118.8 (2C, C-9, C-9'), 99.9 (2C, C-1, C-1'), 72.3 (2C, C-5, C-5'), 72.2 (2C, C-2, C-2'), 70.1 (2C, C-3, C-3'), 68.7 (2C, C-4, C-4'), 62.6 (2C, C-6, C-6'), 53.2 (1C, C-17), 40.0 (2C, C-14, C-14'), 38.8 (1C, C-16), 28.7 (1C, Boc), 26.4 (2C, C-13, C-13'), 20.67 (2C, CH_3), 20.66 (2C, CH_3), 20.52 (2C, CH_3), 20.51 (2C, CH_3). IR (cm^{-1}): 1748.0 (AcO-C=O), 1654.4 (Boc-C=O), 1521.9 (Boc-NH), 1368.2 (Boc). MALDI-TOF: found *m/z* 1264.4520 $[M-H]^-$, calcd for $C_{57}H_{71}N_9O_{24}$ 1265.4612.

5.3.1.35. *General method A*: deprotection and installation of an azide-ending tether to galactoside dimers 51-54

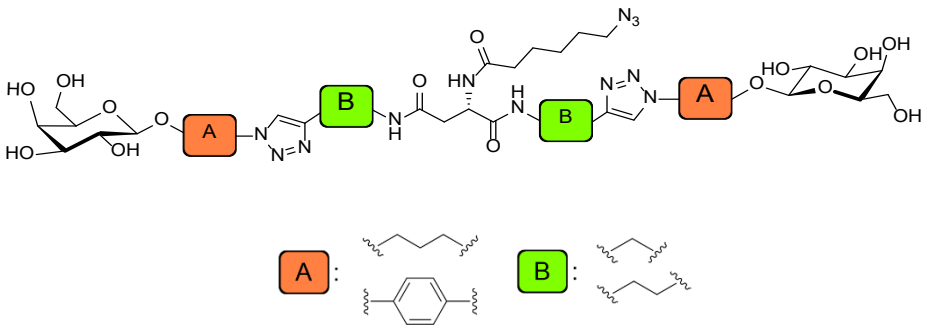

The procedure was adapted from Gao *et al.*[365] This procedure was attempted for the acetylated dimers **51-54**. A solution of 6-azidohexanoic acid (6.3 mg, 0.04 mmol, 1.2 eq) in MeOH (0.5 mL) and TEA (one drop) was stirred with EDC (4.5-9.2 mg, 0.01-0.03 mmol, 1.2 eq) for 45 minutes. Meanwhile, the peracetylated Boc-protected dimer (**51-54**, 15-30 mg, 0.02 mmol, 1 eq) was dissolved in TFA (0.5 mL, 0.6 mmol). The mixture was stirred for thirty minutes, at which point the solvent was evaporated under reduced pressure and the residue was redissolved in DCM (0.25 mL). TEA (0.05 mL) was added to the mixture, and the EDC-activated 6-azidohexanoic acid was transferred to the flask, which was further stirred at room temperature overnight. At that point, several spots could be observed by TLC (IPA-NH_4OH-H_2O 6:3:1) and the similar polarity between the different products hindered the isolation of the desired dimers **55-58** (please refer to the discussion in *Chapter 4*).

5.3.2. BSA conjugate synthesis

5.3.2.1. Propargylated BSA (22)

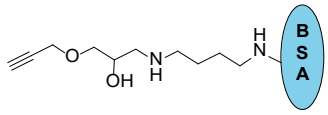

BSA (10.5 mg, 1.6 µmol, 1 eq.) was dissolved in aqueous $NaHCO_3$ (1 mL, 10 mM) in a vial, and glycidyl propargyl ether (5 µL, 0.05 mmol 30 eq) was added. The vials were closed, wrapped in aluminium foil and placed in a heating block at 37 ºC to react overnight without stirring. The reaction crude was dialysed for 48 h (Abcam 3 ml DiaEasy Dialyzer MWCO 12-14 kDa), changing the dialysis Mili-Q water after the first 24 h. The final solution was freeze-dried to obtain BSA conjugate **6** (9 mg, 90%). MALDI-TOF (BSA): found average *m/z* 66569 $[M+H]^+$, in agreement with commercial specifications. MALDI-TOF (reaction) found average *m/z* 69468 $[M+H]^+$. Being M_{BSA} 66569 and M_{alkyne} 112, the average number of alkynes per BSA was calculated as 26.

5.3.2.2. *General method B*: CuAAC reaction for the synthesis of BSA glycoconjugates 23-29

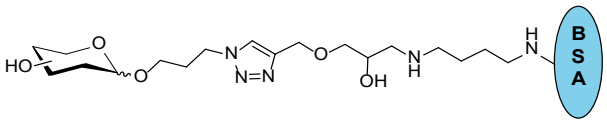

Adapted from Hong *et al.*[230] THPTA (11 µL, 1 M aq., 11 µmol, 750 eq) and $CuSO_4$ (4.4 µL, 1 M, 4.4 µmol, 315 eq.) were pre-mixed (solution A). Propargylated BSA (**22**, 100 µL, 10 mg/mL, 0.014 µmol, 1 eq) was added to a 2 mL Eppendorf tube and was then diluted with Mili-Q water (865 µL). The azidopropyl glycoside (**13-17**/**20**/**21,** 17.4 µL, 50 mM, 0.9 µmol, 65 eq) was added the Eppendorf and mixed in a vortex. Shortly after, solution A was added to the tube. Finally, NaAsc (1.1 µL, 1 M, 1.1 µmol, 80 eq.) was added to the mixture and the reaction was vortexed and set in a heating block at 37 ºC overnight without stirring. The reaction crude was then dialysed for 24 h in Mili-Q water and the glycoconjugate was freeze-dried, redissolved in water to 1 mg/mL and stored at -20 ºC. Yields and MALDI-TOF data for all the glycoconjugates are summarized in **Table 5.3**.

Table 5.3. Yields and mass spectrometry data for the glycoconjugates **23-29** synthesised in this thesis. M_{found}: *m/z* average for the product of the bioconjugation. $M_{glycoside}$: molecular weight of the glycoside used for the bioconjugation. n: number of glycans installed on the BSA, resulting from the difference of mass observed between the glycosylated (M_{found}) and propargylated BSA ($M_{alk\text{-}BSA}$ = 69468), divided by the molecular weight of the glycoside ($M_{glycoside}$).

Glycoconjugate	Glycoside	Amount (mg) / yield	M_{found}	ΔM	$M_{glycoside}$	n
23	Gal (**13**)	0.70 / 70%	70322	854	263	3
24	Lac (**14**)	0.75 / 75%	70138	670	425	2
25	2'FL (**15**)	0.60 / 60%	70596	1128	571	2
26	Glc (**16**)	0.70 / 70%	70539	1071	263	4
27	Man (**17**)	0.70 / 70%	71094	1626	263	6
28	α3α6 (**20**)	0.65 / 65%	70539	1071	587	2
29	3'SL (**21**)	0.60 / 60%	71267	1799	716	3

5.3.3. Glyco AuNPs / AuNSs synthesis

5.3.3.1. *General method C*: passive adsorption of BSA conjugates on 40 nm AuNPs for the synthesis of BSA-AuNPs (30-37)

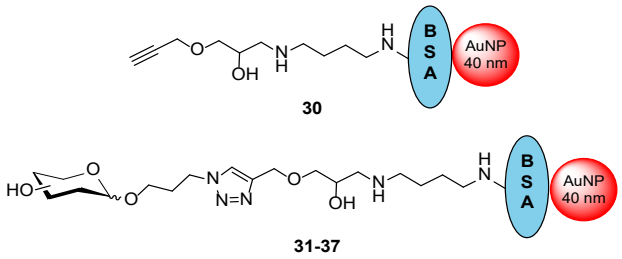

A solution of BSA conjugate (**22-29**) was prepared in citric acid buffer 2 mM pH 5.3 (200 µL, 250 µg/mL). Tween-20 (5 µL, 1% (w/v)) was added to 40 nm AuNPs (100 µl, OD 10). The nanoparticles were spun down (1,650 x g, 10 min). The pellet of the nanoparticles was resuspended in the BSA adduct solution. The mixture was gently pipetted up and down several times. The reaction was set in a rotating mixer at gentle speed for one hour at room temperature, then left covered in aluminium foil at room temperature overnight without further rotation. After the reaction, Tween-20 (1 µL, 10% (w/v)) was added. The AuNPs were spun down (1,650 x g, 10 min), resuspended in 200 µL of PBT (10 mM, pH 7.4), the procedure

was repeatedthree times, then finally resuspended in 100 µL PBT and the OD was measured at 527 nm in agreement with the reported maximum of absorbance for 40 nm AuNPs.[366]

The characterisation of all AuNPs and AuNSs was performed *via* UV-Vis absorption and DLS, data shown in **Table 5.4**.

Table 5.4. Characterisation data for all the glyconanomaterials synthesised in this work. The maximum of absorbance (λ_{max}) is reported together with the semi-height of the peak. (*) Particle diameter was measured through DLS, and the standard deviation was calculated from at least 15 scans.

Particle	Ligand	λ_{max} ± h/2 (nm)	Diameter ± sd (nm) (*)
AuNP	Citrate	525 ± 32	33.6 ± 0.9
AuNP (**30**)	Propargylated BSA	528 ± 32	40.9 ± 0.6
AuNP (**31**)	Gal-BSA	528 ± 32	41.9 ± 0.9
AuNP (**32b**)	Gal_{14}-BSA	526 ± 38	38.9 ± 0.6
AuNP (**32**)	Lac-BSA	528 ± 32	42.2 ± 0.4
AuNP (**33**)	2'FL-BSA	528 ± 32	42.6 ± 0.6
AuNP (**34**)	Glc-BSA	527 ± 32	41.4 ± 0.6
AuNP (**35**)	Man-BSA	527 ± 32	41.0 ± 0.3
AuNP (**36**)	α3α6Man-BSA	527 ± 32	42.6 ± 0.6
AuNP (**37**)	3'SL-BSA	527 ± 32	42.0 ± 0.8
AuNP	NHS ester	530 ± 34	52.3 ± 0.5
AuNP (**39**)	Gal	530 ± 34	57.1 ± 1.5
AuNP (**40**)	Propyl	530 ± 34	52.4 ± 0.5
AuNS	NHS ester	800 ± 186	140.2 ± 0.5
AuNS (**41**)	Gal	800 ± 186	145.4 ± 0.6
AuNS (**42**)	Propyl	800 ± 186	140.5± 0.5

5.3.3.2. *General method D*: NHS-coupling of 3-aminopropyl galactoside to 40 nm AuNPs and 150 nm AuNSs to synthesise Gal-AuNPs (39) and Gal-AuNSs (41)

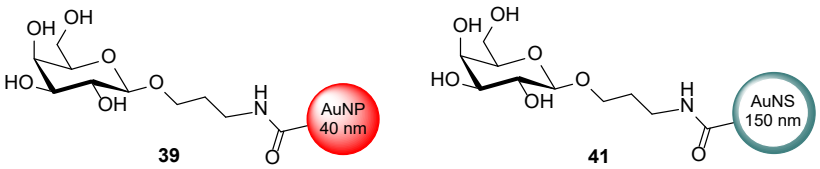

A lyophilised reaction kit (CytoDiagnostics for 40 nm / AuNPs NanoComposix for 150 AuNSs, equivalent to 100 µL OD 20) was allowed to room temperature (20 minutes). Aminopropyl galactoside (**38**, 500 µL in HEPES-PEG reaction buffer, 1 mM for AuNSs). The defrosted AuNPs or AuNSs were resuspended in HEPES-PEG reaction buffer (500 µL) and transferred to the glycoside solution. The reaction tube was kept in the rotating mixer at a gentle rotation speed at room temperature for 6 hours, after which it was quenched with propylamine (10.8 µL, 0.13 mmol). The mixture was spun down (2,200 x g, 15 minutes). The pellet was resuspended in HEPES-PEG reaction buffer (200 µL). The centrifugation and resuspension in reaction buffer steps were repeated three times in total. The pellet was finally resuspended in conjugate diluent [100 of 10 mM PBS, 0.5 % (w/v) BSA, 0.5% (w/v) Tween-20, 0.05% (w/v) NaN_3] to have an OD 20 solution of the functionalised AuNSs or AuNPs.

The characterisation of all AuNPs/AuNSs was performed *via* UV-Vis absorption and DLS, data shown in **Table 5.4**.

5.3.3.3. *General method E*: NHS-coupling of propylamine to 40 nm AuNPs and 150 nm AuNSs to synthesise propyl-AuNPs (40) and propyl-AuNSs (42)

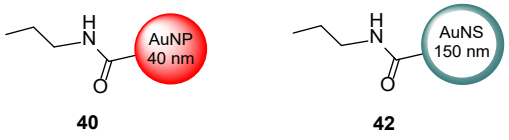

A lyophilised reaction kit (CytoDiagnostics for 40 nm / AuNPs NanoComposix for 150 AuNSs, equivalent to 100 µL OD 20) was allowed to room temperature (20 minutes). The defrosted AuNPs or AuNSs were resuspended in HEPES-PEG reaction buffer (500 µL) and transferred to a solution of propylamine (10.8 µL in 500 µL of HEPES-PEG reaction buffer). The reaction tube was kept in the rotating mixer at gentle rotation speed at room temperature for 6 hours. The mixture was spun down (2,200 x g, 15 minutes). The pellet was resuspended in HEPES-PEG

reaction buffer (200 µL). The centrifugation and resuspension in reaction buffer steps were repeated three times in total. The pellet was finally resuspended in conjugate diluent [100 of 10 mM PBS, 0.5 % (w/v) BSA, 0.5% (w/v) Tween-20, 0.05% (w/v) NaN_3] to have an OD 20 solution of the functionalised AuNSs or AuNPs.

The characterisation of all AuNPs/AuNSs was performed *via* UV-Vis absorption and DLS, data shown in **Table 5.4**.

5.4. Dipstick assay

5.4.1. Assessment of nanoparticle performance *via* dipstick assay

The correct functionalisation and the efficiency of both gold nanoparticles and nanoshells were investigated by their performance using a dipstick assays format. A dipstick consist in a simplified version of a lateral flow device. A schematic representation is shown in **Figure 5.1A**) and it is formed by three components. A nitrocellulose layer with specific characteristics such as the content of surfactant, the porosity, and thickness. On top of the nitrocellulose strip, the cotton wick is generating a pulling force to allow the sample to flow through the nitrocellulose strip. The nitrocellulose and the wick are supported by an underlying a layer of a plastic adhesive backing card holding all the components. Unless differently specified, the usual nitrocellulose employed for the assays was Immunopore RP-90-150. Once assembled the dipsticks are stored under dry conditions in a Falcon tube containing a desiccant pouch. Slightly higher than the middle of the nitrocellulose strip, 0.5 µL of a specified concentration of a selected lectin is deposited as a test spot (**Figure 5.1B**). An performed with a dipstick system consists of four steps (**Figure 5.1C**). In a microfuge tube, 20 µL of stock solution of dipstick buffer, consisting of 10 mM PB, 1% PVP, 50 mM NaCl and 0.05% Tween-20, are added. The corners of the lower edge of the dipstick are cut to give a sharp shape, and the dipstick is introduced in the microfuge tube containing the dipstick buffer. The solution will travel along the nitrocellulose conditioning the strip. In the following step the dipstick is transferred to a second microfuge tube containing 20 µL of running solution. The composition the running solution is, unless specified differently, OD 1 AuNPs, 10 mM PB, 1% (w/v) PVP, 50 mM NaCl, 0.05% (w/v) Tween-20 for AuNPs, or OD 1 AuNSs, 10 mM PB, 1% (w/v) PVP, 150 mM NaCl 1%

(w/v) Triton X100 and 1% (w/v) BSA for AuNSs. The second run was left for 10 minutes, after which the presence or absence of the coloured spot can be observed. The signal intensities were quantified with a gel electrophoresis imager Chemidoc (Biorad).

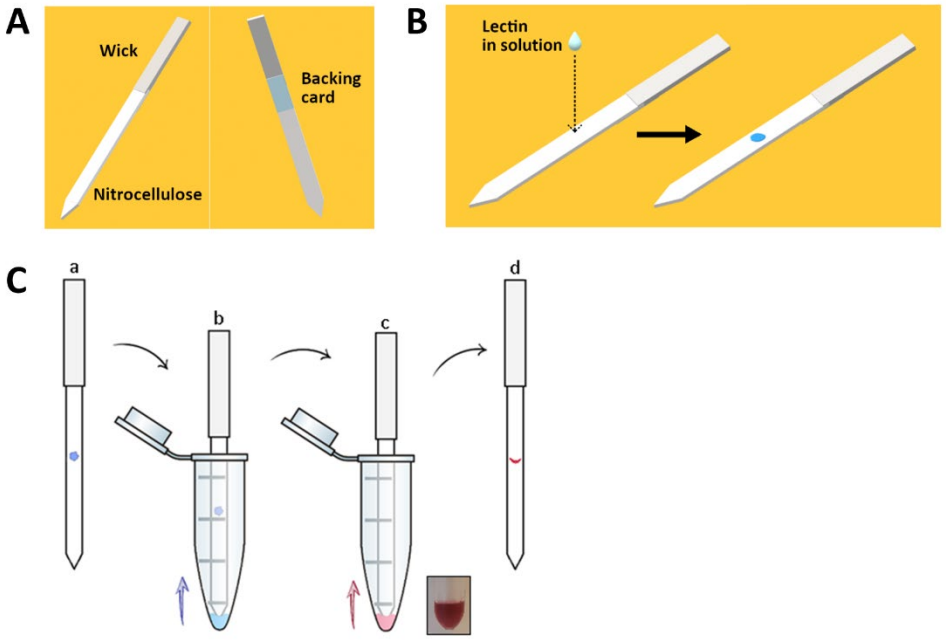

Figure 5.1. (**A**): (*left*) schematic representation of the dipstick front and (*right*) backside. (**B**): an aqueous solution containing the lectin of interest (typically 0.5 µL at a concentration of 5 mg/mL) is spotted on the nitrocellulose strip. (**C**): workflow scheme of the dipstick assay, starting with (**a**) depositing the lectin, (**b**) eluting 20 µL of running buffer to condition the strip, (**c**) eluting the solution of nanoparticles in dipstick buffer and (**d**) development of the signal, typically red-coloured due to the plasmon resonance absorbance of 40 nm AuNPs. The inset shows a photographic image of an Eppendorf vial containing AuNPs at OD 1.

5.5. Microbiology methods

5.5.1. Bacterial growth assays

Pseudomonas aeruginosa strain PAO1 was grown under sterile conditions in 5 mL LB liquid media (1% (m/v) NaCl, 1% (m/v) tryptone, 0.5% (m/v) yeast extract). The culture was incubated overnight at 37 ^{o}C with agitation (200 rpm), after which the OD was measured at 600 nm in a spectrophotometer. The overnight culture was used to inoculate a liquid culture at OD 0.01 in LB media (5 mL). An OD_{600} of 1 was estimated to correspond to 10^8 cells/mL.

5.5.2. FITC-labelling of bacteria

From an overnight culture of *P. aeruginosa*, the cells were diluted in PBS to a final concentration of $5x10^7$ cells in 100 µL. The bacteria were incubated with FITC (10 µL/mL, in the dark) for 1 hour at room temperature in carbonate buffer (10 mM, pH 8.5).

5.5.3. Sample preparation for flow cytometry analysis

For FCM analysis, *P. aeruginosa* (either $5x10^7$ or $5x10^8$ cells in 100 µL) or FITC-labelled *P. aeruginosa* ($5x10^7$ cells in 100 µL) were diluted in PBS (total 800 µL), centrifuged three times (11,600 xg, 5 min) with washing in between to remove unbound ligands, resuspended in Mili-Q water (250 µL) and analysed as below. FCM was also employed to detect LecA by incubating the unlabelled cell suspension ($5x10^7$ cells in 100 µL) with FITC-labelled anti-LecA antibody 10 mM (Biorbyt) or to study the interaction of *P. aeruginosa* with AuNPs by incubating the unlabelled cell suspension ($5x10^7$ cells in 100 µL) with propargyl-BSA-AuNPs (**30**, OD 1) or Gal-BSA-AuNPs (**31**, OD 1). The suspensions were then diluted in PBS (total 800 µL), centrifuged three times (11,600 xg, 5 min) with washing in between to remove unbound ligands and resuspended in Mili-Q water (250 µL).

5.6 Analytical methods for microbial samples

5.6.1. Western Blot analysis

From an overnight culture of *P. aeruginosa*, 1 mL was centrifuged (11,600 xg, 5 min) and resuspended with Mili-Q water (33 µL). NuPAGE LDS sample buffer (x4, 12 µL) was added together with DTT (x10, 5 µL) and the mixture was incubated at 95°C for 20 min. A control sample was prepared from a stock solution of commercial LecA at 1.5 mg/mL by diluting 5 µL into 27.5 µL of water. Following the addition of NuPAGE LDS sample buffer (12.5 µL) and DTT (5 µL), the sample was incubated at 95 °C for 20 min. Pre-casted 4-20% Bis-Tris BioRad mini gels were assembled in the chamber. The gel was run at 200 V, 50 W, and 300 mA for 30 min in Tris/Gly/SDS buffer. Following electrophoresis, the gel was washed for 5 min in Tris/Gly buffer (20 mL). The gel was imaged and subsequently transferred onto a blot membrane (Trans blot turbo, Bio-Rad). The membrane was incubated in blocking buffer (10 mL EveryBlot

Blocking buffer, BioRad) for 15 min. For immunodetection, two different approaches were taken. In the first method, the membrane was incubated with a 1:500 dilution of FITC-labelled anti-LecA rabbit antibody (250 µg/mL stock solution, Biorbyt) in PBST (PB 10 mM pH 7.6, NaCl 50 mM, Tween-20 0.05%), then washed with PBST for 5 min. In the second method, the membrane was incubated with a 1:1000 dilution of anti-LecA rabbit antibody (250 µg/mL stock solution, Biorbyt) in PBST (PB 10 mM pH 7.6, NaCl 50 mM, Tween-20 0.05%), washed with PBST for 5 min, and then incubated with a secondary alkaline phosphatase-conjugated anti-rabbit antibody (0.67 µL from 1 mg/mL stock in PBS) for 30 min. The membrane was incubated with PBST for 5 min to remove the unbound secondary antibody. The membrane was then incubated with NBT/BCID (Sigma-Aldrich, 1 tablet in 10 mL to give a composition of 0.4 mg/ml NBT, 0.19 mg/ml BCIP, 100 mM Tris buffer pH 9.5, 50 mM $MgSO_4$) until colour development. In both methods, the membrane was then imaged using a gel imager.

5.6.2. Flow cytometry

After appropriate sample preparation, 10,000 events were recorded in a flow cytometer. The data were analysed with FlowJo software (BD). FSC: type A-H-W, voltage 324, threshold 500 (laser Sapphire 561 nm, 100mV). SSC: type A-H-W, voltage 247, threshold 500 (laser Sapphire 561 nm, 100 mV). FITC: type A, voltage 405, threshold 100 (laser Sapphire 488 nm, 150 mV).

5.7 Molecular biology methods

5.7.1. DNA purification from bacterial lysate

Genomic DNA was purified from an overnight *P. aeruginosa* culture using a genomic DNA purification kit (Monarch). Briefly, 1 mL of culture was centrifuged (11,600 xg, 5 min) and the cell pellet was resuspended in Tris-HCl buffer (90 µL, 10 mM, pH 6.8). Lysis buffer (100 µL) was added, followed by lysozyme (10 µL, 1 mg/mL) and the suspension was incubated at 37 ^{o}C with agitation (700 rpm) for 10 min. Proteinase K (10 µL, 1 mg/mL) and RNase A (3 µL, 1 mb/mL) were added and the mixture was incubated at 56 ^{o}C with agitation (700 rpm) for 10 min. Genomic DNA binding buffer (400 µL) was added to the mixture and vortexed for 10 sec. The suspension was transferred onto a purification column pre-inserted into a collection tube.

The column was centrifuged (1,000 xg, 3 min; then 15,000, 1 min) and the liquid in the collection tube was discarded. The column was loaded into a new collection tube and genomic DNA wash buffer (500 µL) was added. The column was centrifuged (15,000 xg, 1 min) and the liquid in the collection tube was discarded. The addition of wash buffer and centrifuge step were repeated. The column was then transferred into a DNase-free tube and genomic DNA elution buffer (100 µL, preheated at 60 ^{o}C) was added. The column was incubated at room temperature for 1 min, after which it was centrifuged (15,000 xg, 1 min). The liquid in the tube was collected. The concentration of the purified DNA was determined following the measurement of absorbance at 280 nm in a spectrophotometer.

5.7.2. Polymerase chain reaction DNA amplification

The purified DNA from bacterial samples (*Section 5.7.1.)* was amplified using DNA primers designed using Artemis/Snapgene. For the LecA gene, these included a forward primer (sequence 5' --> 3': TAT ATT CAA TTC ACT GGC GG) and a reverse primer (sequence 5' --> 3': TTC GAT ACT CTT GTC ATT GG). The PCR reaction consisted of Q5 DNA polymerase (0.02 U/µL) mixed with the primers (each 0.5 µM) and nucleotides triphosphate (dNTP, 200 µM) in Q5 PCR reaction buffer (NewEngland Biolabs) in a thermocycler (Biometra T-Gradient Thermoblock) preheated at 99^{o}C. The DNA was denatured at 98^{o}C (30 s), followed by 34 cycles consisting of 98^{o}C (10 s) – 55^{o}C (20 s) – 72^{o}C (3 min), and a final extension phase at 72^{o}C (2 min). The PCR products were purified using a PCR DNA cleanup kit (Monarch). Briefly, the PCR products were diluted with binding buffer in a buffer-sample 5:1 ratio. The sample was loaded onto a purification column and centrifuged (15,000 xg, 1 min). The column was transferred into a new collection tube and wash buffer (200 µL) was added. After centrifugation (15,000 xg, 1 min), the liquid was discarded. The addition of wash buffer and centrifuge step were repeated. The column was then transferred into a new collection tube, and DNA elution buffer (21 µL) was added to it. The column was centrifuged (15,000 xg, 1 min) and the liquid in the tube was collected. The concentration of the purified DNA was determined following the measurement of absorbance at 280 nm in a spectrophotometer. The DNA was sequenced by Dr David Baker and Dr Rhiannon Evans (Quadram Institute Bioscience). Briefly, the PCR products were indexed using Nextera XT indexing primers (Illumina) and sequenced using Illumina MiSeq. The reads were assembled by Dr Andrew Bell using SPAdes.[367]

CHAPTER 6

REFERENCES

(1) European Commission. *Horizon 2020 Work Programme 2019-2020. Marie Sklodowska-Curie Actions*; 2019.

(2) Dwek, R. A. Glycobiology: Toward Understanding the Function of Sugars. *Chem. Rev.* **1996**, *96* (2), 683–720. https://doi.org/10.1021/cr940283b.

(3) Seeberger, P. H. Monosaccharide Diversity. In *Essentials in Glycobiology*; Varki, A., Commings, R., Esko, J., Stanley, P., Hart, G. W., Aebi, M., Mohnen, D., Kinoshita, T., Packer, N., Prestegard, J., Schnaar, R., Seeberger, P., Eds.; Cold Spring Harbor Laboratory Press: New York, 2022.

(4) Varki, A.; Kornfeld, S. Historical Background and Overview. In *Essentials of Glycobiology.*; Varki A, Cummings R, Esko J, Stanley P, Hart G, Aebi M, Mohnen D, Kinoshita T, Packer N, Prestegard J, Schnaar R, Seeberger P, Eds.; Cold Spring Harbor: New York, 2017. https://doi.org/10.1101/glycobiology.3e.001.

(5) Gaudette, S.; Hughes, D.; Boller, M. The Endothelial Glycocalyx: Structure and Function in Health and Critical Illness. *J. Vet. Emerg. Crit. Care* **2020**, *30* (2), 117–134. https://doi.org/10.1111/vec.12925.

(6) Rillahan, C. D.; Paulson, J. C. Glycan Microarrays for Decoding the Glycome. *Annu. Rev. Biochem* **2011**, *80*, 797–823. https://doi.org/10.1146/annurev-biochem-061809-152236.

(7) Lundquist, J. J.; Toone, E. J. The Cluster Glycoside Effect. *Chem. Rev.* **2002**, *102* (2), 555–578. https://doi.org/10.1021/cr000418f.

(8) Dugan, A. E.; Peiffer, A. L.; Kiessling, L. L. Advances in Glycoscience to Understand Viral Infection and Colonization. *Nat. Methods* **2022**, *19* (4), 384–387. https://doi.org/10.1038/s41592-022-01451-0.

(9) Lewis, A.; Kohler, J.; Aebi, M. Microbial Lectins: Hemagglutinins, Adhesins, and Toxins. In *Essentials in Glycobiology*; Varki, A., Cummings, R., Esko, J., Stanley, P., Hart, G., Aebi, M., Mohnen, D., Kinoshita, T., Packer, N. H., Prestegard, J., Schnaar, R., Seeberger, P., Eds.; Cold Spring Harbor Laboratory Press: New York, 2022.

(10) Day, C. J.; Semchenko, E. A.; Korolik, V. Glycoconjugates Play a Key Role in Campylobacter Jejuni Infection: Interactions between Host and Pathogen. *Front. Cell. Infect. Microbiol.* **2012**, *2*, 9. https://doi.org/10.3389/fcimb.2012.00009.

(11) Sharon, N. Carbohydrate-Lectin Interaction in Infectious Disease. In *Toward Anti-Adhesion Therapy for Microbial Diseases. Advances in Experimental Medicine and Biology*; Kahane I, Ofek I, Eds.; Springer: Boston, 1996; Vol. 408, pp 1–8. https://doi.org/https://doi.org/10.1007/978-1-4613-0415-9_1.

(12) Walz, A.; Odenbreit, S.; Mahdavi, J.; Borén, T.; Ruhl, S. Identification and Characterization of Binding Properties of Helicobacter Pylori by Glycoconjugate Arrays. *Glycobiology* **2005**, *15* (7), 700–708. https://doi.org/10.1093/glycob/cwi049.

(13) Ghazarian, H.; Idoni, B.; Oppenheimer, S. B. A Glycobiology Review: Carbohydrates, Lectins and Implications in Cancer Therapeutics. *Acta Histochem.* **2011**, *113* (3), 236–247. https://doi.org/10.1016/j.acthis.2010.02.004.

(14) Weis, W. I.; Drickamer, K. Structural Basis of Lectin-Carbohydrate Recognition. *Annu. Rev. Biochem.* **1996**, *65*, 441–473. https://doi.org/10.1146/annurev.bi.65.070196.002301.

(15) Johnson, Q. R.; Lindsay, R. J.; Petridis, L.; Shen, T. Investigation of Carbohydrate Recognition via Computer Simulation. *Molecules* **2015**, *20* (5), 7700–7718. https://doi.org/10.3390/molecules20057700.

(16) Del, M.; Fernández-Alonso, C.; Díaz, D.; Berbis, M. Á.; Marcelo, F.; Cañada, J.; Jiménez-Barbero, J. Protein-Carbohydrate Interactions Studied by NMR: From Molecular Recognition to Drug Design. *Curr. Protein Pept. Sci.* **2012**, *13*, 816–830. https://doi.org/10.2174/138920312804871175.

(17) Zelensky, A. N.; Gready, J. E. The C-Type Lectin-like Domain Superfamily. *FEBS Journal* **2005**, *272* (24), 6179–6217. https://doi.org/10.1111/j.1742-4658.2005.05031.x.

(18) Imberty, A.; Gautier, C.; Lescar, J.; Pérez, S.; Wyns, L.; Loris, R. An Unusual Carbohydrate Binding Site Revealed by the Structures of Two Maackia Amurensis Lectins Complexed with Sialic Acid-Containing Oligosaccharides. *J. Biol. Chem.* **2000**, *275* (23), 17541–17548. https://doi.org/10.1074/jbc.M000560200.

(19) Lambright, D. G. Membrane Recruitment of Signaling Domains. In *Comprehensive Biophysics*; Egelman, E. H., Ed.; Elsevier Inc., 2012; Vol. 5, pp 239–240. https://doi.org/10.1016/B978-0-12-374920-8.00519-1.

(20) Popovych, N.; Sun, S.; Ebright, R. H.; Kalodimos, C. G. Dynamically Driven Protein Allostery. *Nat. Struct. Mol. Biol.* **2006**, *13* (9), 831–838. https://doi.org/10.1038/nsmb1132.

(21) Allen, M. D.; Grummitt, C. G.; Hilcenko, C.; Min, S. Y.; Tonkin, L. M.; Johnson, C. M.; Freund, S. M.; Bycroft, M.; Warren, A. J. Solution Structure of the Nonmethyl-CpG-

Binding CXXC Domain of the Leukaemia-Associated MLL Histone Methyltransferase. *EMBO Journal* **2006**, *25* (19), 4503–4512. https://doi.org/10.1038/sj.emboj.7601340.

(22) Celie, P. H. N.; Kasheverov, I. E.; Mordvintsev, D. Y.; Hogg, R. C.; van Nierop, P.; van Elk, R.; van Rossum-Fikkert, S. E.; Zhmak, M. N.; Bertrand, D.; Tsetlin, V.; Sixma, T. K.; Smit, A. B. Crystal Structure of Nicotinic Acetylcholine Receptor Homolog AChBP in Complex with an α-Conotoxin PnIA Variant. *Nat. Struct. Mol. Biol.* **2005**, *12* (7), 582–588. https://doi.org/10.1038/nsmb951.

(23) Dam, T. K.; Roy, R.; Das, S. K.; Oscarson, S.; Brewer, C. F. Binding of Multivalent Carbohydrates to Concanavalin A and Dioclea Grandiflora Lectin. Thermodynamic Analysis of the "Multivalency Effect." *J. Biol. Chem.* **2000**, *275* (19), 14223–14230. https://doi.org/10.1074/jbc.275.19.14223.

(24) Hirabayashi, J.; Yamada, M.; Kuno, A.; Tateno, H. Lectin Microarrays: Concept, Principle and Applications. *Chem. Soc. Rev.* **2013**, *42* (10), 4443–4458. https://doi.org/10.1039/c3cs35419a.

(25) Blixt, O.; Head, S.; Mondala, T.; Scanlan, C.; Huflejt, M. E.; Alvarez, R.; Bryan, M. C.; Fazio, F.; Calarese, D.; Stevens, J.; Razi, N.; Stevens, D. J.; Skehel, J. J.; van Die, I.; Burton, D. R.; Wilson, I. A.; Cummings, R.; Bovin, N.; Wong, C.-H.; Paulson, J. C. Printed Covalent Glycan Array for Ligand Profiling of Diverse Glycan Binding Proteins. *PNAS* **2004**, *101* (49), 17033–17038. https://doi.org/https://doi.org/10.1073/pnas.0407902101.

(26) Mccoy, J. P.; Varani, J.; Goldstein, I. J. Enzyme-Linked Lectin Assay (ELLA) II. Detection of Carbohydrate Groups on the Surface of Unfixed Cells. *Exp. Cell. Res.* **1984**, *151*, 96–103. https://doi.org/10.1016/0014-4827(84)90359-8.

(27) Kohn, M.; Benito, J. M.; Mellet, C. O.; Lindhorst, T. K.; Garcia Fernández, J. M. Functional Evaluation of Carbohydrate-Centred Glycoclusters by Enzyme-Linked Lectin Assay: Ligands for Concanavalin A. *ChemBioChem* **2004**, *5* (6), 771–777. https://doi.org/10.1002/cbic.200300807.

(28) Boguszewska, K.; Szewczuk, M.; Urbaniak, S.; Karwowski, B. T. Review: Immunoassays in DNA Damage and Instability Detection. *Cell. Mol. Life Sci.* **2019**, *76* (23), 4689–4704. https://doi.org/10.1007/s00018-019-03239-6.

(29) Karamanska, R.; Clarke, J.; Blixt, O.; MacRae, J. I.; Zhang, J. Q.; Crocker, P. R.; Laurent, N.; Wright, A.; Flitsch, S. L.; Russell, D. A.; Field, R. A. Surface Plasmon Resonance Imaging for Real-Time, Label-Free Analysis of Protein Interactions with Carbohydrate Microarrays. *Glycoconj. J* **2008**, *25* (1), 69–74. https://doi.org/10.1007/s10719-007-9047-y.

(30) Dhayal, M.; Ratner, D. M. XPS and SPR Analysis of Glycoarray Surface Density. *Langmuir* **2009**, *25* (4), 2181–2187. https://doi.org/10.1021/la8031122.

(31) Prien, J. M.; Ashline, D. J.; Lapadula, A. J.; Zhang, H.; Reinhold, V. N. The High Mannose Glycans from Bovine Ribonuclease B Isomer Characterization by Ion Trap MS. *J. Am.*

Soc. Mass Spectrom. **2009**, *20* (4), 539–556. https://doi.org/10.1016/j.jasms.2008.11.012.

(32) Katz, E.; Willner, I. Integrated Nanoparticle-Biomolecule Hybrid Systems: Synthesis, Properties, and Applications. *Angew. Chem. Int. Ed.* **2004**, *43* (45), 6042–6108. https://doi.org/10.1002/anie.200400651.

(33) Baron, R.; Willner, B.; Willner, I. Biomolecule-Nanoparticle Hybrids as Functional Units for Nanobiotechnology. *Chem. Comm.* **2007**, No. 4, 323–332. https://doi.org/10.1039/b610721b.

(34) Peng, X.; Wickham, J.; Alivisatos, A. P. Kinetics of II-VI and III-V Colloidal Semiconductor Nanocrystal Growth: "Focusing" of Size Distributions [15]. *J. Am. Chem. Soc.* **1998**, *120* (21), 5343–5344. https://doi.org/10.1021/ja9805425.

(35) Schultz, D. A. Plasmon Resonant Particles for Biological Detection. *Curr. Opin. Biotechnol.* **2003**, *14* (1), 13–22. https://doi.org/10.1016/S0958-1669(02)00015-0.

(36) Liz-Marzán, L. M. Tailoring Surface Plasmons through the Morphology and Assembly of Metal Nanoparticles. *Langmuir* **2006**, *22* (1), 32–41. https://doi.org/10.1021/la0513353.

(37) Schofield, C. L.; Haines, A. H.; Field, R. A.; Russell, D. A. Silver and Gold Glyconanoparticles for Colorimetric Bioassays. *Langmuir* **2006**, *22* (15), 6707–6711. https://doi.org/10.1021/la060288r.

(38) de la Fuente, J. M.; Barrientos, A. G.; Rojas, T. C.; Rojo, J.; Cañada, J.; Fernández, A.; Penadés, S. Gold Glyconanoparticles as Water-Soluble Polyvalent Models To Study Carbohydrate Interactions. *Angew. Chem. Int. Ed.* **2001**, *40* (12), 2257–2261. https://doi.org/https://doi.org/10.1002/1521-3773(20010618)40:12<2257::AID-ANIE2257>3.0.CO;2-S.

(39) Barrientos, Á. G.; de la Fuente, J. M.; Rojas, T. C.; Fernández, A.; Penadés, S. Gold Glyconanoparticles: Synthetic Polyvalent Ligands Mimicking Glycocalyx-like Surfaces as Tools for Glycobiological Studies. *Chem. Eur. J.* **2003**, *9* (9), 1909–1921. https://doi.org/10.1002/chem.200204544.

(40) de la Fuente, J. M.; Penadés, S. Glyconanoparticles: Types, Synthesis and Applications in Glycoscience, Biomedicine and Material Science. *Biochim. Biophys. Acta Gen. Subj.* **2006**, *1760* (4), 636–651. https://doi.org/10.1016/j.bbagen.2005.12.001.

(41) Compostella, F.; Pitirollo, O.; Silvestri, A.; Polito, L. Glyco-Gold Nanoparticles: Synthesis and Applications. *Beilstein J. Org. Chem.* **2017**, *13*, 1008–1021. https://doi.org/10.3762/bjoc.13.100.

(42) Richards, S. J.; Fullam, E.; Besra, G. S.; Gibson, M. I. Discrimination between Bacterial Phenotypes Using Glyco-Nanoparticles and the Impact of Polymer Coating on Detection Readouts. *J. Mater. Chem. B* **2014**, *2* (11), 1490–1498. https://doi.org/10.1039/c3tb21821j.

(43) Poonthiyil, V.; Golovko, V. B.; Fairbanks, A. J. Size-Optimized Galactose-Capped Gold Nanoparticles for the Colorimetric Detection of Heat-Labile Enterotoxin at Nanomolar Concentrations. *Org. Biomol. Chem*. **2015**, *13* (18), 5215–5223. https://doi.org/10.1039/c5ob00447k.

(44) Poonthiyil, V.; Nagesh, P. T.; Husain, M.; Golovko, V. B.; Fairbanks, A. J. Gold Nanoparticles Decorated with Sialic Acid Terminated Bi-Antennary N-Glycans for the Detection of Influenza Virus at Nanomolar Concentrations. *ChemistryOpen* **2015**, *4* (6), 708–716. https://doi.org/10.1002/open.201500109.

(45) Hernando, P. J.; Dedola, S.; Marín, M. J.; Field, R. A. Recent Developments in the Use of Glyconanoparticles and Related Quantum Dots for the Detection of Lectins, Viruses, Bacteria and Cancer Cells. *Front. Chem.* **2021**, *9*, 668509. https://doi.org/10.3389/fchem.2021.668509.

(46) Marín, M. J.; Schofield, C. L.; Field, R. A.; Russell, D. A. Glyconanoparticles for Colorimetric Bioassays. *Analyst* **2015**, *140* (1), 59–70. https://doi.org/10.1039/c4an01466a.

(47) Marín, M. J.; Rashid, A.; Rejzek, M.; Fairhurst, S. A.; Wharton, S. A.; Martin, S. R.; McCauley, J. W.; Wileman, T.; Field, R. A.; Russell, D. A. Glyconanoparticles for the Plasmonic Detection and Discrimination between Human and Avian Influenza Virus. *Org. Biomol. Chem.* **2013**, *11* (41), 7101–7107. https://doi.org/10.1039/c3ob41703d.

(48) Zheng, L.; Wei, J.; Lv, X.; Bi, Y.; Wu, P.; Zhang, Z.; Wang, P.; Liu, R.; Jiang, J.; Cong, H.; Liang, J.; Chen, W.; Cao, H.; Liu, W.; Gao, G. F.; Du, Y.; Jiang, X.; Li, X. Detection and Differentiation of Influenza Viruses with Glycan-Functionalized Gold Nanoparticles. *Biosens. Bioelectron.* **2017**, *91* (December 2016), 46–52. https://doi.org/10.1016/j.bios.2016.12.037.

(49) Uzawa, H.; Ohga, K.; Shinozaki, Y.; Ohsawa, I.; Nagatsuka, T.; Seto, Y.; Nishida, Y. A Novel Sugar-Probe Biosensor for the Deadly Plant Proteinous Toxin, Ricin. *Biosens. Bioelectron.* **2008**, *24* (4), 923–927. https://doi.org/10.1016/j.bios.2008.07.049.

(50) Schofield, C. L.; Mukhopadhyay, B.; Hardy, S. M.; McDonnell, M. B.; Field, R. A.; Russell, D. A. Colorimetric Detection of Ricinus Communis Agglutinin 120 Using Optimally Presented Carbohydrate-Stabilised Gold Nanoparticles. *Analyst* **2008**, *133* (5), 626–634. https://doi.org/10.1039/b715250g.

(51) Turnbull, W. B.; Precious, B. L.; Homans, S. W. Dissecting the Cholera Toxin-Ganglioside GM1 Interaction by Isothermal Titration Calorimetry. *J. Am. Chem. Soc.* **2004**, *126* (4), 1047–1054. https://doi.org/10.1021/ja0378207.

(52) Schofield, C. L.; Field, R. A.; Russell, D. A. Glyconanoparticles for the Colorimetric Detection of Cholera Toxin. *Anal. Chem.* **2007**, *79* (4), 1356–1361. https://doi.org/10.1021/ac061462j.

(53) Schofield, C. L.; Marín, M. J.; Rejzek, M.; Crocker, P. R.; Field, R. A.; Russell, D. A. Detection of MSiglec-E, in Solution and Expressed on the Surface of Chinese Hamster

Ovary Cells, Using Sialic Acid Functionalised Gold Nanoparticles. *Analyst* **2016**, *141* (20), 5799–5809. https://doi.org/10.1039/c6an01230b.

(54) García Calavia, P.; Chambrier, I.; Cook, M. J.; Haines, A. H.; Field, R. A.; Russell, D. A. Targeted Photodynamic Therapy of Breast Cancer Cells Using Lactose-Phthalocyanine Functionalized Gold Nanoparticles. *J. Colloid Interface Sci.* **2018**, *512*, 249–259. https://doi.org/10.1016/j.jcis.2017.10.030.

(55) Barondess, S. H.; Cooper$, D. N. W.; Gitts, M. A.; Lefflerm, H. Galectins: Structure and Function of a Large Family of Animal Lectins. *J. Biol. Chem.* **1994**, *269* (33), 20807–20810. https://doi.org/https://doi.org/10.1016/S0021-9258(17)31891-4.

(56) Zhang, Z.; Schepens, B.; Nuhn, L.; Saelens, X.; Schotsaert, M.; Callewaert, N.; de Rycke, R.; Zhang, Q.; Moins, S.; Benali, S.; Mespouille, L.; Hoogenboom, R.; de Geest, B. G. Influenza-Binding Sialylated Polymer Coated Gold Nanoparticles Prepared via RAFT Polymerization and Reductive Amination. *Chem. Comm.* **2016**, *52* (16), 3352–3355. https://doi.org/10.1039/c6cc00501b.

(57) Reynolds, M.; Marradi, M.; Imberty, A.; Penadés, S.; Pérez, S. Multivalent Gold Glycoclusters: High Affinity Molecular Recognition by Bacterial Lectin PA-IL. *Chem. Eur. J.* **2012**, *18* (14), 4264–4273. https://doi.org/10.1002/chem.201102034.

(58) Reynolds, M.; Marradi, M.; Imberty, A.; Penadés, S.; Pérez, S. Influence of Ligand Presentation Density on the Molecular Recognition of Mannose-Functionalised Glyconanoparticles by Bacterial Lectin BC2L-A. *Glycoconj. J.* **2013**, *30* (8), 747–757. https://doi.org/10.1007/s10719-013-9478-6.

(59) Chiodo, F.; Marradi, M.; Tefsen, B.; Snippe, H.; van Die, I.; Penadés, S. High Sensitive Detection of Carbohydrate Binding Proteins in an ELISA-Solid Phase Assay Based on Multivalent Glyconanoparticles. *PLoS One* **2013**, *8* (8), 1–11. https://doi.org/10.1371/journal.pone.0073027.

(60) Arosio, D.; Chiodo, F.; Reina, J. J.; Marelli, M.; Penadés, S.; van Kooyk, Y.; Garcia-Vallejo, J. J.; Bernardi, A. Effective Targeting of DC-Sign by α-Fucosylamide Functionalized Gold Nanoparticles. *Bioconjug. Chem.* **2014**, *25* (12), 2244–2251. https://doi.org/10.1021/bc500467u.

(61) Scanlan, C. N.; Pantophlet, R.; Wormald, M. R.; Ollmann Saphire, E.; Stanfield, R.; Wilson, I. A.; Katinger, H.; Dwek, R. A.; Rudd, P. M.; Burton, D. R. The Broadly Neutralizing Anti-Human Immunodeficiency Virus Type 1 Antibody 2G12 Recognizes a Cluster of A1→2 Mannose Residues on the Outer Face of Gp120. *J. Virol.* **2002**, *76* (14), 7306–7321. https://doi.org/10.1128/jvi.76.14.7306-7321.2002.

(62) Budhadev, D.; Poole, E.; Nehlmeier, I.; Liu, Y.; Hooper, J.; Kalverda, E.; Akshath, U.; Hondow, N.; Turnbull, W. B.; Pöhlmann, S.; Guo, Y.; Zhou, D. Glycan-Gold Nanoparticles as Multifunctional Probes for Multivalent Lectin−Carbohydrate Binding: Implications for Blocking Virus Infection and Nanoparticle Assembly. *J. Am. Chem. Soc.* **2020**, *142*, 18022–18034. https://doi.org/https://doi.org/10.1021/jacs.0c06793.

(63) Ajish, J. K.; Kanagare, A. B.; Kumar, K. S. A.; Subramanian, M.; Ballal, A. D.; Kumar, M. Self-Assembled Glycobis(Acrylamide)-Stabilized Gold Nanoparticles for Fluorescent Turn-on Sensing of Lectin and Escherichia Coli. *ACS Appl. Nano. Mater.* **2020**, *3* (2), 1307–1317. https://doi.org/10.1021/acsanm.9b02127.

(64) Wang, A.; Perera, Y. R.; Davidson, M. B.; Fitzkee, N. C. Electrostatic Interactions and Protein Competition Reveal a Dynamic Surface in Gold Nanoparticle-Protein Adsorption. *J. Phys. Chem. C* **2016**, *120* (42), 24231–24239. https://doi.org/10.1021/acs.jpcc.6b08469.

(65) Jazayeri, M. H.; Amani, H.; Pourfatollah, A. A.; Pazoki-Toroudi, H.; Sedighimoghaddam, B. Various Methods of Gold Nanoparticles (GNPs) Conjugation to Antibodies. *Sens. Biosensing Res.* **2016**, *9*, 17–22. https://doi.org/10.1016/j.sbsr.2016.04.002.

(66) Sánchez-Pomales, G.; Morris, T. A.; Falabella, J. B.; Tarlov, M. J.; Zangmeister, R. A. A Lectin-Based Gold Nanoparticle Assay for Probing Glycosylation of Glycoproteins. *Biotechnol. Bioeng* **2012**, *109*, 2240–2249. https://doi.org/10.1002/bit.24513/abstract.

(67) Kong, Y.; Liu, F.; Liu, Z.; Zhao, J.; Wu, Q.; Zhang, X.; Liu, M.; Zhang, H.; Liu, S.; Zhang, X.; Chen, M. Synthesis of Globotriose-Modified Peptides for the Preparation of a Colorimetric Biosensor to Detect Shiga Toxins. *Talanta* **2022**, *243*. https://doi.org/10.1016/j.talanta.2022.123353.

(68) Mukhopadhyay, B.; Martins, M. B.; Karamanska, R.; Russell, D. A.; Field, R. A. Bacterial Detection Using Carbohydrate-Functionalised CdS Quantum Dots: A Model Study Exploiting E. Coli Recognition of Mannosides. *Tetrahedron Lett.* **2009**, *50* (8), 886–889. https://doi.org/10.1016/j.tetlet.2008.12.029.

(69) Ahn, K. S.; Lim, K. R.; Jeong, D.; Lee, B. Y.; Kim, K. S.; Lee, W. Y. Fluorescence Energy Transfer Inhibition Bioassay for Cholera Toxin Based on Galactose-Stabilized Gold Nanoparticles and Amine-Terminated Quantum Dots. *Microchem. J.* **2016**, *124*, 9–14. https://doi.org/10.1016/j.microc.2015.07.007.

(70) Ajish, J. K.; Ajish Kumar, K. S.; Ruhela, A.; Subramanian, M.; Ballal, A. D.; Kumar, M. AIE Based Fluorescent Self Assembled Glycoacrylamides for E.Coli Detection and Cell Imaging. *Sens. Actuators B Chem.* **2018**, *255*, 1726–1734. https://doi.org/10.1016/j.snb.2017.08.188.

(71) Zhang, C.; Shi, D. T.; Yan, K. C.; Sedgwick, A. C.; Chen, G. R.; He, X. P.; James, T. D.; Ye, B.; Hu, X. le; Chen, D. A Glycoconjugate-Based Gold Nanoparticle Approach for the Targeted Treatment of Pseudomonas Aeruginosa Biofilms. *Nanoscale* **2020**, *12* (45), 23234–23240. https://doi.org/10.1039/d0nr05365a.

(72) Zhang, Z.; Qi, X.; Chai, J.; Wu, P.; Lv, X.; Cheng, S.; Li, X. Detection of Glycan-Binding Proteins Using Glycan-Functionalized Quantum Dots and Gold Nanoparticles. *J. Carbohydr. Chem.* **2018**, *37* (4), 199–209. https://doi.org/10.1080/07328303.2018.1451875.

(73) Hooper, J.; Liu, Y.; Budhadev, D.; Ainaga, D. F.; Hondow, N.; Zhou, D.; Guo, Y. Polyvalent Glycan Quantum Dots as a Multifunctional Tool for Revealing Thermodynamic, Kinetic, and Structural Details of Multivalent Lectin-Glycan Interactions. *ACS Appl. Mater. Interfaces* **2022**, *14* (42), 47385–47396. https://doi.org/10.1021/acsami.2c11111.

(74) Weeramange, C. J.; Fairlamb, M. S.; Singh, D.; Fenton, A. W.; Swint-Kruse, L. The Strengths and Limitations of Using Biolayer Interferometry to Monitor Equilibrium Titrations of Biomolecules. *Prot. Sci.* **2020**, *29* (4), 1018–1034. https://doi.org/10.1002/pro.3827.

(75) Wallner, J.; Sissolak, B.; Sommeregger, W.; Lingg, N.; Striedner, G.; Vorauer-Uhl, K. Lectin Bio-Layer Interferometry for Assessing Product Quality of Fc- Glycosylated Immunoglobulin G. *Biotechnol. Prog.* **2019**, *35* (5). https://doi.org/10.1002/btpr.2864.

(76) Samuel, E. L. G.; Holmes, S. L.; Young, D. W. Processing Binding Data Using an Open-Source Workflow. *J. Cheminform.* **2021**, *13* (99). https://doi.org/10.1186/s13321-021-00577-1.

(77) Bai, N.; Roder, H.; Dickson, A.; Karanicolas, J. Isothermal Analysis of ThermoFluor Data Can Readily Provide Quantitative Binding Affinities. *Sci. Rep.* **2019**, *9* (1). https://doi.org/10.1038/s41598-018-37072-x.

(78) Bhayani, J. A.; Ballicora, M. A. Determination of Dissociation Constants of Protein Ligands by Thermal Shift Assay. *Biochem. Biophys. Res. Commun.* **2022**, *590*, 1–6. https://doi.org/10.1016/j.bbrc.2021.12.041.

(79) Musshoff, F.; Madea, B. Ricin Poisoning and Forensic Toxicology. *Drug Test Anal.* **2009**, *1* (4), 184–191. https://doi.org/10.1002/dta.27.

(80) Rutenber, E.; Katzin, B. J.; Ernst, S.; Collins, E. J.; Mlsna, D.; Ready, M. P.; Robertus, J. D. Crystallographic Refinement of Ricin to 2.5 A. *Proteins: Struct. Funct. Genet.* **1991**, *10*, 240–250. https://doi.org/10.1002/prot.340100308.

(81) Ler, S. G.; Lee, F. K.; Gopalakrishnakone, P. Trends in Detection of Warfare Agents. Detection Methods for Ricin, Staphylococcal Enterotoxin B and T-2 Toxin. *J. Chromatogr. A* **2006**, *1133* (1–2), 1–12. https://doi.org/10.1016/j.chroma.2006.08.078.

(82) Etemad, L.; Moshiri, M.; Hamid, F. Ricin Toxicity: Clinical and Molecular Aspects. *Rep. Biochem. Mol. Biol.* **2016**, *4* (2).

(83) Sandvig, K.; Grimmer, S.; Lauvrak, S.; Torgersen, M.; Skretting, G.; van Deurs, B.; Iversen, T. Pathways Followed by Ricin and Shiga Toxin into Cells. *Histochem. Cell. Biol.* **2002**, *117* (2), 131–141. https://doi.org/10.1007/s00418-001-0346-2.

(84) Konareva, N. V.; Gabdulkhakov, A. G.; Eschenburg, S.; Stoeva, S.; Popov, A. N.; Krauspenhaar, R.; Andrianova, M. E.; Savochkina, Yu.; Agapov, I. I.; Tonevitskii, A. G.; Kornev, A. N.; Kornilov, V. v.; Zaitsev, V. N.; Voelter, W.; Betzel, Ch.; Nikonov, S. v.;

Vainshtein, B. K.; Mikhailov, A. M. Topology of the Polypeptide Chain in the Complex of Agglutinin from Castor Bean Seeds with B-D Galactose in the Crystalline State. *Crystallogr. Rep.* **2001**, *46* (5), 792–800. https://doi.org/10.1134/1.1405866.

(85) Sweeney, E. C.; Tonevitsky, A. G.; Temiakov, D. E.; Agapov, I. I.; Saward, S.; Palmer, R. A. Preliminary Crystallographic Characterization of Ricin Agglutinin. *Proteins: Struct. Funct. Genet.* **1996**, *28*, 586–589. https://doi.org/10.1002/(sici)1097-0134(199708)28:4<586::aid-prot12>3.0.co;2-c.

(86) Lord, J. M.; Roberts, L. M.; Robertus, J. D. Ricin: Structure, Mode of Action, and Some Current Applications. *The FASEB Journal* **1994**, *8* (2), 201–208. https://doi.org/10.1096/fasebj.8.2.8119491.

(87) Baenziger, J. U.; Fiete, D. Structural Determinants of Ricinus Communis Agglutinin and Toxin Specificity for Oligosaccharides. *J. Biol. Chem.* **1979**, *254* (19), 9795–9799. https://doi.org/10.1016/s0021-9258(19)83586-x.

(88) Green, E. D.; Brodbeck, R. M.; Baenziger, J. U. Lectin Affinity High-Performance Liquid Chromatography. Interactions of N-Glycanase-Released Oligosaccharides with Ricinus Communis Agglutinin I and Ricinus Communis Agglutinin II. *J. Biol. Chem.* **1987**, *262* (25), 12030–12039. https://doi.org/10.1016/s0021-9258(18)45313-6.

(89) Itakura, Y.; Nakamura-Tsuruta, S.; Kominami, J.; Sharon, N.; Kasai, K. I.; Hirabayashi, J. Systematic Comparison of Oligosaccharide Specificity of Ricinus Communis Agglutinin I and Erythrina Lectins: A Search by Frontal Affinity Chromatography. *J Biochem* **2007**, *142* (4), 459–469. https://doi.org/10.1093/jb/mvm153.

(90) Tateno, H.; Mori, A.; Uchiyama, N.; Yabe, R.; Iwaki, J.; Shikanai, T.; Angata, T.; Narimatsu, H.; Hirabayashi, J. Glycoconjugate Microarray Based on an Evanescent-Field Fluorescence-Assisted Detection Principle for Investigation of Glycan-Binding Proteins. *Glycobiology* **2008**, *18* (10), 789–798. https://doi.org/10.1093/glycob/cwn068.

(91) Wang, Y.; Yu, G.; Han, Z.; Yang, B.; Hu, Y.; Zhao, X.; Wu, J.; Lv, Y.; Chai, W. Specificities of Ricinus Communis Agglutinin 120 Interaction with Sulfated Galactose. *FEBS Lett.* **2011**, *585* (24), 3927–3934. https://doi.org/10.1016/j.febslet.2011.10.035.

(92) Shang, J.; Piskarev, V. E.; Xia, M.; Huang, P.; Jiang, X.; Likhosherstov, L. M.; Novikova, O. S.; Newburg, D. S.; Ratner, D. M. Identifying Human Milk Glycans That Inhibit Norovirus Binding Using Surface Plasmon Resonance. *Glycobiology* **2013**, *23* (12), 1491–1498. https://doi.org/10.1093/glycob/cwt077.

(93) Horejsi, V. Properties of Ulex Europaeus II Lectin Isolated by Affinity Chromatography. *Biochim. Biophys. Acta* **1979**, *577*, 389–393. https://doi.org/https://doi.org/10.1016/0005-2795(79)90042-4.

(94) Debray, H.; Decout, D.; Strecker, G.; Spik, G.; Montreuil, J. Specificity of Twelve Lectins Towards Oligosaccharides and Glycopeptides Related to N-Glycosylproteins. *Eur. J. Biochem.* **1981**, *117* (1), 41–51. https://doi.org/10.1111/j.1432-1033.1981.tb06300.x.

(95) Matsumoto, I.; Osawa, T. Purification and Characterization of an Anti-H(O) Phytohemagglutinin of Ulex Europaeus. *Biochim. Biophys. Acta,* **1966**, *194*, 180–189. https://doi.org/10.1016/0005-2795(69)90193-7.

(96) Allen, H. J.; Johnson, E. A. Z.; Matta, K. L. A Comparison of the Binding Specificities of Lectins from Europaeus and Lotus Tetragonolobus. *Immunol. Commun.* **1977**, *6* (6), 585–602. https://doi.org/10.3109/08820137709093469.

(97) Uchiyama, N.; Kuno, A.; Tateno, H.; Kubo, Y.; Mizuno, M.; Noguchi, M.; Hirabayashi, J. Optimization of Evanescent-Field Fluorescence-Assisted Lectin Microarray for High-Sensitivity Detection of Monovalent Oligosaccharides and Glycoproteins. *Proteomics* **2008**, *8* (15), 3042–3050. https://doi.org/10.1002/pmic.200701114.

(98) Miettinen, M.; Holthofer, H.; Lehto, V.-P. Ulex Europaeus / Lectin as a Marker for Tumors Derived from Endothelial Cells. *Am. J. Clin. Pathog.* **1983**, *79* (1), 32–36. https://doi.org/10.1093/ajcp/79.1.32.

(99) Blonski, K.; Krankenhaus, E.; Bad, S.; Milde-Langosch, K.; Schumacher, U. Ulex Europeus Agglutinin-I Binding as a Potential Prognostic Marker in Ovarian Cancer. *Anticancer Res.* **2007**, *27* (1), 2785–2790.

(100) Peters, B. P.; Ebisu, S.; Goldstein, I. J.; Flashner, M. Interaction of Wheat Germ Agglutinin with Sialic Acid. *Biochem.* **1979**, *18* (24), 5505–5511. https://doi.org/https://doi.org/10.1021/bi00591a038.

(101) Goldstein ~, I. J.; Hammarstrom, S.; Sundblad, G. Precipitation and Carbohydrate-Binding Specificity Studies on Wheat Germ Agglutinin. *Biochem. Biophys. Acta* **1975**, 53–61. https://doi.org/10.1016/0005-2795(75)90313-x.

(102) Maget-Dana, R.; Veh, R. W.; Sander, M.; Roche, A. -C; Schauer, R.; Monsigny, M. Specificities of Limulin and Wheat-Germ Agglutinin Towards Some Derivatives of GM3 Gangliosides. *Eur. J. Biochem.* **1981**, *114* (1), 11–16. https://doi.org/10.1111/j.1432-1033.1981.tb06164.x.

(103) Blanco, J. L. J.; Haseley, S. R.; Kamerling, J. P.; Vliegenthart, J. F. G. Analysis of the Interaction between Lectins and Tetra-and Tri-Saccharide Mimics of the Sd a Determinant by Surface Plasmon Resonance Detection. *Biochimie* **2001**, *83*, 653–658. https://doi.org/https://doi.org/10.1016/S0300-9084(01)01302-5.

(104) Varghese, J. N.; McKimm-Breschkin, J. L.; Caldwell, J. B.; Kortt, A. A.; Colman CSIRO, P. M. The Structure of the Complex Between Influenza Virus Neuraminidase and Sialic Acid, the Viral Receptor. *Proteins: Struct. Funct. Genet.* **1992**, *14*, 327–332. https://doi.org/https://doi.org/10.1002/prot.340140302.

(105) Varki, A. Diversity in the Sialic Acids. *Glycobiology* **1992**, *2* (1), 25. https://doi.org/https://doi.org/10.1093/glycob/2.1.25.

(106) Parasuraman, P.; Murugan, V.; Selvin, J. F. A.; Gromiha, M. M.; Fukui, K.; Veluraja, K. Insights into the Binding Specificity of Wild Type and Mutated Wheat Germ Agglutinin

towards Neu5Acα(2-3)Gal: A Study by in Silico Mutations and Molecular Dynamics Simulations. *J. Mol. Recognit.* **2014**, *27* (8), 482–492. https://doi.org/10.1002/jmr.2369.

(107) Sumner, J. B.; Howell, S. F. The Identification of the Hemagglutinin of the Jack Bean with Concanavalin A. *J. Bacteriol.* **1936**, *32* (2), 227–237. https://doi.org/https://doi.org/10.1128/jb.32.2.227-237.19.

(108) Reeke, G. N.; Becker, J. W.; Cunningham, B. A.; Wang, J. L.; Yahara, I.; Edelman, G. M. Structure and Function of Concanavalin A. *Adv. Exp. Med. Biol.* **1975**, *55* (1), 13–33. https://doi.org/https://doi.org/10.1007/978-1-4684-0949-9_2.

(109) Senear, D. F.; Teller, D. C. Thermodynamics of Concanavalin A Dimer-Tetramer Self-Association: Sedimentation Equilibrium Studies1. *Biochemistry* **1981**, *20*, 3076–3083. https://doi.org/10.1021/bi00514a014.

(110) Mega, T.; Hase, S. Determination of Lectin-Sugar Binding Constants by Microequilibrium Dialysis Coupled with High Performance Liquid Chromatography. *J. Biochem.* **1991**, *109*, 600–603. https://doi.org/https://doi.org/10.1093/oxfordjournals.jbchem.a123426.

(111) Mandal, D. K.; Bhattacharyya, L.; Koenig, I. H.; Brown, R. D.; Oscarson, S.; Brewer, C. F. Studies of the Binding Specificity of Concanavalin A. Nature of the Extended Binding Site for Asparagine-Linked Carbohydrates. *Biochemistry* **1994**, *33*, 1157–1162. https://doi.org/https://doi.org/10.1021/bi00171a015.

(112) Gupta, D.; Oscarson, S.; Raju, T. S.; Stanley, P.; Toone, E. J.; Brewer, C. F. A Comparison of the Fine Saccharide-Binding Specificity of Dioclea Grandiflora Lectin and Concanavalin A. *Eur. J. Biochem.* **1996**, *242* (2), 320–326. https://doi.org/10.1111/j.1432-1033.1996.0320r.x.

(113) Hofer, U. The Cost of Antimicrobial Resistance. *Nat. Rev. Microbiol.* **2019**, *17* (1), 3. https://doi.org/https://doi.org/10.1038/s41579-018-0125-x.

(114) Bloom, D. E.; Cadarette, D. Infectious Disease Threats in the Twenty-First Century: Strengthening the Global Response. *Front. Immunol.* **2019**, *10* (549), 1–12. https://doi.org/10.3389/fimmu.2019.00549.

(115) Tacconelli, E.; Magrini, N.; Carmeli, Y.; Harbarth, S.; G., K.; J., K. Global Priority List of Antibiotic-Resistant Bacteria to Guide Research, Discovery, and Development of New Antibiotics. *World Health Organisation* **2017**, 1–7.

(116) Wu, W.; Jin, Y.; Bai, F.; Jin, S. Pseudomonas Aeruginosa. In *Molecular Medical Microbiology*; Tang, Y., Sussman, M., Liu, D., Poxton, I., Schwartzman, J., Eds.; Academic Press, 2015; Vol. 2, pp 753–767. https://doi.org/https://doi.org/10.1016/B978-0-12-397169-2.00041-X.

(117) Bodey, G. P.; Bolivar, R.; Fainstein, V.; Jadeja, L. Infections Caused by Pseudomonas Aeruginosa. *Rev. Infect. Dis.* **1983**, *5* (2), 279–313. https://doi.org/10.1159/000414328.

(118) Mittal, R.; Aggarwal, S.; Sharma, S.; Chhibber, S.; Harjai, K. Urinary Tract Infections Caused by Pseudomonas Aeruginosa: A Minireview. *J. Infect. Public Health* **2009**, *2* (3), 101–111. https://doi.org/10.1016/j.jiph.2009.08.003.

(119) Govan, J. R. W.; Deretic, V. Microbial Pathogenesis in Cystic Fibrosis: Mucoid Pseudomonas Aeruginosa and Burkholderia Cepacia. *Microbiol. Rev.* **1996**, *60* (3), 539–574. https://doi.org/10.1128/mmbr.60.3.539-574.1996.

(120) Fujitani, S.; Sun, H. Y.; Yu, V. L.; Weingarten, J. A. Pneumonia Due to Pseudomonas Aeruginosa: Part I: Epidemiology, Clinical Diagnosis, and Source. *Chest* **2011**, *139* (4), 909–919. https://doi.org/10.1378/chest.10-0166.

(121) Gilboa-Garber, N. Inhibition of Broad Spectrum Hemagglutinin from Pseudomonas Aeruginosa by D-Galactose and Its Derivatives. *FEBS Lett.* **1972**, *20* (2), 242–244. https://doi.org/10.1016/0014-5793(72)80805-6.

(122) Gilboa-Garber, N. Pseudomonas Aeruginosa Lectins. In *Methods in Enzymology*; Academic Press, 1982; Vol. 83, pp 378–385. https://doi.org/https://doi.org/10.1016/0076-6879(82)83034-6.

(123) Doig, P.; Todd, T.; Sastry, P. A.; Lee, K. K.; Hodges, R. S.; Paranchych, W.; Irvin', R. T. Role of Pili in Adhesion of Pseudomonas Aeruginosa to Human Respiratory Epithelial Cells. *Infect. Immun.* **1988**, *56* (6), 1641–1646. https://doi.org/10.1128/iai.56.6.1641-1646.1988.

(124) Baker, N.; Hansson, G. C.; Leffler, H.; Riise, G.; Svanborg-Edenl, C.; Francisco, S. Glycosphingolipid Receptors for Pseudomonas Aeruginosa. *Infect. Immun.* **1990**, *58* (7), 2361–2366. https://doi.org/10.1128/iai.58.7.2361-2366.1990.

(125) Chemani, C.; Imberty, A.; de Bentzmann, S.; Pierre, M.; Wimmerová, M.; Guery, B. P.; Faure, K. Role of LecA and LecB Lectins in Pseudomonas Aeruginosa-Induced Lung Injury and Effect of Carbohydrate Ligands. *Infect. Immun.* **2009**, *77* (5), 2065–2075. https://doi.org/10.1128/IAI.01204-08.

(126) Loris, R.; Tielker, D.; Jaeger, K. E.; Wyns, L. Structural Basis of Carbohydrate Recognition by the Lectin LecB from Pseudomonas Aeruginosa. *J. Mol. Biol.* **2003**, *331* (4), 861–870. https://doi.org/10.1016/S0022-2836(03)00754-X.

(127) Lanne, B.; Cîopraga, J.; Bergström, J.; Motas, C.; Karlsson, K. A. Binding of the Galactose-Specific Pseudomonas Aeruginosa Lectin, PA-I, to Glycosphingolipids and Other Glycoconjugates. *Glycoconj. J.* **1994**, *11* (4), 292–298. https://doi.org/10.1007/BF00731201.

(128) Englen, M. D.; Fedorka-Cray, P. J. Evaluation of a Commercial Diagnostic PCR for the Identification of Campylobacter Jejuni and Campylobacter Coli. *Lett Appl Microbiol* **2002**, *35* (4), 353–356. https://doi.org/10.1046/j.1472-765X.2002.01193.x.

(129) Ghosh, R.; Uppal, B.; Aggarwal, P.; Chakravarti, A.; Jha, A. K.; Dubey, A. P. A Comparative Study of Conventional and Molecular Techniques in Diagnosis of Campylobacter Gastroenteritis in Children. *Ann. Clin. Lab. Sci.* **2014**, *44* (1), 42–48.

(130) Varki, A.; Cummings, R. D.; Aebi, M.; Packer, N. H.; Seeberger, P. H.; Esko, J. D.; Stanley, P.; Hart, G.; Darvill, A.; Kinoshita, T.; Prestegard, J. J.; Schnaar, R. L.; Freeze, H. H.; Marth, J. D.; Bertozzi, C. R.; Etzler, M. E.; Frank, M.; Vliegenthart, J. F. G.; Lütteke, T.; Perez, S.; Bolton, E.; Rudd, P.; Paulson, J.; Kanehisa, M.; Toukach, P.; Aoki-Kinoshita, K. F.; Dell, A.; Narimatsu, H.; York, W.; Taniguchi, N.; Kornfeld, S. Symbol Nomenclature for Graphical Representations of Glycans. *Glycobiology* **2015**, *25* (12), 1323–1324. https://doi.org/10.1093/glycob/cwv091.

(131) Liu, Y.; Palma, A. S.; Feizi, T. Carbohydrate Microarrays: Key Developments in Glycobiology. *Biol. Chem.* **2009**, *390* (7), 647–656. https://doi.org/10.1515/BC.2009.071.

(132) Bernardes, G. J. L.; Castagner, B.; Seeberger, P. H. Combined Approaches to the Synthesis and Study of Glycoproteins. *ACS Chem. Biol.* **2009**, *4* (9), 703–713. https://doi.org/10.1021/cb900014n.

(133) Laurent, N.; Voglmeir, J.; Flitsch, S. L. Glycoarrays - Tools for Determining Protein-Carbohydrate Interactions and Glycoenzyme Specificity. *Chem. Comm.* **2008**, No. 37, 4400–4412. https://doi.org/10.1039/b806983m.

(134) Dimick, S. M.; Powell, S. C.; McMahon, S. A.; Moothoo, D. N.; Naismith, J. H.; Toone, E. J. On the Meaning of Affinity: Cluster Glycoside Effects and Concanavalin A. *J Am Chem Soc* **1999**, *121* (44), 10286–10296. https://doi.org/10.1021/ja991729e.

(135) Branderhorst, H. M.; Ruijtenbeek, R.; Liskamp, R. M. J.; Pieters, R. J. Multivalent Carbohydrate Recognition on a Glycodendrimer-Functionalized Flow-through Chip. *ChemBioChem* **2008**, *9* (11), 1836–1844. https://doi.org/10.1002/cbic.200800195.

(136) di Maio, A.; Cioce, A.; Achilli, S.; Thépaut, M.; Vivès, C.; Fieschi, F.; Rojo, J.; Reichardt, N. C. Controlled Density Glycodendron Microarrays for Studying Carbohydrate-Lectin Interactions. *Org. Biomol. Chem.* **2021**, *19* (34), 7357–7362. https://doi.org/10.1039/d1ob00872b.

(137) Mende, M.; Tsouka, A.; Heidepriem, J.; Paris, G.; Mattes, D. S.; Eickelmann, S.; Bordoni, V.; Wawrzinek, R.; Fuchsberger, F. F.; Seeberger, P. H.; Rademacher, C.; Delbianco, M.; Mallagaray, A.; Loeffler, F. F. On-Chip Neo-Glycopeptide Synthesis for Multivalent Glycan Presentation. *Chem. Eur. J.* **2020**, *26* (44), 9954–9963. https://doi.org/10.1002/chem.202001291.

(138) Valles, D. J.; Naeem, Y.; Rozenfeld, A. Y.; Aldasooky, R. W.; Wong, A. M.; Carbonell, C.; Mootoo, D. R.; Braunschweig, A. B. Multivalent Binding of Concanavalin A on Variable-

Density Mannoside Microarrays. *Faraday Discuss.* **2019**, *219*, 77–89. https://doi.org/10.1039/c9fd00028c.

(139) Valles, D. J.; Zholdassov, Y. S.; Korpanty, J.; Uddin, S.; Naeem, Y.; Mootoo, D. R.; Gianneschi, N. C.; Braunschweig, A. B. Glycopolymer Microarrays with Sub-Femtomolar Avidity for Glycan Binding Proteins Prepared by Grafted-To/Grafted-From Photopolymerizations. *Angew. Chem. Int. Ed.* **2021**, *60* (37), 20350–20357. https://doi.org/10.1002/anie.202105729.

(140) Renaudet, O. Recent Advances on Cyclopeptide-Based Glycoclusters. *Mini Rev. Org. Chem.* **2008**, *5* (4), 274–286. https://doi.org/10.2174/157019308786242142.

(141) Schwefel, D.; Maierhofer, C.; Beck, J. G.; Seeberger, S.; Diederichs, K.; Möller, H. M.; Welte, W.; Wittmann, V. Structural Basis of Multivalent Binding to Wheat Germ Agglutinin. *J. Am. Chem. Soc.* **2010**, *132* (25), 8704–8719. https://doi.org/10.1021/ja101646k.

(142) Rohse, P.; Weickert, S.; Drescher, M.; Wittmann, V. Precipitation-Free High-Affinity Multivalent Binding by Inline Lectin Ligands. *Chem. Sci.* **2020**, *11* (20), 5227–5237. https://doi.org/10.1039/d0sc01744b.

(143) Švajger, U.; Anderluh, M.; Jeras, M.; Obermajer, N. C-Type Lectin DC-SIGN: An Adhesion, Signalling and Antigen-Uptake Molecule That Guides Dendritic Cells in Immunity. *Cell. Signal.* **2010**, *22* (10), 1397–1405. https://doi.org/10.1016/j.cellsig.2010.03.018.

(144) Ordanini, S.; Varga, N.; Porkolab, V.; Thépaut, M.; Belvisi, L.; Bertaglia, A.; Palmioli, A.; Berzi, A.; Trabattoni, D.; Clerici, M.; Fieschi, F.; Bernardi, A. Designing Nanomolar Antagonists of DC-SIGN-Mediated HIV Infection: Ligand Presentation Using Molecular Rods. *Chem. Comm.* **2015**, *51* (18), 3816–3819. https://doi.org/10.1039/c4cc09709b.

(145) Marradi, M.; Chiodo, F.; García, I.; Penadés, S. Glyconanoparticles as Multifunctional and Multimodal Carbohydrate Systems. *Chem. Soc. Rev.* **2013**, *42* (11), 4728–4745. https://doi.org/10.1039/c2cs35420a.

(146) Reily, C.; Stewart, T. J.; Renfrow, M. B.; Novak, J. Glycosylation in Health and Disease. *Nat Rev Nephrol* **2019**, *15* (6), 346–366. https://doi.org/10.1038/s41581-019-0129-4.

(147) Pergolizzi, G.; Dedola, S.; Field, R. A. Contemporary Glycoconjugation Chemistry. *Carbohydr. Chem.* **2017**, *42*, 1–46. https://doi.org/10.1039/9781782626657-00001.

(148) Kubler-Kielb, J.; Pozsgay, V. A New Method for Conjugation of Carbohydrates to Proteins Using an Aminooxy-Thiol Heterobifunctional Linker. *J. Org. Chem.* **2005**, *70* (17), 6987–6990. https://doi.org/10.1021/jo050934b.

(149) Li, F.-Q.; Su, H.; Chen, X.; Qin, X.-J.; Liu, J.-Y.; Zhu, Q.-G.; Hu, J.-H. Mannose 6-Phosphate-Modified Bovine Serum Albumin Nanoparticles for Controlled and Targeted Delivery of Sodium Ferulate for Treatment of Hepatic Fibrosis. *J. Pharm. Pharmacol.* **2009**, *61* (9), 1155–1161. https://doi.org/10.1211/jpp/61.09.0004.

(150) Dubois, M.; Gilles, K. A.; Hamilton, J. K.; Rebers, P. A.; Smith, F. Colorimetric Method for Determination of Sugars and Related Substances. *Anal. Chem.* **1956**, *28* (3), 350–356. https://doi.org/https://doi.org/10.1021/ac60111a017.

(151) Kong, L.; Vijayakrishnan, B.; Kowarik, M.; Park, J.; Zakharova, A. N.; Neiwert, L.; Faridmoayer, A.; Davis, B. G. An Antibacterial Vaccination Strategy Based on a Glycoconjugate Containing the Core Lipopolysaccharide Tetrasaccharide Hep2 Kdo2. *Nat. Chem.* **2016**, *8* (3), 242–249. https://doi.org/10.1038/nchem.2432.

(152) Adak, A. K.; Leonov, A. P.; Ding, N.; Thundimadathil, J.; Kularatne, S.; Low, P. S.; Wei, A. Bishydrazide Glycoconjugates for Lectin Recognition and Capture of Bacterial Pathogens. *Bioconjug. Chem.* **2010**, *21* (11), 2065–2075. https://doi.org/10.1021/bc100288c.

(153) Yang, Y.; Jia, T. W.; Xu, F.; Li, W.; Tao, S.; Chu, L. Q.; He, Y.; Li, Y.; Iyer, S. S.; Yu, P. Fluorescent Neomannosyl Bovine Serum Albumin as Efficient Probe for Mannose Receptor Imaging and MCF-7 Cancer Cell Targeting. *ACS Appl. Nano. Mater.* **2018**, *1* (3), 1058–1065. https://doi.org/10.1021/acsanm.7b00134.

(154) Wang, J. W.; Asnani, A.; Auzanneau, F. I. Synthesis of a BSA-Lex Glycoconjugate and Recognition of Le x Analogues by the Anti-Lex Monoclonal Antibody SH1: The Identification of a Non-Cross Reactive Analogue. *Bioorg. Med. Chem.* **2010**, *18* (20), 7174–7185. https://doi.org/10.1016/j.bmc.2010.08.040.

(155) Ganesh, N. V.; Sadowska, J. M.; Sarkar, S.; Howells, L.; McGiven, J.; Bundle, D. R. Molecular Recognition of Brucella A and M Antigens Dissected by Synthetic Oligosaccharide Glycoconjugates Leads to a Disaccharide Diagnostic for Brucellosis. *J. Am. Chem. Soc.* **2014**, *136* (46), 16260–16269. https://doi.org/10.1021/ja5081184.

(156) Lemieux, R. U.; Bundle, D. R.; Baker2, D. A. The Properties of a “Synthetic” Antigen Related to the Human Blood-Group Lewis a. *J. Am. Chem. Soc.* **1975**, *97* (14), 4076–4083. https://doi.org/https://doi.org/10.1021/ja00847a035.

(157) Zhong, M.; Yu, Y.; Song, J. Q.; Jia, T. W.; Liu, A. Y.; Zhao, T. F.; He, H. J.; Yang, M. B.; Zhang, W. X.; Yang, Y. Amide-Sialoside Protein Conjugates as Neomucin Bioshields Prevent Influenza Virus Infection. *Carbohydr. Res.* **2020**, *495*. https://doi.org/10.1016/j.carres.2020.108088.

(158) Munneke, S.; Dangerfield, E. M.; Stocker, B. L.; Timmer, M. S. M. The Versatility of N-Alkyl-Methoxyamine Bi-Functional Linkers for the Preparation of Glycoconjugates. *Glycoconj. J.* **2017**, *34* (5), 633–642. https://doi.org/10.1007/s10719-017-9785-4.

(159) Zhang, H.; Laaf, D.; Elling, L.; Pieters, R. J. Thiodigalactoside-Bovine Serum Albumin Conjugates as High-Potency Inhibitors of Galectin-3: An Outstanding Example of Multivalent Presentation of Small Molecule Inhibitors. *Bioconjug Chem* **2018**, *29* (4), 1266–1275. https://doi.org/10.1021/acs.bioconjchem.8b00047.

(160) Böcker, S.; Laaf, D.; Elling, L. Galectin Binding to Neo-Glycoproteins: LacDiNAc Conjugated BSA as Ligand for Human Galectin-3. *Biomolecules* **2015**, *5* (3), 1671–1696. https://doi.org/10.3390/biom5031671.

(161) Mir, M. M.; Fazili, K. M.; Qasim, M. A. Chemical Modification of Buried Lysine Residues of Bovine Serum Albumin and Its Influence on Protein Conformation and Bilirubin Binding. *Biochim. Biophys. Acta. I* **1992**, *119*, 261–267. https://doi.org/https://doi.org/10.1016/0167-4838(92)90212-V.

(162) Huang, Z.; Gengenbach, T.; Tian, J.; Shen, W.; Garnier, G. Effect of Bovine Serum Albumin Treatment on the Aging and Activity of Antibodies in Paper Diagnostics. *Front. Chem.* **2018**, *6* (161). https://doi.org/10.3389/fchem.2018.00161.

(163) Zhu, W.; Li, H.; Wan, A. EDC-Induced Self-Assembly of BSA-Au NCs. *J. Fluoresc.* **2019**, *29* (3), 627–630. https://doi.org/10.1007/s10895-019-02369-1.

(164) Kolb, H. C.; Finn, M. G.; Sharpless, K. B. Click Chemistry: Diverse Chemical Function from a Few Good Reactions. *Angew. Chem. Int. Ed.* **2001**, *40* (11), 2004–2021. https://doi.org/10.1002/1521-3773(20010601)40:11<2004::AID-ANIE2004>3.0.CO;2-5.

(165) Tornøe, C. W.; Christensen, C.; Meldal, M. Peptidotriazoles on Solid Phase: [1,2,3]-Triazoles by Regiospecific Copper(I)-Catalyzed 1,3-Dipolar Cycloadditions of Terminal Alkynes to Azides. *J. Org. Chem.* **2002**, *67* (9), 3057–3064. https://doi.org/10.1021/jo011148j.

(166) Rostovtsev, V. v; Green, L. G.; Fokin, V. v; Barry Sharpless, K. A Stepwise Huisgen Cycloaddition Process: Copper(I)-Catalyzed Regioselective "Ligation" of Azides and Terminal Alkynes. *Angew. Chem. Int. Ed* **2002**, *41* (14), 2596–2599. https://doi.org/https://doi.org/10.1002/1521-3773(20020715)41:14<2596::AID-ANIE2596>3.0.CO;2-4.

(167) Sawa, M.; Hsu, T.-L.; Itoh, T.; Sugiyama, M.; Hanson, S. R.; Vogt, P. K.; Wong, C.-H. Glycoproteomic Probes for Fluorescent Imaging of Fucosylated Glycans in Vivo. *PNAS* **2006**, *103* (33), 12371–12376. https://doi.org/https://doi.org/10.1073/pnas.060541810.

(168) Chikae, M.; Fukuda, T.; Kerman, K.; Idegami, K.; Miura, Y.; Tamiya, E. Amyloid-β Detection with Saccharide Immobilized Gold Nanoparticle on Carbon Electrode. *Bioelectrochemistry* **2008**, *74* (1), 118–123. https://doi.org/10.1016/j.bioelechem.2008.06.005.

(169) Trieger, G. W.; Verespy, S.; Gordts, P. L. S. M.; Godula, K. Efficient Synthesis of Heparinoid Bioconjugates for Tailoring FGF2 Activity at the Stem Cell-Matrix Interface. *Bioconjug. Chem.* **2019**, *30* (3), 833–840. https://doi.org/10.1021/acs.bioconjchem.8b00921.

(170) Parker, R. E.; Isaacs, N. S. Mechanisms of Epoxide Reactions. *Chem. Rev.* **1959**, *59* (4), 737–799. https://doi.org/https://doi.org/10.1021/cr50028a006.

(171) Thomas, E. W.; McKelvy, J. F.; Sharon, N. Specific and Irreversible Inhibition of Lysozyme by 2',3'-Epoxypropyl β-Glycosides of N-Acetyl-D-Glucosamine Oligomers. *Nature* **1969**, *222* (3), 485–486. https://doi.org/https://doi.org/10.1038/222485a0.

(172) Azizi, N.; Saidi, M. R. Highly Chemoselective Addition of Amines to Epoxides in Water. *Org Lett* **2005**, *7* (17), 3649–3651. https://doi.org/10.1021/ol051220q.

(173) Lederer, M. O. Reactivity of Lysine Moieties toward γ-Hydroxy-α,β-Unsaturated Epoxides: A Model Study on Protein-Lipid Oxidation Product Interaction. *J. Agric. Food Chem.* **1996**, *44* (9), 2531–2537. https://doi.org/https://doi.org/10.1021/jf950837r.

(174) Chen, G.; Heim, A.; Riether, D.; Yee, D.; Milgrom, Y.; Gawinowicz, M. A.; Sames, D. Reactivity of Functional Groups on the Protein Surface: Development of Epoxide Probes for Protein Labeling. *J. Am. Chem. Soc.* **2003**, *125* (27), 8130–8133. https://doi.org/10.1021/ja034287m.

(175) Takaoka, Y.; Tsutsumi, H.; Kasagi, N.; Nakata, E.; Hamachi, I. One-Pot and Sequential Organic Chemistry on an Enzyme Surface to Tether a Fluorescent Probe at the Proximity of the Active Site with Restoring Enzyme Activity. *J. Am. Chem. Soc.* **2006**, *128* (10), 3273–3280. https://doi.org/10.1021/ja057926x.

(176) Gratzer, P. F.; Santerre, J. P.; Lee, J. M. The Effect of Chemical Modification of Amino Acid Side-Chains on Collagen Degradation by Enzymes. *J. Biomed. Mater. Res. B Appl. Biomater.* **2007**, *81* (1), 1–11. https://doi.org/10.1002/jbm.b.30629.

(177) Lu, X.; Xu, Y.; Zheng, C.; Zhang, G.; Su, Z. Ethylene Glycol Diglycidyl Ether as a Protein Cross-Linker: A Case Study for Cross-Linking of Hemoglobin. *J. Chem. Technol. Biotechnol.* **2006**, *81* (5), 767–775. https://doi.org/10.1002/jctb.1441.

(178) Fan, J.; Lei, T. da; Li, J.; Zhai, P. Y.; Wang, Y. H.; Cao, F. Y.; Liu, Y. High Protein Content Keratin/Poly (Ethylene Oxide) Nanofibers Crosslinked in Oxygen Atmosphere and Its Cell Culture. *Mater. Des.* **2016**, *104*, 60–67. https://doi.org/10.1016/j.matdes.2016.05.022.

(179) Cardenas Turner, J.; Collins, G.; Blaber, E. A.; Almeida, E. A. C.; Arinzeh, T. L. Evaluating the Cytocompatibility and Differentiation of Bone Progenitors on Electrospun Zein Scaffolds. *J. Tissue Eng. Regen. Med.* **2020**, *14* (1), 173–185. https://doi.org/10.1002/term.2984.

(180) Liu, L.; Jiang, J.; Jin, X.; Li, R.; Huang, L.; Wang, N.; Reddy, N.; Liu, W.; Jiang, Q. Epoxide Cross-Linked and Lysine-Blocked Zein Ultrafine Fibrous Scaffolds with Prominent Wet Stability and Cytocompatibility. *ACS Appl. Polym. Mater.* **2021**, *3* (8), 3855–3866. https://doi.org/10.1021/acsapm.1c00439.

(181) Liu, Y.; Tu, F.; Li, H.; Shi, P.; Yin, Y.; Dong, F.; Wang, J. Preparation, Characterization and in Vivo Graft Patency of a Silk Fibroin Tubular Scaffold. *Mater. Technol.* **2018**, *33* (3), 227–234. https://doi.org/10.1080/10667857.2017.1405889.

(182) Stoessel, P. R.; Krebs, U.; Hufenus, R.; Halbeisen, M.; Zeltner, M.; Grass, R. N.; Stark, W. J. Porous, Water-Resistant Multifilament Yarn Spun from Gelatin. *Biomacromolecules* **2015**, *16* (7), 1997–2005. https://doi.org/10.1021/acs.biomac.5b00424.

(183) Connell, L. S.; Romer, F.; Suárez, M.; Valliant, E. M.; Zhang, Z.; Lee, P. D.; Smith, M. E.; Hanna, J. v.; Jones, J. R. Chemical Characterisation and Fabrication of Chitosan-Silica Hybrid Scaffolds with 3-Glycidoxypropyl Trimethoxysilane. *J. Mater. Chem. B* **2014**, *2* (6), 668–680. https://doi.org/10.1039/c3tb21507e.

(184) Chao, A. C. Preparation of Porous Chitosan/GPTMS Hybrid Membrane and Its Application in Affinity Sorption for Tyrosinase Purification with Agaricus Bisporus. *J. Memb. Sci.* **2008**, *311* (1–2), 306–318. https://doi.org/10.1016/j.memsci.2007.12.032.

(185) Shirosaki, Y.; Tsuru, K.; Hayakawa, S.; Osaka, A.; Lopes, M. A.; Santos, J. D.; Costa, M. A.; Fernandes, M. H. Physical, Chemical and in Vitro Biological Profile of Chitosan Hybrid Membrane as a Function of Organosiloxane Concentration. *Acta Biomater.* **2009**, *5* (1), 346–355. https://doi.org/10.1016/j.actbio.2008.07.022.

(186) Liu, Y. L.; Su, Y. H.; Lai, J. Y. In Situ Crosslinking of Chitosan and Formation of Chitosan-Silica Hybrid Membranes with Using γ-Glycidoxypropyltrimethoxysilane as a Crosslinking Agent. *Polymer (Guildf)* **2004**, *45* (20), 6831–6837. https://doi.org/10.1016/j.polymer.2004.08.006.

(187) Xu, D.; Hein, S.; Wang, K. Chitosan Membrane in Separation Applications. *Mater. Sci. Technol.* **2008**, *24* (9), 1076–1087. https://doi.org/10.1179/174328408X341762.

(188) Shirosaki, Y.; Botelho, C. M.; Lopes, M. A.; Santos, J. D. Synthesis and Characterization of Chitosan-Silicate Hydrogel as Resorbable Vehicle for Bonelike® Bone Graft. *J. Nanosci. Nanotechnol.* **2009**, *9* (6), 3714–3719. https://doi.org/10.1166/jnn.2009.NS56.

(189) Zhu, Z. Y.; Cui, D.; Gao, H.; Dong, F. Y.; Liu, X. C.; Liu, F.; Chen, L.; Zhang, Y. M. Efficient Synthesis and Activity of Beneficial Intestinal Flora of Two Lactulose-Derived Oligosaccharides. *Eur. J. Med. Chem.* **2016**, *114*, 8–13. https://doi.org/10.1016/j.ejmech.2016.03.007.

(190) Xu, P.; Yang, J. Y.; Kováč, P. Observations on the Preparation of β-Lactose Octaacetate. *J. Carbohydr. Chem.* **2012**, *31* (9), 711–720. https://doi.org/10.1080/07328303.2012.739230.

(191) Vazquez, I. M.; Thezl, I. M. E.; Deferrari, J. 0. Preparation and Structure of 1,2,6,2',3',4',6'-Hepta-O-Benzoyl-β-Cellobiose and 6-O-Benzoylcellobiose. *Carbohydr Res* **1976**, *47*, 241–244. https://doi.org/https://doi.org/10.1016/S0008-6215(00)84189-0.

(192) Yi, X.; Venot, A.; Glushka, J.; Prestegard, J. H. Glycosidic Torsional Motions in a Bicelle-Associated Disaccharide from Residual Dipolar Couplings. *J. Am. Chem. Soc.* **2004**, *126* (42), 13636–13638. https://doi.org/10.1021/ja045697t.

(193) Wang, Z.; Matin, M.; Sheikh, S. Facile Preparation of Peracetates and Per-3-Bromobenzoates of α-Mono-and Disaccharides. *Molecules* **2005**, *10*, 1325–1334. https://doi.org/10.3390/10101325.

(194) Dass, A. V.; Georgelin, T.; Westall, F.; Foucher, F.; de Los Rios, P.; Busiello, D. M.; Liang, S.; Piazza, F. Equilibrium and Non-Equilibrium Furanose Selection in the Ribose Isomerisation Network. *Nat. Commun.* **2021**, *12* (1). https://doi.org/10.1038/s41467-021-22818-5.

(195) Percec, V.; Leowanawat, P.; Sun, H. J.; Kulikov, O.; Nusbaum, C. D.; Tran, T. M.; Bertin, A.; Wilson, D. A.; Peterca, M.; Zhang, S.; Kamat, N. P.; Vargo, K.; Moock, D.; Johnston, E. D.; Hammer, D. A.; Pochan, D. J.; Chen, Y.; Chabre, Y. M.; Shiao, T. C.; Bergeron-Brlek, M.; André, S.; Roy, R.; Gabius, H. J.; Heiney, P. A. Modular Synthesis of Amphiphilic Janus Glycodendrimers and Their Self-Assembly into Glycodendrimersomes and Other Complex Architectures with Bioactivity to Biomedically Relevant Lectins. *J. Am. Chem. Soc.* **2013**, *135* (24), 9055–9077. https://doi.org/10.1021/ja403323y.

(196) Stevens, J. D. Preparation and Properties of the Aldohexofuranose Pentaacetates. *Carbohydr. Res.* **2012**, *347* (1), 9–15. https://doi.org/10.1016/j.carres.2011.09.009.

(197) Rudrum, B. M.; Shaw, D. F. The Structure and Conformation of Some Monosaccharides in Solution. *J. Chem. Soc.* **1965**, 52–57. https://doi.org/https://doi.org/10.1039/JR9650000052.

(198) Keyari, C. M.; Polt, R. Serine and Threonine Schiff Base Esters React with β-Anomeric Peracetates in the Presence of BF3·Et2O to Produce β-Glycosides. *J. Carbohydr. Chem.* **2010**, *29* (4), 181–206. https://doi.org/10.1080/07328303.2010.508295.

(199) Lee, C. C.; Grandinetti, G.; McLendon, P. M.; Reineke, T. M. A Polycation Scaffold Presenting Tunable "Click" Sites: Conjugation to Carbohydrate Ligands and Examination of Hepatocyte-Targeted PDNA Delivery. *Macromol. Biosci.* **2010**, *10* (6), 585–598. https://doi.org/10.1002/mabi.200900431.

(200) Brusa, C.; Muzard, M.; Rémond, C.; Plantier-Royon, R. β-Xylopyranosides: Synthesis and Applications. *RSC Adv.* **2015**, *5* (110), 91026–91055. https://doi.org/10.1039/c5ra14023d.

(201) Singh, Y.; Demchenko, A. v. Koenigs–Knorr Glycosylation Reaction Catalyzed by Trimethylsilyl Trifluoromethanesulfonate. *Chem. Eur. J.* **2019**, *25* (6), 1461–1465. https://doi.org/10.1002/chem.201805527.

(202) Ness, R. K.; Fletcher, H. G.; Hudson, C. S. The Reaction of 2,3,4,6-Tetrabenzoyl-a-D-Glucopyranosyl Bromide and 2,3,4,6-Tetrabenzoyl-a-D-Mannopyranosyl Bromide with Methanol. Certain Benzoylated Derivatives of D-Glucose and D-Mannose. *J. Am. Chem. Soc.* **1950**, *72* (5), 2200–2205. https://doi.org/https://doi.org/10.1021/ja01161a091.

(203) Oscarson, S.; Tidén, A. K. Syntheses of the Octyl and Tetradecyl Glycosides of 3,6-Di-O-α-d-Mannopyranosyl-α-d-Mannopyranose and of 3,4-Di-O-α-d-Mannopyranosyl-α-d-Mannopyranose. A New Way for 2,4-Di-O-Protection of Mannopyranosides. *Carbohydr. Res.* **1993**, *247* (C), 323–328. https://doi.org/10.1016/0008-6215(93)84266-9.

(204) Lebedel, L.; Ardá, A.; Martin, A.; Désiré, J.; Mingot, A.; Aufiero, M.; Aiguabella Font, N.; Gilmour, R.; Jiménez-Barbero, J.; Blériot, Y.; Thibaudeau, S. Structural and Computational Analysis of 2-Halogeno-Glycosyl Cations in the Presence of a Superacid: An Expansive Platform. *Angew. Chem. Int. Ed.* **2019**, *58* (39), 13758–13762. https://doi.org/10.1002/anie.201907001.

(205) Fekete, A.; Borbás, A.; Antus, S.; Lipták, A. Synthesis of 3,6-Branched Arabinogalactan-Type Tetra- and Hexasaccharides for Characterization of Monoclonal Antibodies. *Carbohydr. Res.* **2009**, *344* (12), 1434–1441. https://doi.org/10.1016/j.carres.2009.04.025.

(206) Lu, W. Y.; Sun, X. W.; Zhu, C.; Xu, J. H.; Lin, G. Q. Expanding the Application Scope of Glycosidases Using Click Chemistry. *Tetrahedron* **2010**, *66* (3), 750–757. https://doi.org/10.1016/j.tet.2009.11.044.

(207) Šardzík, R.; Noble, G. T.; Weissenborn, M. J.; Martin, A.; Webb, S. J.; Flitsch, S. L. Preparation of Aminoethyl Glycosides for Glycoconjugation. *Beilstein J. Org. Chem.* **2010**, *6*, 699–703. https://doi.org/10.3762/bjoc.6.81.

(208) Demchenko, A. v.; Boons, G. J. A Highly Convergent Synthesis of a Complex Oligosaccharide Derived from Group B Type III Streptococcus. *J. Org. Chem.* **2001**, *66* (8), 2547–2554. https://doi.org/10.1021/jo001477w.

(209) Yu, H.; Chokhawala, H.; Karpel, R.; Yu, H.; Wu, B.; Zhang, J.; Zhang, Y.; Jia, Q.; Chen, X. A Multifunctional Pasteurella Multocida Sialyltransferase: A Powerful Tool for the Synthesis of Sialoside Libraries. *J. Am. Chem. Soc.* **2005**, *127* (50), 17618–17619. https://doi.org/10.1021/ja0561690.

(210) Wang, G. N.; André, S.; Gabius, H. J.; Murphy, P. v. Bi- to Tetravalent Glycoclusters: Synthesis, Structure-Activity Profiles as Lectin Inhibitors and Impact of Combining Both Valency and Headgroup Tailoring on Selectivity. *Org. Biomol. Chem.* **2012**, *10* (34), 6893–6907. https://doi.org/10.1039/c2ob25870f.

(211) Scheppokat, A. M.; Bretting, H.; Thiem, J. Fast and Efficient Synthesis of a Novel Homologous Series of L-Fucosylated Trisaccharides Using the Helix Pomatia α-(1→ 2)-L-Galactosyltransferase. *Carbohydr. Res.* **2003**, *338* (20), 2083–2090. https://doi.org/10.1016/S0008-6215(03)00344-6.

(212) Michihata, N.; Kaneko, Y.; Kasai, Y.; Tanigawa, K.; Hirokane, T.; Higasa, S.; Yamada, H. High-Yield Total Synthesis of (-)-Strictinin through Intramolecular Coupling of Gallates. *J. Org. Chem.* **2013**, *78* (9), 4319–4328. https://doi.org/10.1021/jo4003135.

(213) Huang, K.; Parmeggiani, F.; Ledru, H.; Hollingsworth, K.; Mas Pons, J.; Marchesi, A.; Both, P.; Mattey, A. P.; Pallister, E.; Bulmer, G. S.; van Munster, J. M.; Turnbull, W. B.; Galan, M. C.; Flitsch, S. L. Enzymatic Synthesis of N-Acetyllactosamine from Lactose Enabled by Recombinant B1,4-Galactosyltransferases. *Org. Biomol. Chem.* **2019**, *17* (24), 5920–5924. https://doi.org/10.1039/c9ob01089k.

(214) Sail, D.; Kováč, P. Benzoylated Ethyl 1-Thioglycosides: Direct Preparation from per-O-Benzoylated Sugars. *Carbohydr. Res.* **2012**, *357*, 47–52. https://doi.org/10.1016/j.carres.2012.05.012.

(215) Meldal, M.; Christensen, M. K.; Bock, K. Large-Scale Synthesis of D-Mannose 6-Phosphate and Other Hexose 6-Phosphates. *Carbohydr. Res.* **1992**, *235*, 115–127. https://doi.org/https://doi.org/10.1016/0008-6215(92)80082-C.

(216) King, J. F.; Allbutt, A. D. Remarkable Stereoselectivity in the Hydrolysis of Dioxolenium Ions and Orthoesters Fused to Anchored Six-Membered Rings. *Can. J. Chem.* **1970**, *48* (11), 1754–1769. https://doi.org/10.1139/v70-288.

(217) Oscarson, S.; Szönyi, M. Acidic Opening of 4,6-O-Orthoesters of Pyranosides. *J. Carbohydr. Chem.* **1989**, *8* (4), 663–668. https://doi.org/10.1080/07328308908048024.

(218) Lindhorst, T. K.; Bruegge, K.; Fuchs, A.; Sperling, O. A Bivalent Glycopeptide to Target Two Putative Carbohydrate Binding Sites on FimH. *Beilstein J. Org. Chem.* **2010**, *6*, 801–809. https://doi.org/10.3762/bjoc.6.90.

(219) Angata, T.; Varki, A. Chemical Diversity in the Sialic Acids and Related α-Keto Acids: An Evolutionary Perspective. *Chem. Rev.* **2002**, *102* (2), 439–469. https://doi.org/10.1021/cr000407m.

(220) Almagro-Moreno, S.; Boyd, E. F. Sialic Acid Catabolism Confers a Competitive Advantage to Pathogenic Vibrio Cholerae in the Mouse Intestine. *Infect. Immun.* **2009**, *77* (9), 3807–3816. https://doi.org/10.1128/IAI.00279-09.

(221) Cavalcante, T.; Medeiros, M. M.; Mule, S. N.; Palmisano, G.; Stolf, B. S. The Role of Sialic Acids in the Establishment of Infections by Pathogens, With Special Focus on Leishmania. *Front. Cell. Infect. Microbiol.* **2021**, *11*. https://doi.org/10.3389/fcimb.2021.671913.

(222) Harrison, J. A.; Kartha, K. P. R.; Fournier, E. J. L.; Lowary, T. L.; Malet, C.; Nilsson, U. J.; Hindsgaul, O.; Schenkman, S.; Naismith, J. H.; Field, R. A. Probing the Acceptor Substrate Binding Site of Trypanosoma Cruzi Trans-Sialidase with Systematically Modified Substrates and Glycoside Libraries. *Org. Biomol. Chem.* **2011**, *9* (5), 1653–1660. https://doi.org/10.1039/c0ob00826e.

(223) Todeschini, A. R.; Mendonça-Previato, L.; Previato, J. O.; Varki, A.; van Halbeek, H. Trans-Sialidase from Trypanosoma Cruzi Catalyzes Sialoside Hydrolysis with Retention of Configuration. *Glycobiology* **2000**, *10* (2), 213–221. https://doi.org/10.1093/glycob/10.2.213.

(224) Spiro, R. G. Studies on Fetuin, a Glycoprotein of Fetal Serum. Isolation, Chemical Composition and Physicochemical Properties. *J. Biol. Chem.* **1960**, *235* (10). https://doi.org/https://doi.org/10.1016/S0021-9258(18)64553-3.

(225) Guttman, M.; Lee, K. K. Site-Specific Mapping of Sialic Acid Linkage Isomers by Ion Mobility Spectrometry HHS Public Access. *Anal. Chem.* **2016**, *88* (10), 5212–5217. https://doi.org/10.1021/acs.anal-chem.6b00265.

(226) Wu, X.; Ye, J.; DeLaitsch, A. T.; Rashidijahanabad, Z.; Lang, S.; Kakeshpour, T.; Zhao, Y.; Ramadan, S.; Saavedra, P. V.; Yuzbasiyan-Gurkan, V.; Kavunja, H.; Cao, H.; Gildersleeve, J. C.; Huang, X. Chemoenzymatic Synthesis of 9NHAc-GD2 Antigen to Overcome the Hydrolytic Instability of O-Acetylated-GD2 for Anticancer Conjugate Vaccine Development. *Angew. Chem. Int. Ed.* **2021**, *60* (45), 24179–24188. https://doi.org/10.1002/anie.202108610.

(227) Isom, D. G.; Castañeda, C. A.; Cannon, B. R.; García-Moreno, B. Large Shifts in PK a Values of Lysine Residues Buried inside a Protein. *PNAS* **2011**, *108* (13), 5260–5265. https://doi.org/10.1073/pnas.1010750108/-/DCSupplemental.

(228) Presolski, S. I.; Hong, V. P.; Finn, M. G. Copper-Catalyzed Azide–Alkyne Click Chemistry for Bioconjugation. *Curr. Protoc. Chem. Biol.* **2011**, *3* (4), 153–162. https://doi.org/10.1002/9780470559277.ch110148.

(229) Presolski, S. I.; Hong, V.; Cho, S. H.; Finn, M. G. Tailored Ligand Acceleration of the Cu-Catalyzed Azide-Alkyne Cycloaddition Reaction: Practical and Mechanistic Implications. *J. Am. Chem. Soc.* **2010**, *132* (41), 14570–14576. https://doi.org/10.1021/ja105743g.

(230) Hong, V.; Presolski, S. I.; Ma, C.; Finn, M. G. Analysis and Optimization of Copper-Catalyzed Azide-Alkyne Cycloaddition for Bioconjugation. *Angew. Chem. Int. Ed.* **2009**, *48* (52), 9879–9883. https://doi.org/10.1002/anie.200905087.

(231) Posthuma-Trumpie, G. A.; Korf, J.; van Amerongen, A. Lateral Flow (Immuno)Assay: Its Strengths, Weaknesses, Opportunities and Threats. A Literature Survey. *Anal. Bioanal. Chem.* **2009**, *393* (2), 569–582. https://doi.org/10.1007/s00216-008-2287-2.

(232) di Nardo, F.; Chiarello, M.; Cavalera, S.; Baggiani, C.; Anfossi, L. Ten Years of Lateral Flow Immunoassay Technique Applications: Trends, Challenges and Future Perspectives. *Sensors* **2021**, *21* (15). https://doi.org/10.3390/s21155185.

(233) Hu, J.; Wang, S. Q.; Wang, L.; Li, F.; Pingguan-Murphy, B.; Lu, T. J.; Xu, F. Advances in Paper-Based Point-of-Care Diagnostics. *Biosens. Bioelectron.* **2014**, *54*, 585–597. https://doi.org/10.1016/j.bios.2013.10.075.

(234) Bührer-Sékula, S.; Smits, H. L.; Gussenhoven, G. C.; van Leeuwen, J.; Amador, S.; Fujiwara, T.; Klatser, P. R.; Oskam, L. Simple and Fast Lateral Flow Test for Classification of Leprosy Patients and Identification of Contacts with High Risk of Developing Leprosy. *J. Clin. Microbiol.* **2003**, *41* (5), 1991–1995. https://doi.org/10.1128/JCM.41.5.1991-1995.2003.

(235) Rivas, L.; de la Escosura-Muñiz, A.; Serrano, L.; Altet, L.; Francino, O.; Sánchez, A.; Merkoçi, A. Triple Lines Gold Nanoparticle-Based Lateral Flow Assay for Enhanced and Simultaneous Detection of Leishmania DNA and Endogenous Control. *Nano. Res.* **2015**, *8* (11), 3704–3714. https://doi.org/10.1007/s12274-015-0870-3.

(236) Kwon, J. H.; Kim, H. T.; Sim, S. J.; Cha, Y. J.; Lee, J. Performance of Point-of-Care Diagnosis of AIDS: Label-Free One-Step-Immunoassay: Vs. Lateral Flow Assay. *Analyst* **2018**, *143* (4), 936–942. https://doi.org/10.1039/c7an01748k.

(237) Hang, V. T.; Nguyet, N. M.; Trung, D. T.; Tricou, V.; Yoksan, S.; Dung, N. M.; Ngoc, T. van; Hien, T. T.; Farrar, J.; Wills, B.; Simmons, C. P. Diagnostic Accuracy of NS1 ELISA and Lateral Flow Rapid Tests for Dengue Sensitivity, Specificity and Relationship to Viraemia and Antibody Responses. *PLoS Negl. Trop. Dis.* **2009**, *3* (1). https://doi.org/10.1371/journal.pntd.0000360.

(238) Kim, J.; Cao, X. E.; Finkelstein, J. L.; Cárdenas, W. B.; Erickson, D.; Mehta, S. A Two-Colour Multiplexed Lateral Flow Immunoassay System to Differentially Detect Human Malaria Species on a Single Test Line. *Malar. J.* **2019**, *18* (1). https://doi.org/10.1186/s12936-019-2957-x.

(239) Li, Z.; Yi, Y.; Luo, X.; Xiong, N.; Liu, Y.; Li, S.; Sun, R.; Wang, Y.; Hu, B.; Chen, W.; Zhang, Y.; Wang, J.; Huang, B.; Lin, Y.; Yang, J.; Cai, W.; Wang, X.; Cheng, J.; Chen, Z.; Sun, K.; Pan, W.; Zhan, Z.; Chen, L.; Ye, F. Development and Clinical Application of a Rapid IgM-IgG Combined Antibody Test for SARS-CoV-2 Infection Diagnosis. *J. Med. Virol.* **2020**, *92* (9), 1518–1524. https://doi.org/10.1002/jmv.25727.

(240) Vaidya, V. S.; Ford, G. M.; Waikar, S. S.; Wang, Y.; Clement, M. B.; Ramirez, V.; Glaab, W. E.; Troth, S. P.; Sistare, F. D.; Prozialeck, W. C.; Edwards, J. R.; Bobadilla, N. A.; Mefferd, S. C.; Bonventre, J. v. A Rapid Urine Test for Early Detection of Kidney Injury. *Kidney Int.* **2009**, *76* (1), 108–114. https://doi.org/10.1038/ki.2009.96.

(241) Jux, U.; Baginski, R. M.; Arnold, H.-G.; Krönke, M.; Seng, P. N. Detection of Pharmaceutical Contaminations of River, Pond, and Tap Water from Cologne (Germany) and Surroundings. *Int. J. Hyg. Environ. Health* **2002**, *205*, 393–398. https://doi.org/https://doi.org/10.1078/1438-4639-00166.

(242) Li, D.; Wei, S.; Yang, H.; Li, Y.; Deng, A. A Sensitive Immunochromatographic Assay Using Colloidal Gold-Antibody Probe for Rapid Detection of Pharmaceutical Indomethacin in Water Samples. *Biosens. Bioelectron.* **2009**, *24* (7), 2277–2280. https://doi.org/10.1016/j.bios.2008.11.004.

(243) Li, S.; Ge, W.; Suryoprabowo, S.; Liu, J.; Kuang, H.; Zhu, J.; Liu, L.; Xu, C. A Paper-Based Sensor for Rapid and Ultrasensitive Detection of Ibuprofen in Water and Herbal Tea. *Analyst* **2021**, *146* (22), 6874–6882. https://doi.org/10.1039/d1an01533h.

(244) Yang, X.; Wang, Y.; Yang, J.; Sun, Z.; Chu, C.; Yue, Z.; Li, L.; Hu, X. Development of an Immunochromatographic Lateral Flow Strip Test for the Rapid Detection of Diclofenac

in Medicinal Wine. *Food. Agric. Immunol.* **2020**, *31* (1), 205–216. https://doi.org/10.1080/09540105.2020.1712331.

(245) Gandhi, S.; Caplash, N.; Sharma, P.; Raman Suri, C. Strip-Based Immunochromatographic Assay Using Specific Egg Yolk Antibodies for Rapid Detection of Morphine in Urine Samples. *Biosens. Bioelectron.* **2009**, *25* (2), 502–505. https://doi.org/10.1016/j.bios.2009.07.018.

(246) Angelini, D. J.; Biggs, T. D.; Maughan, M. N.; Feasel, M. G.; Sisco, E.; Sekowski, J. W. Evaluation of a Lateral Flow Immunoassay for the Detection of the Synthetic Opioid Fentanyl. *Forensic Sci. Int.* **2019**, *300*, 75–81. https://doi.org/10.1016/j.forsciint.2019.04.019.

(247) Hudson, M.; Stuchinskaya, T.; Ramma, S.; Patel, J.; Sievers, C.; Goetz, S.; Hines, S.; Menzies, E.; Russell, D. A. Drug Screening Using the Sweat of a Fingerprint: Lateral Flow Detection of ’ " 9 -Tetrahydrocannabinol, Cocaine, Opiates and Amphetamine. *J. Anal. Toxicol.* **2019**, *43* (2), 88–95. https://doi.org/10.1093/jat/bky068.

(248) Hatta, M.; Goris, M. G. A.; Heerkens, E.; Gooskens, J.; Smits, H. L. Simple Dipstick Assay for the Detection of Salmonella Typhi-Specific IgM Antibodies and the Evolution of the Immune Response in Patients with Typhoid Fever. *Am. J. Trop. Med. Hyg.* **2002**, *66* (4), 416–421. https://doi.org/10.4269/ajtmh.19-0053.

(249) Shim, W. B.; Kim, M. J.; Mun, H.; Kim, M. G. An Aptamer-Based Dipstick Assay for the Rapid and Simple Detection of Aflatoxin B1. *Biosens. Bioelectron.* **2014**, *62*, 288–294. https://doi.org/10.1016/j.bios.2014.06.059.

(250) Tang, D.; Sauceda, J. C.; Lin, Z.; Ott, S.; Basova, E.; Goryacheva, I.; Biselli, S.; Lin, J.; Niessner, R.; Knopp, D. Magnetic Nanogold Microspheres-Based Lateral-Flow Immunodipstick for Rapid Detection of Aflatoxin B2 in Food. *Biosens. Bioelectron.* **2009**, *25* (2), 514–518. https://doi.org/10.1016/j.bios.2009.07.030.

(251) Jarvis, J. N.; Percival, A.; Bauman, S.; Pelfrey, J.; Meintjes, G.; Williams, G. N.; Longley, N.; Harrison, T. S.; Kozel, T. R. Evaluation of a Novel Point-of-Care Cryptococcal Antigen Test on Serum, Plasma, and Urine from Patients with HIV-Associated Cryptococcal Meningitis. *Clin. Infect. Dis.* **2011**, *53* (10), 1019–1023. https://doi.org/10.1093/cid/cir613.

(252) Mishra, P.; Banga, I.; Tyagi, R.; Munjal, T.; Goel, A.; Capalash, N.; Sharma, P.; Suri, C. R.; Gandhi, S. An Immunochromatographic Dipstick as an Alternate for Monitoring of Heroin Metabolites in Urine Samples. *RSC Adv.* **2018**, *8* (41), 23163–23170. https://doi.org/10.1039/C8RA02018C.

(253) Chen, A.; Yang, S. Replacing Antibodies with Aptamers in Lateral Flow Immunoassay. *Biosens. Bioelectron.* **2015**, *71*, 230–242. https://doi.org/10.1016/j.bios.2015.04.041.

(254) Stine, R.; Pishko, M. v.; Schengrund, C. L. Comparison of Glycosphingolipids and Antibodies as Receptor Molecules for Ricin Detection. *Anal Chem* **2005**, *77* (9), 2882–2888. https://doi.org/10.1021/ac048126s.

(255) Frohnmeyer, E.; Tuschel, N.; Sitz, T.; Hermann, C.; Dahl, G. T.; Schulz, F.; Baeumner, A. J.; Fischer, M. Aptamer Lateral Flow Assays for Rapid and Sensitive Detection of Cholera Toxin. *Analyst* **2019**, *144* (5), 1840–1849. https://doi.org/10.1039/c8an01616j.

(256) Baker, A. N.; Hawker-Bond, G. W.; Georgiou, P. G.; Dedola, S.; Field, R. A.; Gibson, M. I. Glycosylated Gold Nanoparticles in Point of Care Diagnostics: From Aggregation to Lateral Flow Antibody-Based Lateral Flow. *Chem. Soc. Rev.* **2022**. https://doi.org/10.1039/d2cs00267a.

(257) Toyoshima, M.; Oura, T.; Fukuda, T.; Matsumoto, E.; Miura, Y. Biological Specific Recognition of Glycopolymer- Modified Interfaces by RAFT Living Radical Polymerization. *Polym. J.* **2010**, *42* (2), 172–178. https://doi.org/10.1038/pj.2009.321.

(258) Ishii, J.; Toyoshima, M.; Chikae, M.; Takamura, Y.; Miura, Y. Preparation of Glycopolymer-Modified Gold Nanoparticles and a New Approach for a Lateral Flow Assay. *Bull. Chem. Soc. Jpn.* **2011**, *84* (5), 466–470. https://doi.org/10.1246/bcsj.20100303.

(259) Takara, M.; Toyoshima, M.; Seto, H.; Hoshino, Y.; Miura, Y. Polymer-Modified Gold Nanoparticles via RAFT Polymerization: A Detailed Study for a Biosensing Application. *Polym. Chem.* **2014**, *5* (3), 931–939. https://doi.org/10.1039/c3py01001e.

(260) Baker, A. N.; Richards, S. J.; Guy, C. S.; Congdon, T. R.; Hasan, M.; Zwetsloot, A. J.; Gallo, A.; Lewandowski, J. R.; Stansfeld, P. J.; Straube, A.; Walker, M.; Chessa, S.; Pergolizzi, G.; Dedola, S.; Field, R. A.; Gibson, M. I. The SARS-COV-2 Spike Protein Binds Sialic Acids and Enables Rapid Detection in a Lateral Flow Point of Care Diagnostic Device. *ACS Cent. Sci.* **2020**, *6* (11), 2046–2052. https://doi.org/10.1021/acscentsci.0c00855.

(261) Baker, A. N.; Richards, S. J.; Pandey, S.; Guy, C. S.; Ahmad, A.; Hasan, M.; Biggs, C. I.; Georgiou, P. G.; Zwetsloot, A. J.; Straube, A.; Dedola, S.; Field, R. A.; Anderson, N. R.; Walker, M.; Grammatopoulos, D.; Gibson, M. I. Glycan-Based Flow-Through Device for the Detection of SARS-COV-2. *ACS Sens.* **2021**, *6* (10), 3696–3705. https://doi.org/10.1021/acssensors.1c01470.

(262) Baker, A. N.; Muguruza, A. R.; Richards, S. J.; Georgiou, P. G.; Goetz, S.; Walker, M.; Dedola, S.; Field, R. A.; Gibson, M. I. Lateral Flow Glyco-Assays for the Rapid and Low-Cost Detection of Lectins–Polymeric Linkers and Particle Engineering Are Essential for Selectivity and Performance. *Adv. Healthc. Mater.* **2022**, *11* (4). https://doi.org/10.1002/adhm.202101784.

(263) Baker, A. N.; Congdon, T. R.; Richards, S.-J.; Georgiou, P. G.; Walker, M.; Dedola, S.; Field, R. A.; Gibson, M. I. End-Functionalized Poly(Vinylpyrrolidone) for Ligand Display in Lateral Flow Device Test Lines. *ACS Polymers Au* **2022**, *2* (2), 69–79. https://doi.org/10.1021/acspolymersau.1c00032.

(264) Kim, S. H.; Kearns, F. L.; Rosenfeld, M. A.; Casalino, L.; Papanikolas, M. J.; Simmerling, C.; Amaro, R. E.; Freeman, R. GlycoGrip: Cell Surface-Inspired Universal Sensor for Betacoronaviruses. *ACS Cent. Sci.* **2022**, *8* (1), 22–42. https://doi.org/10.1021/acscentsci.1c01080.

(265) Kim, D. S.; Kim, Y. T.; Hong, S. B.; Kim, J.; Huh, N. S.; Lee, M. K.; Lee, S. J.; Kim, B. il; Kim, I. S.; Huh, Y. S.; Choi, B. G. Development of Lateral Flow Assay Based on Size-Controlled Gold Nanoparticles for Detection of Hepatitis B Surface Antigen. *Sensors* **2016**, *16* (12). https://doi.org/10.3390/s16122154.

(266) Zhan, L.; Guo, S. Z.; Song, F.; Gong, Y.; Xu, F.; Boulware, D. R.; McAlpine, M. C.; Chan, W. C. W.; Bischof, J. C. The Role of Nanoparticle Design in Determining Analytical Performance of Lateral Flow Immunoassays. *Nano Lett.* **2017**, *17* (12), 7207–7212. https://doi.org/10.1021/acs.nanolett.7b02302.

(267) Hirsch, L. R.; Jackson, J. B.; Lee, A.; Halas, N. J.; West, J. L. A Whole Blood Immunoassay Using Gold Nanoshells. *Anal. Chem.* **2003**, *75* (10), 2377–2381. https://doi.org/10.1021/ac0262210.

(268) Gonzalez-Moa, M. J.; van Dorst, B.; Lagatie, O.; Verheyen, A.; Stuyver, L.; Biamonte, M. A. Proof-of-Concept Rapid Diagnostic Test for Onchocerciasis: Exploring Peptide Biomarkers and the Use of Gold Nanoshells as Reporter Nanoparticles. *ACS Infect Dis* **2018**, *4* (6), 912–917. https://doi.org/10.1021/acsinfecdis.8b00031.

(269) Khlebtsov, B.; Khlebtsov, N. Enhanced Solid-Phase Immunoassay Using Gold Nanoshells: Effect of Nanoparticle Optical Properties. *Nanotechnology* **2008**, *19* (43). https://doi.org/10.1088/0957-4484/19/43/435703.

(270) Bikkarolla, S. K.; McNamee, S. E.; Vance, P.; McLaughlin, J. High-Sensitive Detection and Quantitative Analysis of Thyroid-Stimulating Hormone Using Gold-Nanoshell-Based Lateral Flow Immunoassay Device. *Biosensors (Basel)* **2022**, *12* (3). https://doi.org/10.3390/bios12030182.

(271) Khullar, P.; Singh, V.; Mahal, A.; Dave, P. N.; Thakur, S.; Kaur, G.; Singh, J.; Singh Kamboj, S.; Singh Bakshi, M. Bovine Serum Albumin Bioconjugated Gold Nanoparticles: Synthesis, Hemolysis, and Cytotoxicity toward Cancer Cell Lines. *J. Phys. Chem. C* **2012**, *116* (15), 8834–8843. https://doi.org/10.1021/jp300585d.

(272) Erickson, H. P. Size and Shape of Protein Molecules at the Nanometer Level Determined by Sedimentation, Gel Filtration, and Electron Microscopy. *Biol. Proced. Online*. 2009, pp 32–51. https://doi.org/10.1007/s12575-009-9008-x.

(273) Wang, H. D.; Niu, C. H.; Yang, Q.; Badea, I. Study on Protein Conformation and Adsorption Behaviors in Nanodiamond Particle-Protein Complexes. *Nanotechnology* **2011**, *22* (14). https://doi.org/10.1088/0957-4484/22/14/145703.

(274) Ju, S.; Yeo, W. S. Quantification of Proteins on Gold Nanoparticles by Combining MALDI-TOF MS and Proteolysis. *Nanotechnology* **2012**, *23* (13). https://doi.org/10.1088/0957-4484/23/13/135701.

(275) Katayama, T.; Sakuma, A.; Kimura, T.; Makimura, Y.; Hiratake, J.; Sakata, K.; Yamanoi, T.; Kumagai, H.; Yamamoto, K. Molecular Cloning and Characterization of Bifidobacterium Bifidum 1,2-α-L-Fucosidase (AfcA), a Novel Inverting Glycosidase (Glycoside Hydrolase Family 95). *J. Bacteriol.* **2004**, *186* (15), 4885–4893. https://doi.org/10.1128/JB.186.15.4885-4893.2004.

(276) Bahl, O. P.; Agrawal, K. M. L. Glycosidases of Aspergillus Niger. *J. Biol. Chem.* **1969**, *244* (11), 2970–2978. https://doi.org/10.1016/s0021-9258(18)91719-9.

(277) Chien, Y. Y.; Jan, M. D.; Adak, A. K.; Tzeng, H. C.; Lin, Y. P.; Chen, Y. J.; Wang, K. T.; Chen, C. T.; Chen, C. C.; Lin, C. C. Globotriose-Functionalized Gold Nanoparticles as Multivalent Probes for Shiga-like Toxin. *ChemBioChem* **2008**, *9* (7), 1100–1109. https://doi.org/10.1002/cbic.200700590.

(278) Koehler, L. H. Differentiation of Carbohydrates by Anthrone Reaction Rate and Color Intensity. *Anal. Chem.* **1954**, *24* (10), 1576–1579. https://doi.org/https://doi.org/10.1021/ac60070a014.

(279) Nyffeler, P. T.; Liang, C. H.; Koeller, K. M.; Wong, C. H. The Chemistry of Amine-Azide Interconversion: Catalytic Diazotransfer and Regioselective Azide Reduction. *J. Am. Chem. Soc.* **2002**, *124* (36), 10773–10778. https://doi.org/10.1021/ja0264605.

(280) Fulton, R. E.; Thompson, H. G. Fluorogenic Hand-Held Immunoassay for the Identification of Ricin: Rapid Analyte Measurement Platform. *J. Immunoassay Immunochem.* **2007**, *28* (3), 227–241. https://doi.org/10.1080/15321810701454730.

(281) Wittmann, V.; Pieters, R. J. Bridging Lectin Binding Sites by Multivalent Carbohydrates. *Chem. Soc. Rev.* **2013**, *42* (10), 4492–4503. https://doi.org/10.1039/c3cs60089k.

(282) Oyelaran, O.; Li, Q.; Farnsworth, D.; Gildersleeve, J. C. Microarrays with Varying Carbohydrate Density Reveal Distinct Subpopulations of Serum Antibodies. *J. Proteome Res.* **2009**, *8* (7), 3529–3538. https://doi.org/10.1021/pr9002245.

(283) Ling, H.; Boodhoo, A.; Hazes, B.; Cummings, M. D.; Armstrong, G. D.; Brunton, J. L.; Read, R. J. Structure of the Shiga-like Toxin I B-Pentamer Complexed with an Analogue of Its Receptor Gb3. *Biochemistry* **1998**, *37*, 1777–1788. https://doi.org/https://doi.org/10.1021/bi971806n.

(284) Lundquist, J. J.; Debenham, S. D.; Toone, E. J. Multivalency Effects in Protein-Carbohydrate Interaction: The Binding of the Shiga-like Toxin 1 Binding Subunit to Multivalent C-Linked Glycopeptides. *J. Org. Chem.* **2000**, *65* (24), 8245–8250. https://doi.org/10.1021/jo000943e.

(285) Kitov, P. I.; Sadowska, J. M.; Mulvey[2], G.; Armstrong[2], G. D.; Ling[3], H.; Pannu, N. S.; Read[23], R. J.; Bundle, D. R. Shiga-like Toxins Are Neutralized by Tailored Multivalent Carbohydrate Ligands. *Nature* **2000**, *403*, 669–672. https://doi.org/10.1038/35001095.

(286) Mulvey, G. L.; Marcato, P.; Kitov, P. I.; Sadowska, J.; Bundle, D. R.; Armstrong, G. D. Assessment in Mice of the Therapeutic Potential of Tailored, Multivalent Shiga Toxin Carbohydrate Ligands. *J. Infect. Dis.* **2003**, *187*, 640–649. https://doi.org/https://doi.org/10.1086/373996.

(287) Nishikawa, K.; Matsuoka, K.; Kita, E.; Okabe, N.; Mizuguchi, M.; Hino, K.; Miyazawa, S.; Yamasaki, C.; Aoki, J.; Takashima, S.; Yamakawa, Y.; Nishijima, M.; Terunuma, D.; Kuzuhara, H.; Natori, Y. A Therapeutic Agent with Oriented Carbohydrates for Treatment of Infections by Shiga Toxin-Producing Escherichia Coli O157:H7. *PNAS* **2002**, *99* (11), 7669–7674. https://doi.org/https://doi.org/10.1073/pnas.112058999.

(288) Fan, E.; Zhang, Z.; Minke, W. E.; Hou, Z.; Verlinde, C. L. M. J.; Hol, W. G. J. Heterobifunctional Multivalent Inhibitor-Adaptor Mediates Specific Aggregation between Shiga Toxin and a Pentraxin. *J. Am. Chem. Soc.* **2005**, *122* (3), 254–259. https://doi.org/10.1021/ol051529.

(289) Ho, J. G. S.; Kitov, P. I.; Paszkiewicz, E.; Sadowska, J.; Bundle, D. R.; Ng, K. K. S. Ligand-Assisted Aggregation of Proteins: Dimerization of Serum Amyloid P Component by Bivalent Ligands. *J. Biol. Chem.* **2005**, *280* (36), 31999–32008. https://doi.org/10.1074/jbc.M504403200.

(290) Kitov, P. I.; Mulvey, G. L.; Griener, T. P.; Lipinski, T.; Solomon, D.; Paszkiewicz, E.; Jacobson, J. M.; Sadowska, J. M.; Suzuki, M.; Yamamura, K.-I.; Armstrong, G. D.; Bundle, D. R. In Vivo Supramolecular Templating Enhances the Activity of Multivalent Ligands: A Potential Therapeutic against the Escherichia Coli O157 AB 5 Toxins. *PNAS* **2008**, *105* (44), 16837–16842. https://doi.org/10.1073/pnas.0804919105.

(291) Jacobson, J. M.; Kitov, P. I.; Bundle, D. R. The Synthesis of a Multivalent Heterobifunctional Ligand for Specific Interaction with Shiga Toxin 2 Produced by E. Coli O157:H7. *Carbohydr. Res.* **2013**, *378*, 4–14. https://doi.org/10.1016/j.carres.2013.05.010.

(292) Dasgupta, S.; Kitov, P. I.; Sadowska, J. M.; Bundle, D. R. Discovery of Inhibitors of Shiga Toxin Type 2 by On-Plate Generation and Screening of a Focused Compound Library. *Angew. Chem. Int. Ed.* **2014**, *53* (6), 1510–1515. https://doi.org/10.1002/anie.201309436.

(293) Matsuoka, K.; Nishikawa, K.; Goshu, Y.; Koyama, T.; Hatano, K.; Matsushita, T.; Watanabe-Takahashi, M.; Natori, Y.; Terunuma, D. Synthetic Construction of Sugar-Amino Acid Hybrid Polymers Involving Globotriaose or Lactose and Evaluation of Their Biological Activities against Shiga Toxins Produced by Escherichia Coli O157:H7. *Bioorg. Med. Chem.* **2018**, *26* (22), 5792–5803. https://doi.org/10.1016/j.bmc.2018.10.023.

(294) Li, X.; Wu, P.; Cheng, S.; Lv, X. Synthesis and Assessment of Globotriose-Chitosan Conjugate, a Novel Inhibitor of Shiga Toxins Produced by Escherichia Coli. *J. Med. Chem.* **2012**, *55* (6), 2702–2710. https://doi.org/10.1021/jm201570s.

(295) Zhang, P.; Paszkiewicz, E.; Wang, Q.; Sadowska, J. M.; Kitov, P. I.; Bundle, D. R.; Ling, C. C. Clustering of PK-Trisaccharides on Amphiphilic Cyclodextrin Reveals Unprecedented Affinity for the Shiga-like Toxin Stx2. *Chem. Comm.* **2017**, *53* (76), 10528–10531. https://doi.org/10.1039/c7cc06299k.

(296) Haksar, D.; Asadpoor, M.; Heise, T.; Shi, J.; Braber, S.; Folkerts, G.; Ballell, L.; Rodrigues, J.; Pieters, R. J. Fighting Shigella by Blocking Its Disease-Causing Toxin. *J. Med. Chem.* **2021**, *64* (9), 6059–6069. https://doi.org/10.1021/acs.jmedchem.1c00152.

(297) Branson, T. R.; McAllister, T. E.; Garcia-Hartjes, J.; Fascione, M. A.; Ross, J. F.; Warriner, S. L.; Wennekes, T.; Zuilhof, H.; Turnbull, W. B. A Protein-Based Pentavalent Inhibitor of the Cholera Toxin B-Subunit. *Angew. Chem. Int. Ed.* **2014**, *53* (32), 8323–8327. https://doi.org/10.1002/anie.201404397.

(298) Jobling, M. G.; Holmes, R. K. Analysis of Structure and Function of the B Subunit of Cholera Toxin by the Use of Site-Directed Mutagenesis. *Mol. Microbiol.* **1991**, *5* (7), 1755–1767. https://doi.org/10.1111/j.1365-2958.1991.tb01925.x.

(299) Vrasidas, I.; de Mol, N. J.; Liskamp, R. M. J.; Pieters, R. J. Synthesis of Lactose Dendrimers and Multivalency Effects in Binding to the Cholera Toxin B Subunit. *Eur. J. Org. Chem.* **2001**, *24*, 4685–4692. https://doi.org/https://doi.org/10.1002/1099-0690(200112)2001:24<4685::AID-EJOC4685>3.0.CO;2-9.

(300) Pukin, A. v.; Branderhorst, H. M.; Sisu, C.; Weijers, C. A. G. M.; Gilbert, M.; Liskamp, R. M. J.; Visser, G. M.; Zuilhof, H.; Pieters, R. J. Strong Inhibition of Cholera Toxin by Multivalent GM1 Derivatives. *ChemBioChem* **2007**, *8* (13), 1500–1503. https://doi.org/10.1002/cbic.200700266.

(301) Sisu, C.; Baron, A. J.; Branderhorst, H. M.; Connell, S. D.; Weijers, C. A. G. M.; de Vries, R.; Hayes, E. D.; Pukin, A. v.; Gilbert, M.; Pieters, R. J.; Zuilhof, H.; Visser, G. M.; Turnbull, W. B. The Influence of Ligand Valency on Aggregation Mechanisms for Inhibiting Bacterial Toxins. *ChemBioChem* **2009**, *10* (2), 329–337. https://doi.org/10.1002/cbic.200800550.

(302) Fu, O.; Pukin, A. v.; Vanufford, H. C. Q.; Branson, T. R.; Thies-Weesie, D. M. E.; Turnbull, W. B.; Visser, G. M.; Pieters, R. J. Tetra- versus Pentavalent Inhibitors of Cholera Toxin. *ChemistryOpen* **2015**, *4* (4), 471–477. https://doi.org/10.1002/open.201500006.

(303) Arosio, D.; Vrasidas, I.; Valentini, P.; Liskamp, R. M. J.; Pieters, R. J.; Bernardi, A. Synthesis and Cholera Toxin Binding Properties of Multivalent GM1 Mimics. *Org. Biomol. Chem.* **2004**, *2* (14), 2113–2124. https://doi.org/10.1039/b405344c.

(304) Wilkins, L. E.; Badi, N.; du Prez, F.; Gibson, M. I. Double-Modified Glycopolymers from Thiolactones to Modulate Lectin Selectivity and Affinity. *ACS Macro. Lett.* **2018**, *7* (12), 1498–1502. https://doi.org/10.1021/acsmacrolett.8b00825.

(305) Liu, S.; Kiick, K. L. Architecture Effects on the Binding of Cholera Toxin by Helical Glycopolypeptides. *Macromolecules* **2008**, *41* (3), 764–772. https://doi.org/10.1021/ma702128a.

(306) Farmer, R. S.; Kiick, K. L. Conformational Behavior of Chemically Reactive Alanine-Rich Repetitive Protein Polymers. *Biomacromolecules* **2005**, *6* (3), 1531–1539. https://doi.org/10.1021/bm049216.

(307) Pickens, J.; Mitchell, D.; Liu, J.; Tan, X.; Zhang, Z.; Verlinde, C. L.; Hol, W.; Fan, E. Nonspanning Bivalent Ligands as Improved Surface Receptor Binding Inhibitors of the Cholera Toxin B Pentamer. *Chem. Biol.* **2004**, *11*, 1205–1215. https://doi.org/1.1016/j.chembiol.2004.06.008.

(308) Merritt, E. A.; Zhang, Z.; Pickens, J. C.; Ahn, M.; Hol, W. G. J.; Fan, E. Characterization and Crystal Structure of a High-Affinity Pentavalent Receptor-Binding Inhibitor for Cholera Toxin and E. Coli Heat-Labile Enterotoxin. *J. Am. Chem. Soc.* **2002**, *124* (30), 8818–8824. https://doi.org/10.1021/ja0202560.

(309) Haataja, S.; Tikkanen, K.; Nilsson, U.; Magnusson, G.; Karlsson, K. A.; Finne, J. Oligosaccharide-Receptor Interaction of the Galα1-4Gal Binding Adhesin of Streptococcus Suis. Combining Site Architecture and Characterization of Two Variant Adhesin Specificities. *J. Biol. Chem.* **1994**, *269* (44), 27466–27472. https://doi.org/10.1016/s0021-9258(18)47008-1.

(310) Joosten, J. A. F.; Loimaranta, V.; Appeldoorn, C. C. M.; Haataja, S.; Ait, F.; Maate, E.; Liskamp, R. M. J.; Finne, J.; Pieters, R. J. Inhibition of Streptococcus Suis Adhesion by Dendritic Galabiose Compounds at Low Nanomolar Concentration. *J. Med. Chem.* **2004**, *47* (26), 6499–6508. https://doi.org/10.1021/jm049476.

(311) Autar, R.; Khan, A. S.; Schad, M.; Hacker, J.; Liskamp, R. M. J.; Pieters, R. J. Adhesion Inhibition of F1C-Fimbriated Escherichia Coli and Pseudomonas Aeruginosa PAK and PAO by Multivalent Carbohydrate Ligands. *ChemBioChem* **2003**, *4* (12), 1317–1325. https://doi.org/10.1002/cbic.200300719.

(312) Appeldoorn, C. C. M.; Joosten, J. A. F.; Ait El Maate, F.; Dobrindt, U.; Hacker, J.; Liskamp, R. M. J.; Khan, A. S.; Pieters, R. J. Novel Multivalent Mannose Compounds and Their Inhibition of the Adhesion of Type 1 Fimbriated Uropathogenic E. Coli. *Tetrahedron Asymmetry* **2005**, *16* (2), 361–372. https://doi.org/10.1016/j.tetasy.2004.11.014.

(313) Haataja, S.; Verma, P.; Fu, O.; Papageorgiou, A. C.; Pöysti, S.; Pieters, R. J.; Nilsson, U. J.; Finne, J. Rationally Designed Chemically Modified Glycodendrimer Inhibits Streptococcus Suis Adhesin SadP at Picomolar Concentrations. *Chem. Eur. J.* **2018**, *24* (8), 1905–1912. https://doi.org/10.1002/chem.201704493.

(314) Ferrando, M. L.; Willemse, N.; Zaccaria, E.; Pannekoek, Y.; van der Ende, A.; Schultsz, C. Streptococcal Adhesin P (SadP) Contributes to Streptococcus Suis Adhesion to the

Human Intestinal Epithelium. *PLoS One* **2017**, *12* (4). https://doi.org/10.1371/journal.pone.0175639.

(315) Yan, X.; Sivignon, A.; Yamakawa, N.; Crepet, A.; Travelet, C.; Borsali, R.; Dumych, T.; Li, Z.; Bilyy, R.; Deniaud, D.; Fleury, E.; Barnich, N.; Darfeuille-Michaud, A.; Gouin, S. G.; Bouckaert, J.; Bernard, J. Glycopolymers as Antiadhesives of E. Coli Strains Inducing Inflammatory Bowel Diseases. *Biomacromolecules* **2015**, *16* (6), 1827–1836. https://doi.org/10.1021/acs.biomac.5b00413.

(316) Yan, X.; Sivignon, A.; Barnich, N.; Gouin, S. G.; Bouckaert, J.; Fleury, E.; Bernard, J. A Library of Heptyl Mannose-Functionalized Copolymers with Distinct Compositions, Microstructures and Neighboring Non-Sugar Motifs as Potent Antiadhesives of Type 1 Piliated E. Coli. *Polym. Chem.* **2016**, *7* (15), 2674–2683. https://doi.org/10.1039/c6py00118a.

(317) Garber, N.; Guempel, U.; Belz, A.; Gilboa-Garber, N.; Doyle, R. J. On the Specificity of the D-Galactose-Binding Lectin (PA-I) of Pseudomonas Aeruginosa and Its Strong Binding to Hydrophobic Derivatives of D-Galactose and Thiogalactose. *Biochim. Biophys. Acta* **1992**, *2226* (3), 331–333. https://doi.org/https://doi.org/10.1016/0304-4165(92)90048-Y.

(318) Kadam, R. U.; Bergmann, M.; Hurley, M.; Garg, D.; Cacciarini, M.; Swiderska, M. A.; Nativi, C.; Sattler, M.; Smyth, A. R.; Williams, P.; Cámara, M.; Stocker, A.; Darbre, T.; Reymond, J. L. A Glycopeptide Dendrimer Inhibitor of the Galactose-Specific Lectin LecA and of Pseudomonas Aeruginosa Biofilms. *Angew. Chem. Int. Ed.* **2011**, *50* (45), 10631–10635. https://doi.org/10.1002/anie.201104342.

(319) Kadam, R. U.; Garg, D.; Schwartz, J.; Visini, R.; Sattler, M.; Stocker, A.; Darbre, T.; Reymond, J. L. CH-π "t-Shape" Interaction with Histidine Explains Binding of Aromatic Galactosides to Pseudomonas Aeruginosa Lectin LecA. *ACS Chem. Biol.* **2013**, *8* (9), 1925–1930. https://doi.org/10.1021/cb400303w.

(320) Siebs, E.; Shanina, E.; Kuhaudomlarp, S.; da Silva Figueiredo Celestino Gomes, P.; Fortin, C.; Seeberger, P. H.; Rognan, D.; Rademacher, C.; Imberty, A.; Titz, A. Targeting the Central Pocket of the Pseudomonas Aeruginosa Lectin LecA. *ChemBioChem* **2022**, *23* (3). https://doi.org/10.1002/cbic.202100563.

(321) Meiers, J.; Zahorska, E.; Röhrig, T.; Hauck, D.; Wagner, S.; Titz, A. Directing Drugs to Bugs: Antibiotic-Carbohydrate Conjugates Targeting Biofilm-Associated Lectins of Pseudomonas Aeruginosa. *J. Med. Chem.* **2020**, *63* (20), 11707–11724. https://doi.org/10.1021/acs.jmedchem.0c00856.

(322) Meiers, J.; Rox, K.; Titz, A. Lectin-Targeted Prodrugs Activated by Pseudomonas Aeruginosa for Self-Destructive Antibiotic Release. *J. Med. Chem.* **2022**, *65* (20), 13988–14014. https://doi.org/10.1021/acs.jmedchem.2c01214.

(323) Deguise, I.; Lagnoux, D.; Roy, R. Synthesis of Glycodendrimers Containing Both Fucoside and Galactoside Residues and Their Binding Properties to Pa-IL and PA-IIL

Lectins from Pseudomonas Aeruginosa. *New J. Chem.* **2007**, *31* (7), 1321–1331. https://doi.org/10.1039/b701237c.

(324) Imberty, A.; Wimmerová, M.; Mitchell, E. P.; Gilboa-Garber, N. Structures of the Lectins from Pseudomonas Aeruginosa: Insights into the Molecular Basis for Host Glycan Recognition. *Microbes Infect.* **2004**, *6* (2), 221–228. https://doi.org/10.1016/j.micinf.2003.10.016.

(325) Mohy El Dine, T.; Jimmidi, R.; Diaconu, A.; Fransolet, M.; Michiels, C.; de Winter, J.; Gillon, E.; Imberty, A.; Coenye, T.; Vincent, S. P. Pillar[5]Arene-Based Polycationic Glyco[2]Rotaxanes Designed as Pseudomonas Aeruginosa Antibiofilm Agents. *J. Med. Chem.* **2021**, *64* (19), 14728–14744. https://doi.org/10.1021/acs.jmedchem.1c01241.

(326) Joseph, R.; Kaizerman, D.; Herzog, I. M.; Hadar, M.; Feldman, M.; Fridman, M.; Cohen, Y. Phosphonium Pillar[5]Arenes as a New Class of Efficient Biofilm Inhibitors: Importance of Charge Cooperativity and the Pillar Platform. *Chem. Comm.* **2016**, *52* (70), 10656–10659. https://doi.org/10.1039/c6cc05170g.

(327) Cecioni, S.; Lalor, R.; Blanchard, B.; Praly, J. P.; Imberty, A.; Matthews, S. E.; Vidal, S. Achieving High Affinity towards a Bacterial Lectin through Multivalent Topological Isomers of Calix[4]Arene Glycoconjugates. *Chem. Eur. J.* **2009**, *15* (47), 13232–13240. https://doi.org/10.1002/chem.200901799.

(328) Cecioni, S.; Faure, S.; Darbost, U.; Bonnamour, I.; Parrot-Lopez, H.; Roy, O.; Taillefumier, C.; Wimmerová, M.; Praly, J. P.; Imberty, A.; Vidal, S. Selectivity among Two Lectins: Probing the Effect of Topology, Multivalency and Flexibility of "Clicked" Multivalent Glycoclusters. *Chem. Eur. J.* **2011**, *17* (7), 2146–2159. https://doi.org/10.1002/chem.201002635.

(329) Soomro, Z. H.; Cecioni, S.; Blanchard, H.; Praly, J. P.; Imberty, A.; Vidal, S.; Matthews, S. E. CuAAC Synthesis of Resorcin[4]Arene-Based Glycoclusters as Multivalent Ligands of Lectins. *Org. Biomol. Chem.* **2011**, *9* (19), 6587–6597. https://doi.org/10.1039/c1ob05676j.

(330) Sicard, D.; Cecioni, S.; Iazykov, M.; Chevolot, Y.; Matthews, S. E.; Praly, J. P.; Souteyrand, E.; Imberty, A.; Vidal, S.; Phaner-Goutorbe, M. AFM Investigation of Pseudomonas Aeruginosa Lectin LecA (PA-IL) Filaments Induced by Multivalent Glycoclusters. *Chem. Comm.* **2011**, *47* (33), 9483–9485. https://doi.org/10.1039/c1cc13097h.

(331) Gening, M. L.; Titov, D. v.; Cecioni, S.; Audfray, A.; Gerbst, A. G.; Tsvetkov, Y. E.; Krylov, V. B.; Imberty, A.; Nifantiev, N. E.; Vidal, S. Synthesis of Multivalent Carbohydrate-Centered Glycoclusters as Nanomolar Ligands of the Bacterial Lectin LecA from Pseudomonas Aeruginosa. *Chem. Eur. J.* **2013**, *19* (28), 9272–9285. https://doi.org/10.1002/chem.201300135.

(332) Chabre, Y. M.; Giguère, D.; Blanchard, B.; Rodrigue, J.; Rocheleau, S.; Neault, M.; Rauthu, S.; Papadopoulos, A.; Arnold, A. A.; Imberty, A.; Roy, R. Combining

Glycomimetic and Multivalent Strategies toward Designing Potent Bacterial Lectin Inhibitors. *Chem. Eur. J.* **2011**, *17* (23), 6545–6562. https://doi.org/10.1002/chem.201003402.

(333) Pertici, F.; Pieters, R. J. Potent Divalent Inhibitors with Rigid Glucose Click Spacers for Pseudomonas Aeruginosa Lectin LecA. *Chem. Comm.* **2012**, *48* (33), 4008–4010. https://doi.org/10.1039/c2cc30234a.

(334) Pertici, F.; de Mol, N. J.; Kemmink, J.; Pieters, R. J. Optimizing Divalent Inhibitors of Pseudomonas Aeruginosa Lectin Leca by Using a Rigid Spacer. *Chem. Eur. J.* **2013**, *19* (50), 16923–16927. https://doi.org/10.1002/chem.201303463.

(335) Yu, G.; Vicini, A. C.; Pieters, R. J. Assembly of Divalent Ligands and Their Effect on Divalent Binding to Pseudomonas Aeruginosa Lectin LecA. *J. Org. Chem.* **2019**, *84* (5), 2470–2488. https://doi.org/10.1021/acs.joc.8b02727.

(336) Fu, O.; Pukin, A. v.; Quarlesvanufford, H. C.; Kemmink, J.; DeMol, N. J.; Pieters, R. J. Functionalization of a Rigid Divalent Ligand for LecA, a Bacterial Adhesion Lectin. *ChemistryOpen* **2015**, *4* (4), 463–470. https://doi.org/10.1002/open.201402171.

(337) Zaree, P.; Sastre Torano, J.; de Haan, C. A. M.; Scheltema, R. A.; Barendregt, A.; Thijssen, V.; Yu, G.; Flesch, F.; Pieters, R. J. The Assessment of Pseudomonas Aeruginosa Lectin LecA Binding Characteristics of Divalent Galactosides Using Multiple Techniques. *Glycobiology* **2021**, *31* (11), 1490–1499. https://doi.org/10.1093/glycob/cwab074.

(338) Visini, R.; Jin, X.; Bergmann, M.; Michaud, G.; Pertici, F.; Fu, O.; Pukin, A.; Branson, T. R.; Thies-Weesie, D. M. E.; Kemmink, J.; Gillon, E.; Imberty, A.; Stocker, A.; Darbre, T.; Pieters, R. J.; Reymond, J. L. Structural Insight into Multivalent Galactoside Binding to Pseudomonas Aeruginosa Lectin LecA. *ACS Chem. Biol.* **2015**, *10* (11), 2455–2462. https://doi.org/10.1021/acschembio.5b00302.

(339) Pertici, F.; Varga, N.; van Duijn, A.; Rey-Carrizo, M.; Bernardi, A.; Pieters, R. J. Efficient Synthesis of Phenylene-Ethynylene Rods and Their Use as Rigid Spacers in Divalent Inhibitors. *Beilstein J. Org. Chem.* **2013**, *9*, 215–222. https://doi.org/10.3762/bjoc.9.25.

(340) Zahorska, E.; Kuhaudomlarp, S.; Minervini, S.; Yousaf, S.; Lepsik, M.; Kinsinger, T.; Hirsch, A. K. H.; Imberty, A.; Titz, A. A Rapid Synthesis of Low-Nanomolar Divalent LecA Inhibitors in Four Linear Steps from d-Galactose Pentaacetate. *Chem. Comm.* **2020**, *56* (62), 8822–8825. https://doi.org/10.1039/d0cc03490h.

(341) Hanwell, M. D.; Curtis, D. E.; Lonie, D. C.; Vandermeersch, T.; Zurek, E.; Hutchison, G. R. Access Avogadro: An Advanced Semantic Chemical Editor, Visualization, and Analysis Platform. *J. Cheminform.* **2012**, *4*, 17. https://doi.org/https://doi.org/10.1186/1758-2946-4-17.

(342) Imberty, A.; Wimmerová, M.; Mitchell, E. P.; Gilboa-Garber, N. Structures of the Lectins from Pseudomonas Aeruginosa: Insights into the Molecular Basis for Host

Glycan Recognition. *Microbes Infect.* **2004**, *6* (2), 221–228. https://doi.org/10.1016/j.micinf.2003.10.016.

(343) Kawano, S. I.; Tamaru, S. I.; Fujita, N.; Shinkai, S. Sol-Gel Polycondensation of Tetraethyl Orthosilicate (TEOS) in Sugar-Based Porphyrin Organogels: Inorganic Conversion of a Sugar-Directed Porphyrinic Fiber Library through Sol-Gel Transcription Processes. *Chem. Eur. J.* **2004**, *10* (2), 343–351. https://doi.org/10.1002/chem.200305042.

(344) Cao, S.; Hernández-Matéo, F.; Roy, R. Scope and Applications of "Active and Latent" Thioglycosyl Donors. Part 4. *J. Carbohydr. Chem.* **1998**, *17* (4–5), 609–631. https://doi.org/10.1080/07328309808002341.

(345) Kumar, V.; Giri, S. K.; Venugopalan, P.; Kartha, K. P. R. Synthesis of Cross-Linked Glycopeptides and Ureas by a Mechanochemical, Solvent-Free Reaction and Determination of Their Structural Properties by TEM and X-Ray Crystallography. *Chempluschem* **2014**, *79* (11), 1605–1613. https://doi.org/10.1002/cplu.201402185.

(346) Saman, E.; Claeyssens, M.; Kefsters-Hilderson, H.; de Bruyne, C. K. Azido Compounds as Potential Affinity Labels for Glycosidases. *Carbohydr. Res.* **1973**, *30*, 207–210. https://doi.org/https://doi.org/10.1016/S0008-6215(00)82193-X.

(347) Molander, G. A.; Cadoret, F. Synthesis of the Stereogenic Triad of the Halicyclamine A Core. *Tetrahedron Lett.* **2011**, *52* (17), 2199–2202. https://doi.org/10.1016/j.tetlet.2010.11.162.

(348) Creary, X.; Anderson, A.; Brophy, C.; Crowell, F.; Funk, Z. Method for Assigning Structure of 1,2,3-Triazoles. *J. Org. Chem.* **2012**, *77* (19), 8756–8761. https://doi.org/10.1021/jo301265t.

(349) Huggins, M. T.; Kesharwani, T.; Buttrick, J.; Nicholson, C. Variable Temperature NMR Experiment Studying Restricted Bond Rotation. *J. Chem. Educ.* **2020**, *97* (5), 1425–1429. https://doi.org/10.1021/acs.jchemed.0c00057.

(350) Cegielska, B.; Kacprzak, K. M. Simple and Convenient Protocol for Staining of Organic Azides on TLC Plates by Ninhydrin. A New Application of an Old Reagent. *Chem. Analityczna* **2009**, *54* (4), 807–812.

(351) Priyadarshi, N.; Ambule, M. D.; Kaushal, S.; Kumar, A.; Sagar, P.; Srivastava, A. K.; Singhal, N. K. Nanoglycocluster Based Diagnostic Platform for Colorimetric Detection of Bacteria; A Comparative Study Analysing the Effect of AuNPs Size, Linker Length, and Glycan Diversity. *Biosens Bioelectron* **2022**, *201*. https://doi.org/10.1016/j.bios.2022.113969.

(352) Moore, B. A. Developing Targeted Photodynamic Therapy Using Glyconanoparticles [Unpublished Doctoral Thesis], University of East Anglia, Department of Biological Chemistry, John Innes Centre, 2019.

(353) LaBauve, A. E.; Wargo, M. J. Growth and Laboratory Maintenance of Pseudomonas Aeruginosa. *Curr. Protoc. Microbiol.* **2012**, *25* (6E.1), 1–8. https://doi.org/10.1002/9780471729259.mc06e01s25.

(354) Diggle, S. P.; Winzer, K.; Lazdunski, A.; Williams, P.; Cámara, M. Advancing the Quorum in Pseudomonas Aeruginosa: MvaT and the Regulation of N-Acylhomoserine Lactone Production and Virulence Gene Expression. *J. Bacteriol.* **2002**, *184* (10), 2576–2586. https://doi.org/10.1128/JB.184.10.2576-2586.2002.

(355) Jeffers, F.; Fuell, C.; Tailford, L. E.; MacKenzie, D. A.; Bongaerts, R. J.; Juge, N. Mucin-Lectin Interactions Assessed by Flow Cytometry. *Carbohydr. Res.* **2010**, *345* (10), 1486–1491. https://doi.org/10.1016/j.carres.2010.05.012.

(356) Lamprinaki, D.; Garcia-Vello, P.; Marchetti, R.; Hellmich, C.; McCord, K. A.; Bowles, K. M.; Macauley, M. S.; Silipo, A.; de Castro, C.; Crocker, P. R.; Juge, N. Siglec-7 Mediates Immunomodulation by Colorectal Cancer-Associated Fusobacterium Nucleatum Ssp. Animalis. *Front. Immunol.* **2021**, *12*. https://doi.org/10.3389/fimmu.2021.744184.

(357) Pital, A.; Janowitz, S. L.; Hudak, C. E.; Lewis, E. E. Direct Fluorescent Labeling of Microorganisms as a Possible Life-Detection Technique. *Appl. Microbiol.* **1966**, *14* (1), 119–123.

(358) Winsor, G. L.; Griffiths, E. J.; Lo, R.; Dhillon, B. K.; Shay, J. A.; Brinkman, F. S. L. Enhanced Annotations and Features for Comparing Thousands of Pseudomonasgenomes in the Pseudomonas Genome Database. *Nucleic Acids Res.* **2016**, *44* (D1), D646–D653. https://doi.org/10.1093/nar/gkv1227.

(359) Sohrabi, H.; Majidi, M. R.; Fakhraei, M.; Jahanban-Esfahlan, A.; Hejazi, M.; Oroojalian, F.; Baradaran, B.; Tohidast, M.; Guardia, M. de la; Mokhtarzadeh, A. Lateral Flow Assays (LFA) for Detection of Pathogenic Bacteria: A Small Point-of-Care Platform for Diagnosis of Human Infectious Diseases. *Talanta* **2022**, *243* (123330). https://doi.org/10.1016/j.talanta.2022.123330.

(360) Donnier-Maréchal, M.; Abdullayev, S.; Bauduin, M.; Pascal, Y.; Fu, M. Q.; He, X. P.; Gillon, E.; Imberty, A.; Kipnis, E.; Dessein, R.; Vidal, S. Tetraphenylethylene-Based Glycoclusters with Aggregation-Induced Emission (AIE) Properties as High-Affinity Ligands of Bacterial Lectins. *Org Biomol. Chem.* **2018**, *16* (45), 8804–8809. https://doi.org/10.1039/c8ob02035c.

(361) Xu, Y.; Zhang, Q.; Xiao, Y.; Wu, P.; Chen, W.; Song, Z.; Xiao, X.; Meng, L.; Zeng, J.; Wan, Q. Practical Synthesis of Latent Disarmed S-2-(2-Propylthio)Benzyl Glycosides for Interrupted Pummerer Reaction Mediated Glycosylation. *Tetrahedron Lett.* **2017**, *58* (24), 2381–2384. https://doi.org/10.1016/j.tetlet.2017.05.014.

(362) Tesch, M.; Kudruk, S.; Letzel, M.; Studer, A. Orthogonal Click Postfunctionalization of Alternating Copolymers Prepared by Nitroxide-Mediated Polymerization. *Chemistry - A European Journal* **2017**, *23* (25), 5915–5919. https://doi.org/10.1002/chem.201605639.

(363) Bensoussan, C.; Rival, N.; Hanquet, G.; Colobert, F.; Reymond, S.; Cossy, J. Iron-Catalyzed Cross-Coupling between C-Bromo Mannopyranoside Derivatives and a Vinyl Grignard Reagent: Toward the Synthesis of the C31-C52 Fragment of Amphidinol 3. *Tetrahedron* **2013**, *69* (36), 7759–7770. https://doi.org/10.1016/j.tet.2013.05.067.

(364) Ligeour, C.; Dupin, L.; Marra, A.; Vergoten, G.; Meyer, A.; Dondoni, A.; Souteyrand, E.; Vasseur, J. J.; Chevolot, Y.; Morvan, F. Synthesis of Galactoclusters by Metal-Free Thiol "Click Chemistry" and Their Binding Affinities for Pseudomonas Aeruginosa Lectin Leca. *Eur. J. Org. Chem.* **2014**, *2014* (34), 7621–7630. https://doi.org/10.1002/ejoc.201402902.

(365) Gao, Y.; Chen, L.; Zhang, Z.; Gu, W.; Li, Y. Linear Cationic Click Polymer for Gene Delivery: Synthesis, Biocompatibility, and in Vitro Transfection. *Biomacromolecules* **2010**, *11* (11), 3102–3111. https://doi.org/10.1021/bm100906m.

(366) He, Y. Q.; Liu, S. P.; Kong, L.; Liu, Z. F. A Study on the Sizes and Concentrations of Gold Nanoparticles by Spectra of Absorption, Resonance Rayleigh Scattering and Resonance Non-Linear Scattering. *Spectrochim. Acta A Mol. Biomol. Spectrosc.* **2005**, *61* (13–14), 2861–2866. https://doi.org/10.1016/j.saa.2004.10.035.

(367) Bankevich, A.; Nurk, S.; Antipov, D.; Gurevich, A. A.; Dvorkin, M.; Kulikov, A. S.; Lesin, V. M.; Nikolenko, S. I.; Pham, S.; Prjibelski, A. D.; Pyshkin, A. v.; Sirotkin, A. v.; Vyahhi, N.; Tesler, G.; Alekseyev, M. A.; Pevzner, P. A. SPAdes: A New Genome Assembly Algorithm and Its Applications to Single-Cell Sequencing. *J. Comput. Biol.* **2012**, *19* (5), 455–477. https://doi.org/10.1089/cmb.2012.0021.

APPENDIX 1

EXPRESSION AND PURIFICATION OF *TRYPANOSOMA CRUZI* TRANS-SIALIDASE

The work described in this appendix was performed prior to the course of this thesis, at Iceni Glycoscience, by Dr Simona Chessa.

S1.1. TcTS expression incubation at RT overnight

For this study, 10 mL of ampicillin (10 µL of 100 mg/mL) supplemented LB medium were inoculated from cryo-glycerol stocks and incubated overnight at 37 °C with shaking at 200 rpm.

1 mL of this culture was used to inoculate 100 mL of ampicillin (100 µL of 100 mg/mL) supplemented LB medium, which was incubated at 37 °C with orbital shaking at 200 rpm overnight. 20 mL of this culture were used to inoculate 1 L of ampicillin (1 mL of 100 mg/mL) supplemented LB medium, which was incubated at 37 °C for 4 h with orbital shaking at 200 rpm until it reached an OD_{600nm} of 1. The culture was then induced with 0.2 mM isopropyl β-D-1-thiogalactopyranoside (IPTG, 200 µL of 1M) and incubated overnight at 18 °C.

S1.2. Lysis and purification

The culture was centrifuged at 12,000 × g at 4 °C for 20 minutes, and the pellets harvested for lysis. The pellets were suspended in B-PER complete bacterial protein extraction reagent, (Termofisher).

5 mL of B-PER were added per gramme of the pellets, followed by Protease Inhibitor cocktail (final concentration 2 mM benzamidine, 2 mM pepstatin, 2 mM leupeptine, 10 µL of solution per mL of suspension) and lysozyme (50 mg/ml stock solution, 10 µL per ml of suspension, for a final concentration of 250 µg/mL)

The suspension was incubated for 30 minutes at room temperature under gentle mixing and centrifuged at 4000 x g, 4 °C, for 20 min and the supernatant was collected.

S1.3. Purification of the Enzyme by Immobilized Metal Ion Affinity Chromatography IMAC

Purification of the enzyme was performed from *E. coli* soluble extracts containing enzyme, using a 1-mL-column HisTrap™ High Performance (Cytiva).

Following cell lysis and centrifugation, the supernatant was transferred into a 1 mL HisTrap HP column cartridge and the following purification protocol was performed using an AKTA-FPLC equipped with an UV detector. Using a flow of 1 mL/min, the column was washed with 5 CV of cold buffer A (20 mM imidazole, 0.5 M NaCl, 50 mM glycine, 50 mM TRIS-HCL, pH 8). Elution was performed using 5 CV of cold buffer B (200 mM imidazole, 0.5 M NaCl, 50 mM glycine, 50 mM TRIS-HCL, pH 8). The purified fractions 18-22 were collected and pooled together (**Figure S1.1**). The column was finally regenerated with 5 CV of buffer B, and re-equilibrated with 5 CV of buffer A.

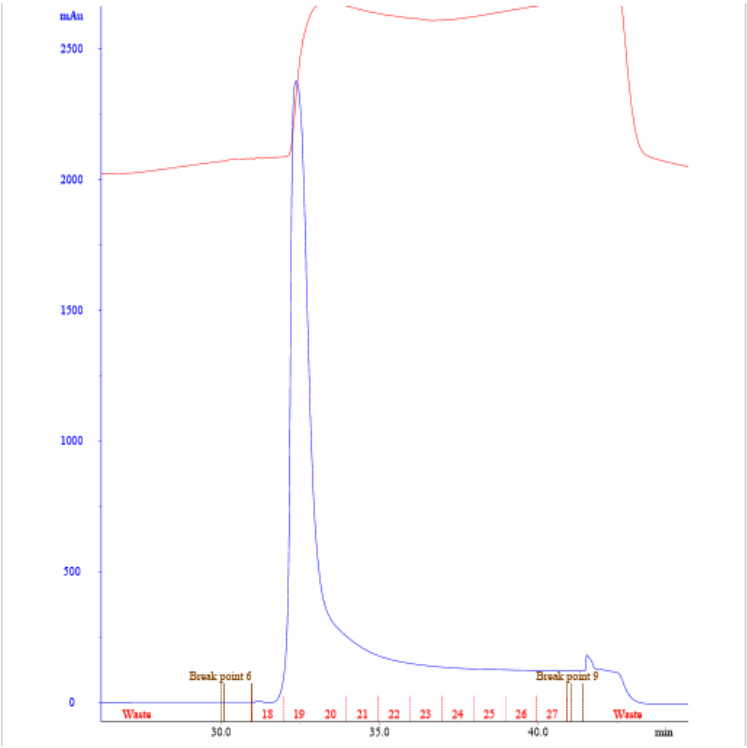

Figure S.1.1. Elution profile of the His-Trap purification step

The eluates were desalted by gel filtration chromatography, using a NAP-10 column (Sephadex G-25 Medium; Sigma) to eliminate the imidazole and evaluated by SDS-PAGE (**Figure S1.2**). The mass of protein obtained was 4.73 mg.

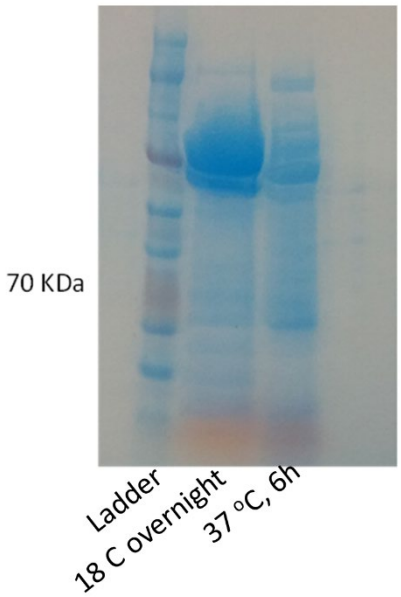

Figure S1.2. SDS gel analysis of purified lysate (18 C overnight) and aliquot taken after incubation at 37 ºC for 6 h.

APPENDIX 2

LECTIN SPECIFICITY ASSESSMENT THROUGH A FLUORESCENCE PLATE ASSAY

The work described in this appendix was performed before the course of this thesis, at Iceni Glycoscience, by Dr Simona Chessa, Dr Simone Dedola, Dr Paula García, Dr Stephan Goetz and Dr María J. Marín.

S2.1. Lectins of study

All the lectins used in this study are commercially available and fluorescein-labelled, with an excitation maximum is at 495 nm and an emission maximum is at 515 nm.

S2.1.1. Concanavalin A (ConA)

ConA recognizes α-mannose present as part of a core oligosaccharide in many serum and membrane glycoproteins. At neutral and alkaline pH, Con A exists as a tetramer of four identical subunits; below pH 5.6, Con A dissociates into active dimers of 52 kDa. Acetylation, succinylation, or other derivatizations can also produce stable forms with dimeric structures.

ConA requires calcium or manganese ions at each of its four saccharide binding sites. Although these divalent metal ions are bound tightly to the polypeptide structure, buffers which can bind calcium (such as phosphate) generally should be avoided in diluting ConA, since a gradual loss in activity may occur.

S2.1.2. Peanut agglutinin (PNA)

PNA binds preferentially to the T-antigen, a galactosyl (β-1,3) N-acetylgalactosamine structure present in many glycoconjugates such as M and N blood groups, gangliosides, and many other soluble and membrane-associated glycoproteins and glycolipids. A major cell surface receptor for PNA may be asialo GM1 ganglioside. With certain exceptions, the receptor sequence for PNA is normally sialylated, preventing the lectin from binding to its receptor oligosaccharide. Even sialic acid which is not bound directly to the receptor sugars may inhibit binding. The presence of calcium ions in diluents can enhance the binding of PNA to receptors, possibly by neutralizing the negative charges on sialic acid residues adjacent to the receptor sequence.

S2.1.3. *Ricinus communis agglutinin 120* (RCA$_{120}$)

This lectin consists of two subunits of 60 kDa which can be dissociated by reducing agents into closely related chains between 27 kDa and 33 kDa. One of the chains appears to be common to the B chain of another castor bean lectin, ricin, while the other chain is unique to RCA I. The B chain binds to galactose or N-acetylgalactosamine residues of membrane glycoconjugates.

S2.1.4. *Sambucus nigra* lectin (SNA)

SNA, isolated from elderberry bark, binds preferentially to sialic acid attached to terminal galactose in α-2,6 and to a lesser degree, α-2,3 linkage. Binding is also inhibited to some extent by lactose or galactose. This lectin does not appear to bind sialic acid linked to N-acetylgalactosamine. SNA has been reported to inhibit cell-free protein synthesis.

S2.1.5. *Dolichos biflorus* agglutinin (DBA)

DBA is a glycoprotein with a molecular weight of about 111 kDa and consists of 4 subunits of approximately equal size. This lectin has a carbohydrate specificity toward α-linked N-acetylgalactosamine. It has been used to establish secretor status in blood group A individuals by hemagglutination inhibition techniques and for blood typing. This lectin has also been used as a general marker of developing renal collecting ducts.

S2.1.6. *Ulex europaeus I* (UEA I)

UEA I binds to many glycoproteins and glycolipids containing α-linked fucose residues, such as ABO blood group glycoconjugates. This lectin preferentially binds blood group O cells and has been used to determine secretor status. It has been established as an excellent marker for human endothelial cells.

S2.1.7. Soybean agglutinin (SBA)

SBA is a family of closely related isolectins composed of four subunits of approximately equal size. This glycoprotein has a molecular weight of about 120 kDa and an isoelectric point near pH 6.0. SBA preferentially binds to oligosaccharide structures with terminal α- or β-linked N-acetylgalactosamine, and a lesser extent, galactose residues. Binding can be blocked by substitutions on penultimate sugars, such as fucose attached to the penultimate galactose in blood group B substance.

An important application for SBA is the separation of pluripotent stem cells from human bone marrow. Cells fractionated by SBA do not produce graft vs host disease and can be used in bone marrow transplantation across histocompatibility barriers.

S2.1.8. Wheat germ agglutinin (WGA)

This derivative has been reported to have properties distinct from the native lectin. Evidence suggests that succinylated WGA does not bind to sialic acid residues, unlike the native form, but retains its specificity toward N-acetylglucosamine. Using conjugates of the native lectin and the succinylated form can provide a system to distinguish between sialylated glycoconjugates and those containing only N-acetylglucosamine structures.

S2.2. Non-competitive plate assay for the detection of fluorescently-labelled lectins

The protocol below was developed and performed for the detection of the lectins described in *Section S2.1.*

1. A black 384-well plate is coated with BSA conjugates in bicarbonate buffer (50 µg/mL) for 1 h at 37 °C.
2. Following incubation, the plate is washed with 100 µL of PBST three times.
3. The lectins (10 µL) are added to the wells and incubated for 2 h at room temperature. The concentrations of the lectins needed in this step are the following: 20 µg/mL for PNA, DBA, UEA-I, ConA, WGA and RCA_{120}; and 50 µg/mL for SNA and SBA. The dilutions for the lectins are done in the HEPES-T buffer.
4. Following incubation with the lectin, the plate is washed with 100 µL of PBST twice.
5. The wells are then resuspended in 50 µL of PBST.
6. The fluorescence is measured at 485/520 nm.

S2.3. Glycoconjugates assayed

The figure below shows the commercially available BSA glycoconjugates used in this study.

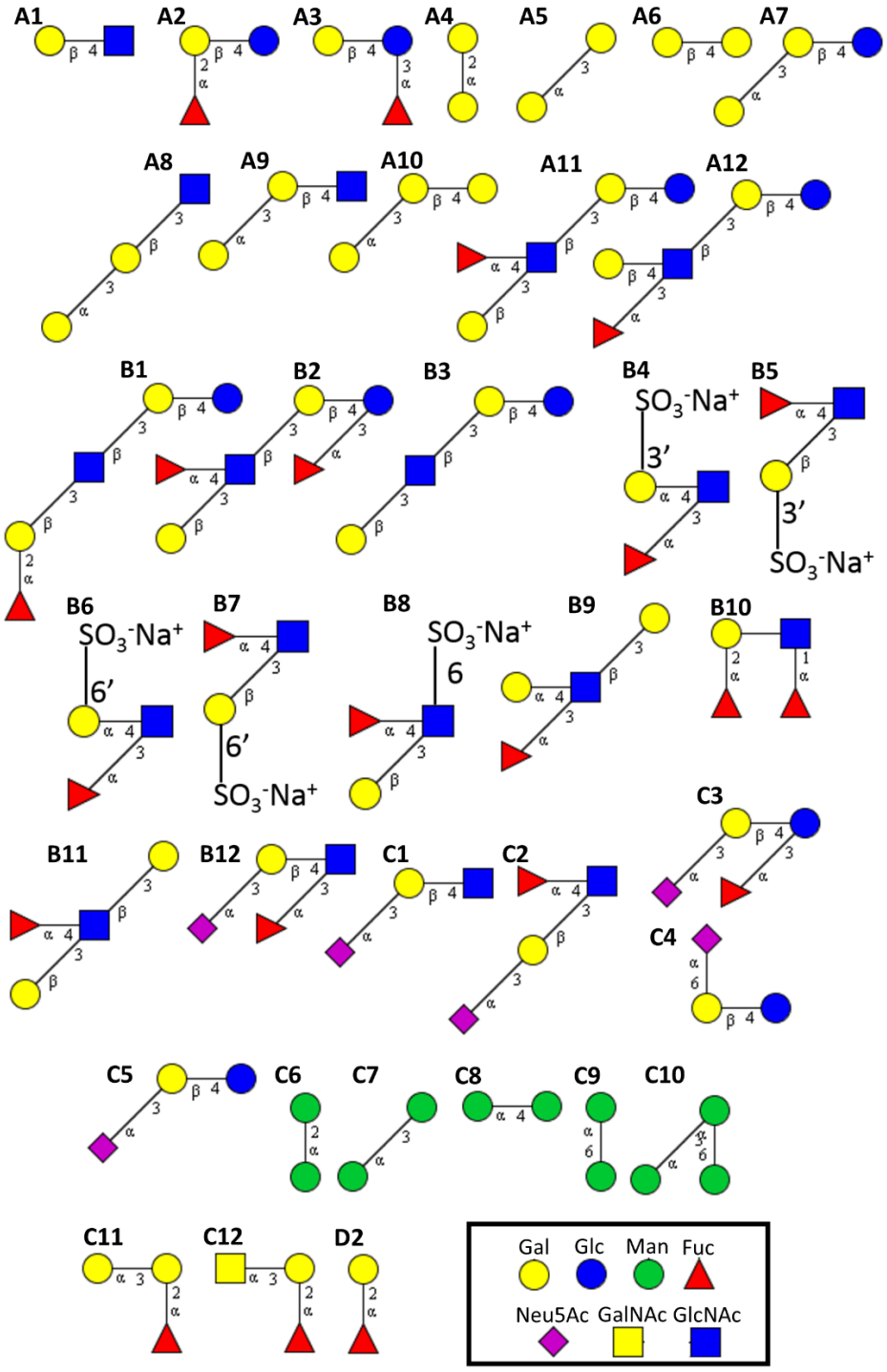

Figure S2.1. Carbohydrate moieties of the BSA glycoconjugates used in the fluorescence plate assay

S2.3. Fluorescence data

Figures S2.2-9 show the fluorescence data relating to the assay described in this appendix.

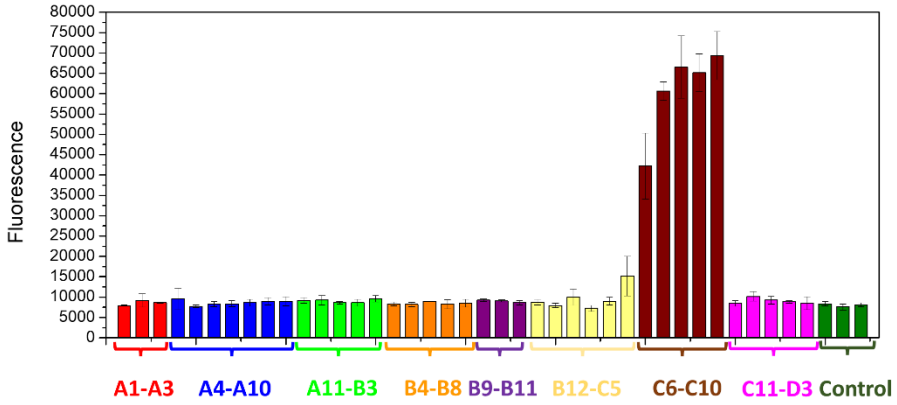

Figure S2.2. Fluorescence assay binding data of ConA and a library of BSA glycoconjugates.

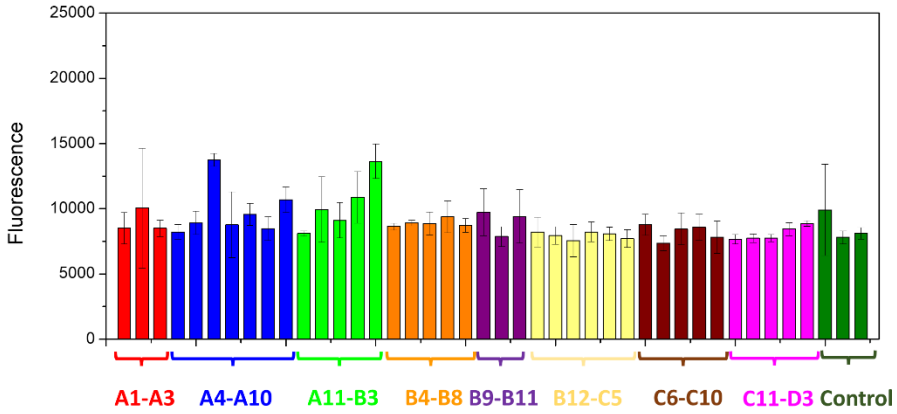

Figure S2.3. Fluorescence assay binding data of PNA and a library of BSA glycoconjugates.

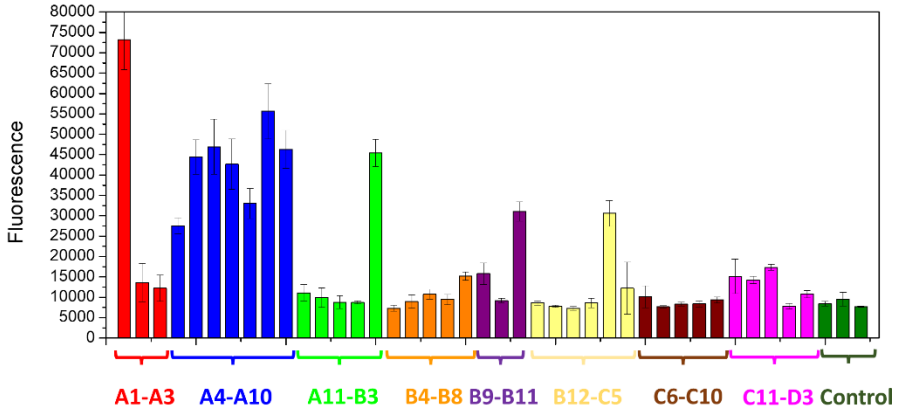

Figure S2.4. Fluorescence assay binding data of RCA_{120} and a library of BSA glycoconjugates.

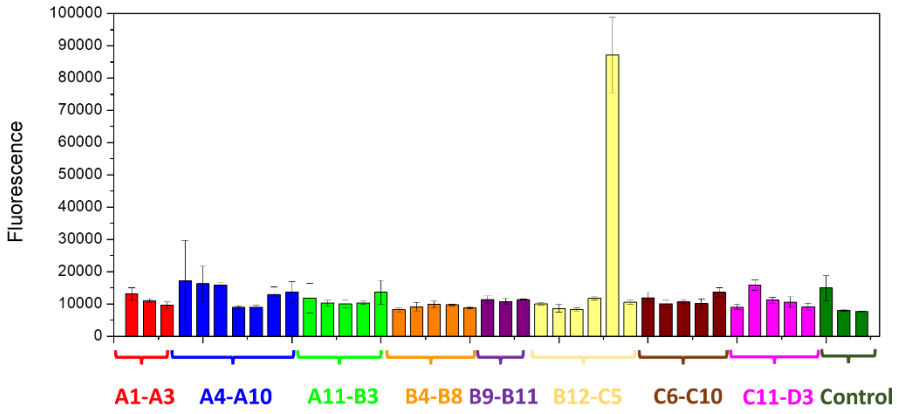

Figure S2.5. Fluorescence assay binding data of SNA and a library of BSA glycoconjugates.

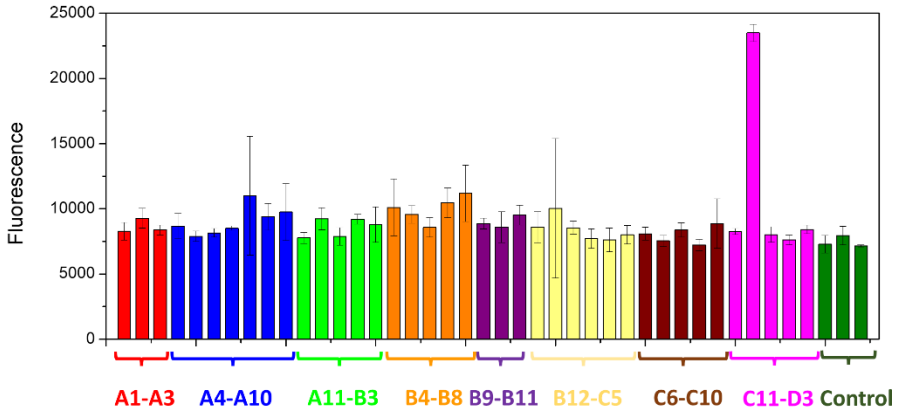

Figure S2.6. Fluorescence assay binding data of DBA and a library of BSA glycoconjugates.

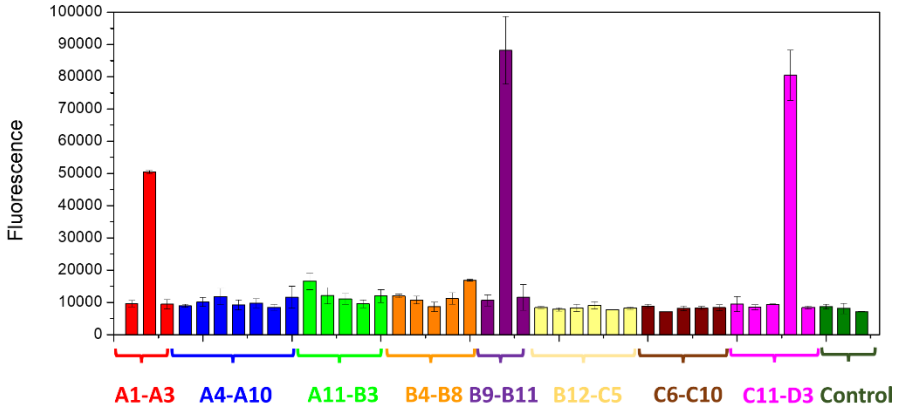

Figure S2.7. Fluorescence assay binding data of UEA I and a library of BSA glycoconjugates.

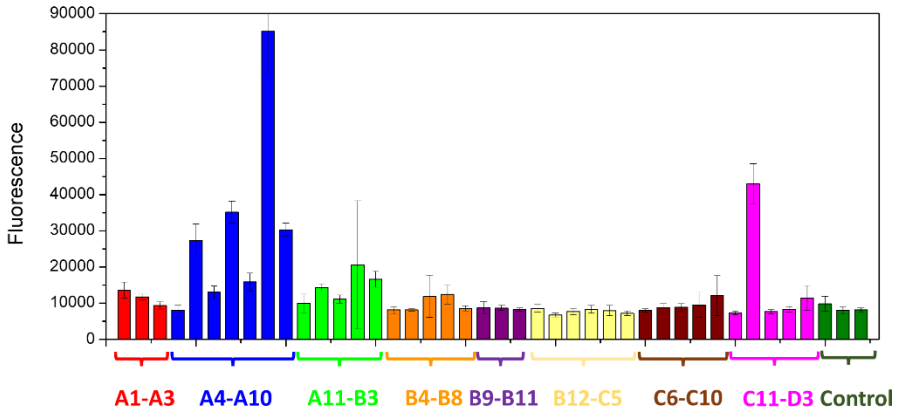

Figure S2.8. Fluorescence assay binding data of SBA and a library of BSA glycoconjugates.

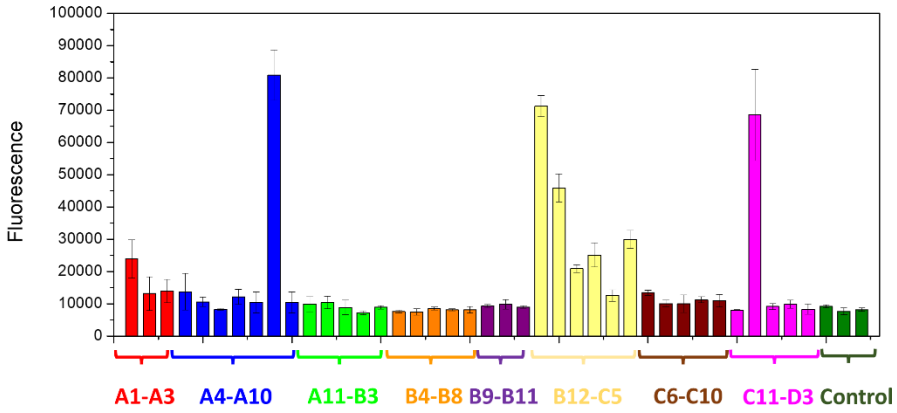

Figure S2.9. Fluorescence assay binding data of WGA and a library of BSA glycoconjugates.

The heatmap in **Figure S2.10** summarises all the binding data found in this set of experiments.

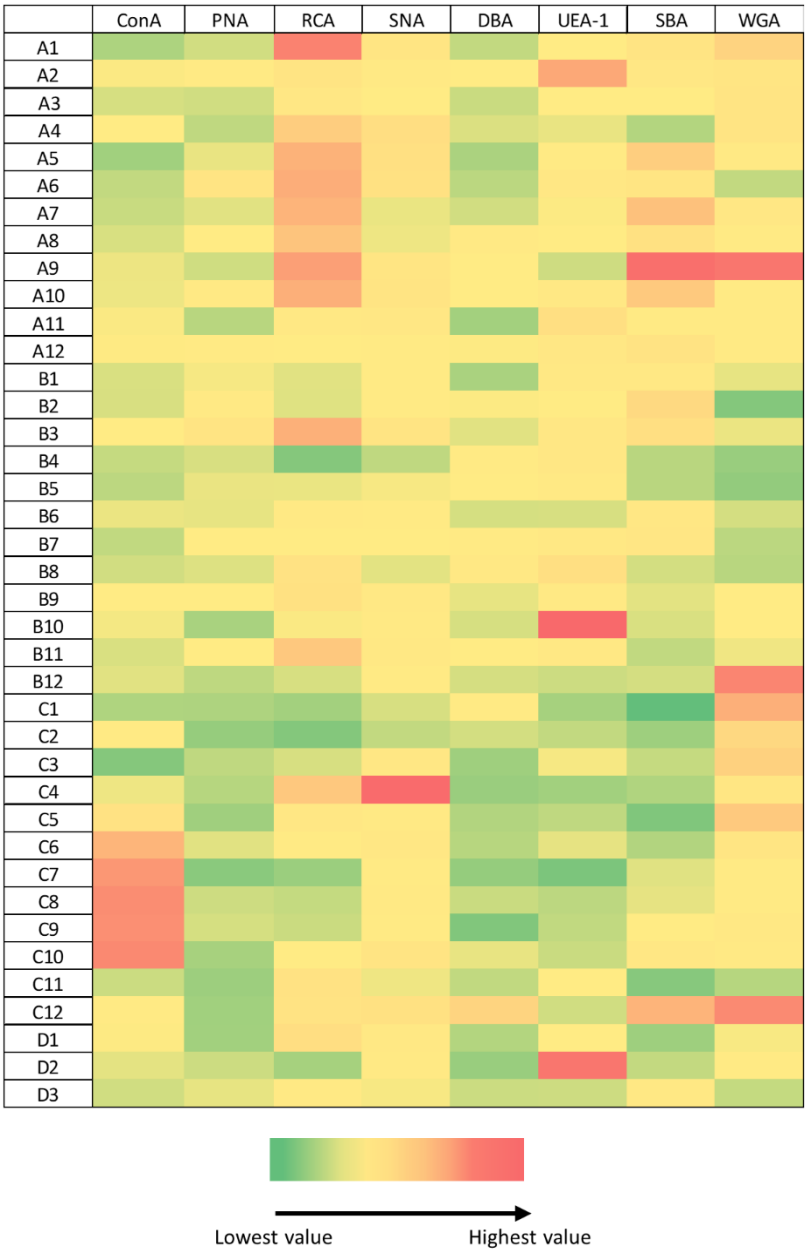

Figure S2.10. Heatmap showing the fluorescence assay binding data of a set of fluorescently labelled lectins and a library of BSA glycoconjugates.